# Nano-electronic components built from DNA templates

Von der Fakultät für Physik und Geowissenschaften
der Universität Leipzig
genehmigte

**DISSERTATION**

zur Erlangung des akademischen Grades

doctor rerum naturalium
Dr. rer. nat.

vorgelegt

von M.Sc. Jingjing Ye

geboren am 23.09.1991 in Zhejiang, China

Gutachter: Prof. Dr. Ralf Seidel
Prof. Dr. Tim Liedl

Tag der Verleihung: 30.04.2020

Die vorgelegte Arbeit entstand zwischen März 2016 und Oktober 2019
am Peter Debye Institut für Physik der weichen Materie
Linnéstraße 5
04103 Leipzig
Deutschland

Die Arbeit wurde betreut von
Prof. Dr. Ralf Seidel

Dedicated to my grandpa

I miss you

# List of Publications

**P1:** *Fabrication of Metal Nanostructures with Programmable Length and Patterns Using a Modular DNA Platform*

Jingjing Ye, Seham Helmi, Josephine Teske, Ralf Seidel

Nano Letter 2019, 19, 4, 2707-2714

**P2:** *DNA-Mold Templated Assembly of Conductive Gold Nanowires*

Türkan Bayrak,* Seham Helmi,* Jingjing Ye,* Dominik Kauert, Jeffrey Kelling, Tommy Schönherr, Artur Erbe, Ralf Seidel

Nano Letter 2018, 18, 3, 2116-2123

*These authors contributed equally to this work

**P3:** *DNA-Mediated Self-Assembly and Metallization of Semiconductor Nanorods for the Fabrication of Nanoelectronic Interfaces*

Richard Weichelt,* Jingjing Ye,* Uri Banin, Alexander Eychmüller, Ralf Seidel

CHEMISTRY-A European Journal 2019, 25, 9012-9016

*These authors contributed equally to this work

**P4:** *Complex Metal Nanostructures with Programmable Shapes from Simple DNA Building Blocks*

Jingjing Ye, Ralf Seidel

Submitted

**P5:** *Casting Gold Nanoparticles with High Aspect Ratios inside DNA Origami Molds*

Jingjing Ye,* Richard Weichelt,* Vaibhav Gupta, Tobias A. F. König, Alexander Eychmüller, Ralf Seidel

Submitted

*These authors contributed equally to this work

**P6:** *Sequential pull down for specific DNA nanostructure purification*

Jingjing Ye,* Josephine Teske,* Ralf Seidel

Manuscript in preparation

*These authors contributed equally to this work

**P7:** *A Hybrid Carrier System Based on Origami Nanostrucutures and Layer-by-Layer Microparticles*

Florian Scheffler, Mandy Brueckner, Jingjing Ye, Ralf Seidel, Uta Reibetanz

Advanced Functional Materials 2019, 29, 180811

The work from P4, P5 and P6 were conducted within the Ph.D. time frame. Under the regulation of *'Promotionsordnung der Fakultät für Physik und Geowissenschaften der Universität Leipzig'*, only published paper can be presented in the cumulative dissertation. Therefore, the results from P4, P5 and P6 were not included in this thesis.

## Bibliographic Description

Ye, Jingjing

**Nano-electronic components built from DNA templates**

University Leipzig, Dissertation

144 pages, 155 references, 16 figures and 2 tables (excluding publications)

## Abstract

Building metal nanomaterials with tailored electrical properties is in high demand for electronic device fabrication. However, scalable and inexpensive fabrication of such metallic structures with nanometer precision remains a challenge. DNA origami is a versatile and robust self-assembly method which allows fabrication of arbitrary structures at the nanoscale. In this thesis, DNA origami templated metal nanostructure fabrication method is introduced. Continuous metal nanostructures with controlled geometry as well as the selective deposition of multi-nanomaterials (metals and semiconductors) at specific sites on origami templates play an important role in the fabrication of DNA based nanoelectronics system. A mold DNA origami with quadratic cross-section was constructed and used as template for the gold nanoparticles metal growth. Each individual mold element acted as a lego-brick in this modular mold system. (1) Linear metallic nanostructures with controlled length and programmable patterns were fabricated at superior yields by systematically investigating the interface of each mold element. (2) A versatile fabrication modular mold platform for metallic nanostructures with complex shapes was further developed by integrating particular molds with different diameters, additional docking sites, and junctions. Caged metal nanostructures, constrained gold growth and branched structures with extensions in two dimensions were successfully realized. (3) Micrometer long, homogeneous and continuous gold nanowires were obtained with exceeding quality. Using electron-beam lithography and low-temperature conductance measurements, ohmic behavior of such nanowires were observed, confirming metallic conductive property. (4) A method for the synthesis and DNA functionalization of semiconducting nanorods was established. Metal-semiconductor heterostructures were fabricated based on the modular mold system. Semiconducting nanorods, as well as gold nanoparticles, were placed at defined positions on the DNA modular platform and a direct metal-semiconductor interface was achieved after the electroless metal deposition. (5) An improved and optimized metallization of DNA origami templated gold nanowires were further developed to increase the conductivity performance. Various reaction parameters were investigated and the obtained gold nanowires with a reduced number of AuNPs achieved an anisotropic

growth. This developed DNA origami template mold modular platform addresses the size, pattern, and geometry controls over the metallic nanostructures. For the application prospect, the conductivity of such metallic nanostructures and controlled placement of different nanomaterials enable an important step towards the nanodevices and systems fabrication based on DNA.

## Bibliographische Beschreibung

Ye, Jingjing

**Nano-electronic components built from DNA templates**

Universität Leipzig, Dissertation

144 Seiten, 155 Literaturangaben, 16 Abbildungen und 2 Tabellen (ausgenommen Veröffentlichungen)

## Zusammenfassung

Der Aufbau metallischer Nanomaterialien mit angepassten elektrischen Eigenschaften ist für die Verwendung in elektronischen Bauteilen von großer Bedeutung. Dabei ist die skalierbare und günstige Herstellung metallischer Strukturen im Nanometerbereich weiterhin eine Herausforderung. Die DNA Origami Technik bietet hier eine vielseitig einsetzbare und stabile Methode zur Selbstassemblierung, welche die Herstellung beliebiger nanoskalierter Strukturen ermöglicht. In dieser Arbeit wird ein neuer Ansatz zur Herstellung metallischer Nanostrukturen mit Hilfe von DNA Origami Templaten vorgestellt. Kontinuierliche Metallnanostrukturen mit einer definierten Geometrie, sowie die selektive Anbindung verschiedener Nanomaterialien (Metalle und Halbleiter) an spezifischen Anbindungsstellen des Origamitemplates spielen eine wichtige Rolle bei der Herstellung DNA basierter nanoelektrischer Systeme. Ein DNA Origami Mold mit einem quadratischen Querschnitt wurde als Templat für die Metallisierung von Goldnanopartikeln verwendet. Das legostein-artige Design der einzelnen Origami Molds ermöglicht die Assemblierung in einem modularen System. (1) Lineare metallische Nanostrukturen mit kontrollierter Länge und programmierbarem Muster wurden mit hohen Ausbeuten assembliert, indem das Interface der einzelnen Origamistrukturen systematisch untersucht wurde. (2) Weiterhin wurde eine vielseitige, sowie modulare Plattform für metallische Nanostrukturen mit komplexen Formen entwickelt. Dabei wurden spezielle Origamistrukturen mit unterschiedlichem Durchmesser, sowie zusätzlichen Anbindungsstellen und Verzweigungen integriert. Die erfolgreiche Metallisierung linearer und verzweigter Nanostrukturen in zwei Dimensionen wurde durch ein restriktives Goldwachstum im Inneren der Origamistrukturen realisiert. (3) Homogene und kontinuierliche Goldnanodrähte mit Mikrometerlänge und außerordentlicher Qualität wurden fabriziert. Mit Hilfe von Elektronenstrahllithographie wurde die Leitfähigkeit der Strukturen im Niedrigtemperaturbereich untersucht, wobei ein ohmsches Ladungstransportverhalten der Nanodrähte nachgewiesen werden konnte, welches die metallische Leitfähigkeit der Strukturen bestätigte. (4) Eine Methode zur Synthese und DNA Funktionalisierung von Halbleiternanostäbchen wurde eingeführt. Zudem konnten Metall-

Halbleiterheterostrukturen hergestellt werden, basierend auf dem entworfenen modularen Origamisystem. Halbleiternanostäbchen und Goldnanopartikel wurden an definierten Positionen der DNA Origami platziert. Durch eine anschließende Metallisierung konnte ein direktes Metall-Halbleiterinterface hergestellt werden. (5) Eine verbesserte und optimierte Metallisierung der DNA Origami basierten Goldnanodrähte zur Erhöhung der Leitfähigkeit wurde entwickelt. Dazu wurden verschiedene Reaktionsparameter optimiert, so dass ein anisotropes Wachstum mit einer reduzierten Anzahl von Goldnanopartikel ermöglicht werden konnte. Die, in dieser Arbeit entwickelte DNA Origami Plattform ermöglicht die Kontrolle über Größe, Struktur und Geometrie metallischer Nanostrukturen. Die ohmsche Leitfähigkeit dieser Nanostrukturen und die zusätzliche Assemblierung verschiedener Nanomaterialien stellen dabei einen wichtigen Schritt für eine potentielle Verwendung in elektrischen Nanogeräten dar.

# Table of Contents

# 1. Introduction

## 1.1 DNA Nanotechnology

Nanotechnology and nanoscience cover the study, manipulation, design, and engineering of particles, materials, structures and functional devices on dimensions from 1 nm to 100 nm. Materials at the nanometer scale (the scale of atoms and molecules) can often exhibit different electrical, optical, thermal and mechanical properties than their macro-scale counterparts due to finite-size and quantum mechanical effects. Because of their intrinsic properties, nanomaterials are being widely used in applications including electronics, optics, photonics and medicine. Two distinct approaches are used to produce nanomaterials: the 'top-down' and 'bottom-up' methodology. Top-down approaches, such as electron beam lithography, employ large devices to fabricate smaller objects with designed dimensions and patterns. It is often costly and requires advanced instrumentation. Bottom-up approaches follow the arrangement of smaller components into larger and more sophisticated structures. This arrangement is often based on molecular recognition properties in the self-assembly process and it allows for a highly parallel production of nanostructures.

Deoxyribonucleic acid (DNA) has become a widely used building material [1], [2] due to the specificity of Watson-Crick base pairing. DNA has exclusive molecular recognition properties which allows building of predefined micro and nanostructures by programming intra- and intermolecular interactions [3]–[5]. DNA is a rigid biomolecule that can be cost-effectively synthesized [6], [7]. Because of the aforementioned reasons, DNA has been remarkably used as a building material in nanotechnology for applications in numerous fields [8], [9].

### 1.1.1 Deoxyribonucleic Acid

Deoxyribonucleic acid (DNA) is a molecule that stores genetic information and encodes the necessary functions. In 1869, Friedrich Miescher isolated DNA from the leukocytes' nuclei (white blood cells) and named as "nuclein" [10], which later was evaluated to "nucleic acid", and eventually to "deoxyribonucleic acid" or "DNA". In 1994, DNA was confirmed as the genetic information carrier by Oswald Avery and co-workers [11], and later confirmed by the Hershey-Chase experiment [12]. In 1953, James Watson and Francis Crick developed the double helical molecular model of DNA [13] based on the X-ray crystallography data (**Figure 1**a) from Rosalind Franklin and Maurice Wilkins [14] and the chemical prediction from Erwin Chargaff [15].

## The DNA Structure

DNA is a long polymer composed of many repeating units, so-called "nucleotides". Each nucleotide (nt) is composed of a five-carbon sugar (deoxyribose), a phosphate group and one of four nitrogenous nucleobases, in particular adenine (A), thymine (T), cytosine (C) and guanine (G). The nucleobases are divided into two groups: purines (A and G) and pyrimidines (T and C).

The DNA double helix structure contains two complementary DNA chains. For right-handed double helix, it has 2 nm diameter, 0.34 nm center-to-center distance between two following nucleotides and the helical pitch is 10.5 nucleotides [16], see **Figure 1**b. Alternating sugar and phosphate residues form the DNA double helix backbone. Sugar residues are interconnected by phosphodiester bonds between the third and fifth carbon atoms of the adjacent sugar rings. Due to these asymmetric bonds, a single DNA strand has a chemical polarity. It has a terminal phosphate group at the 5' end and a terminal hydroxyl group at the 3' end [17]. The two DNA strands are hybridized via hydrogen bonds between the bases, see **Figure 1**c. The DNA double helix has two grooves: a major groove (2.2 nm width) and a minor groove (1.2 nm width) [18]. There are different DNA forms including right-handed B-DNA, A-DNA and left-handed Z-DNA [19]. Depending on the base sequence and the environmental factors (metal ions, hydration level, and polyamines), DNA can have different conformation [20]. B-form DNA is the most common form under physiological conditions.

## Base Pairing and Base Stacking

The DNA double strands are held together by Watson-Crick base pairing. A-T base pairs have two hydrogen bonds and G-C base pairs have three hydrogen bonds [17], [21], [22]. DNA with rich G-C content is more stable [23]. The complementary base pairing leads to an energetically favorable base pair packing at the inner double helix. The hydrogen bonding is a relatively weak molecular interaction (5-30 kJ/mol) compare to covalent binding energy (100 kJ/mol) [24]. DNA double helix structure is preserved primarily by base stacking (π-stacking) interaction between adjacent bases caused by the overlapping delocalized π-electron systems [25]. Both base stacking and base-pairing interactions (cooperative effect) contribute to the formation of the DNA double helix structure. DNA length, percentage of G-C content (base pairing), sequence (base stacking), concentration and the ionic strength all contribute to the thermodynamic stability of the DNA double helix conformation. The melting temperature is often used to determine the DNA stability, when half of the double-stranded DNA molecules fall apart into single-stranded DNA molecules [26], [27].

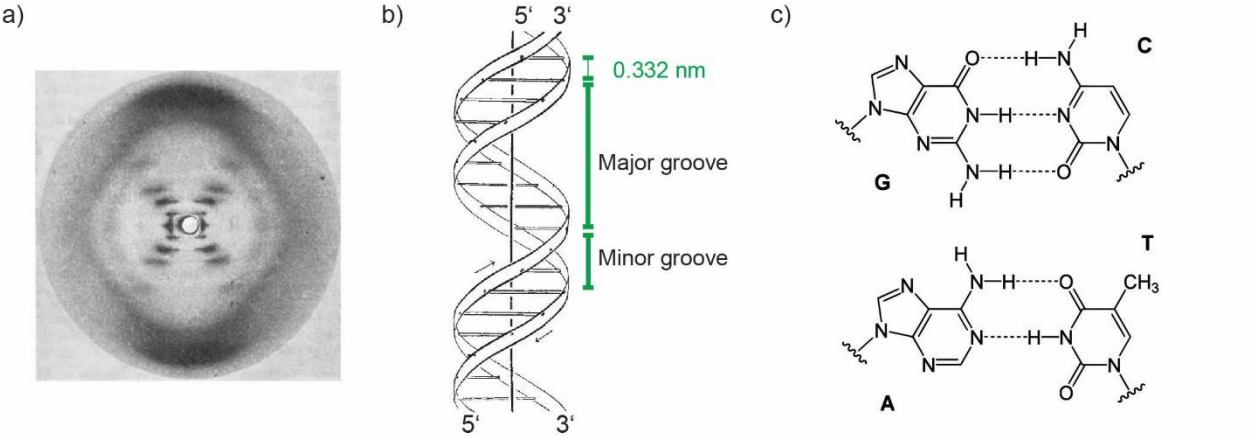


**Figure 1** DNA structure. (a) X-ray fiber diffraction pattern of B-form DNA [14]. (b) Three-dimensional B-form DNA double helix model [13]. (c) Watson-Crick base pairing of the DNA double helix [28]. There are three hydrogen bonds (dashed lines) between C and G (top) and two hydrogen bonds between A and T (bottom).

### 1.1.2 DNA as Building Material

In 1982, Nadrian Seeman [29] introduced the revolutionary idea that DNA is not only a genetic information carrier but can also be used as a molecular building material. A tremendous development has since then occurred in the field of structural DNA nanotechnology. DNA architectures with increasing complexity and rigidity have been created with accurate control down to the atomic scale [30]. Nanoscale size, molecular recognition properties, stability, programmability and also the biocompatibility, all these DNA molecule's unique material properties promote the nanoscale engineering utilizing DNA.

#### Nanoscale Size, Programmability and Producibility

DNA molecule has 2 nm diameter, 0.34 nm separation distance between the adjacent bases and 3.5 nm helical pitch per turn and 53 nm persistence length for double-stranded DNA [31]. All these nanometer size conditions make DNA double helix a perfect building material for design and construct complex three-dimensional nano-objects. The DNA sequence can be programmed to almost any specific sequence that is designed to construct the DNA nanostructures. The synthesize of this individual arbitrary sequence can be industrially achieved with different length and functionalization [32]. Commercial technology can produce custom oligonucleotides with a high yield up to 60 nucleotides. The availability of custom single-stranded DNA and its programmability is the foundation of programmable DNA nanoconstructs.

#### DNA Hybridization

The bottom-up self-assembly process in structural DNA nanotechnology is based on the hybridization between complementary DNA strands. It is specific and energetically favored of the complementary Watson-Crick base pairing: bases A with T, bases G with C. Furthermore, double-

stranded DNA molecules are programmed to interact with each other. This uses single-strand extensions of either the 5' or the 3'-end of the DNA duplex, which are called "sticky ends" [33]. Via hydrogen bonding, the sticky ends of one double-stranded DNA can hybridize with the complementary sticky ends of a second double-stranded DNA (**Figure 2**a).

**Stability of Branched DNA Constructs**

To create arbitrary shaped two-dimension (2D) and two-dimension (3D) DNA constructs, DNA motifs with branched helical axis can self-assemble via sticky-end interactions into compact structures. It is crucial that these branched motifs are mechanically rigid for such a construct building. One example in nature of such branched DNA motifs is the four-arm branched junction [34], also called Holliday junction. It occurs naturally during genetic recombination when homologous chromosome pairs exchange adjacent sequences by crossing over to each other. This allows creating increased genetic diversity for the next generation by "mixing" genes of both parents. In a Holliday junction four DNA strands are linked together, to form a 4-arm branch point (**Figure 2**b). In biology, Holliday junctions usually have symmetric sequences and the branch point of the four-arm junction can migrate throughout the molecule. This movement is called branch migration [35]. To prevent the dynamic process of branch migration, the sequences of the DNA can be designed to be asymmetric near the branch point. Two and three-dimensional lattices (**Figure 2**b, c) can be created by connecting multiple Holliday junctions via sticky end interaction [29], [36].

DNA with all these abovementioned different characteristics can self-assembled to predictable and stable nanoscale constructs. 3D crystals can be fabricated using DNA branched-junctions with single-stranded overhangs (**Figure 2**a, b). This 3D crystal can also be used as a template for the precise arrangement of proteins and other bio-macromolecules [37]. A DNA 3D cube (**Figure 2**c) was successfully fabricated by hybridizing the three-arm junctions through sticky-ends [38]. Furthermore, double-crossover [39] and triple-crossover [40], [41] molecules were also utilized as building units to increase rigidity. Periodic 2D crystal lattices were constructed via sticky-ends association [42], [43]. With further developed computational design, 2D and 3D nanostructures built from single-stranded DNA tiles can also be realized [44], [45]. The concept established by Nadrian Seeman introduced an important breakthrough for DNA nanotechnology.

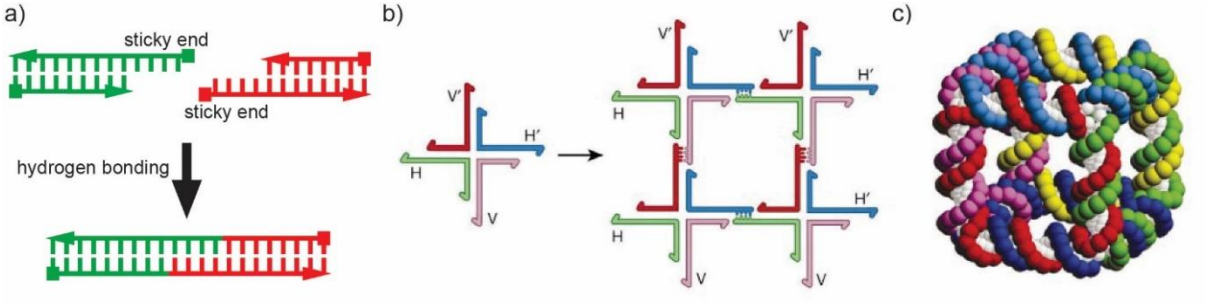


**Figure 2** Self-assembly of DNA. (a) Sticky-end hybridization via hydrogen bonding. (b) Self-assembly of DNA branched-junctions into a 2D crystal via sticky-end hybridization [37]. (c) Cube-like DNA structure by ligation of six single DNA strands [38].

### 1.1.3 The DNA Origami Technique

In 2006, Paul Rothemund introduced the concept of 'scaffolded DNA origami' to construct DNA nanostructures [46]. It followed a somewhat similar concept as the traditional Japanese paper folding art. Instead of folding a sheet of paper into an arbitrary shape, a long single-stranded viral DNA scaffold molecule was folded into 2D or 3D structures. The 7249 nt single-stranded DNA was so-called "scaffold DNA" and was derived from the bacteriophage M13. With the help of hundreds of short oligonucleotides called "staple strands" , the ssDNA could be folded into the designed shape through the hybridization of these individual short oligonucleotides to different complementary position on the 'scaffold strand' that shall be brought into proximity (see **Figure 3**a). The folding process was one-pot reaction. The scaffold strand and the staple strands were mixed in salt-containing buffer and subjected to an annealing process with samples heated up to 65 º and cooled down through a nonlinear temperature ramp over hours. A set of desired flat shapes with around 100 nm diameter (two-dimensional squares, stars, smiley face, and triangles) was achieved (**Figure 3**b) with high folding yields up to 90 % and spatial resolution of 6 nm.

Further on, more complex 3D DNA structures by stacking the multiple layers of DNA helices were realized by Douglas and co-workers [47] in 2009 (**Figure 3**c), which increased the complexity and rigidity of DNA origami structures. The helices from multiple layers were interconnected to three neighbors through staple and scaffold crossovers at the position where the corresponding bases were pointing towards each other. When assuming every 10.5 bases B-form DNA with one full turn, thus at the position of every 7 bases, it gave the spatial orientation of 120º and 240º via these three neighbor helices which resulted in a honeycomb lattice. Helices could also be placed on a square lattice [48] where one helix was connected to four neighbor helices with 90º angle between the helices with a distance of multiple of 8 bases (**Figure 3**d). The 90º angle of square lattice did not match the rotational properties of B-DNA and it caused a general twist in the structure, which could be manually corrected by additional insertion or deletions. The complex DNA

origami design could be achieved with a computer-aided user-friendly software called caDNAno [49], that was also developed in the same year 2009 by Douglas and co-workers. It is a graphical interface-based program, which easier the design of DNA origami and can automatically generate the sequence of the final staple strand.

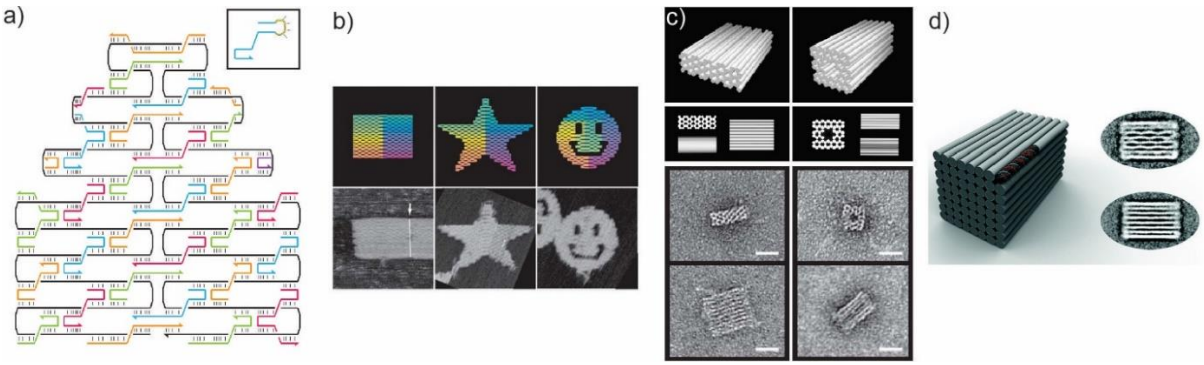


**Figure 3** DNA origami structures. (a) The scheme demonstrates the folding path of a DNA origami structure. (b) Examples of 2D origami structures. Top: Schematic diagrams of the structures including a rectangle, a star, a smiley face, and a triangle; bottom: AFM images of the fabrucated 2D DNA origami shapes [50]. (c) 3D origami structures based on a honeycomb lattice [51]. Scale bar: 20 nm. (d) 3D DNA origami structures based on a square lattice[48]. Scale bar: 20 nm.

Numerous DNA nanostructures have been assembled using the origami technique, such that in the following only a small selection is highlighted. A DNA box with a controllable lid [52] could be fabricated by connecting 6 origami sheets at their edges. By manually introducing the base insertions/deletions to change the distance between staple crossovers, twisted and curved structures could be introduced [53] (**Figure 4**a). Dietz *et al.* demonstrated that the curvature of DNA origami structure could be quantitatively controlled down curvature radii of 6 nm [53]. A molecular robot could also be built based on the shape-complementarity of the 3D DNA origami [54]. They could change their conformation by cation concentration or temperature, thus introducing a dynamic system, including an actuator, a switchable gear and a nanorobot (**Figure 4**b). In addition to conventional DNA origami structures from closely packed helices, wireframe 3D DNA origami meshes have been created by using a computer algorithm to convert the desired structure into a triangulated mesh [55]–[57] (**Figure 4**c).

Each individual staple oligonucleotide is highly addressable, thus different functional materials can also be integrated into the DNA origami structure via these staple oligonucleotides. The oligonucleotides end can be directly modified with chemical linkers for integration or an extension of the specific staples strands for the attachment of functional materials with complementary sequence. Various functional elements, such as proteins [58], fluorescent dye [59] and Raman-active molecules [60], [61], semiconducting polymers [62] and metallic nanoparticles [63], [64]

have been introduced to the DNA origami structures to achieve different functionalities and properties. DNA origami proved to be a useful method to design and fabricate nanostructures with a broad range of functionalities.

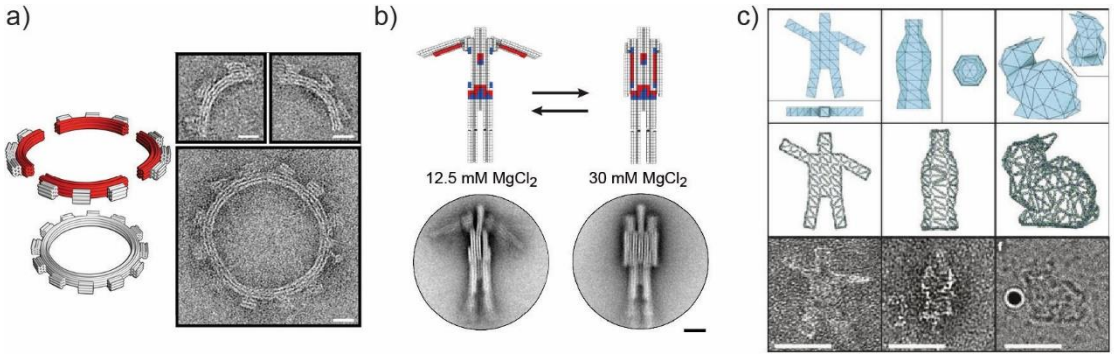


**Figure 4** DNA origami structures. (a) Curved structures bend into a quarter circle to form 12-tooth gears [53]. Scale bar: 20 nm. (b) DNA origami nanorobot [54]. Scale bar: 25 nm. (c) 3D wireframe DNA structures: waving stickman, a bottle and a version of the Stanford bunny [55]. Scale bar: 50 nm.

### 1.1.4 Hierarchical Assembly of DNA Origami Structures

Large DNA origami structures, both in size and molecular weight, are highly desired for creating complex higher-order structures [65]. However, the size of an individual DNA origami structure is limited by the scaffold length of ~8000 nt (~300 kDa). To scale up the size of DNA origami structures, each DNA origami can be used as a building block and form higher-order structures through hierarchical self-assembly [66]. There are two principles for the higher-order DNA origami assembly that utilizes and stabilizes DNA structures: (1) sequence-specific Watson-Crick base pairing via sticky-end association; (2) non-sequence-specific base stacking at the blunt ends of the DNA helices.

**Base pairing via sticky ends:** Iinuma *et al.* [67] fabricated 3D polyhedrons from DNA origami "tripod" monomers, whose inter-arm angles can be tuned by the length of supporting struts (**Figure 5**a). Different polyhedral shapes were constructed (consist of 4-12 monomers) from tripod monomers with different angles, reaching molecular weights of up to 60 MDa. 2D crystalline DNA origami structures can also be achieved based on this principle. Seeman and co-workers [68] constructed a DNA origami array where the cross-shaped origami tiles had available connecting sites in two independent directions (**Figure 5**b). These sticky ends found the complementary parts and hybridized, leading to large 2D arrays. In addition, lattice arrays can be assembled from sets of hexagonal DNA origami tiles [69]. One important aspect for higher-order DNA origami structure assembly is the rigidity and correct folding of the origami monomers. In addition, minimizing the global twist and avoiding strong association improves the higher-order assembly.

**Base stacking at blunt ends:** Yan *et al.* reported that simple base stacking at helical blunt ends of DNA origami can be utilized for higher-order assembly [70]. In 2011, Woo and Rothemund systematically studied the assembly rule based on base stacking. They found that base stacking was a directional bond force and it favored an antiparallel stacking polarity. Furthermore, this force can be used to guide DNA origami towards high-order assembly [71]. They summarized three main factors that need to be considered when implementing base stacking into the higher-order DNA origami self-assembly: (1) the sequences of the bases, which defined the interaction strength; (2) global twist, which influences the stacking sites' accessibility; and (3) crossovers near the blunt-end region, which can cause deformation and reduce its efficiency. Following these rules, a set of base stacking interactions have been designed with complementary codes to achieve specific hybridization associations resulting in different patterns (**Figure 5**c). Dietz *et al.* constructed 3D multilayered DNA origami bricks based on this concept (**Figure 5**d) [72]. In addition, they showed that temperature and salt concentration could be tuned to switch on or off interactions between these origami units.

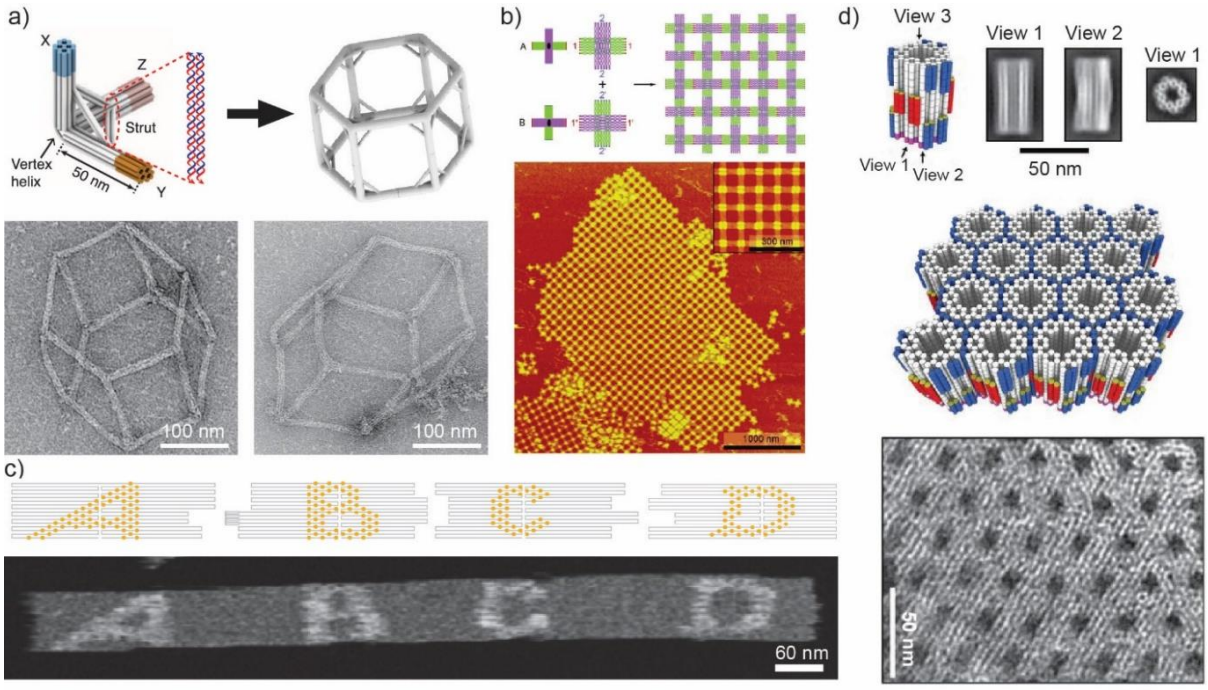


**Figure 5** Hierarchical assembly of DNA origami via base-pairing and base-stacking. (a) Hexagonal prisms containing 12 DNA origami tripods via sticky ends hybridization [67]. (b) 2D DNA origami arrays assembled from cross-shaped DNA origami tiles via sticky ends hybridization [68]. (c) A linear DNA origami array assembled via blunt-end stacking and shape complementarities [71]. (d) 2D lattice structures were created based on shape complementarity of the origami monomers [72].

**Combination of two principles (base pairing via sticky ends and base stacking at blunt ends):** In addition, base stacking (based on shape complementarity DNA blunt ends ) and base pairing (based on hybridization of sticky ends) can be simultaneously combined and applied [73]–[75]. This has extensively expanded the complexity of self-assembled patterns. Three-dimensional crystalline DNA origami lattices (**Figure 6**a) were assembled from DNA building blocks and it could site-specifically host nano-objects [76]. Gigadalton-scale DNA structures (**Figure 6**b) with sizes comparable with viruses and cellular organelles have been achieved with a high yield around 90 % [77]. Mona Lisa structures (**Figure 6**c) can be produced with DNA origami arrays by 'fractal assembly' [78]. Increasing size (up to16 individual monomer) and arbitrary pattern reached a yield of 2-4 %.

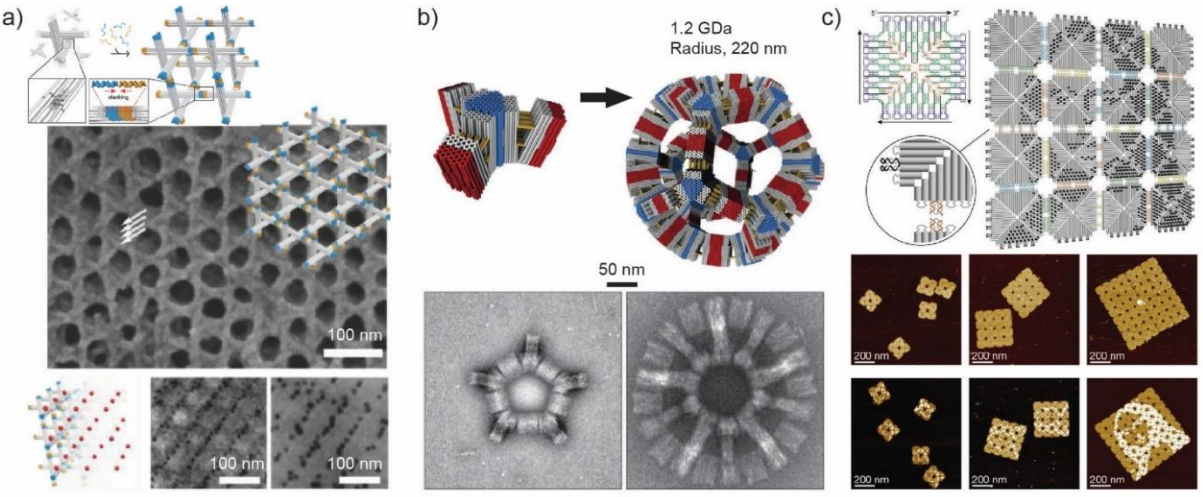


**Figure 6** Higher-order DNA origami assembly. (a) A rhombohedral DNA origami lattice via triangular DNA origami building blocks [76]. Gold nanoparticles can be hosted in this DNA origami lattices. (b) DNA dodecahedron formed from V-brick, with 1.2 GDa mass and 220 nm radius [77]. (c) Strand-level diagram of square DNA origami tiles which can form a picture of Mona Lisa [78]. AFM images of plain arrays and Mona Lisa were presented.

**Other strategies to obtain large origami structures**: Much longer scaffolds for DNA origami can be produced to increase the size of DNA origami. Such scaffolds, achieved by a variety of biotechnological methods, have been used to construct large-sized DNA origami structures [79], [80]. Multiple scaffolds could be utilized for one DNA origami design to achieve larger sizes [81]. Moreover, some single-stranded staples in the origami structure can be replaced with complex nanostructures, for example, DNA tiles or origami structures themselves to increases the complexity and size of an individual origami [82], [83]. For the latter, the assembly yield of 85% can be achieved with a molecular weight up to 45.5 MDa. In addition, external templates can be used to assemble the DNA origami structure into a large scale. Woo and Rothemund [84] demonstrated that controlling the stepwise diffusion of origami onto the mica substrate can medicate higher-

order latticed DNA origami structures. Lipid bilayer can also be utilized to direct the growth of DNA origami into 2D arrays [85].

## 1.2 Metallic Nanostructure Fabrication based on DNA

Top-down lithography method to scale down metal structure reaches limitations, building arbitrary metal nanostructures in a parallel fashion are highly demanded. Bottom-up self-assembly based on DNA nanotechnology for fabricating metallic nanomaterials is widely developed.

### 1.2.1 Metallization of DNA

#### Metal-ion Interactions with DNA

The key aspect of DNA metallization is the interaction between DNA and metal ions. DNA with its negatively charged phosphate backbone can attract charged species due to electrostatic interactions [86], which dominate in particular for alkali metal ions like $Li^+$, $Na^+$, $K^+$, $Cs^+$. It has been proven that they can electrostatically bind to the DNA backbone. In addition to electrostatic interactions, divalent metal cations like $Mn^{2+}$, $Ni^{2+}$, $Cu^{2+}$, $Pd^{2+}$, have specific interactions with bases on the purine and pyrimidine rings [87]. These metal ions interact more strongly with the bases than with the phosphates, except for $Cu^{2+}$, which binds strongly to both of these groups. However a too strong base affinity can disturb the hydrogen bonding the between base pairs, destabilizing the B-form DNA [87]. Different metal ions interact with either phosphate backbone or nucleotide bases, and it is of critical importance for several methods of DNA metallization.

#### Electroless Plating

Electroless plating is a method of depositing metals without the usage of an electrochemical reduction process. It can therefore also applied to non-conductive substrates. A solution containing the desired metal ions is applied to a substrate to initiate the metal deposition. The first deposited metal layer catalyzes subsequent plating and allows the metal deposition to continue. The plating process thus follows an autocatalytic mechanism [88].

The underlying principle can be described as a reduction-oxidation (redox) reaction and is divided into two steps: oxidation (anodic reaction) and reduction (cathodic reaction). The reducing agent ($Red$) provides the required electrons by reacting to its oxidized form ($Ox$); afterward, the electrons reduce the metal ions ($M^{z^+}$).

$$\begin{aligned} Oxidation\ reaction&: Red \rightarrow Ox + ne^- \\ Reduction\ reaction&: M^{z^+} + ze^- \rightarrow M \end{aligned} \tag{1}$$

The above reactions do not show the actual stoichiometry for the electroless plating.

An electroless plating bath typically consists in addition to metal ions and a reducing agent also of suitable complexing agents, and stabilizers. Complexing agents are normally organic acids or their salts to maintain the pH of the plating solution [88], [89]. Complexing agents can also form stable complexes with metal ions and enhance the metal ion stability and the plating reaction's selectivity [88]. Stabilizers help to prevent the homogeneous reaction that leads to random decomposition [88], [90].

**Metallization of dsDNA**

Double-stranded DNA (dsDNA) can be directly metallized by electroless plating via initial binding of seed ions, formation of nucleation centers during the reduction of seeds, and subsequent growth of the nucleation centers into metallic structures. In 1996, the first case of exploiting DNA structures for a templated growth of nanoparticle was described by Coffer *et al.* [91]. They used 3455 bp long circular plasmid DNA molecule as a template for the fabrication of semiconductor nanoparticle rings (Q-CdS, $Cd^{2+}$ ions reduced by $H_2S$). It demonstrated that it was possible to use biological macromolecules as templates for the self-assembly of semiconductor nanostructures.

In 1998, Braun *et al.* [92] described a two-step procedure for using DNA in the construction of a functional electric circuit. It was the first realization of DNA metallization. The DNA they used was λ-DNA (48502 base pairs), a linear dsDNA from lambda phage. They fabricated silver nanowires on this DNA scaffold which were previously stretched between two electrodes. $Ag^{+}$-ions were bound to the DNA backbone via electrostatic interaction. Hydroquinone (HQ) was added as a reducing agent, resulting in continuous, grainy silver wires (12 μm long and 100 nm wide, see Figure 7a). Measurements of the I-V curves showed interesting results, revealing a non- linear, and history-dependent characteristic. It demonstrated that nanoscale functional electric devices based on DNA are possible. Different growth conditions and metal types need to be further developed to achieve wires with metallic conductivity for future applications and still remained a challenge up to now.

The conductive properties of DNA based wires have been improved by using palladium for the metallization as reported by Richter *et al*. [93]. λ-DNA was again used as a scaffold (placed between macroscopic Au electrodes), and reduction of a palladium chloride solution allowed the groth of metallic Pd wires using the reducing agent dimethylamine borane (DMAB) (Figure 7b). Conductivity measurements were performed and linear I-V curve was achieved. The nanowires exhibited ohmic transport behavior at room temperature. Their research again confirmed that DNA is highly applicable for metallic nanowires production.

Metallization of DNA with other metals has also been reported, for examples, DNA with platinum (Pt) [94], [95] and linear nickel (Ni) wires on λ-DNA [96] were fabricated, DNA nanowires made of zinc oxide (ZnO) [97] were achieved, gold (Au) nanowires and networks [98], [99], as well as copper (Cu) nanowires [100] were also realized. For future application in nanoelectronics, metallic nanowires with smaller diameters under continuous and homogenous growth are needed. It requires better confinement over the growing seeds to construct thinner conductive wires.

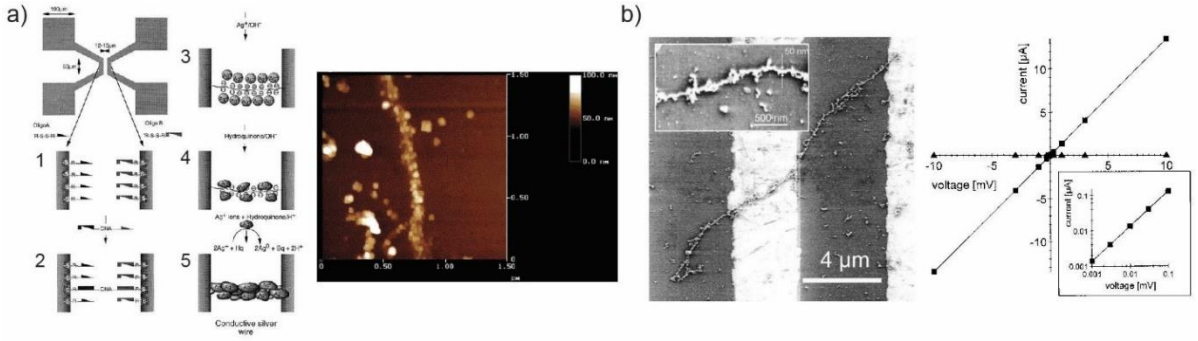


**Figure 7** Metallization of dsDNA. (a) Construction of a silver wire between two gold electrodes [92]. Left: scheme; right: atomic force microscopy image. (b) Fabrication of palladium nanowire based on DNA strand [93]. Left: scanning electron microscope image; right: two-terminal current-voltage curves.

## Site Specific Metallization of DNA

Keren and co-workers [101] developed sequence-specific molecular lithography on dsDNA molecules substrate. During the metallization, a nucleoprotein filament found in recombination (ssDNA polymerized with RecA) was used as a site-specific mask. The filament could invade into dsDNA with complementary sequence, which created a section of three DNA strands, leading to a pattern over the whole DNA strands. Subsequently, during the gold metallization, RecA would prohibit the Ag ions binding and thus the formation of Ag seeds on the dsDNA. The subsequent electroless gold deposition resulted in gold-wires with an insulating gap (see **Figure 8**). In this molecular lithography, DNA molecules were used as the masks as in the conventional microelectronics, and the RecA protein behaved as the resist. This molecular lithography can be a useful tool for further metal construct building.

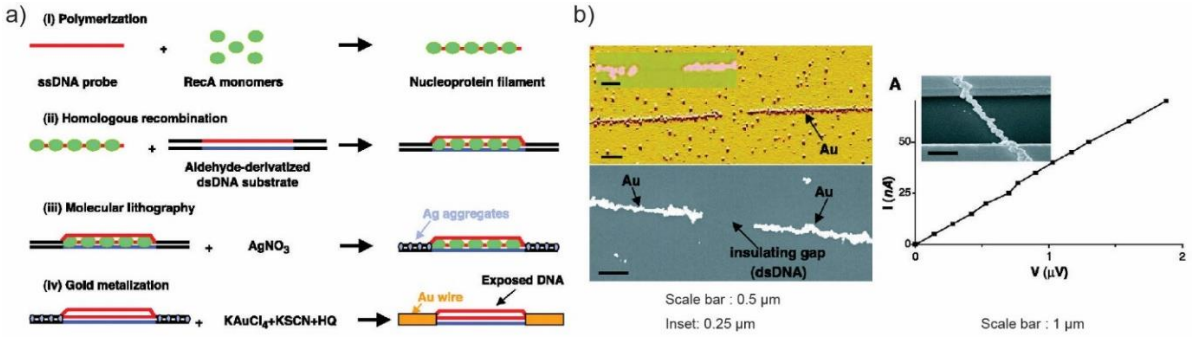


**Figure 8** Site specific metallization of DNA [101]. (a) Schematics of Ssquence-specific molecular lithography on a single DNA molecule. (b) AFM, SEM images and current-voltage (I-V) curve of DNA-templated gold nanowire.

## Metallization of DNA tiles

With advances in DNA nanotechnology fabrication, metallization of complex DNA nanostructures such as DNA tiles has also been achieved. In 2003, H. Yan *et al.* metallized a tile-based nanoribbon structure into highly conductive and equally wide silver nanowires (43 ± 2 nm width and ~5 μm length) [102]. The nanoribbons were comprised of 4 × 4 DNA tiles and displayed periodic square cavities. The nanoribbons were first mixed with Ag ion solution for the seeding procedure, followed by the commercial metallization kit. Current-voltage characterization revealed the ohmic behavior of the silver nanowires (**Figure 9**a). The 4 × 4 DNA tiles could be further programmed with different sticky ends to form various arrays for molecular device fabrication. The same "two-step metallization" process was optimized to fabricate continuous silver nanowires from DNA nanotubes assembled from thiol-modified triple-crossover tiles (**Figure 9**b) [103]. They demonstrated that the nanowire formation was programmable and easily reproducible, and resulted in nanowires with high conductivity (corresponded to a bulk resistivity of $2.4 \times 10^{-6}$ ohm·m) for potential usage in electrical devices.

In 2006, C. Mao *et al.* designed a single oligonucleotide for self-assemble micrometer-long nanotubes [104]. The nanotubes (30-70 nm widths and 60 μm length) were assembled from double-crossover (DX) tile-like structures via hybridization of complementary overhangs. Nanotubes were first immobilized on mica substrate followed by incubating in $Pd^{2+}$ -solution and subsequent chemical reduction. Pd metallic nanowires were formed with 30-80 nm width and up to 30 μm length (**Figure 9**c).

Via DNA tiles based metallization, long linear nanowires can be built and less randomized nucleation and high conductivity were observed. Furthermore, interconnections can be introduced at specific positions as needed for larger electronic circuits. However, the metallic nanowires were still not perfectly constrained and controlled. To fabricate metallic structures with complex ge-

ometries and patterns in a controlled manner, DNA origami was further used as metallization template.

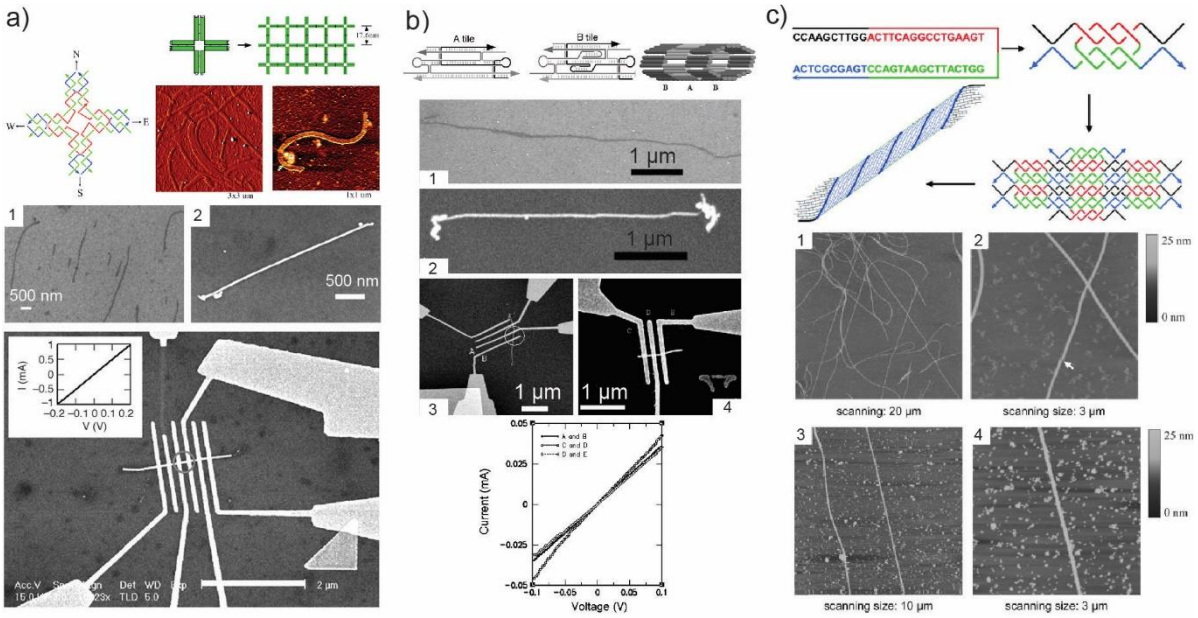


**Figure 9** Metallization of DNA tiles based nanostructures. (a) Silver nanoribbons using 4 × 4 DNA tile [102]. Top: scheme and AFM images of the nanoribbons (left: amplitude-mode; right: height mode); bottom: SEM image of nonmetallized nanoribbons, silver nanoribbon and the conductivity measurement (inset: current-voltage curve). (b) Silver nanowires from DNA nanotubes [103]. Top: scheme; bottom: SEM images of nanotube before metallization and fully metallized silver nanotube. (c) Palladium (Pd) nanowires derived from DNA nanotubes originated from one DNA single strand [104]. Top: scheme; bottom: AFM images of DNA nanotubes and palladium (Pd) nanowires.

## 1.2.2 DNA Origami Metallization

Transformation of DNA origami structures with different shapes into inorganic nanomaterials has originated different DNA origami metallization protocols.

### Electroless Deposition through Metal ion/Metal complex

The group of Adam T. Woolley has made several attempts in the metallization of DNA origami structures. In 2011, metallization of branched Y-shaped DNA origami has been reported [105]. They used 4-aminomethyltrioxsalen to crosslink DNA origami and it can further react with glutaraldehyde to introduce aldehyde groups, which allow the high-density Ag seeds deposition onto the DNA. Electroless Au plating solution was applied and selectively a gold layer with the shape of the underlying DNA nanostructures has been achieved (Figure 10a). They showed that magnesium ions ($Mg^{2+}$) are crucial for maintaining the DNA structure, and it facilitates the adhesion of the negatively charged DNA nanostructures to the negatively charged mica substrate. Several other experimental conditions were optimized to achieve relatively high selectivity of metal dep-

osition for small DNA origami templates. However, the metal deposition presented in this study was not highly continuous and often grainy shapes were observed.

Subsequently, within the same group, a rapid DNA origami metallization compared to λ-DNA was reported and branched Au nanostructures (T-shape, 200-250 nm length and ~40 nm diameters) were achieved (Figure 10b) [106]. The updated metallization method consisted of three steps: Pd ions activation with DNA, reduction for forming seeds, and Au electroless plating of the seeded structures. Sufficient activation time (10-30 min) allowed a significant increase in the seeding density and at the same time avoided partial DNA removal from the substrate. Interestingly under identical seeding conditions, DNA origami showed a higher nucleation site density than λ-DNA. This improved procedures showed potential for using DNA molecules as templates in bottom-up nanoelectronics circuit fabrication.

Different geometries such as circuit-like DNA origami have also been employed for two types of metal deposition (Au and Cu), showing increased seed uniformity and density due to multiple Pd seeding steps [107]. Gold and copper circuit-like structures were achieved with electrical resistance measurements showing ohmic behavior (Figure 10c).

Liedl *et al.* demonstrated a universal strategy for arbitrarily shaped metal nanoparticles generation [108]. It was achieved by a two-step metallization procedure. DNA origami structures with defined shapes and dimensions were mixed with positively charged 1.4 nm gold clusters. By a subsequent electroless gold ions deposition from solution, metallized objects with defined shape and dimensions were obtained retaining their original shapes (Figure 10d). The continuously metallized structures showed a narrow size distribution yet still rather bumpy and grainy morphologies with grains of different diameters. However, this site-directed metallization constituted a general and easy route to more complex structures with high yield and fidelity.

DNA origami structures with a wide variety of shapes and sizes can be programmed and constructed, leading to the fabrication of complex metal materials with different shapes with unprecedented optical and electronic behavior. The possibility to selectively address DNA origami structures with metallic nanoparticles and chemical groups will enable the controlled metallization with nanometer precision.

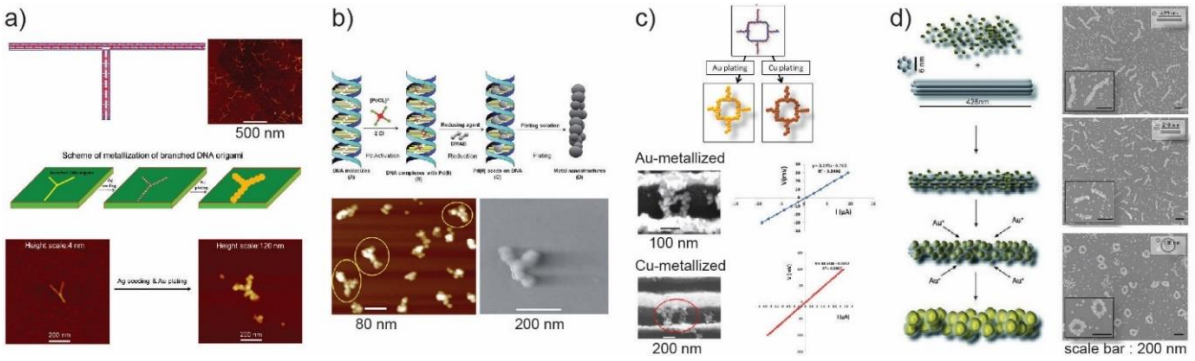


**Figure 10** Electroless deposition directly on DNA origami. (a) Y-shaped branched origami metallization [105]. Top: design and illustration of the metallization process; bottom: AFM images of branched origami before and after metallization on mica surface. (b) T-shaped branched origami metallization [106]. Top: schematic of Pd seeding and plating on double-stranded DNA; bottom: AFM and SEM images of metallized T-shape DNA origami on mica surface. (c) Circuit-liked origami metallization [107]. Top: fabrication scheme; bottom: SEM images and current-voltage curves for Au- and Cu-metallized circuit-like structure. (d) The two-step process of DNA origami metallization with defined shape [108]. Left: metallization strategy; right: SEM images of metallized six-helix bundles, 14-helix bundles, and nanodonuts on the silicon wafer.

## Metallic Nanoparticles Conjugated with DNA

Chemically-synthesized metallic nanoparticles (NPs) have gained broad interest [109], [110]. These NPs are prepared by the reduction of metal salts typically in a seeded growth reaction scheme. The particle shapes can be altered by using suitable surfactants or reagents. Various metallic NPs with different shapes (spherical particles [111], [112], rods [113], triangles [114], and hexagons [115]) have been produced. The assembled particles are normally stabilized using protective agents or additional layers (electrostatic, *e.g.* ionic double layer or steric stabilization *e.g.* organic molecules).

Typically, functionalization of metallic NPs is achieved by chemical modifications of the NPs' surface *e.g*. by replacing the protective or capping layer with ligand molecules. The ligand molecules are usually attached to the metallic surface via a linker or terminal group. One of the most important linker group for modifying AuNPs is thiol. This concept was introduced by Brust *et al.* for the fabrication of gold nanoparticles (AuNPs) with a thiol-modified surface [116]. In 1996, Mirkin [117] and Alivisatos [118] at the same time reported the DNA functionalization of AuNPs. Mirkin *et al.* successfully assembled colloidal gold nanoparticles into macroscopic aggregates using complementary DNA oligonucleotide sequences **(Figure 11**a) [117]. Based on Watson-Crick base-pairing interaction, Alivisatos organized complex nanocrystals into spatially defined structures (**Figure 11**b) [118]. Citrate stabilized AuNPs underwent a ligand exchange with thiolated ssDNA, due to the large energy difference between the gold-oxygen (ΔH (Au-O) = 222 kJ/mol) and the gold-sulfur (ΔH (Au-S) = 418 kJ/mol) bonds. Thiolated ssDNA replaced the cit-

rate ligand on AuNPs and arranged the AuNPs into defined patterns. In addition, short DNA linkers have been successfully used to create assemblies of nanoparticles with tunable interparticle distances (**Figure 11**c) [119].

AuNPs are broadly used in the field of DNA nanotechnology for a wide range of with their robust synthesis and versatile modification possibilities, specially AuNPs functionalized with thiolated oligonucleotides via sequence-complementarity applications [120]–[124]. The programmable base sequence of the oligonucleotides enables a highly specific attachment of AuNPs together with different materials into one system, while the interparticle distances can be finely controlled. The usage of DNA origami as a template for the precise arrangement of AuNPs is particularly interesting in metallic nanostructure fabrication.

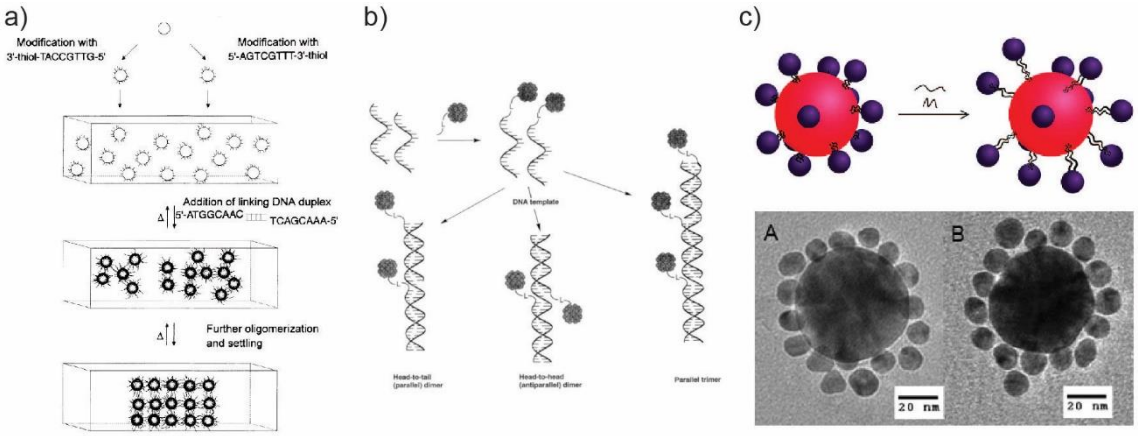


**Figure 11** ssDNA conjugated AuNPs. (a) Scheme of DNA-based colloidal nanoparticle assembly strategy [117]. (b) Nanocrystal assembly based on Watson-Crick base-pairing interactions, nanocrystal (shaded) attached to oligonucleotide [118]. (c) Core (50 nm) - satellite (13 nm) expansion through modulation of a double-helical DNA linker [119].

### Electroless Deposition Using Metallic Nanoparticle Seeds

Site-specific attachment of preformed metallic nanoparticles as nucleation seeds, instead of the non-specific seeds generation all over the DNA structure, has been employed as a promising strategy for electroless metallization of DNA nanostructures. M. Pilo-Pais *et al.* demonstrated the site-specific silver metallization of AuNPs on DNA origami structures with programmable locations for AuNPs binding [125]. 5 nm AuNPs were functionalized with complementary single-stranded DNA which can hybridize to staple extensions at the desired binding sites on the DNA origami structures. The DNA structures were deposited on mica and $SiO_2$ substrates. Silver deposition was conducted and different metal patterns were achieved, including a four-corners structure, two parallel bars, ring and H-shapes (**Figure 12**a). All the designed patterns retained the intended features after the metallization. The growth speed of the AuNPs was also investigated on

four-corner bound AuNP origami structures. With the increasing metallization time, the nanoparticles' size increased linearly. Although the results showed still granular nanostructures, it represented a first step for site-specific metal deposition on DNA nanostructures.

A similar procedure to site-specific metallization through AuNP attachment for gold deposition was applied to achieve conductive gold nanowires [126]. T-shaped origami structures were fabricated with a high density of staple overhangs on the select regions (11 nm spacing) to hybridize AuNPs. A commercial kit together with the previously mentioned plating protocol was applied to the tightly-packed seeds (4.1 nm gap size), resulting in continuous nanowires (**Figure 12**b). However, the nanowires achieved showed variable widths (20-30 nm) and resistance values were up to 2.4 kΩ by the electrical conductivity measurements. Another method to fabricate gold nanowires based on DNA origami nanotubes and AuNPs has been reported by Teschome *et al*. [127]. 6-helix bundles origami was assembled with attachment strands protruding for AuNPs and followed by Au plating with various incubation times. 5 nm AuNPs have grown to ~30 nm diameter, resulting in continuous gold nanowires. Electron beam lithography was used to fabricate electrode contacts for selected nanowires and electrical conductance was measured at various temperatures (room temperature to 4.2 K). At room temperature, the gold nanowires showed ohmic behavior whereas at lower temperatures, different charge transport mechanisms (tunneling and thermally assisted charge transport, discussed in 1.3.1) start to dominate (**Figure 12**c). The selective contact fabrications using electron beam lithography presented in this study demonstrated nanoelectronics devices assembly combined with top-down and bottom-up methods is possible.

Instead of one single metal type, two different metals can also be assembled on one DNA origami nanostructure with selective deposition in sequential steps [128]. At first, AuNPs were attached to the left side of the origami, then followed by sequential Au plating using a commercial kit. Octadecane thiol was used as a 'chemical mask' to cover the gold structure. In a second step, ionic Pd seeding and Cu plating were applied on the uncovered side of the origami. Using this strategy, gold and copper were directed to the designed locations on the origami and a heterogeneous Cu–Au junction was formed, as confirmed with compositional and morphological investigation (**Figure 12**d). This work showed the ability to deposit different metal components to designed sections on DNA templates, which can be further adapted for hybrid DNA-templated nanosystems fabrication.

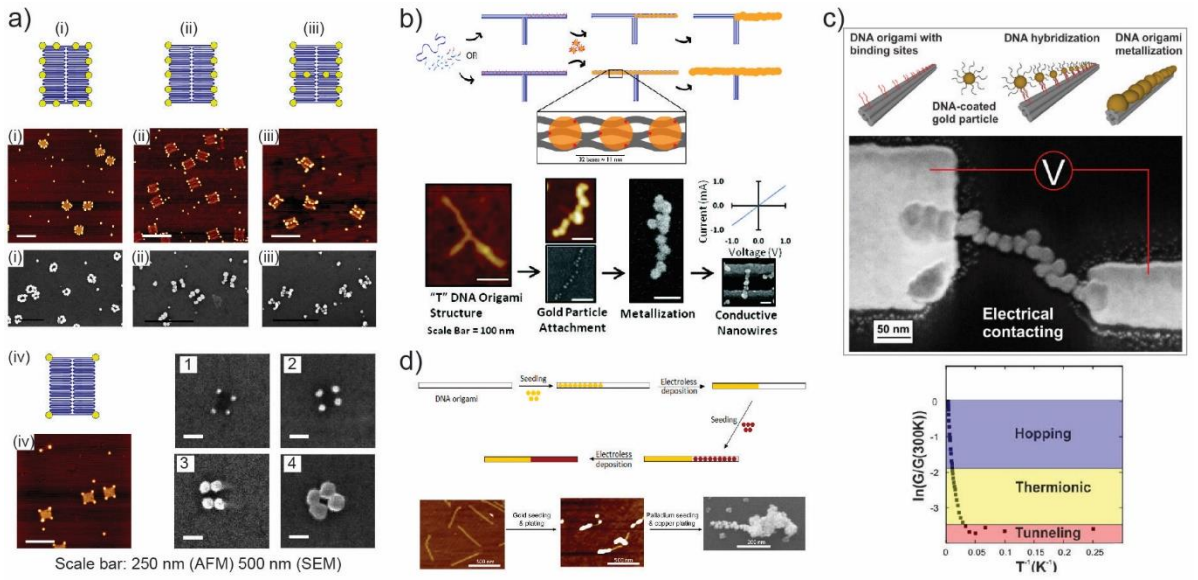


**Figure 12** Electroless deposition through metallic particles (NPs) on DNA origami. (a) Site-specific DNA origami metallization [125]. Top: Schemes of the designed structures; bottom: AFM and SEM images of different metallic nanostructures, (i) a pair of parallel bars, (ii) ring, (iii) H shape and (iv) a four-corner with increasing metallization. (b) Conductive gold nanowire fabricated in T-shaped origami [126]. Top: scheme of site-specific seeding; bottom: AFM, SEM and I-V curve of the nanostructures. (c) Gold nanowire contact by electron beam lithography [127]. Top: schematic; bottom: different charge transport mechanism under different temperature ranges. (d) Heterogeneous metal junction on a DNA origami template [128]. Top: scheme demonstrated the two metal metallization in a sequential step; bottom: AFM image of bar origami, Au plating on the Au-seeded section and SEM image of Au-Cu junction.

## Electroless Deposition Employing Metallic Nanorods (NRs)

Nanorods are rod-shaped nanoparticles with length ranges from 10-100 nm at different aspect ratios (length over width). The potential usage of metallic nanorods as seed particles to improve the quality of metal deposition on DNA origami templates has been previously investigated. In 2017, Uprety *et al.* [129] demonstrated a metallization process based on gold nanorods on DNA origami template and achieved conductive gold nanowires with diameters as small as 13 nm (**Figure 13**a). Gold nanorods were attached to the origami followed by an electroless gold deposition to fill the gaps between individual nanorods to create continuous nanowires. Interestingly, gold growth in the distal direction exhibited a faster growth rate than in the lateral direction, which better controlled the final metallized width of the structure. The resistivity values of nanowires (13-29 nm diameter) were as low as $8.9 \times 10^{-7}$ Ω·m.

Continued with the similar strategy, different shapes of quasi-continuous metallic structures were fabricated, including rectangular, square, and T shapes [130]. The main difference to the previous study is the site-specific deposition of DNA functionalized gold nanorods on DNA origami templates. Anisotropic growth of nanorods was observed such that it filled up the gaps between

neighboring nanorods (11-13 nm), and resulting in continuous structures with diameters as small as 10 nm (**Figure 13**b). The metallization process was highly selective with low background deposition compared to the previous study.

Following the anisotropic growth of the site-specific Au nanorods, several self-assembled Au nanowire arrangements on DNA origami tiles were fabricated [131]. Additional attachment sites were used to provide more effective linking of DNA-functionalized Au nanorods to the desired sites, resulting in 6-fold increased yields of the final desired nanostructures. A four-point measurement technique was applied to each individual Au nanowire for conductivity measurement (~130 nm long, 10 nm diameter, and 40 nm spacing between measurement points). This technique utilized electron beam induced metal deposition to form probe electrodes. The C-shaped Au nanowires exhibited resistivity as low as $4.24 \times 10^{-5}$ Ω·m (**Figure 13**c).

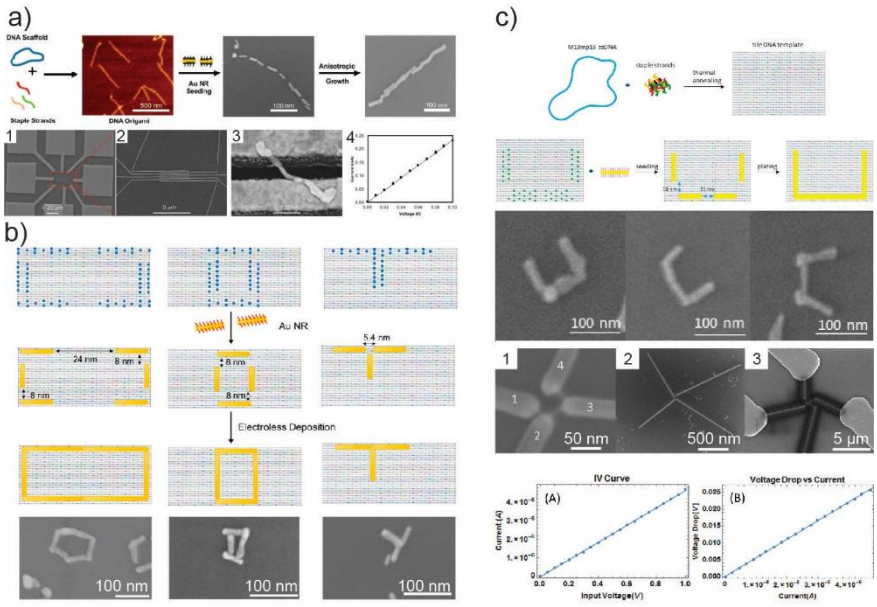


**Figure 13** Electroless deposition through metallic nanorods (NRs) on DNA origami. (a) Conductive gold nanowires with nanorods as seeds [129]. Top: schematic demonstration of the wire fabrication; bottom: SEM images and current-voltage curve of the nanowire. (b) The directional continuous growth of site-specific gold nanorods on DNA origami template [130]. Top: design scheme; bottom: SEM images of metal structures after electroless plating (rectangular, square, and T-shaped). (c) Gold nanowires with four-point probe electrical measurements [131]. Top: schematic diagram; bottom: SEM images of C-shaped nanowire with four distinct platinum contacts and I-V curve from one C-shaped nanowire.

### 1.2.3 DNA Origami Mold Templated Metal Deposition

All the above mentioned strategies for depositing inorganic material on DNA templates rely on introducing nucleation centers (metal ions/metal complexes, metal nanoparticles/ nanorods). Since the growth occurs on top of the DNA origami, the electroless deposition of inorganic mate-

rial is inhomogeneous. To achieve a tight control of the metal deposition, a new strategy has recently been developed in which DNA origami structures were used as nanoscopic molds. This allowed to confine the metal growth and to imprint the shape of the DNA mold onto the resulting nanoparticle (see Figure 14a).

Sun *et al.* designed barrel-like structures, where DNA handles for capturing ssDNA-AuNPs through hybridization were placed in the middle of the cavity [132]. Once the conjugated AuNPs were captured, DNA origami lids were added to create in a caged chamber. The electroless deposition has been initiated, using $AgNO_3$ as a metal precursor, and ascorbic acid as a reducing agent. The AuNP seeded growth was confined within the mold cavity and replicated their 3D shapes. Different silver and gold metal nanostructures were fabricated with tunable dimensions and more than one cavity segment, as shown in Figure 14b. The metallized silver nanostructures reached a yield of ~40 % with 3 nm resolution. Gold nanoparticles growth was more difficult since the gold precursor buffer contained ethylenediaminetetraacetic acid (EDTA) which might cause a chelating effect. Removing EDTA improved the growth rate but lead to a significantly lower yield of 6 %. The electromagnetic behavior and the plasmonic spectra of these metal nanostructures further proved the feasibility of this technique.

At the same time, Helmi *et al.* in our group fabricated cuboid gold nanostructures in a similar fashion [133]. Tube-like DNA origamis with quadratic cross-sections were constructed and AuNP seeds were captured in the middle through complementary DNA strands. The AuNP decorated origamis were first premixed with a reducing agent (hydroxylamine) in the salt-containing buffer, and $HAuCl_4$ was gradually added to initiate gold growth. The growth is a self-terminate process since only a certain amount of gold ions was added for the reaction. The particle can fully adapt the shape of the mold structure and the growth can be controlled with stepwise addition of gold precursor (see Figure 14b). Furthermore, dimer structures with side-by-side and head-to-tail geometries were also investigated for the larger composition of mold-casted nanoparticles. However, enlarged particles with sizes exceeding the diameter of the mold cavity were observed, which indicated that DNA origami double layer is not sufficient enough to completely constrain the gold growth. Furthermore, the outgrown cuboid particles tended to aggregate at the open sites. To address these challenges, multiple layers of DNA origami can be designed to have better control over the gold growth as well as extra lid structure to create caged space to avoid aggregation.

Nevertheless, the resolution of mold-templated metal deposition is limited by the stiffness of the DNA origami, since often outgrowth from the mold can be observed. Despite that, this method enables metal nanostructure fabrication with homogenous composition. Moreover, each individual staple from the 3D origami can be designed to attach different functional elements and metallic

nanoparticles in one system, which can be used for further nanoelectronics and plasmonics applications.

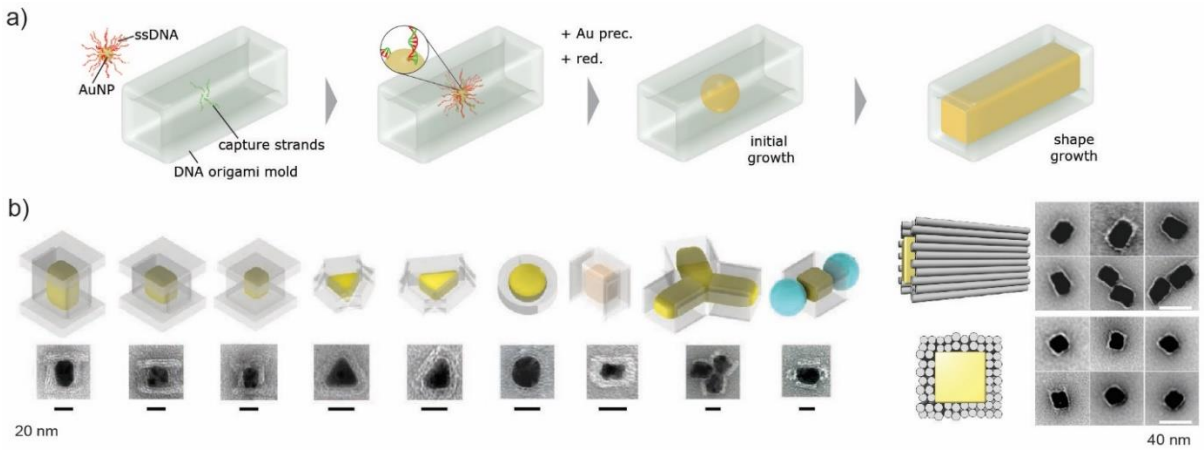


**Figure 14** DNA origami mold templated metal deposition. (a) Scheme of the metal nanostructure casting using DNA nanostructure molds [133]. (b) Experimental results of the metal particles from Sun *at el.* [132] and Helmi *at el.* [133].

### 1.2.4 Metallization Summary

DNA-templated metal nanowires obtained with different methods are summarized in **Table 1** (adopted from reference [134]). The widespread resistance values ranging from a few Ω up to several GΩ indicated the quality of the metal layers played an important role in their electronic performance. The low conductivities compared to bulk metal materials mainly came from the electron scattering at the metal grain boundaries which could be avoided with development of metal growth conditions. The seed-based metallization schemes suffered from granular structures and discontinuities, while the controlled growth using DNA origami mold served as a highly promising approach to form arbitrarily-shaped metallic nanoparticles with homogeneous and continuous growth. The possible applicability of this self-organization scheme based on the DNA origami mold enabled the formation of complex structures for nanoelectronic applications. Strategies to incorporate different metals or active electronic building blocks into this mold system will be investigated as the next step towards self-assembled nanoelectronics.

**Table 1** Summary of resistance values and construction properties of DNA templated metal nanowires [134].

| DNA Building | Contact Method | NP | DNA Structure | Resistances | Metal Source/Metallization | Contact Metal | Substrate | Temp. | Height | Length | Width |
|---|---|---|---|---|---|---|---|---|---|---|---|
| DNA Metallization | EBL | Pd | λ-DNA | 800 GΩ | $Pd(Ac)_2$/Chemical Reduction | Cr/Au, Au, & Pd | Mica | 120–300 K | NA | 1–2 μm | 7 nm |
| | | Pd | λ-DNA | 743 Ω and <5 kΩ | $Pd(CH_3COO)_2$/Chemical Reduction | Au | $SiO_2$ | RT | NA | 6.5 μm | 50 nm |
| | | Ag | λ-DNA/ds-DNA | 30 MΩ, 7 MΩ | $AgNO_3$/Chemical Reduction | Au | Glass | RT | NA | 1.2 μm | 100 nm |
| | | Ag | TX-DNA | 1.42–1.21 kΩ | $AgNO_3$/Chemical Reduction | Cr/Au | Si | RT | (1.8 ± 2) nm | 16.5 nm | 320 and 430 nm |
| | | Ag | λ-DNA/ds-DNA | 597 Ω–895 Ω (30 & 500 Ω at 77 K) | $AgNO_3$/Chemical Reduction | Cr/Au | Si | 77–300 K | NA | 7 μm | 15–35 nm |
| | | Ag | DNA nanoribbons | 200 Ω | Protein Array | NA | NA | RT | 25 nm | 5 μm | 43 nm |
| | | Ag | ds-DNA | 500 Ω | $AgNO_3$/Chemical Reduction | NA | PDMS transferred to Si | RT | NA | 60 nm | NA |
| | | Ag | TX-DNA | 2.80 kΩ, 2.35 kΩ, 2.82 kΩ | $AgNO_3$/Chemical Reduction | Cr/Au | Si | RT | 35 nm | 5 μm | 40 nm |
| | | Au | ds-DNA | 103 kΩ | Pyridine modified gold nanoparticles/Gold-enhancer solution | Au | $SiO_2$ | RT | 20 nm | 1.25 μm | 40 nm |
| | | Au | λ-DNA/ds-DNA | 44.3 Ω (60 nm) and 7.7 Ω (80 nm) | E-beam Evaporation Gold | Ti/Au | $Si/SiO_2$ | RT | NA | 800 nm | 60 nm and 80 nm |
| | | Au | λ-DNA | 30–140 Ω | Thermal Evaporation Gold | Au | Pillars on Si or $CF_4$ substrate | RT | 5–350 nm in diameter | >5 mm | 5–350 nm in diameter |
| | | Au | ss-DNA | <20 Ω | Gold nanoparticles/Gold-enhancer solution | Au | Polycarbonate memranes | RT | NA | 10 ± 1.4 μm | NA |
| | AFM | Cu | ds-DNA | 107 MΩ | $Cu(NO_3)_2$/Chemical Reduction | NA | TMS modified $Si/SiO_2$ | RT | 11–20 nm | 1.5 μm | 20 nm |
| | | Pd | λ-DNA/ds-DNA | 0.4–0.8 GΩ with DMAB and 2–8 GΩ with $NaBH_4$ | $K_2PdCl_4$/Chemical Reduction | Au | $SiO_2$ | RT | NA | NA | 5–45 nm diameter |
| | | Au | DNA | 2.4 kΩ | THP-AuNPs/Chemical reduction | Au | Si | RT | NA | 2 μm | 30–40 nm |
| | | Au | DNA | 3 kΩ to 1 GΩ | Au seeds/Chemical reduction | Au | Mica | RT | (10 ± 2, 13 ± 2 and 27 ± 3) nm | 10–700 nm | 25 nm |
| | AFM | Rh | λ-DNA | 400–650 MΩ and 250–350 MΩ | $RhCl_3(H_2O)$/Chemical and electrochemical reduction | NA | $SiO_2$ | RT | 3–31 nm in diameter | NA | 3–31 nm in diameter |
| | Dielectro-phoresis | Au | TX-DNA tiles | Coulomb Blockade | DNA modified gold nanoparticles | Au | $Si/SiO_2$ | 4.2–300 K | 1.5 nm | 50–60 nm | NA |
| | Micro-channel | Ag | ds-DNA | 9 Ω | Chemical modification of gold nanoparticles | Au | PDMS | RT | NA | 1 μm | 40 nm |
| Metalized DNA Origami | EBL | Au | T-shaped | 1.5–2.3 kΩ | DNA modified gold nanoparticles/Chemical Reduction | Au | $SiO_2$ | RT | NA | 120 nm to 240 nm | 33 nm |
| | | Pd | CC | 1–5 kΩ for Au/40 kΩ–1 MΩ Cu | $(NH_4)_2PdCl_4$/Chemical Reduction and Gold-enhancer solution | Au | Si | RT | NA | 150 nm | 35/30 for Au, 40 nm for Cu |
| | | Au | Nanotube | 116 MΩ–2.8 GΩ | DNA modified gold nanoparticles/Gold-enhancer solution | Ti/Au | $SiO_2$ | 4.2 K–300 K | 40 nm | 400 nm | 30nm |
| | | Au rod | Rectangular | 435 Ω–36.9 MΩ | DNA modified gold rod/Chemical Reduction | Cr/Au | $SiO_2$ | RT | NA | < 410 nm | 13–29 nm |
| | | Au | Nanopillars | Highly resistive | DNA modified gold nanoparticles/Chemical Reduction | Pt | $SiO_2$ | RT | NA | NA | NA |
| | | Au | Mold | 90 Ω–30 GΩ | DNA modified gold nanoparticles/Chemical Reduction | Ti/Au | $SiO_2$ | 4.2 K–300 K | 20–30 nm in diameter | NA | 20–30 nm in diameter |
| | EBID | Au rod | plus, cross, c-shaped | 5.58 kΩ–76 MΩ | DNA modified gold rod/Chemical Reduction | Cr/Au-Pd | Si | RT | NA | 130 nm | 12 nm |

NP: nanoparticle; EBL: electron beam lithography; NA: not available; RT: room temperature; TX: triple-crossover; PDMS: polydimethylsiloxane; AFM: atomic force microscopy; TMS: tetramethylsilane; THP: negatively charged tris(hydroxymethyl)- phosphine-capped; CC: circular circuit; EBID: electron beam induced deposition.

## 1.3 Characterization of Metal Nanostructures

For nanoelectronic devices, proper interconnections between the individual electronic components are essential. Different charge transport mechanisms occur even for metallic structures due to the unique geometries as well as a significantly smaller contact surface [135]. Several charge transport mechanisms will be discussed in this chapter, together with techniques for electrical characterization and structural inspection of DNA-based metallic nanostructures. Furthermore, microscopy techniques to visualize nanometer-sized structures will be explained.

### 1.3.1 Charge Transport Mechanisms

During metallization, each of the nucleation centres grows to a certain particle size and eventually touches its neighbors to form a continuous nanostructure. These granular nanoparticle assemblies (mostly from gold) exhibit electronic properties that depend on the architecture and composition of the materials [136], [137]. Extensive studies have shown that the electronic properties of granular nanoparticle arrays can be categorized into three distinct regimes: an insulating regime, a bulk regime (metallic), and a transition regime [138]. Charge transport mechanisms in these regimes, however, have not yet been fully understood [138]. Several phenomena such as tunneling, thermionic emission, hopping, and single-electron charging are particularly important.

**Large and highly coupled nanoparticles** In this case the metal nanostructures typically exhibit metallic behavior and the charge transport can be described by classical theory. The conductivity of metals can be expressed as [138],

$$\sigma = \frac{nq^2\tau}{m} \tag{2}$$

where $n$ is the electron density, $q$ is the electron charge, $\tau$ is the mean free time between collisions, and $m$ is the electron mass. Since the mean free time $\tau$ is determined by both elastic and inelastic electronic scattering, the total mean free time can be written as [138],

$$\frac{1}{\tau} = \frac{1}{\tau_{elastic}} + \frac{1}{\tau_{inelastic}} \tag{3}$$

In granular metal nanoparticle assemblies, impurities and defects cause elastic electron scattering whereas electron-electron or electron-phonon interactions cause inelastic scattering. Unlike elastic scattering, inelastic scattering has a strong temperature dependence. At higher temperature, inelastic scattering becomes dominate and affects the conductivity of metals. The conductivity of metals can, therefore, be rewritten as

$$\sigma^{-1} = {\sigma_0}^{-1} + \sigma(T)^{-1} \tag{4}$$

**Small and weakly coupled nanoparticles** The electronic properties are between the metallically conducting and the insulating regime, also known as metal-insulator transition (MIT) regime. Here quantum effects such as quantum confinement and tunneling become important. Depending on the different conditions, such as applied electric field, temperature and the arrangement of the nanoparticles, various competing mechanisms dominate the transport behavior. In particular, tunneling, thermionic emission, hopping conduction, single-electron transport, which will be explained in the following.

### Tunneling

One important charge transport mechanism in absence of metallic interparticle contacts is tunneling. Tunneling enables the charge between weakly coupled sites, where the wave functions are mainly localized on each site. In direct tunneling, an electron has a finite probability of crossing a potential barrier, even in case the electron's energy is smaller than the barrier. The tunneling probability $P$ is exponentially dependent on the thickness of the tunneling barrier $L$ and is given by [138], [139]

$$P \approx \exp\left(-\frac{2\pi\sqrt{2m\Phi}}{h}L\right) \tag{5}$$

where $h$ is Planck's constant, $m$ is the mass of the electron and $\Phi$ is the barrier height.

The tunnelling behaviour qualitatively differs dependent on the applied voltage:

**At low bias voltage** the tunnel current density $J$ can be expressed using the Wentzel–Kramers–Brillouin (WKB) approximation, as [140],

$$J \sim V\exp\left(-\frac{4\pi L}{h}\sqrt{2m\Phi}\right) \tag{6}$$

where $V$ is the applied voltage. Thus, the current density has a linear voltage dependence. Although direct tunneling is an important charge transport mechanism in granular metal nanoparticle assemblies, it is difficult to extract the necessary parameters such as the barrier height from the tunneling current [138].

**At high bias voltage** the shape of the barrier potential changes from an idealized rectangular to a triangular form allowing more electrons to penetrate the lower barrier. This field-dependent tunneling is known as Fowler-Nordheim (F-N) tunneling. The current density at high bias voltage can be calculated according to [138]

$$J \sim V^2 exp\left(-\frac{8\pi L}{3qhV}\sqrt{2m}\Phi^{\frac{3}{2}}\right) \tag{7}$$

For F-N tunneling, $In\left(\frac{J}{V^2}\right)$ should have a linear dependence on $1/V$, allowing the barrier height to be extracted from the I-V curve. In addition, such an F-N plot is normally used to specify the transition voltage, where the transport mechanism jumped from direct tunneling to F-N tunneling.

**Thermionic Emission**

In addition to tunneling, which is temperature independent, also thermally activated processes have to be considered for the charge transport. Due to thermal excitation, electrons acquire sufficient energy to overcome the potential barrier instead of tunneling at a certain temperature. It is called thermionic or Schottky emission. The current density, in this case, is given as [140],

$$J \sim T^2 \exp\left(-\frac{\Phi - q\sqrt{qV/4\pi\varepsilon L}}{kT}\right) \tag{8}$$

where $T$ is the temperature, $\varepsilon$ is the dielectric constant, and $k$ is the Boltzmann's constant. In the thermionic emission regime, $In\left(\frac{J}{T^2}\right)$ has then a linear dependence over $1/V$.

**Hopping Conduction**

Due to thermal fluctuations, thermally activated electrons can escape from one isolated state to another. This charge transport mechanism is called hopping. If the hopping distance is comparable with the distance between neighboring sites, nearest-neighbor hopping (NNH) [138] dominates the transport mechanism, and the conductance shows activated Arrhenius behavior. The temperature dependence of the current density can be expressed as,

$$J \sim V \exp\left(-\frac{E_a}{kT}\right) \tag{9}$$

where $E_a$ is the activation energy. In this thermally activated transport regime, $In\ (G)$ has linear dependency over $\frac{1}{T}$, and the activation energy $E_a$ can be extracted from the slope.

These abovementioned transport mechanisms with their characteristic current-, temperature-, and voltage-dependencies are summarized in **Table 2** [141].

**Table 2** Summary of several charge transport (conduction) mechanisms [141].

| Conduction Mechanism | Characteristic Behavior | Temperature Dependence | Voltage Dependence |
|---|---|---|---|
| Direct Tunneling (low bias regime) | $J \sim V \exp\left(-\frac{4\pi L}{h}\sqrt{2m\Phi}\right)$ | none | $J \sim V$ |
| Fowler-Nordheim Tunneling | $J \sim V^2 exp\left(-\frac{8\pi L}{3qhV}\sqrt{2m}\Phi^{\frac{3}{2}}\right)$ | none | $In\left(\frac{J}{V^2}\right) \sim \frac{1}{V}$ |
| Thermionic Emission | $J \sim T^2 \exp\left(-\frac{\Phi - q\sqrt{qV/4\pi\varepsilon L}}{kT}\right)$ | $In\left(\frac{J}{T^2}\right) \sim \frac{1}{V}$ | $In(J) \sim V^{1/2}$ |
| Hopping Conduction | $J \sim V \exp\left(-\frac{E_a}{kT}\right)$ | $In\left(\frac{J}{V}\right) \sim \frac{1}{T}$ | $J \sim V$ |

### Single-Electron Transport

Given the small size of metal nanoparticles used in many nanotechnology applications, the charging of a nanoparticle by a single electron can also strongly influence the transport properties. When an electron tunnels, it charges or discharges the metal nanoparticles. At absolute zero, a sufficiently large external bias is required to enable the current flow. Below a certain voltage threshold, current and conductance of the system are zero. This is known as "Coulomb blockade" (CB) [138]. When the temperature increases, electrons are able to overcome the Coulomb blockade thermally, and current and conductance increase. Multi-electron charging and discharging can give stepwise increases in the current at certain higher voltages at which these charging processes become energetically favorable. These steps in current are known as "Coulomb staircase" (**Figure 15**). Coulomb blockade and often Coulomb staircases have been observed in many studies of nanostructures [142], [143].

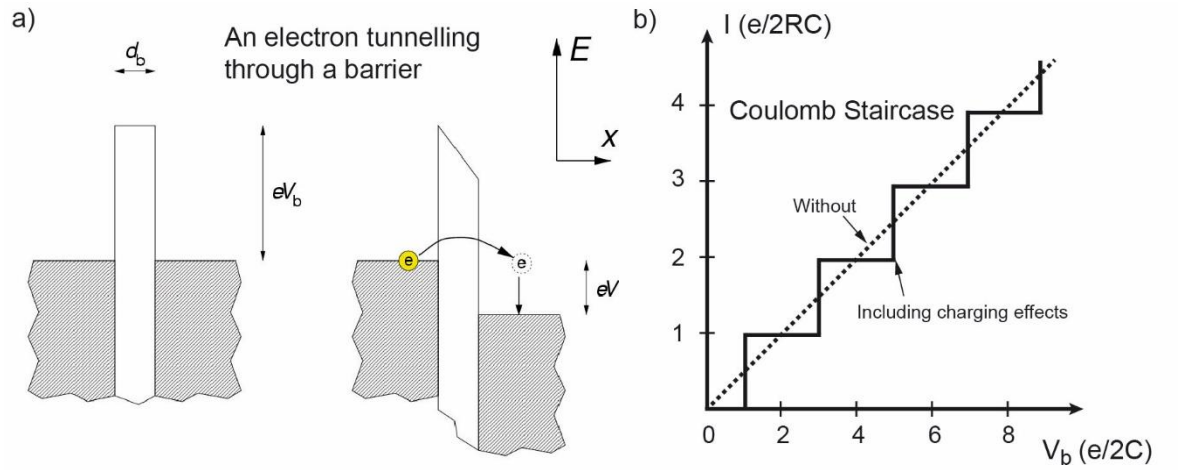


**Figure 15** Schematic presentation of single-eletron charging. (a) Schematic representation (similar to band diagram) of an electron tunneling through a barrier [144]. (b) I-V curve diagram of Coulomb Staircase when including charging effect of each single elctron [145].

### 1.3.2 Measuring Charge Transport in Nanostructures

To characterize the different charge transport mechanisms, current-voltage curves are normally measured using two- or four-point measurements. Electron-beam lithography (EBL) is used to fabricate electrode contacts on nanometer-sized metal nanostructure for the characterization of their electrical properties [127], [146]–[148]. EBL uses a highly focused beam of electrons (spot size of 1-2 nm and even below) to irradiate an electron-sensitive film (resist) and create a desired nano-pattern with sub-10 nm resolution [149]. The pattern can be programmed and directly written by the electron beams without a physical mask compared to other lithography technics [150].

The first step in EBL is developing the patterns. A resist layer is a special molecular film deposited on the substrate by spin coating and it is sensitive to electrons. With electron irradiation, its molecular structure and solubility can be changed. They can be positive resist (*e.g.* polymethyl methacrylate (PMMA) of different molecular weight), where the already existing molecular bonds can be cleaved and led to smaller molecules, thus the positive resist becomes soluble in the appropriate developer. They can also be negative resist (for instance, hydrogen silsesquioxane (HSQ)), where new bonds between the resist molecules are formed, leading to larger molecules, thus the exposed areas of the negative resist become insoluble (**Figure 16**a-c).

After exposing and developing, the resist layer can be used as a mask for transferring the pattern onto the substrate. There are two main types of process for pattern transfer. The first is an additive process, where a metal layer is deposited all over the sample, followed by 'lift-off' to remove the remaining resist layer (**Figure 16**d). The second is a subtractive process that etches material away where resist layer is not covered (**Figure 16**e) [151]. Metal nanostructures that are random-

ly distributed on a wafer surface can be contacted with high precision using EBL and it provides an important step towards the integration of self-assembled metal nanostructures to devices and systems.

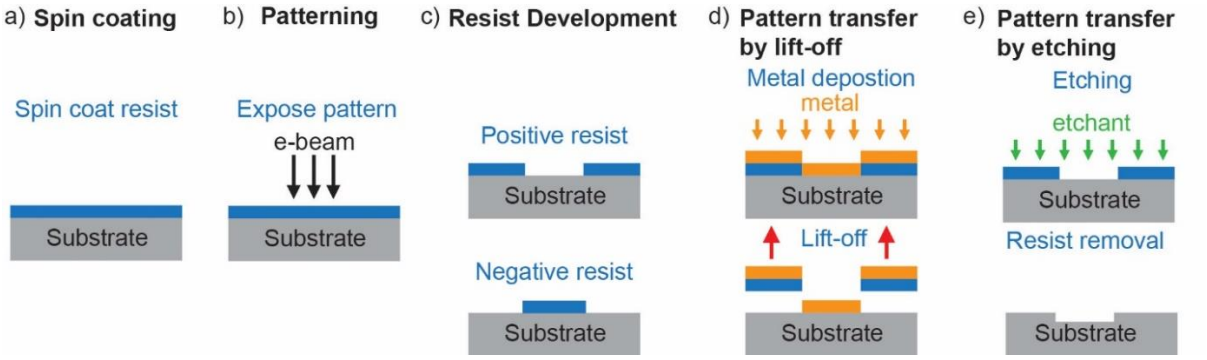


**Figure 16** Schematic illustration of the EBL development. (a) The resist layer (positive or negative) is spin-coated to the substrate. (b)The resist layer is subsequently exposed to an electron beam to achieve a defined pattern. (c) Two different resist layer types show different patterns after resist development. For the positive resist, the exposed areas are washed off; for the negative resist, the exposed areas remained after the development. (d) Pattern transfer by lift-off: metal layer is deposited onto the whole area, subsequently the remaining resist layer together with the metal layer on top of it are lifted from the substrate, leaving the final pattern. (e) Pattern transfer by etching: either wet chemical etching or dry etching is applied to the whole area, subsequently the resist layer is removed, leaving the final pattern.

### 1.3.3 Scanning Electron Microscopy in Transmission Mode (tSEM)

Transmission electron microscopy (TEM) or scanning electron microscopy in transmission mode (tSEM) are commonly used to characterize DNA origami objects and metal nanoparticles with high spatial resolution [152]. According to Louis de Broglie laws, the electron wavelength $\lambda_e$ is dependent on its kinetic energy $E$:

$$\lambda_e \approx \frac{h}{\sqrt{2m_0E(1+\frac{E}{2m_0c^2})}} \tag{10}$$

Where $h$ is the Planck constant, $m_0$ is the electron rest mass, and $c$ is the speed of light. With an operation voltage $V$ between 80 kV to 100 kV ($E = eV$), a wavelength of about 4 pm can be achieved, which is sufficient to resolve DNA origami objects with feature sizes down to 2 nm (corresponding to the DNA helix diameter). DNA origami samples are usually negatively stained with heavy ions (*e.g.* uranyl acetate) to increase the contrast during the imaging. The staining increases the atomic number of the specimen, leading to the proportional increase of the scattering efficiency by the electron beam. STEM or tSEM operates in a similar fashion as a scanning electron microscope (SEM). With a wide range of possible scattering signals from the sample,

two commonly used modes are bright-field (BF) and high angle annular dark-field (HAADF) [153].

# 2. Objective

As detailed in the sections before, advances in DNA nanotechnology allowed to fabricate rigid DNA templates that could be utilized to synthesize metal nanostructures. However, for a convenient and successful usage of DNA-templated metal nanostructures in nanoelectronic applications, a number of key challenges still need to be addressed: (1) The traditional external metal deposition on DNA templates lacks size-control during particles growth and is prone to inhomogeneities. Thus, a better metal deposition concept is required. (2) The new metal deposition scheme should allow for homogeneous and continuous metal growth to avoid formation of isolated grains with pure electric contacts. (3) The new concept should allow the assembly of complex higher-order metal nanostructures with controlled multi-dimensional geometry and high addressability. (4) The new concept should allow the integration of multiple materials with distinct electronic properties to allow the construction of nanoscale structures with electronic functionality.

This thesis addresses these challenges using a metal deposition concept based on DNA molds which can be programmably assembled into complex high-order structures. Furthermore, techniques for the selective placement of different materials on the DNA templates including metallic and semi-conducting nanomaterials are examined, as a crucial requirement for the fabrication of DNA-based electronic devices. The primary objective of this study is to develop a universal modular platform using the DNA mold-based fabrication of metal nanoparticles. Particularly, metal nanostructures with programmable and controlled size, morphology and conductivity should be fabricated. Furthermore, the integration of different materials into this scheme should be established.

The results achieved in this thesis are presented in the following order:

**Chapter 3** describes a modular platform that allows linear DNA origami molds to be assembled into controlled higher-order superstructures at a high yield. This allows to fabricate linear gold nanostructures with defined length as well defined metal patterns by site-specific metal deposition. **Chapter 4** describes the synthesis of conductive linear gold nanowires. For this the wires were contacted by E-beam lithography and characterized in temperature-depended conductivity measurements. **Chapter 5** reveals the integration of semiconducting rods into the mold platform. Simultaneous arrangement of the nanorods and gold nanoparticles with defined spatial orientation and interparticle distances allowed to create metal-semiconductor heterostructures. In **Chapter 6**, the obtained results are summarized and perspectives for the future application of the established mold-based nanostructures fabrication scheme are discussed. Additionally, within the Ph.D. time frame, extra work were conducted for the development of the modular platform and they were

summarized in unpublished manuscripts (**P4** and **P5**, refer to **List of Publications**). Manuscript **P4** demonstrates that the modular mold platform allows to integrate different mold shapes, such us molds with different diameter and even a junction. This allows the programmable fabrication of metal nanoparticles with complex geometries that contain branches as well as constrictions. In manuscript **P5**, a procedure for the highly anisotropic metal growth inside DNA molds is described. This allows to grow metal nanowires from a minimal number of seeds numbers that promise improved conductivity.

# 3. Fabrication of Metal Nanostructures with Programmable Length and Patterns using a Modular DNA Platform

## 3.1 Introduction

The field of DNA nanotechnology has seen a tremendous boost in the fabrication of complex and atomically-precise nanostructures in a fully programmable manner. However, for many technological purposes, it would be highly desirable if one could synthesize inorganic nanostructures in a similar fashion. This idea has inspired the usage of DNA nanostructures as templates for guiding and thus structuring metal deposition. Recently, a promising approach was developed in our research group and the group of Peng Yin in which DNA origami structures are used as molds in which metal is "casted". This approach allows the formation of homogenous and continuous metal structures.

This chapter significantly improved the capabilities of the mold-based approach, which was so far limited to single DNA origami structures or to origami superstructures with undefined length. Particularly, specific docking interfaces between mold monomers were created, such that linear mold superstructures of programmable length could be formed. By carefully improving the affinity and specificity between the monomer structures, mold superstructures containing up to nine monomers at superior yields could also be formed. In a subsequent metallization step, linear metal structures could be fabricated whose length was fully predetermined by the interfaces of the used molds. Importantly, each monomer remained specifically addressable in the mold superstructures. This allowed to create specific patterns of nucleation seeds for the gold deposition and thus specific metallization pattern within the molds.

This chapter furthermore expands the mold-based modular platform for metallic nanostructures and demonstrates the flexibility of interfaces for higher-order structure fabrication. The established platform provides a crucial basis for the assembly of even more complex nanostructures, *e.g.* by implementing branch points and extra elements like presented in manuscript **P4**, or different materials including semiconducting nanorods as presented in **Chapter 5**. Furthermore, it facilities the creation of well-defined and large interparticle distances which is further utilized in manuscript **P5**. Therefore, this modular platform opens a new route to self-assemble functional nanodevices.

## 3.2 Associated Publication P1

**Fabrication of Metal Nanostructures with Programmable Length and Patterns Using a Modular DNA Platform**

by

Jingjing Ye, Seham Helmi, Josephine Teske, Ralf Seidel

published in

Nano Letter 2019, 19, 4, 2707-2714

NANO LETTERS
Cite This: Nano Lett. 2019, 19, 2707−2714
Letter
pubs.acs.org/NanoLett

# Fabrication of Metal Nanostructures with Programmable Length and Patterns Using a Modular DNA Platform

Jingjing Ye,[†,‡] Seham Helmi,[‡,§] Josephine Teske,[‡] and Ralf Seidel*[,†,‡]

[†]Cluster of Excellence Center for Advancing Electronics Dresden (cfaed), TU Dresden, 01062 Dresden, Germany
[‡]Molecular Biophysics group, Peter Debye Institute for Soft Matter Physics, Universität Leipzig, 04103 Leipzig, Germany

Supporting Information

**ABSTRACT:** Recently introduced DNA nanomolds allow the shape-controlled growth of metallic nanoparticles. Here we demonstrate that this approach can be used to fabricate longer linear metal nanostructures of controlled lengths and patterns. To this end, we establish a set of different interfaces that enable mold interactions with high affinity and specificity. These interfaces enable and control the modular assembly of mold monomers into larger mold superstructure with programmable dimension in which each mold monomer remains uniquely addressable. Preloading the molds with nanoparticle seeds subsequently allows the growth of linear gold nanostructures whose lengths are controlled by the DNA structure. Exploiting the addressability of individual mold monomers furthermore allows achievement of site-specific metallization, that is, to create defined metal patterns. We think that the introduced approach provides a useful basis to fabricate nanomaterials with complex shapes and material composition in a fully programmable and modular fashion.

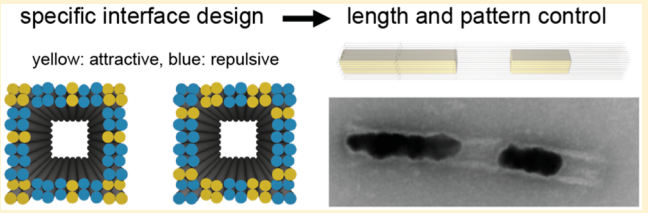


**KEYWORDS:** *Metal nanoparticles, seeded growth, DNA metallization, DNA nanostructures, DNA origami, DNA template*



Over the past decade, DNA nanotechnology[1,2] has become a rapidly emerging field for building complex two- and three-dimensional nano- and submicrometer structures. In comparison to top-down lithography techniques, it offers inexpensive and highly parallel fabrication with large diversity, complexity, and almost atomic resolution.[3,4] A number of pioneering techniques[5−9] have been developed that allow a computer-aided design and a simple fabrication of DNA nanostructures of many different shapes. Among others, the scaffold-based DNA origami technique[9,10] is markedly attractive due to its high yield in assembling large molecular weight structures. Because of available unique binding sequences, functional elements, such as proteins,[11] fluorescent[12] and Raman-active[13,14] molecules, semiconducting polymers,[15] and metallic nanoparticles,[16,17] can be bound and arranged at DNA origami structures. This allowed the synthesis of novel nanomaterials for applications in nanoelectronics,[18] nanophotonics,[19,20] nanomedicine,[21,22] and biology.[23]

While the DNA-aided placement of separated functional groups and nanomaterials has become routine, an analogous DNA templated deposition of continuous layers particularly of inorganic materials remains challenging. By employing metal seeds as nucleation sites for electroless deposition, elongated metal assemblies from silver,[24] platinum,[25] palladium,[26] copper,[27] and cobalt[28] have been fabricated on linear DNA molecules[29−31] as well as rigid DNA nanostructures.[32−36] To overcome problems with discontinueties[31] or inhomogeneitis[26] of the deposited metal films in earlier works, recent promising approaches employed elongated nanoparticles to reduce the number of seeds[37] as well as DNA-based molds.[18,38,39] For the latter, a DNA origami-based mold that harbors an internal nucleation seed confines and guides the metal growth enabling the fabrication of metallic cuboids of different dimensions and shapes as well as micrometer-sized metallic wires.

So far, the material deposition has been concentrating on single DNA (origami) nanostructures[33,37−41] as well as structures of uncontrolled length.[18] However, to enable applications in nanoelectronics and nano-optics, DNA-templated nanostructures have to become larger as well as more complex regarding their shapes and material composition. This mandates a programmable assembly of individual DNA templates into well-defined and fully addressable higher-order structures. Such structures, including DNA filaments,[42] twisted DNA structures,[43,44] three-dimensional (3D) polyhedrons[45] as well as 2D[46,47] and 3D[48] crystalline DNA origami structures could be fabricated using sticky DNA ends between the individual DNA units. Considerably higher efficiencies were obtained using the base-stacking interactions between blunt DNA ends allowing the assembly of linear[49] as well as complex three-dimensional origami structures up to gigadalton molecular masses.[50] In these approaches, higher-order structures were typically assembled using periodic patterns of interfaces such that the final size of the assembly was either random or controlled by self-limiting hierarchical oligomerization. Higher-order assembly that allows free addressability of

**Received:** February 19, 2019
**Revised:** March 15, 2019
**Published:** March 19, 2019




DOI: 10.1021/acs.nanolett.9b00740
Nano Lett. 2019, 19, 2707−2714

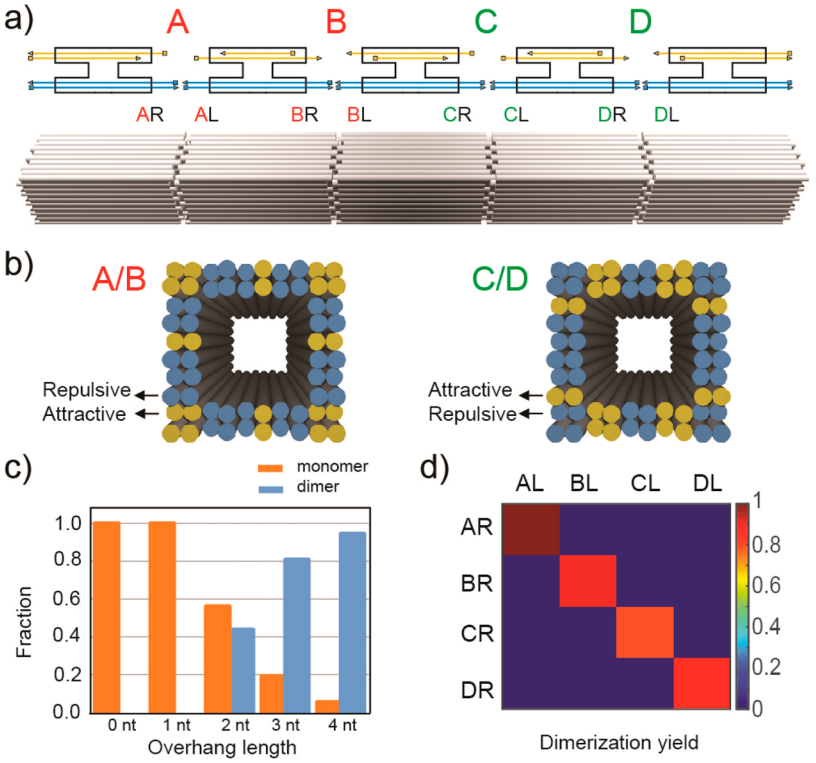


**Figure 1.** Construction scheme for DNA mold superstructures based on four orthogonal interfaces. (a) Design scheme of a hollow pentameric mold superstructure based on the specific interfaces A, B, C and D (see three-dimensional model at the bottom). DNA ends at the interfaces are either attractive (yellow in cartoons at the top) or repulsive (blue in cartoons at the top). The 5′-staple and 3′ staple ends are marked with squares and triangles, respectively. Attractive ends contain either protruding 5′-staple ends or correspondingly recessed 3′-staple ends (A and C interfaces) or protruding 3′-staple ends and recessed 5′-staple ends (B and D interfaces). Repulsive ends contain overhangs on both staple ends. A mold R-end of a particular interface shall only interact with a mold L-end of the same interface such that monomers with different interface combinations at their L- and R-ends can be assembled into a defined higher-order structure. (b) View onto the end of mold monomers with A or B (left) and C or D (right) interface. Attractive helix ends are colored in yellow, repulsive helix ends in blue. Both patterns have 24 attractive and 40 repulsive helix ends. (c) Fraction of mold monomers and dimers in solution as a function of the overhang length at attractive helix ends. Dimer formation was tested between two molds carrying either an L-end or an R-end of the C-interface (Figure S1). (d) Dimerization yield for all possible combinations of interface L-ends with interface R-ends (Figure S2). The overhang lengths were 3 nt throughout.

each single monomer has been more difficult.[51] Recently up to 16 individual monomers could be assembled albeit reaching yields of 2−4%.[52]

Here, we report a fully addressable metal deposition on controlled higher-order DNA origami assemblies comprising up to nine individual mold elements. The fabrication scheme is based on a modular platform. Individual elements share the same (mold-) core but are guided to their position in the final linear superstructure via specific interfaces. Key for this method was the assembly of the origami superstructures at a high yield. To this end, affinity and specificity of four different mold−mold interfaces were carefully tuned and optimized. Subsequent metal deposition inside the seed-preloaded DNA templates allowed us to obtain linear metal structures with controllable lengths. To demonstrate the addressability and site-selectivity of the origami superstructure, particular origami elements were either equipped or not equipped with metallization seeds. This allowed us to obtain programmable metal patterns within the mold-based system. Overall, the presented method provides a promising route to assemble much more complex inorganic nanostructures with potential applications in nanoelectronics and plasmonics.

To design four orthogonal high-yield interfaces for origami docking, we base our approach on the previously established mold-based metallization scheme.[18] A mold monomer is a 40 nm long DNA tube with quadratic cross-section (see Figure 1a) consisting of 64 helices. It is asymmetric with respect to its ends, one further called the L-end (left end) and the other the R-end (right end). When an L-end of one mold binds to an R-end of another mold, all 64 DNA-helix ends of one mold can stack without a gap onto the helix ends of the other mold. We therefore used an L-to-R docking to design specific mold−mold interactions. We previously observed that specific L-to-R docking (i.e., without formation of unspecific L-to-L or R-to-R self-dimers) requires that only a subset of the helix ends interact attractively with each other with the remaining helix ends interacting repulsively.[18]

To assemble addressable mold superstructures, we designed four different orthogonal interfaces A, B, C and D, for mold docking each carrying 40 repulsive helix ends and 24 attractive helix ends (Figure 1b, Figures 10−13). The repulsive helix ends carried 6 nucleotide (nt) single-stranded DNA (ssDNA) overhangs. The A and B interfaces shared a particular pattern of attractive helices while the C and D interfaces shared a different pattern of attractive helices (Figure 1b). The two different patterns were fully orthogonal, that is, attractive helix ends of the A/B and the C/D patterns did not overlap when correctly docked. For the A and C interfaces, the staples at helix ends (further called end staples) were extended by few nt at their 5′-ends with respect to the terminal scaffold crossing



DOI: 10.1021/acs.nanolett.9b00740
Nano Lett. 2019, 19, 2707−2714

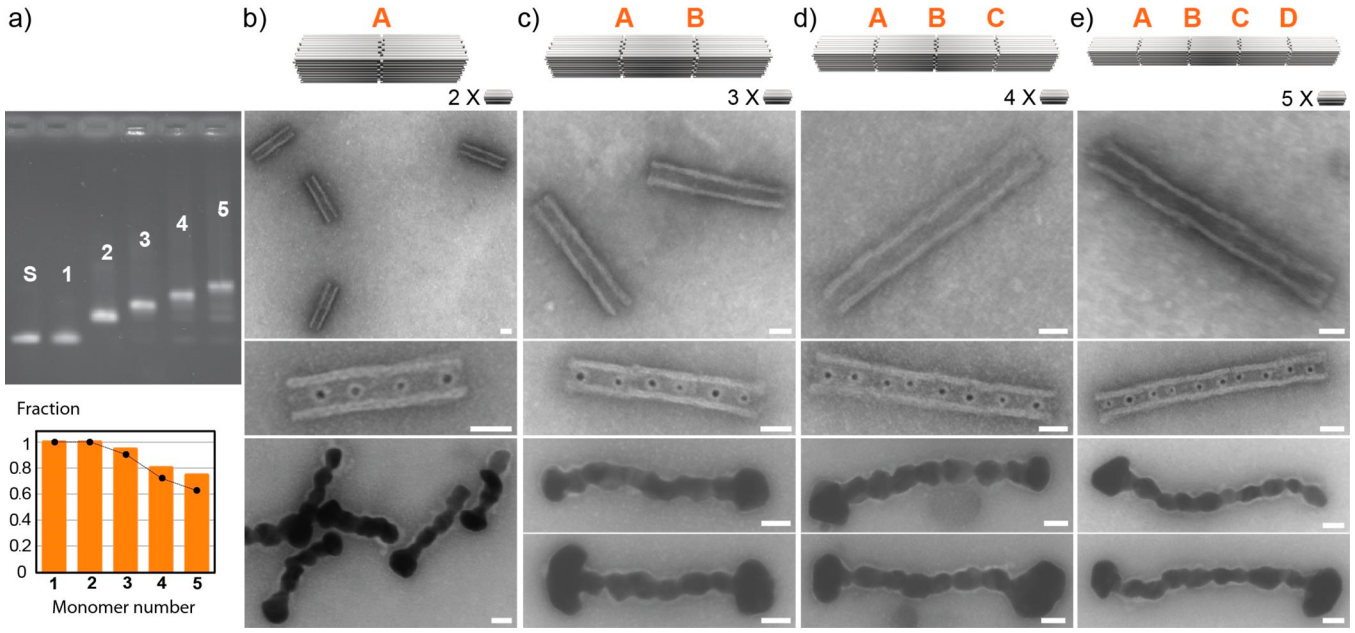


**Figure 2.** Formation of length-controlled mold and gold structures. (a) Formation of mold multimers analyzed by gel electrophoreses (top). Numbers at the lanes refer to the number of monomers in the desired superstructure. S indicates the scaffold lane. Quantification of the corresponding band intensities allowed to determine the yields of the desired multimer structures (orange bars in the bottom graph). The expected values calculated from the dimerization efficiencies of the individual interfaces are shown as black circles. (b–e) tSEM images of the formed mold superstructures in absence of seeds (top), loaded with seeds (center) and after metallization (bottom). The 3D schemes of the intended mold structures are shown above the tSEM images with letters indicating the employed interfaces. The scale bars correspond to 20 nm in all images.

and correspondingly recessed at their 3′- ends. The sequence of the overhangs was chosen to allow hybridization with the scaffold of the docked structure (Figures S10–13). In contrast, the end staples of the B and D interfaces were recessed at their 5′-ends and extended at their 3′-ends (Figure 1a). Each interface carried thus a unique combination of overhang type and pattern of attractive helices, such that a mold L-end of a given interface should only interact with a mold R-end of the same interface. The establishment of four different interfaces should then allow the controlled formation of a linear mold pentamer in which each monomer would be individually addressable.

We first tested which overhang length of an attractive helix end was sufficient to support efficient mold docking. To this end, we prepared different versions of two interacting molds with either a CL or a CR end in which the end staples had 0 nt, 1 nt, 2 nt, 3 nt, or 4 nt 5′-overhangs and correspondingly recessed 3′-ends. The other end of the molds was made fully repulsive, such that only dimers could form. After mixing the monomer versions, mold dimerization started to appear at an overhang length of 2 nt and saturated at overhang lengths of 3–4 nt (Figure 1c, Figure S1). Because of the rather high efficiency of mold dimerization and to avoid unspecific binding for longer overhangs based on the study of DNA origami dimerization,[51] we therefore chose 3 nt as overhang length for all further interface designs.

We next evaluated whether the designed interfaces were specific. Therefore, we assembled eight different mold monomers with one repulsive end and one L- or R-end of one of the interfaces. We then prepared pairwise mixtures of the different mold versions to test dimerization. Particularly we tested all 16 combinations to combine an L- and an R-ends. Any dimerization was absent for pairs of monomers from different interfaces, demonstrating the high specificity of the designed interfaces (Figure 1d, Figure S2). Only L and R monomers of the same interface interacted with dimerization yields of 100%, 90%, 79% and 86% for the A, B, C and D interfaces, respectively (Figure 1d, Figure S2). The dimerization yield of each interface is either higher or at the similar level with the reported 86% dimerization yield[51] within the optimized condition. Dimer formation was in this case tested near the stoichiometric optimum (see Figure S3).

For controlled assembly of a mold pentamer, we next tested whether the four interfaces can be employed for assembling mold superstructures with a controlled number of mold monomers, i.e., of a controlled length. For that, five monomers using the interface combinations depicted in Figure 1a were assembled and purified. We then formed mold dimer, trimer, tetramer, and pentamer structures by mixing a subset (the left-most molds depicted in Figure 1a) or all the five monomers at equal stoichiometry in a buffer supplemented with 350 mM NaCl. Gel electrophoreses confirmed the stepwise length increase of the resulting structures (Figure 2a), i.e., dimer formation upon mixing the (left-most) two monomers, trimer formation when mixing three monomers, and so forth. Quantification of the gel electrophoreses images allowed to estimate the formation yields of the designed structures, which agreed within error the expected yields calculated from the dimerization efficiencies for each interface (Figure 2a, bottom). The yield of formation of the pentamer reached 74%, which is higher than the typical yields obtained for origami tetramers being in the range of 40–50%.[52] Thus, the four orthogonal interfaces allow a highly efficient superstructure assembly. Scanning electron microscope in transmission mode (tSEM) imaging additionally confirmed the correct and efficient formation of the different multimers (Figure 2b-e).

To allow metal deposition inside the cavities of the mold superstructures, mold monomers containing two seed binding



DOI: 10.1021/acs.nanolett.9b00740
Nano Lett. 2019, 19, 2707–2714

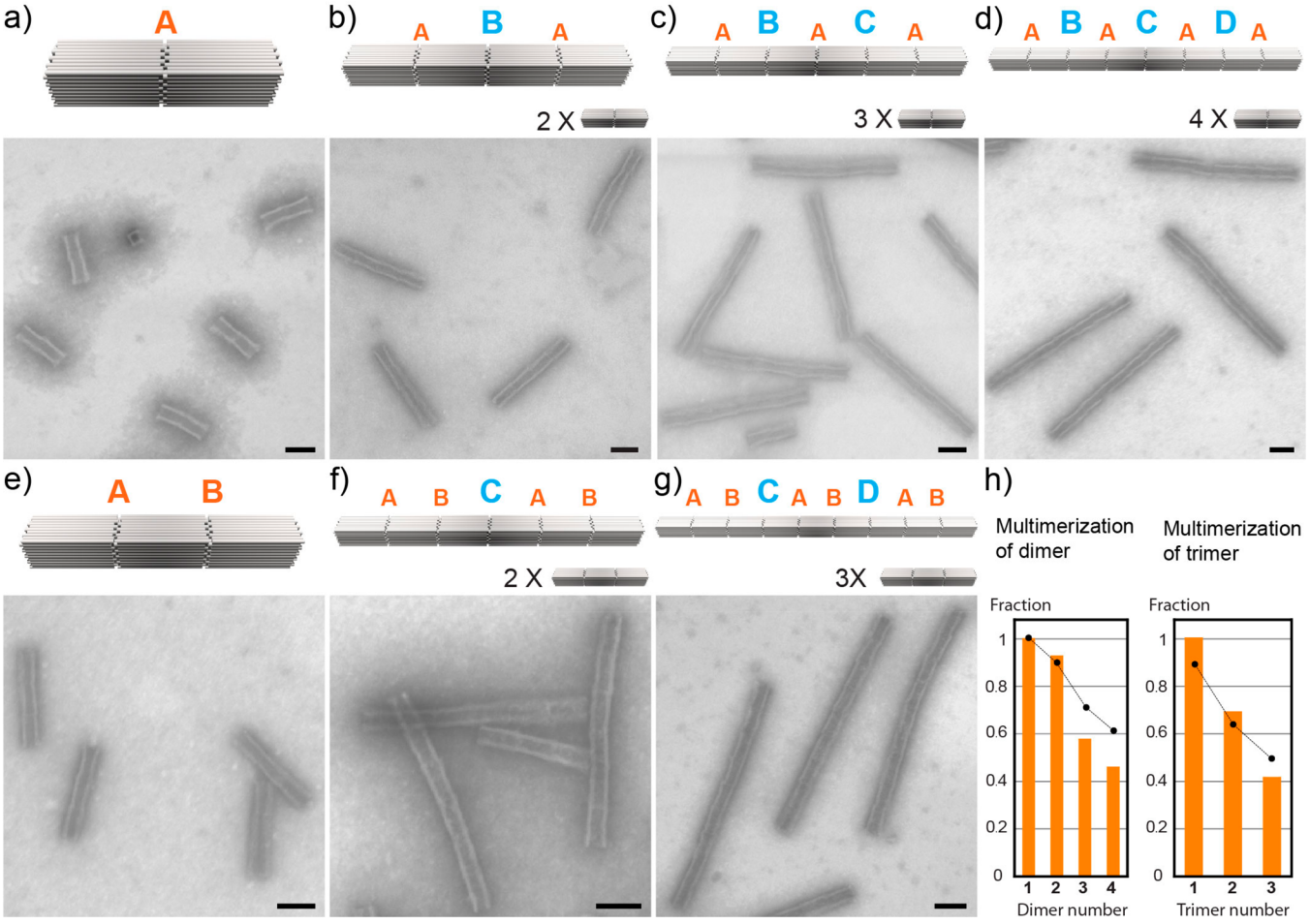


**Figure 3.** Formation of length-controlled mold octamers and nonamers using just four interfaces. The schemes in the subfigures indicate the employed interfaces for the particular structure. tSEM images reveal the correct structure formation. (a) Mold-dimer structure based on interface A that was used in a subsequent step as building block for dimer multimers. (b–d) Assembly of dimers, trimers, and tetramers of the dimer intermediate using the B, C, and D interfaces. (e) Mold-trimer structure based on interfaces A and B used to assembly trimer multimers. (f,g) Assembly of dimers and trimers of the trimer intermediate using the C and D interfaces. (h) Assembly yields (orange bars) of the intended structure for the different dimer multimers (left) and trimer multimers (right) (gel electrophoreses, see Figure S5). The expected values calculated from the dimerization efficiencies of the individual interfaces (Figure 1d) are shown as black circles. The scale bars in all tSEM images are 50 nm.

sites were preloaded with 5 nm AuNP seeds prior to the assembly of the mold superstructure. This allowed one to obtain mold structures with high seed decoration yields (95% ± 2%) (Figure 2b–e). For gold deposition on the seeds an optimized procedure compared to previous work[18] was employed to minimize the presence of occasional gaps between the individually growing gold grains. A gold plating solution containing 225 $\mu$M $H[AuCl_4]$ and 1350 $\mu$M $NH_2OH$ was supplemented with 50 mM NaCl (see Methods), which was found to improve the continuity of the deposited metal. tSEM imaging confirmed the successful metal deposition inside the mold structures. The continuity of the structures was dependent on the amount of gold precursor employed in the reaction. When using 2 nM of seeds and 450 $\mu$M of $H[AuCl_4]$ the gold grains remained largely individual (Figure S4a). Increasing the gold precursor concentration to 675 $\mu$M provided the formation of continuous rodlike gold structures whose length increased with the length of the mold superstructure (Figure 2b–e, bottom). Inside of the molds the width of the structures was confined by the DNA walls as demonstrated by the rather small variation in diameter. At the open mold ends, unconstrained metal growth partially occurred, such that dumbbell-like metal structures formed (Figure 2b–e, bottom). The unprotected metal at the mold ends led to some aggregation during deposition on the imaging grids (Figure S4c). The average lengths of the confined regions of the rod structures were 80 ± 5.4 nm for the mold dimer ($N$ = 70), 118.5 ± 10.7 nm for the trimer ($N$ = 60), 161 ± 15 nm for the tetramer ($N$ = 70), and 197.3 ± 14 nm for the pentamer ($N$ = 50). This agrees with the length of the designed mold superstructure considering a length of 40 nm per mold monomer. These results show that mold superstructures can be formed in a modular manner at high yield and used to fabricate gold-rod structures of controlled length.

To further explore the modular assembly concept for the assembly of octameric and nonameric mold superstructures, we tested the assembly of even larger mold superstructures of defined length. In a first step, we formed mold dimers or mold trimers from corresponding monomers using the high-affinity interfaces A or A and B, respectively (Figure 3a,e) at almost 100% yield. These structures were then used as building blocks in a second step without any further purification and assembled into superstructures using the remaining interfaces. This way, up to four mold dimers can in principle be



DOI: 10.1021/acs.nanolett.9b00740
Nano Lett. 2019, 19, 2707–2714

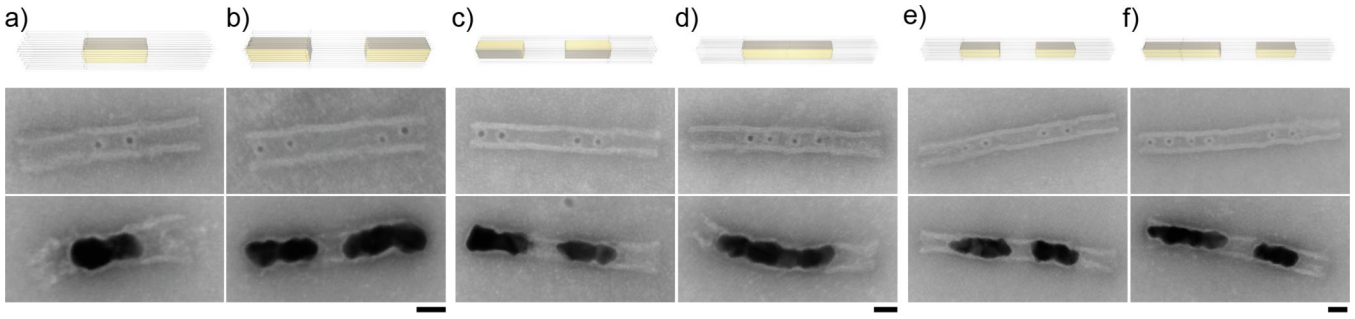


**Figure 4.** Site-specific metal deposition inside trimeric, tetrameric, and pentameric mold superstructures. Schemes on top of the subfigures depict the intended lengths and sites of selective metal deposition. tSEM images reveal the obtained patterns of seeds (middle) and of metal growth within each structure. (a,b) Mold trimers with either a central or two terminal gold blocks. (c,d) Mold tetramers with either two separate or two connected central gold blocks. (e,f) Mold pentamer with two disconnected or three asymmetrically placed gold blocks. The scale bars in all tSEM images are 20 nm. Figures S6–8 for overview.

specifically connected by the interfaces B, C, D (see scheme in Figure 3d) and up to three mold trimers can be specifically connected by the interfaces C and D (see scheme in Figure 3h). The high yield and the stability of the preformed dimers and trimers are crucial for the realization of such superstructure assemblies. To test this concept, we formed multimers of increasing length of mold dimers (Figure 3b–d) as well as of mold trimers (Figure 3f–h). tSEM microscopy demonstrated the successful assembly of these structures. Inspecting the assembly using gel electrophoreses (Figure S5) provided high yields for such large origami superstructures of 46% for the mold octamer and 41.3% for the mold nonamer, in agreement with the dimerization yields of the single interfaces (Figure 3h). Furthermore, it showed only products corresponding to multimers of dimers or trimers and no larger structures than designed confirming the high purity and stability of the intermediate building blocks. We note that a particular dimer or trimer of such a structure remains uniquely addressable due to its interfaces. Since each mold monomer within such a dimer or trimer assemblies is also uniquely addressable, a single mold will therefore even be uniquely addressable in the final superstructure.

So far, we judged the success of the modular superstructure assembly using the length of the formed structures. As stated earlier, each mold in the assembly should be uniquely addressable. To verify this more stringently, we tested whether we can achieve a site-specific metallization within the produced mold superstructures. To this end, we loaded only a subset of the molds of a superstructure with seeds prior to the final assembly. Each addressed, that is, preloaded, mold should according to the design contain two seeds, while each nonaddressed, that is, not preloaded, mold should not contain any seeds. By choosing different subsets of molds, we fabricated two trimer, two tetramer, and two pentamer versions according to the design scheme of Figure 2 that should exhibit different "digital" patterns of seed loading (Figure 4a–f). tSEM imaging verified the correct formation of seed patterns with high yield. Nonsymmetric arrangements of addressed mold elements further confirmed the full addressability of each individual mold (Figure 4f). The molds with the site-selectively loaded seeds were used in a subsequent metallization step to produce corresponding metallization patterns (Figure 4a–f, bottom row, Figures S6–8 for overview). This demonstrated that the modular mold superstructure assembly can indeed be applied to achieve site-specific/site-selective metallization of DNA templates. This did not require any alteration of the design of the DNA structures but just a simple selection of mold elements for preloading.

To provide a proof of principle that the assembled structures can be arranged into much larger, higher-order structures, while still maintaining their local pattern, we used the established four interfaces to generate linear periodic metal patterns with tunable periodicity. To achieve assembly of periodic chains with tunable metallization pattern, the ends of defined mold multimers were not made repulsive but rather an attractive interface was introduced to support binding of another multimer and thus chain formation. Using a total of two, three, and four interfaces should therefore allow one to achieve a periodicity of two, three, and four mold monomers (Figure 5a–c). Preloading of only a subset of the different

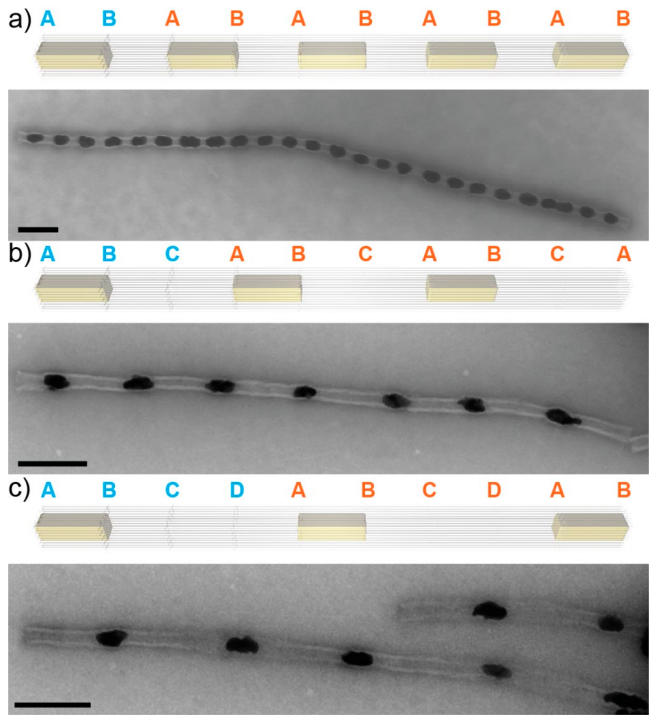


**Figure 5.** Schematics and tSEM images demonstrating the formation of pattern in the length frame of chain. (a) Alternating chain pattern with one empty and one gold block by using two interfaces. (b) Chain pattern with two empties and one gold block by using three interfaces. (c) Chain pattern with three empties and one gold blocks by using four interfaces. The scale bars in all tSEM images are 100 nm.



DOI: 10.1021/acs.nanolett.9b00740
*Nano Lett.* 2019, 19, 2707–2714

molds with seeds and subsequent metallization allows testing the designed periodicity in the final structure. Using a single seed-preloaded monomer we assembled mold chains with periodicities of two, three, and four. The length of the obtained chains was in the submicrometer to micrometer range. The chains reproduced the designed periodicity typically over their entire length (Figure 5a–c, Figure S9), demonstrating that potentially large and complex structures self-assemble through this modular approach.

In conclusion, we demonstrated the synthesis of metal structures with programmable lengths and patterns using a modular DNA-based mold platform. Key for this platform was the establishment of four orthogonal high-affinity interfaces between mold monomers that allowed the reliable fabrication of higher-order mold superstructures. By preparing different mold monomers with different terminal interfaces, the shape of the final structure could be programmed. Optimization of the interface affinities while preserving specificity allowed one to obtain yields of 74%, 46%, and 41.3% for pentameric, octameric, and nonameric mold assemblies, respectively. This is substantially higher than previously obtained for the assembly of addressable origami superstructures.[52] The modular concept uniquely allows an easy expansion to generate even larger and more complex higher-order DNA template structures and in turn inorganic nanostructures in a fully programmable manner. Larger structures can be obtained by designing further specific interfaces using different patterns of attractive and repulsive helices and fine-tuned affinities. More complex structures can be obtained by employing mold elements with other shapes and functionalities, such as mold elements with integrated walls, turns, junctions, different seeds for the deposition of other materials, and so forth. In this case, the combination of different structural or functional core modules with a common set of shared interfaces will allow the design and fabrication of nanostructures with very different shapes and functions based on practically the same building blocks. We envision that this is a promising concept to enable the self-assembly of switchable electronic or optical devices or even device networks.

**Materials and Methods.** *Preparation of Seed-Loaded DNA Mold Monomers.* The DNA origami molds with different interfaces on the L- and the R-side (Supporting Information, Figures S10–13) were designed for an arrangement of parallel helices on a square lattice[53] using the software-tool CaDNAno.[54] The origami structures were assembled in folding buffer (FB) containing 5 mM Tris-HCl, 1 mM EDTA and 11 mM $MgCl_2$ (pH 8.0) following a one-pot assembly reaction protocol.[18] Subsequently, the mold monomers were purified using precipitation with polyethylene glycol to remove excess staples.[55] AuNPs (5 nm, Sigma-Aldrich) were densely coated with 15 nt poly thymidine oligonucleotides carrying a 5′-thiol modification using the method of salt aging.[38,56,57] The particle concentration was estimated from the absorbance at 520 nm. DNA-functionalized gold nanoparticles were mixed with the purified DNA origami molds in the presence of 350 mM NaCl at a molar ratio of 6:1 for two seed binding sites. The mixture was slowly heated to 40 °C and afterward cooled down to 23 °C over a duration of 5 h to allow hybridization of the AuNPs with the complementary capture strands on the mold. The seed-loaded monomers were purified by precipitation with PEG to remove excess seeds.

*Formation of Linear Mold Superstructures.* Mold monomers of a particular superstructure carrying corresponding end staples to allow specific docking their L- or R-ends (see Supporting Information, Figures S10–13 for the design details of interfaces) were mixed at equal stoichiometry in FB supplemented with 350 mM NaCl and incubated overnight. For the assembly of mold octamer and nonamer structures, eight and nine monomers were assembled separately. At first different sets of mold dimers and trimers were preformed and these different sets of dimers or trimers were then mixed and incubated to yield the final structures. The prepared mold structures were analyzed with gel-electrophoresis (0.8% agarose gels, 0.5× TBE buffer, 11 mM $MgCl_2$, separation at 3.5 V/cm, 18 min staining with 0.2% EtBr), and tSEM imaging. For tSEM imaging, 5 $\mu$L of a 2–5 nM solution of origami structures were placed onto glow-discharged carbon-coated TEM grids for 5 min. The sample was subsequently stained using a filtered 2% solution of uranyl formate in 5 mM NaOH for 1–2 min, followed by 2 washing steps with 5 $\mu$L of ultrapure water for 10 s. tSEM imaging was performed on a Gemini SEM500 scanning electron microscope (Zeiss) operated in transmission mode at 25 kV.

*Seeded-Growth of Gold within Mold Superstructures.* For seed-mediated deposition of gold inside the mold superstructures, their concentration was adjusted, such that the solution contained a total of 1 nM mold monomers in folding buffer supplemented with 50 mM NaCl. A 1350 $\mu$M solution of the reducing agent hydroxyl amine ($NH_2OH$) was added by stirring the solution with a magnetic stirrer for 1 min, such that the final hydroxyl amine concentration was in 6-fold molar excess over the final concentration of gold precursor. The gold deposition was initiated by injecting either 1.8 or 2.7 $\mu$L of 25 mM $H[AuCl_4]$ into 100 $\mu$L final volume of the $NH_2OH$ containing mold solution and the self-terminating growth reaction was allowed to proceed for 1 min.[18] Only the larger amount of precursor allowed to prepare structures that were mostly continuous (see main text).

*Analysis of Assembly Efficiencies.* Assembly efficiencies of higher-order mold structures were estimated by quantification of the corresponding band intensities from agarose gel electrophoresis. Band intensities were obtained by ChemiDoc MP imaging system with Image Lab software. For background subtraction, a hypothetical rolling disk (1–99 mm) was applied. With a smaller disk, more background in the lane was subtracted; with larger disk, less background was subtracted.[58] For all the multimer yield calculation, 10 mm rolling disk was applied.

## ■ ASSOCIATED CONTENT

### Supporting Information

The Supporting Information is available free of charge on the ACS Publications website at DOI: 10.1021/acs.nanolett.9b00740.

Additional electrophoresis gel images, electron microscopy micrographs as well as design files for the origami mold interface construction(PDF)

## ■ AUTHOR INFORMATION

### Corresponding Author

*E-mail: ralf.seidel@physik.uni-leipzig.de. Tel. +49 341 97 32501.

### ORCID

Ralf Seidel: 0000-0002-6642-053X



DOI: 10.1021/acs.nanolett.9b00740
Nano Lett. 2019, 19, 2707–2714

**Present Address**

[§](S.H.) Department of Physics, University of Oxford, Oxford OX13PU, U.K.

**Funding**

This work was supported by the Deutsche Forschungsgemeinschaft within the Cluster of Excellence Center for Advancing Electronics Dresden (cfaed/TU Dresden) as well as grant SE 1646/8-1 to R.S.

**Notes**

The authors declare no competing financial interest.

## ■ ACKNOWLEDGMENTS

We gratefully acknowledge Markus Löffler and the Dresden Center for Nanoanalysis for access, training, and support for the tSEM imaging. We furthermore acknowledge Dominik Kauert and Fatih N. Gür for useful discussions. We thank Martin Göse and Pierre Aldag for proof reading.

## ■ REFERENCES

(1) Seeman, N. C.; Sleiman, H. F. DNA Nanotechnology. *Nat. Rev. Mater.* **2017**, *3* (1), 17068.

(2) Bathe, M.; Rothemund, P. W. K. DNA Nanotechnology: A Foundation for Programmable Nanoscale Materials. *MRS Bull.* **2017**, *42* (12), 882−888.

(3) Seeman, N. C. Nanomaterials Based on DNA. *Annu. Rev. Biochem.* **2010**, *79* (1), 65−87.

(4) Hong, F.; Zhang, F.; Liu, Y.; Yan, H. DNA Origami: Scaffolds for Creating Higher Order Structures. *Chem. Rev.* **2017**, *117* (20), 12584−12640.

(5) Benson, E.; Mohammed, A.; Gardell, J.; Masich, S.; Czeizler, E.; Orponen, P.; Högberg, B. DNA Rendering of Polyhedral Meshes at the Nanoscale. *Nature* **2015**, *523* (7561), 441−444.

(6) Gerling, T.; Wagenbauer, K. F.; Neuner, A. M.; Dietz, H. Dynamic DNA Devices and Assemblies Formed by Shape-Complementary, Non−Base Pairing 3D Components. *Science* **2015**, *347* (6229), 1446−1452.

(7) Han, D.; Pal, S.; Nangreave, J.; Deng, Z.; Liu, Y.; Yan, H. DNA Origami with Complex Curvatures in Three-Dimensional Space. *Science* **2011**, *332* (6027), 342−346.

(8) Wei, B.; Dai, M.; Yin, P. Complex Shapes Self-Assembled from Single-Stranded DNA Tiles. *Nature* **2012**, *485* (7400), 623−626.

(9) Rothemund, P. W. K. Folding DNA to Create Nanoscale Shapes and Patterns. *Nature* **2006**, *440* (7082), 297−302.

(10) Douglas, S. M.; Dietz, H.; Liedl, T.; Högberg, B.; Graf, F.; Shih, W. M. Self-Assembly of DNA into Nanoscale Three-Dimensional Shapes. *Nature* **2009**, *459* (7245), 414−418.

(11) Scheffler, F.; Brueckner, M.; Ye, J.; Seidel, R.; Reibetanz, U. A Hybrid Carrier System Based on Origami Nanostrucutures and Layer-by-Layer Microparticles. *Adv. Funct. Mater.* **2019**, *29* (8), 1808116.

(12) Acuna, G. P.; Möller, F. M.; Holzmeister, P.; Beater, S.; Lalkens, B.; Tinnefeld, P. Fluorescence Enhancement at Docking Sites of DNA-Directed Self-Assembled Nanoantennas. *Science* **2012**, *338* (6106), 506−510.

(13) Heck, C.; Kanehira, Y.; Kneipp, J.; Bald, I. Placement of Single Proteins within the SERS Hot Spots of Self-Assembled Silver Nanolenses. *Angew. Chem., Int. Ed.* **2018**, *57* (25), 7444−7447.

(14) Thacker, V. V.; Herrmann, L. O.; Sigle, D. O.; Zhang, T.; Liedl, T.; Baumberg, J. J.; Keyser, U. F. DNA Origami Based Assembly of Gold Nanoparticle Dimers for Surface-Enhanced Raman Scattering. *Nat. Commun.* **2014**, *5*, 3448.

(15) Zessin, J.; Fischer, F.; Heerwig, A.; Kick, A.; Boye, S.; Stamm, M.; Kiriy, A.; Mertig, M. Tunable Fluorescence of a Semiconducting Polythiophene Positioned on DNA Origami. *Nano Lett.* **2017**, *17* (8), 5163−5170.

(16) Gür, F. N.; Schwarz, F. W.; Ye, J.; Diez, S.; Schmidt, T. L. Toward Self-Assembled Plasmonic Devices: High-Yield Arrangement of Gold Nanoparticles on DNA Origami Templates. *ACS Nano* **2016**, *10* (5), 5374−5382.

(17) Kuzyk, A.; Schreiber, R.; Fan, Z.; Pardatscher, G.; Roller, E.-M.; Högele, A.; Simmel, F. C.; Govorov, A. O.; Liedl, T. DNA-Based Self-Assembly of Chiral Plasmonic Nanostructures with Tailored Optical Response. *Nature* **2012**, *483* (7389), 311−314.

(18) Bayrak, T.; Helmi, S.; Ye, J.; Kauert, D.; Kelling, J.; Schönherr, T.; Weichelt, R.; Erbe, A.; Seidel, R. DNA-Mold Templated Assembly of Conductive Gold Nanowires. *Nano Lett.* **2018**, *18* (3), 2116−2123.

(19) Liu, N.; Liedl, T. DNA-Assembled Advanced Plasmonic Architectures. *Chem. Rev.* **2018**, *118* (6), 3032−3053.

(20) Gür, F. N.; McPolin, C. P. T.; Raza, S.; Mayer, M.; Roth, D. J.; Steiner, A. M.; Löffler, M.; Fery, A.; Brongersma, M. L.; Zayats, A. V. DNA-Assembled Plasmonic Waveguides for Nanoscale Light Propagation to a Fluorescent Nanodiamond. *Nano Lett.* **2018**, *18*, 7323.

(21) Hu, Q.; Li, H.; Wang, L.; Gu, H.; Fan, C. DNA Nanotechnology-Enabled Drug Delivery Systems. *Chem. Rev.* **2018**. DOI: 10.1021/acs.chemrev.7b00663

(22) Douglas, S. M.; Bachelet, I.; Church, G. M. A Logic-Gated Nanorobot for Targeted Transport of Molecular Payloads. *Science* **2012**, *335* (6070), 831−834.

(23) Chandrasekaran, A. R.; Anderson, N.; Kizer, M.; Halvorsen, K.; Wang, X. Beyond the Fold: Emerging Biological Applications of DNA Origami. *ChemBioChem* **2016**, *17* (12), 1081−1089.

(24) Wirges, C. T.; Timper, J.; Fischler, M.; Sologubenko, A. S.; Mayer, J.; Simon, U.; Carell, T. Controlled Nucleation of DNA Metallization. *Angew. Chem., Int. Ed.* **2009**, *48* (1), 219−223.

(25) Seidel, R.; Colombi Ciacchi, L.; Weigel, M.; Pompe, W.; Mertig, M. Synthesis of Platinum Cluster Chains on DNA Templates: Conditions for a Template-Controlled Cluster Growth. *J. Phys. Chem. B* **2004**, *108* (30), 10801−10811.

(26) Richter, J.; Seidel, R.; Kirsch, R.; Mertig, M.; Pompe, W.; Plaschke, J.; Schackert, H. K. Nanoscale Palladium Metallization of DNA. *Adv. Mater.* **2000**, *12* (7), 507−510.

(27) Monson, C. F.; Woolley, A. T. DNA-Templated Construction of Copper Nanowires. *Nano Lett.* **2003**, *3* (3), 359−363.

(28) Gu, Q.; Cheng, C.; Haynie, D. T. Cobalt Metallization of DNA: Toward Magnetic Nanowires. *Nanotechnology* **2005**, *16* (8), 1358.

(29) Braun, E.; Eichen, Y.; Sivan, U.; Ben-Yoseph, G. DNA-Templated Assembly and Electrode Attachment of a Conducting Silver Wire. *Nature* **1998**, *391* (6669), 775−778.

(30) Keren, K.; Krueger, M.; Gilad, R.; Ben-Yoseph, G.; Sivan, U.; Braun, E. Sequence-Specific Molecular Lithography on Single DNA Molecules. *Science* **2002**, *297* (5578), 72−75.

(31) Mertig, M.; Colombi Ciacchi, L.; Seidel, R.; Pompe, W.; De Vita, A. DNA as a Selective Metallization Template. *Nano Lett.* **2002**, *2* (8), 841−844.

(32) Teschome, B.; Facsko, S.; Schönherr, T.; Kerbusch, J.; Keller, A.; Erbe, A. Temperature-Dependent Charge Transport through Individually Contacted DNA Origami-Based Au Nanowires. *Langmuir* **2016**, *32* (40), 10159−10165.

(33) Schreiber, R.; Kempter, S.; Holler, S.; Schüller, V.; Schiffels, D.; Simmel, S. S.; Nickels, P. C.; Liedl, T. DNA Origami-Templated Growth of Arbitrarily Shaped Metal Nanoparticles. *Small* **2011**, *7* (13), 1795−1799.

(34) Liu, J.; Geng, Y.; Pound, E.; Gyawali, S.; Ashton, J. R.; Hickey, J.; Woolley, A. T.; Harb, J. N. Metallization of Branched DNA Origami for Nanoelectronic Circuit Fabrication. *ACS Nano* **2011**, *5* (3), 2240−2247.

(35) Schreiber, R.; Do, J.; Roller, E.-M.; Zhang, T.; Schüller, V. J.; Nickels, P. C.; Feldmann, J.; Liedl, T. Hierarchical Assembly of Metal Nanoparticles, Quantum Dots and Organic Dyes Using DNA Origami Scaffolds. *Nat. Nanotechnol.* **2014**, *9* (1), 74−78.

(36) Uprety, B.; Gates, E. P.; Geng, Y.; Woolley, A. T.; Harb, J. N. Site-Specific Metallization of Multiple Metals on a Single DNA Origami Template. *Langmuir* **2014**, *30* (4), 1134−1141.

(37) Gates, E. P.; et al. Optimizing Gold Nanoparticle Seeding Density on DNA Origami. *RSC Adv.* **2015**, *5* (11), 8134−8141.



DOI: 10.1021/acs.nanolett.9b00740
*Nano Lett.* 2019, 19, 2707−2714

(38) Helmi, S.; Ziegler, C.; Kauert, D. J.; Seidel, R. Shape-Controlled Synthesis of Gold Nanostructures Using DNA Origami Molds. *Nano Lett.* **2014**, *14* (11), 6693−6698.
(39) Sun, W.; Boulais, E.; Hakobyan, Y.; Wang, W. L.; Guan, A.; Bathe, M.; Yin, P. Casting Inorganic Structures with DNA Molds. *Science* **2014**, *346* (6210), 1258361.
(40) Uprety, B.; Westover, T.; Stoddard, M.; Brinkerhoff, K.; Jensen, J.; Davis, R. C.; Woolley, A. T.; Harb, J. N. Anisotropic Electroless Deposition on DNA Origami Templates To Form Small Diameter Conductive Nanowires. *Langmuir* **2017**, *33* (3), 726−735.
(41) Stern, A.; Eidelshtein, G.; Zhuravel, R.; Livshits, G. I.; Rotem, D.; Kotlyar, A.; Porath, D. Highly Conductive Thin Uniform Gold-Coated DNA Nanowires. *Adv. Mater.* **2018**, *30* (26), 1800433.
(42) Pfeifer, W.; Lill, P.; Gatsogiannis, C.; Saccà, B. Hierarchical Assembly of DNA Filaments with Designer Elastic Properties. *ACS Nano* **2018**, *12* (1), 44−55.
(43) Jungmann, R.; Scheible, M.; Kuzyk, A.; Pardatscher, G.; Castro, C. E.; Simmel, F. C. DNA Origami-Based Nanoribbons: Assembly, Length Distribution, and Twist. *Nanotechnology* **2011**, *22* (27), 275301.
(44) Dietz, H.; Douglas, S. M.; Shih, W. M. Folding DNA into Twisted and Curved Nanoscale Shapes. *Science* **2009**, *325* (5941), 725−730.
(45) Iinuma, R.; Ke, Y.; Jungmann, R.; Schlichthaerle, T.; Woehrstein, J. B.; Yin, P. Polyhedra Self-Assembled from DNA Tripods and Characterized with 3D DNA-PAINT. *Science* **2014**, *344* (6179), 65−69.
(46) Liu, W.; Zhong, H.; Wang, R.; Seeman, N. C. Crystalline Two-Dimensional DNA-Origami Arrays. *Angew. Chem., Int. Ed.* **2011**, *50* (1), 264−267.
(47) Wang, P.; Gaitanaros, S.; Lee, S.; Bathe, M.; Shih, W. M.; Ke, Y. Programming Self-Assembly of DNA Origami Honeycomb Two-Dimensional Lattices and Plasmonic Metamaterials. *J. Am. Chem. Soc.* **2016**, *138* (24), 7733−7740.
(48) Zhang, T.; Hartl, C.; Frank, K.; Heuer-Jungemann, A.; Fischer, S.; Nickels, P. C.; Nickel, B.; Liedl, T. 3D DNA Origami Crystals. *Adv. Mater.* **2018**, *30* (28), 1800273.
(49) Woo, S.; Rothemund, P. W. K. Programmable Molecular Recognition Based on the Geometry of DNA Nanostructures. *Nat. Chem.* **2011**, *3* (8), 620−627.
(50) Wagenbauer, K. F.; Sigl, C.; Dietz, H. Gigadalton-Scale Shape-Programmable DNA Assemblies. *Nature* **2017**, *552* (7683), 78−83.
(51) Liber, M.; Tomov, T. E.; Tsukanov, R.; Berger, Y.; Popov, M.; Khara, D. C.; Nir, E. Study of DNA Origami Dimerization and Dimer Dissociation Dynamics and of the Factors That Limit Dimerization. *Small* **2018**, *14* (23), 1800218.
(52) Tikhomirov, G.; Petersen, P.; Qian, L. Fractal Assembly of Micrometre-Scale DNA Origami Arrays with Arbitrary Patterns. *Nature* **2017**, *552* (7683), 67−71.
(53) Ke, Y.; Douglas, S. M.; Liu, M.; Sharma, J.; Cheng, A.; Leung, A.; Liu, Y.; Shih, W. M.; Yan, H. Multilayer DNA Origami Packed on a Square Lattice. *J. Am. Chem. Soc.* **2009**, *131* (43), 15903−15908.
(54) Douglas, S. M.; Marblestone, A. H.; Teerapittayanon, S.; Vazquez, A.; Church, G. M.; Shih, W. M. Rapid Prototyping of 3D DNA-Origami Shapes with CaDNAno. *Nucleic Acids Res.* **2009**, *37* (15), 5001−5006.
(55) Stahl, E.; Martin, T. G.; Praetorius, F.; Dietz, H. Facile and Scalable Preparation of Pure and Dense DNA Origami Solutions. *Angew. Chem., Int. Ed.* **2014**, *53* (47), 12735−12740.
(56) Ding, B.; Deng, Z.; Yan, H.; Cabrini, S.; Zuckermann, R. N.; Bokor, J. Gold Nanoparticle Self-Similar Chain Structure Organized by DNA Origami. *J. Am. Chem. Soc.* **2010**, *132* (10), 3248−3249.
(57) Hill, H. D.; Mirkin, C. A. The Bio-Barcode Assay for the Detection of Protein and Nucleic Acid Targets Using DTT-Induced Ligand Exchange. *Nat. Protoc.* **2006**, *1* (1), 324−336.
(58) Bio-Rad. ChemiDoc Mp imaging system with Image Lab software, http://www.bio-rad.com/webroot/web/pdf/lsr/literature/10000076957.pdf.



DOI: 10.1021/acs.nanolett.9b00740
*Nano Lett.* 2019, 19, 2707−2714

# 4. DNA Mold Templated Assembly of Conductive Gold Nanowires

## 4.1 Introduction

Based on the mold modular platform, different mold superstructures can be fabricated with controlled length, pattern as well as geometries as shown in **Chapter 3** and **P4**. A highly homogeneous metal deposition was obtained for this modular platform. However, for nanoelectronic applications, whether the assembled metal nanostructures exhibit metallic behaviour comparable with bulk material, is a key question that we need to address.

Thus, the electronic behaviour of linear gold nanowires was investigated. Two different mold monomers with alternating interfaces were introduced to form periodic chain structures. With two gold nanoparticles decoration within each mold monomer, a micrometer long chain formation was achieved with high seed decoration affinity. By following similar metal deposition strategy as before, highly homogeneous gold nanowires that exceeded significantly the quality of previous reported gold nanowires were obtained. This could be attributed to the mold walls around all the evenly aligned gold nanoparticle seeds, which uniquely controlled the internal metal deposition. The gold nanowires were deposited on a silicon dioxide layer and site-specific electron beam lithography was performed to construct gold electrodes for two- or even four-terminal current-voltage measurements. Conductance measurements were operated under different temperatures to reveal the charge transport mechanisms within the gold nanowires. Some of the measured wires were indeed metallically conductive comparable with bulk material, whereas other exhibited large resistance values.

This chapter depicts a further step towards nanoelectronic devices made from DNA templates. The metallic conductive nanowires fulfil one important requirement for future applications. Based on this, more complex structures containing different materials were fabricated in **Chapter 5**. Following, achieving high yield of conductive wires within this scheme would increase the homogeneity and avoid granular boundaries produced during this process. Such improvements were implemented in manuscript **P5**.

## 4.2 Associated Publication P2

### DNA-Mold Templated Assembly of Conductive Gold Nanowires

by

Türkan Bayrak,* Seham Helmi,* Jingjing Ye,* Dominik Kauert, Jeffrey Kelling, Tommy Schönherr, Artur Erbe, Ralf Seidel

*equal contribution

published in

Nano Letter 2018, 18, 3, 2116-2123

NANO LETTERS
Letter
Cite This: Nano Lett. 2018, 18, 2116−2123
pubs.acs.org/NanoLett

# DNA-Mold Templated Assembly of Conductive Gold Nanowires

Türkan Bayrak,[†,§,▽] Seham Helmi,[⊥,#,▽] Jingjing Ye,[§,⊥,▽] Dominik Kauert,[⊥] Jeffrey Kelling,[‡] Tommy Schönherr,[†] Richard Weichelt,[∥,§] Artur Erbe,[*,†,§] and Ralf Seidel[*,§,⊥]

[†]Institute of Ion Beam Physics and Materials Research and [‡]Department of Information Services and Computing, Helmholtz-Zentrum Dresden-Rossendorf, 01328 Dresden, Germany

[§]Cluster of Excellence Center for Advancing Electronics Dresden (cfaed) and [∥]Institute of Physical Chemistry, TU Dresden, 01062 Dresden, Germany

[⊥]Molecular Biophysics Group, Peter Debye Institute for Soft Matter Physics, Universität Leipzig, 04103 Leipzig, Germany

Supporting Information

**ABSTRACT:** We introduce a new concept for the solution-based fabrication of conductive gold nanowires using DNA templates. To this end, we employ DNA nanomolds, inside which electroless gold deposition is initiated by site-specific attached seeds. Using programmable interfaces, individual molds self-assemble into micrometer-long mold superstructures. During subsequent internal gold deposition, the mold walls constrain the metal growth, such that highly homogeneous nanowires with 20−30 nm diameters are obtained. Wire contacting using electron-beam lithography and electrical conductance characterization at temperatures between 4.2 K and room temperature demonstrate that metallic conducting wires were produced, although for part of the wires, the conductance is limited by boundaries between gold grains. Using different mold designs, our synthesis scheme will, in the future, allow the fabrication of complex metal structures with programmable shapes.

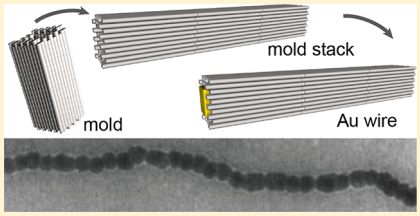


**KEYWORDS:** *Metal nanowires, seeded growth, DNA metallization, DNA nanostructures, DNA template, nanoelectronics*



The past decade has seen a boost in the field of DNA nanotechnology. A number of pioneering techniques[1−6] were developed that allow the self-assembly of large two- and three-dimensional DNA structures with complex shapes. The basis of these techniques are specific interactions between complementary DNA strands. By appropriate sequence design of the involved DNA molecules, a desired structure can thus be obtained in a fully programmable, sequence-encoded manner. The beauty, the complexity[1−6] and the increased rigidity[7] of the down-to-the-atomic-level defined objects instantaneously motivated the usage of DNA nanostructures to assemble non-DNA materials in defined patterns. Examples include the arrangements of proteins,[8] chemical[9] and photoactive groups,[10,11] the assembly of metal nanoparticles into plasmonic nanostructures,[12−14] and the sculpting of lipid membranes.[15,16]

DNA nanotechnology is particularly successful in generating soft nanostructures. However, many applications in "hard-matter nanotechnology", particularly in nano-optics and nanoelectronics, require structures made from inorganic, e.g., metallic and semiconducting, rather than biological materials. In particular, the low electrical conductance found in contacts to single DNA duplexes is detrimental for applications in nanoelectronics.[17] Therefore, it would be highly desirable if one could "replace" the DNA structure atom by atom site-specifically with a material of choice to enable a programmable synthesis of inorganic nanostructures. Though a direct replacement will be practically impossible, the outlined idea inspired the usage of DNA as a template for inorganic material growth. Hereby, the biomolecule would donate its shape to the growing material film. In first approaches, linear DNA molecules were metallized by so-called electroless deposition, in which metal seeds are first deposited on the molecule that are subsequently grown to more-continuous structures. This way, elongated metal particle assemblies could be fabricated.[18−20] Later, this concept could be extended to many different materials, including gold, silver, platinum, palladium, copper, and cobalt.[21] With the advances in DNA nanotechnology, rigid DNA template structures with more-complex shapes became available enabling the growth of elongated wires,[22] metal rings,[23] junctions,[24] and spheres[25] as well as structures consisting of two types of metals.[26] The deposited metal films were, however, not homogeneous and typically contained many distinct grains. This made the resulting structures either discontinuous[20] or inhomogeneous,[27] depending on the amount of deposited material.

Nonetheless, wires produced this way were often found to conduct electric current when contacted either by electron-beam-lithography-fabricated electrodes[19,28−32] or by conductive AFM tips.[33,34] Reported resistance values spanned several orders of magnitude. Typically, the observed resistivities were significantly larger than expected for the respective metal forming the wire, indicating that grain boundaries can act as significant barriers. This was supported by recent temperature-dependent (4.2 to 293 K) conductance measurements on

Received: January 24, 2018
Revised: February 26, 2018
Published: February 27, 2018




DOI: 10.1021/acs.nanolett.8b00344
Nano Lett. 2018, 18, 2116−2123

DNA-origami-based Au nanowires from our laboratory showing that tunneling, thermionic, and hopping conduction mechanisms govern the conductance at low, intermediate, and high temperatures, respectively.[22] In addition, a recent study of 500 nm nanopillars, realized as a multilayer heterostructure of DNA origami tiles and Au nanoparticles, suggested a tunneling or hopping conduction mechanism at room temperature.[28] To limit the number of grain boundaries, recently elongated Au nanorods were deposited in an aligned manner on DNA origami templates and connected using limited electroless Au-plating.[35] This provided resistance values for wires of 12 to 30 nm widths in the range of 440 Ω to 37 MΩ with resistivities close to bulk gold for the wires with the highest conductances. This further supports the idea that grain boundaries due to inhomogeneous growth conditions appear to be one of the challenges in DNA-templated fabrication of metallic wires.

A key problem for the traditional external deposition on DNA templates is the lack of size control for the particles that grow at the different positions along the DNA chain. This makes the methodology prone to inhomogeneities. Inspired by internal metal deposition schemes inside protein shells,[36,37] we and others recently developed a DNA mold-based nanoparticle fabrication scheme.[38,39] Here, the metal deposition occurs on a nucleation seed inside the cavity of a DNA origami mold, such that the mold wall influences the shape of the resulting particle. This way, it was possible to synthesize gold and silver cuboids of different dimensions and shapes.

Here, we extend the mold-based nanostructure fabrication scheme by coupling mold monomers into large linear mold superstructures (Figure 1). This enables the growth of highly homogeneous, micrometer-long nanowires with ∼30 nm width that in part exhibit metallic conductance. To this end, we assembled DNA molds using the DNA origami method[1,2] from an 8064 nucleotide long single-stranded DNA scaffold and corresponding DNA staple oligomers (see the Methods section). The mold monomers had a 40 nm long tube-like shape with a quadratic cross-section.[39] Each side wall of the mold was composed of two layers of 10 parallel DNA helices of equal length (Figure 1) providing a total of 64 helices for the whole mold structure. Fabricated mold monomers were preloaded with 5 nm DNA-functionalized gold nanoparticles[40,41] serving as seeds for the subsequent gold growth. They were attached within the molds via four complementary DNA capture strands extruding from the four cavity faces at the given binding position (Figure 1a).[39]

To allow the formation of long linear mold superstructures via sequential docking of mold monomers, we extended or shortened the staples at the DNA helix ends (further called end staples) by two nucleotides, such that the 2-nt extensions of one mold could invade into the other mold and hybridize with its scaffold (Figure 1a,b).

The mold geometry with helices of identical length is asymmetric with respect to its ends. If we call one mold end the head and the other end the tail side, then a particular DNA helix that is recessed at the head side is extended at the tail side (and vice versa), which results in a symmetry break. Thus, when mold ends bind in a head-to-tail fashion, docking can be obtained at all 64 helix ends, leaving no gap at the interface. However, for head-to-head or tail-to-tail binding, a significantly lower number of docking helices is obtained (44 or 36, respectively). To obtain "neat-less", i.e., gap-free, mold superstructures we therefore designed end staples to support head-to-tail binding. We prepared two different types of

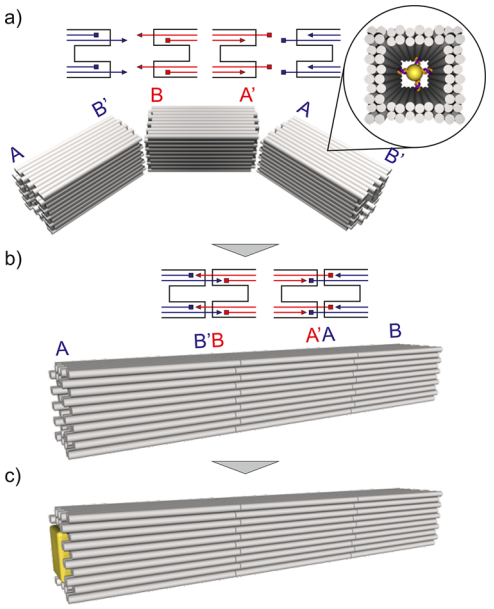


**Figure 1.** Scheme illustrating the mold-based gold nanowire. (a) Design scheme of the mold bricks with specifically interacting ends containing an internally attached 5 nm gold seed (see the inset in the upper right corner). Adhesion of mold ends is obtained by either protruding 5′-staple ends together with correspondingly recessed 3′-staple ends at the mold ends (A−A′ interface; see the sketches in the top row) or protruding 3′-staple ends together with recessed 5′-staple ends (B−B′ interface). (b) Self-assembly of a long mold superstructure using two mold types, each carrying an A or a B interface, being complementary to the A′ or the B′ interface of the other mold type, respectively. (c) Gold nanowire formation by metal deposition at the seeds inside the mold chain.

interfaces: interface A−A′, for which end staples were extended by 2 nt at the 5′-ends and correspondingly recessed at the 3′-ends, as well as interface B−B′ with recessed 5′-ends and extended 3′-ends (Figure 1a). Here, A and B denote the head side of the mold and A′ and B′ the complementary side on a mold tail side, respectively.

For the assembly of linear mold chains a single interface, e.g., monomers with A−A′ ends would suffice. In this case mold chains would already form during origami hybridization, which would, however, inhibit the loading of the molds with gold seeds at internal sites. We therefore designed two different mold monomers: one with AB′ ends and the other with BA′ ends. While each mold type would be monomeric alone, their mixing should result in the desired chain formation (Figures 1 and 2).

Following the outlined approach, we assembled AB′ and BA′ molds, loaded them with gold nanoparticle seeds, and subjected them to TEM imaging (Figures 2a and S1). In contrast to our expectations, both monomers alone formed extended linear, partially staggered, chains, which, in turn, led to poor decoration with seeds. We hypothesized that, due to the large number of "attractive" ends (all 64 helix ends contained 2 nt recessions and extensions), mold monomers could bind to themselves, forming nondesired head-to-head and tail-to-tail interactions. Apparently, the presence of mismatches between staple extension and scaffold did not lower the affinity between single helix ends sufficiently to prevent unspecific binding.

To suppress unspecific interactions, the number of attractive helix ends was reduced by omitting end staples at some of the helix ends, which are in the following called nonattractive ends.



DOI: 10.1021/acs.nanolett.8b00344
Nano Lett. 2018, 18, 2116−2123

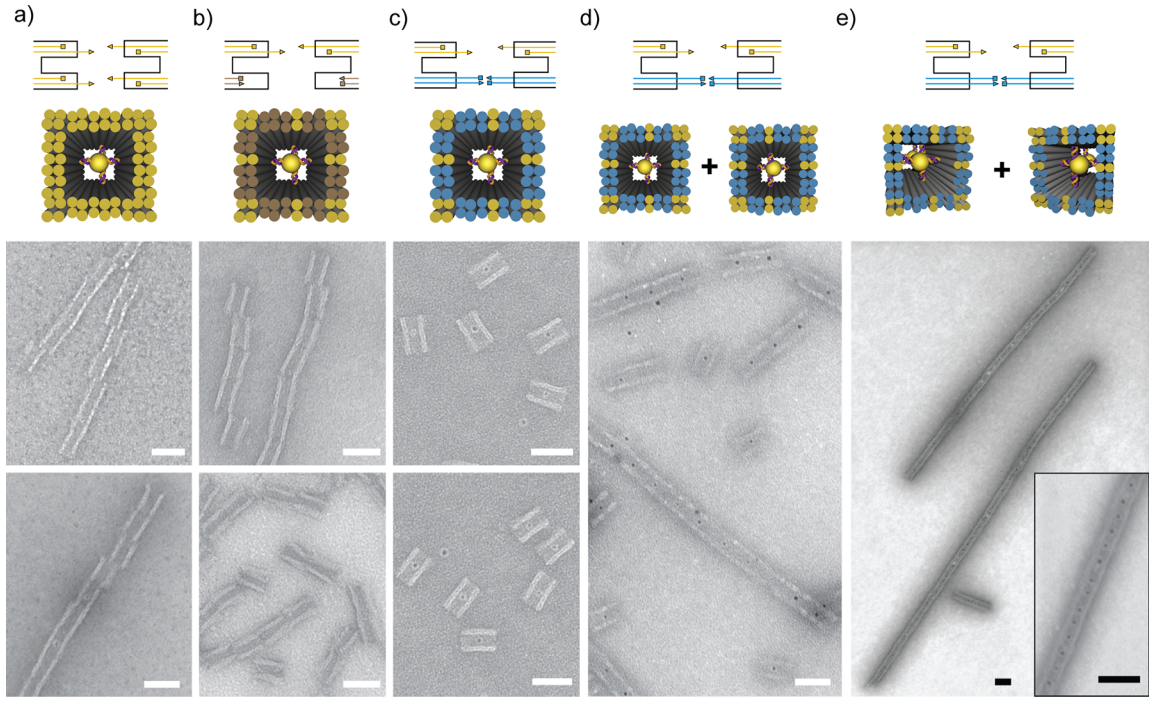


**Figure 2.** Fine-tuning the specificity of adhesive mold ends. (a–c) Type of staple ends used and their positions on the 3D model (upper row) as well as corresponding TEM images of the AB′ and BA′ mold monomers. Tested were (a) attractive ends only (in yellow), (b) attractive ends together with nonattractive ends (in gray, obtained by omitting ends staples), and (c) attractive and repulsive ends (blue, obtained by 6 nt non-complementary 5′-staple overhangs). (d) Mixing AB′ and BA′ mold monomers comprising attractive and repulsive end staples (as in panel c) results in mold oligomer formation. (e) By using optimized multimerization conditions, long linear mold chains are obtained. Preloading of the monomers with two seeds at high decoration efficiency results in a homogeneous loading of seeds inside the mold superstructure (see the inset). The scale bars correspond to 50 nm.

Here, the scaffold forms a dangling loop. For 16 to 24 attractive ends with the remaining ends being nonattractive, considerable unspecific interactions between mold monomers were observed nonetheless (Figures 2b and S1). To further reduce unspecific binding, repulsive interactions between helix ends were incorporated. To this end, the previously nonattractive ends were made repulsive by extending the end staples at these positions by 6 nt for both 5′ and 3′ ends (see the sketch in Figure 2c). The steric clash between these dangling ends should introduce an energetic penalty compared to the nonattractive end configuration. In agreement with this expectation, TEM imaging revealed the monomeric nature of molds containing up to 24 attractive helix ends (Figures 2c and S1). These monomers exhibited a high seed decoration efficiency because gold nanoparticles could freely enter the mold ends.

We next tested whether the optimized molds with attractive and repulsive ends could form specific interactions by mixing seed decorated AB′ and BA′ monomers. While molds with 16 and 20 attractive helix ends remained mostly monomeric (Figure S1), molds with 24 attractive ends supported the formation of linear oligomeric mold assemblies already after 10 min of incubation (Figure 2d). To prepare long mold chains for subsequent metallization, we carried out the following optimizations: (i) addition of 2 seeds per mold monomer to avoid interruption of gold wire in case of missing seeds, (ii) chain formation overnight to obtain long assemblies, and (iii) polyethylene glycol (PEG) precipitation[42] after chain formation to remove unbound gold seeds. All together, these optimizations yielded $\mu$m-long linear mold chains containing evenly 20 nm spaced gold seeds with 96 ± 2% decoration efficiency (Figure 2e).

To fabricate gold nanowires, the linear mold superstructures were used in a previously established seeded growth procedure.[39] Mold chains were premixed with the reducing agent hydroxylamine. Subsequently, a solution of the gold precursor H[$AuCl_4$] was quickly injected into the rapidly stirred solution. The reaction self-terminated due to the consumption of H[$AuCl_4$] after ∼1 min as judged from color changes of the solution. TEM and SEM imaging revealed a homogeneous gold deposition at all seeds (Figure 3). The lengths of the grown structures were in the micrometer range (Figure S2). At low amounts of precursor, the grown gold particles still remained well-separated (Figure 3a), while at larger amounts of precursor, the grown particles appeared more and more connected to each other (Figures 3b,c and S3). At the largest precursor concentration the particles formed quasi-continuous $\mu$m-long wires that were occasionally interrupted by smaller gaps (Figures 3c,d, and S4). These structures were stable in solution for several days. Only at larger precursor concentrations did aggregation occur. We note that the highly homogeneous particle growth and the stability of the wires was only achieved when the seed-loaded mold chains were subjected to the PEG precipitation before metallization. This was most likely due to residual PEG traces because PEG is also used as a surfactant in nanoparticle synthesis.[43] The resulting nanowires (Figure 3d) had diameters of 32 ± 3 nm. Despite occasional gaps, these wires were of excellent homogeneity compared with other DNA-templated metal structures. Thus, the mold-assisted growth of metal nanoparticles can be successfully transferred to large mold superstructures.

To reveal which role residual gaps are playing and whether the wires can exhibit metal-like conductance, we investigated



DOI: 10.1021/acs.nanolett.8b00344
Nano Lett. 2018, 18, 2116–2123

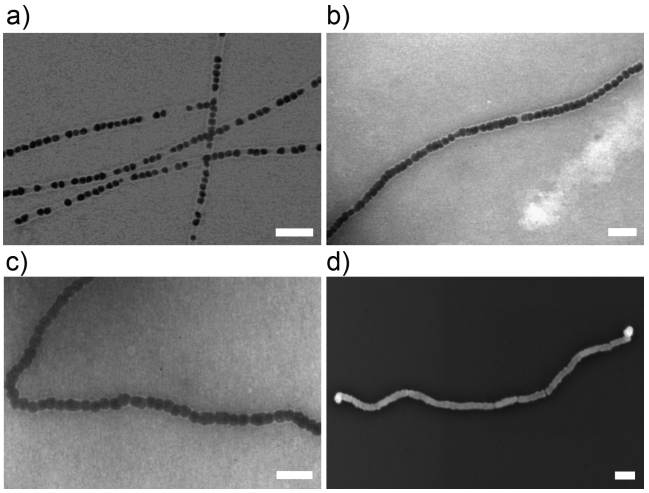


**Figure 3.** Gold nanowires obtained by gold deposition within the seed decorated linear mold superstructures. TEM images of the obtained structures for different relative amounts of gold precursor are shown: (a) 1-fold, (b) 2-fold, and (c) 4-fold $H[AuCl_4]$. (d) SEM image of a gold nanowire on a $SiO_2$ support grown with 4-fold $H[AuCl_4]$. The scale bars correspond to 50 nm.

the electrical transport properties of several fabricated nanowires with 110 to 1000 nm in length. The electrical contacting of individual DNA origami mold-based gold nanowires was performed in three steps. (i) Using electron beam lithography, 45 contact areas (in three parallel arrays) were patterned on top of $SiO_2$ substrates containing the adsorbed gold nanowires. Each contact area had a total of 4 90 $\mu$m × 90 $\mu$m Au contact pads and 144 alignment marks arranged in a square lattice with an 8 $\mu$m distance between neighboring marks (Figure 4a). (ii) Using scanning electron microscopy, the coordinates of the individual wires relative to the alignment marks were recorded (Figure 4b). (iii) The recorded locations of the nanowires were used to obtain corresponding electron-beam exposure positions to place electrical contacts on the nanowires. This procedure allowed to write four electrodes, even on a 600 nm long nanowire (Figure 4c). Overall, the wires adhered well to the substrate, such that they retained their shape during the lithography and the solvent-based ultrasonic lift-off process, as confirmed by SEM imaging.

Two-terminal current−voltage ($I$−$V$) measurements were performed on 22 individual wires. The measured resistance values at room temperature (RT, i.e., 293 K) including the contact resistance between EBL-patterned gold electrodes and nanowires were between 90 Ω and 30 GΩ without showing a clear length dependence (Figure 5).

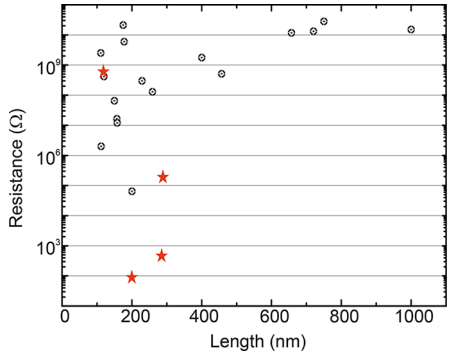


**Figure 5.** Resistance values as a function of length for the characterized gold nanowires. Wires chosen for temperature-dependent measurements are shown by a star-shaped symbol.

The limited resolution of SEM imaging on the $SiO_2$ substrates did not allow to correlate the measured resistance with the wire morphology (Figure S5). Therefore, to understand the large variation in resistance values, we measured the temperature dependence of the charge transport of two highly conductive nanowires (labeled CW-1 and CW-2 with RT resistances of 90 ± 5 Ω and 460 ± 10 Ω) as well as two highly resistive nanowires (labeled RW-1 and RW-2 with RT resistances of 190 ± 5 kΩ and 690 ± 5 MΩ). The inset of Figure 6a depicts a nanowire with a length of 800 nm, which was contacted by four terminal gold contacts. SEM imaging revealed 13−15 nm gaps between the contact points 2 and 3 as well as 3 and 4 leading to insulating behavior in $I$−$V$ measurements (see Figure S6). A high conductance was found for the wire segment between contacts 1 and 2 (CW-1). The $I$−$V$ characteristics of CW-1 (200 nm length and 40 nm width) was linear throughout the considered temperature range between 4.2 K and RT (see Figures 6b and 7a). This indicates an ohmic behavior of the nanowire itself as well as its contacts. The resistance of the wire was weakly decreasing with temperature from 90 Ω at 293 K to 50 Ω at 4.2 K, as expected for a metallic wire. A qualitatively similar behavior was observed for the 285 nm long nanowire CW-2 with a 30 nm average width (see Figures 6b and 7b) for which resistances of 460 and 420 Ω at 293 and 4.2 K were measured, respectively.

Temperature-dependent $I$−$V$ measurements on the more resistive nanowires RW-1 (290 nm length and 36 nm width)

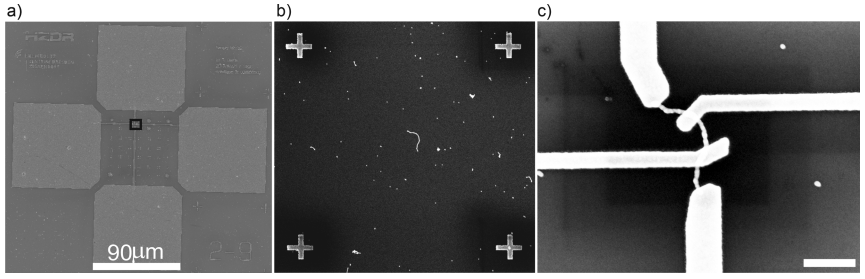


**Figure 4.** Electrical contacting of mold-templated nanowires. (a) SEM images of one out of 45 contact areas comprising four contact pads. Contact pads were fabricated on $SiO_2$ substrates containing the adsorbed gold nanowires. In between the electrodes, 144 alignment markers arranged in a square lattice defined 36 "writing" fields of 8 $\mu$m × 8 $\mu$m size. (b) Enlarged view into a single writing field (corresponding to the black square in panel a) containing a 600 nm long gold nanowire. (c) The gold nanowire shown in panel b after contact writing. Each contact to the wire connects to one of the four contact pads shown in panel a.



DOI: 10.1021/acs.nanolett.8b00344
*Nano Lett.* 2018, 18, 2116−2123

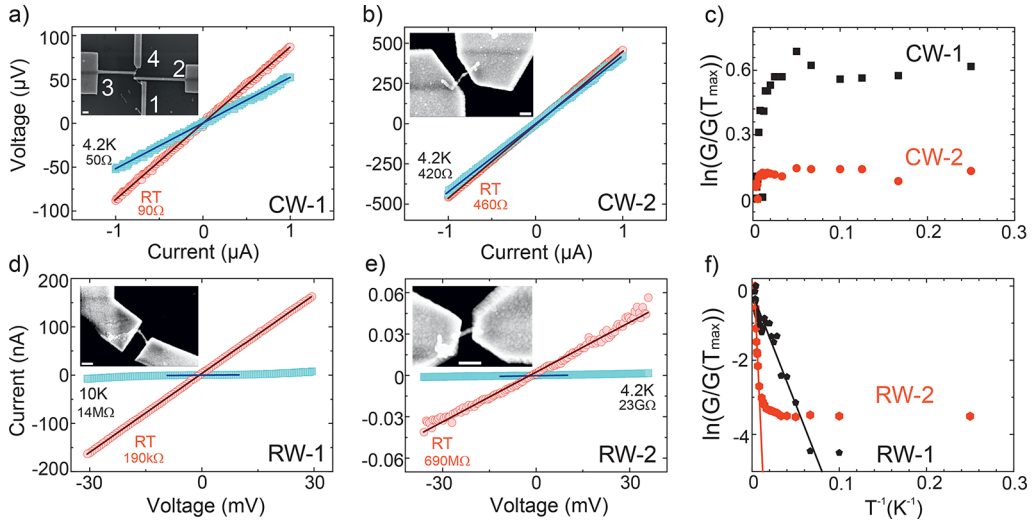


**Figure 6.** *I*−*V* characteristics of the different nanowires measured at the temperatures of 4.2 and 293 K. SEM inset images show the nanowires after contacting (scale bars are 200 nm). (a,b) *I*−*V* curves for the highly conductive wires CW-1 and CW-2 obtained by sourcing the current and measuring the voltage drop across the wire. Resistance values shown next to the curves were obtained from linear fits (solid lines). (c) Normalized natural logarithm of the conductance values as a function of $T^{-1}$ for CW-1 and CW-2. (d,e) *I*−*V* curves for the resistive wires RW-1 and RW-2 obtained by applying a voltage bias and measuring the resulting current. (f) Normalized natural logarithm of the conductance values as a function of $T^{-1}$ for RW-1 and RW-2 (filled circles). Exponential fits to the data in a selected temperature range are shown as solid lines.

and RW-2 (115 nm length and 39 nm width) revealed linear behavior at RT (Figure 6d,e). However, at low temperatures (50 to 4 K), the *I*−*V* curves became nonlinear in between −30 and +30 mV (Figure S7). Therefore, resistance values were calculated from the slope of the linear part of the curves (−10 to 10 mV). The resistance was strongly temperature dependent for both wires; it increased for RW-1 from 190 kΩ at RT to 14 MΩ at 10 K and for RW-2 from 700 MΩ at RT to 23 GΩ at 4 K. Thus, both wires did not show metallic conductance behavior.

To better understand the nature of the charge transport in these nanowires, we plotted the normalized natural logarithm of the conductance $\ln[G/G(T_{max})]$ as a function of the reciprocal temperature ($T^{-1}$). The conductance of both CW-1 and CW-2 increased mildly with decreasing temperature, as discussed above (Figure 6c). Saturation of the conductance at low temperatures (4.2 to 20 K) was observed in CW-1 and CW-2. In contrast, the conductance of the resistive nanowires RW-1 and RW-2 decreased strongly, initially in an exponential fashion with the reciprocal temperature (Figure 6f). While RW-1 exhibited an exponential decrease over the whole temperature range, the conductance of RW-2 saturated for temperatures below 30 K.

An exponential conductance decrease indicates a thermally activated hopping mechanism for the charge transport, e.g., due to low conductance barriers in between conductive wire segments. Here, the conductance is governed by the activation energy, $E_a$, necessary to overcome the barrier according to $G \approx \exp(-E_a/k_BT)$, where $k_B$ is the Boltzmann constant.[44−46]

The activation energies of the wires were obtained from the slope of the linear sections in the conductance yielding 5 ± 0.5 meV for RW-1 (temperature range from 10K to RT) and 45 ± 5 meV for the more-resistive wire RW-2 (temperature range from 70 K to RT). While a hopping mechanism seems to dominate the conduction of RW-1 at all temperatures, hopping conductivity is observed for RW-2 only at high temperatures. At low temperatures, between 4 and 30 K, the independence of the conductance of RW-2 on the temperature suggests that direct tunneling of electrons through an energy barrier is the dominant mechanism in this regime. For temperatures in between the tunneling and the hopping regime (30 to 70 K) a thermionic conduction mechanism comes into play[21] due to decreases in the effective barrier height and the excitation of more electrons.

In summary, we successfully demonstrated the fabrication of highly homogeneous and conductive nanowires using DNA molds. An important step was herein the fine-tuning of the specificity of the mold−mold interactions using attractive and repulsive ssDNA overhangs. In only this way did molds of a given type stay monomeric and could thus be efficiently loaded with gold nanoparticle seeds. Mixing two mold types with likewise attractive interfaces resulted in the formation of linear mold superstructures being hundreds of nanometers long and comprising dozens of monomers. The subsequent gold deposition at the seeds produced nanowire structures that consisted of nearly perfectly aligned gold nanoparticles of homogeneous size. This demonstrates that the mold-assisted growth of metal nanoparticles can be applied to large superstructures. Our approach represents thus a new way to DNA-templated nanostructure fabrication.

At elevated amounts of deposited gold, the grown nanoparticles became connected to each other, such that the resulting structures became quasi-continuous. To verify whether actual gold−gold contacts between the particles had been established, we employed temperature-dependent conductance measurements enabled by high-precision contacting of the wires using electron beam lithography. These characterizations provided diverging results. A small part of the wires exhibited high metal-like conductivity, verifying that metallic gold−gold contacts could be successfully formed over 20 to 30 contiguous particle boundaries (being spaced by 20 nm). This is remarkable because only very recently were high conductivities of DNA templated gold structures achieved using long gold nanorods with much fewer interfaces and a surface-based metallization procedure.[35]



DOI: 10.1021/acs.nanolett.8b00344
*Nano Lett.* 2018, 18, 2116−2123

Establishing metallic contacts at the particle−particle interfaces still remains a critical factor because many of the tested wires exhibited significantly reduced conductance values. Comprehensive temperature-dependent characterization of two more resistive wires revealed that the charge transport was dominated by a single effective energy barrier reflected by the single exponential decrease of the conductivity with reciprocal temperature. This suggests that the charge transport was dominated by a single nonmetallic interparticle interface that needed to be overcome by hopping at higher temperatures. The width of such nonmetallic gaps was presumably in the low nanometer range supported by the observation of tunneling dominating the charge transport at low temperatures for one of the tested wires.

Future work will focus on improving the perfection of the obtained wires by increasing the yield for establishing metallic interparticle contacts. Nonetheless, our results represent a considerable advancement in DNA-templated fabrication of electronic devices regarding the homogeneity and the potentially high conductivity of the obtained structures. Beyond that our approach, based on large DNA mold superstructures, opens a versatile route for self-assembly-based device fabrication. Using molds with different geometries (e.g., different diameters, additional docking sites, and junctions) and specific interfaces as well as different materials should enable the fabrication of whole devices including gate electrodes and even device networks.

**Methods.** *DNA-Origami Design, Assembly, and Analysis.* The DNA origami molds (Figures S8 and S9) were designed using CaDNAno[47] and comprised of parallel helices arranged in a square lattice.[48] Reverse-phase cartridge purified oligonucleotides for the DNA origami objects were purchased from Eurofins MWG Operon. Single-stranded p8064 scaffold DNA was purchased from Tilibit Nanosystems (Garching). The one-pot assembly reaction was performed as follows: the 10 nM scaffold p8064 was mixed in folding buffer containing 5 mM Tris−HCl, 1 mM ethylenediaminetetraacetic acid, and 11 mM $MgCl_2$ (pH 8.0) with unpurified staple strands and capture strands in a molar ratio of 1:10:1 (per individual sequence). The reaction was heated to 80 °C for 5 min and cooled to 25 °C over 15 h using a nonlinear temperature ramp, with the slowest temperature decrease occurring between 55 to 45 °C. The folded objects were investigated with gel-electrophoresis (1% agarose gel, 0.5× TBE, 11 mM $MgCl_2$, and 3.5 V/cm). Subsequently, the molds were purified using precipitation with polyethylene glycol to remove excess staples.[42] For TEM imaging, 2−3 μL of a diluted origami sample solution (1−2 nM) was applied to glow-discharged carbon-coated grids. The sample was subsequently stained using a filtered 2% solution of uranyl formate in 5 mM NaOH for 2 min. TEM imaging was performed in a Zeiss Libra 120 or a Phillips CM200 Ultra Twin transmission electron microscope at 80 or 120 kV, respectively.

*Decoration of DNA Molds with Gold Nanoparticle Seeds.* AuNPs (5 nm; Sigma-Aldrich) were densely coated with 15 nt poly thymidine oligonucleotides carrying a 5′-thiol modification as described before using the method of salt aging.[39,40,49] The particle concentration was estimated from the absorbance at 520 nm. DNA-functionalized gold nanoparticles were mixed with the purified DNA origami molds in the presence of 300 mM NaCl at a molar ratio of 3:1 or 6:1 for molds with one or two seed binding sites, respectively. The mixture was slowly heated to 40 °C and afterward cooled down to 23 °C over a duration of 5 h to allow hybridization of the AuNPs with the complementary capture strands on the mold.

*Formation of Linear-Mold Superstructures.* A pair of types of mold monomers (AB′ and BA′) were designed that only allow specific head-to-tail binding to the other monomer type (see Figures S8 and S9 for the design details of the mold ends). After preloading with seeds, both monomers were mixed in a 1:1 molar ratio and incubated for up to 24 h followed by a precipitation with PEG to remove excess seeds.

*Seeded Growth of Gold within Mold Superstructures.* The concentration of the mold superstructures was adjusted with folding buffer (see above), such that 1 nM mold monomers were present in solution, and hydroxyl amine ($NH_2OH$) was added at a 6-fold molar access over the subsequently added gold precursor. The gold growth was initiated by injecting 1×, 2×, or 4× of 0.9 μL of 25 mM $H[AuCl_4]$ into a 100 μL final volume of the $NH_2OH$-containing mold solution.[39] During growth, the solution was vigorously stirred, and after 1 min, the grown wires were deposited on TEM grids or $SiO_2$ substrates.

**Deposition of the Gold Nanowires on Wafer Substrates.** Grown gold nanowires were deposited on p-doped $Si/SiO_2$ (300 nm oxide layer) wafer substrates diced into 1 cm × 1 cm squares. The surface was treated with an $O_2$ plasma (PICO, Diener Electronic-Plasma Surface Technology) at 7 sccm $O_2$ and a power of 240W for 3 min to make the hydrophobic surface more hydrophilic (see Figure S10). The sample was rinsed with ethanol (20 s) and pure-membrane water (20 s). Subsequently, 20 μL of the nanowire sample were placed on the wafer surface for 1 h. Afterward, the substrate was dipped in a 1:1 mixture of ethanol and deionized water for 30 s. To remove the organic DNA layer around the nanowires, the sample was again subjected to $O_2$ plasma at 7 sccm $O_2$ and 300 W for 30 min.

**Electron-Beam Lithography and Electrical Measurements.** The electrical contact pads and markers were fabricated using electron beam lithography (RAITH e-line Plus). ZEP520 electron beam resist was spin-coated on the samples and baked at 150 °C for 10 min. The resist was exposed at a 35 $\mu C/cm^2$ area dose to define contact pads, markers, and small contacts. The resist was developed in n-Amyl acetate for 90s and subsequently in isopropanol for 30 s. A 5 nm Ti adhesion layer followed by a 100 nm gold layer were deposited at 0.2 and 2 Å/s with electron-beam evaporation (Bestec UHV Evaporation Tool). Lift-off was performed by immersion in ZDMAC (Dimethylacetamide) and subsequent washing with IPA, followed by drying in a $N_2$-stream. Electrical measurements were carried out using a semiconductor parameter analyzer (Agilent 4156-C) in vacuum ($10^{-5}$ mbar) and in the dark using two probes. A helium flow cryostat system was used for temperature-dependent electrical measurements. The samples were cooled to 4.2 K, and measurements were performed while heating up. $I-V$ measurements were performed by sweeping of the voltage (0 to 30 mV and 0 to −30 mV) or the current (0 to 1 μA and 0 to −1 μA) for resistive or conductive wires, respectively. The resistances or conductances of the were determined by least-squares fitting of a linear function to the measured $V-I$ or $I-V$ curves, respectively. For wires that showed nonlinear $I-V$ relations at low temperatures (RW-1 and RW-2), we determined the zero-bias resistance (conductance) as the slope of the curve at the inflection point near zero current (voltage).



DOI: 10.1021/acs.nanolett.8b00344
Nano Lett. 2018, 18, 2116−2123

## ■ ASSOCIATED CONTENT

### Supporting Information

The Supporting Information is available free of charge on the ACS Publications website at DOI: 10.1021/acs.nanolett.8b00344.

Figures showing additional electron microscopy micrographs, conductance measurements, temperature-dependent $I-V$ behavior, design templates for the origami mold construction, and contact angles and surface energies. (PDF)

## ■ AUTHOR INFORMATION


### Corresponding Authors

*E-mail: a.erbe@hzdr.de. Phone: +49-351-260-2366.
*E-mail: ralf.seidel@uni-leipzig.de. Phone: +49-341-97-32501.

### ORCID

Ralf Seidel: 0000-0002-6642-053X

### Present Address

[#]Department of Physics, University of Oxford, Oxford OX13PU, U.K.

### Author Contributions

[▽]T.B., S.H., and J.Y. contributed equally to the presented work.



### Funding

This work was supported by the Deutsche Forschungsgemeinschaft within the Cluster of Excellence Center for Advancing Electronics Dresden (cfaed/TU Dresden) as well as grant no. SE 1646/8-1 to R.S. and by the Helmholtz Association through IHRS for Nanoelectronic Networks NanoNet (VH-KO-606).


### Notes

The authors declare no competing financial interest.

## ■ ACKNOWLEDGMENTS


We gratefully acknowledge Martin Bähler, Oliver Oeckler, Roger Gläser, Marius Grundmann, Jörg Lenzner, Markus Löffler, and the Dresden Center for Nanoanalysis for access, training, and support with respect to TEM and SEM imaging. We furthermore acknowledge Matthias Krause, Angela Schneider, and Claudia Neisser for their help with and access to the drop-shape analysis system and the helium flow for the cryostat. We thank Peter Zahn for useful discussions on the data of the electrical measurements.


## ■ REFERENCES


(1) Rothemund, P. W. K. Folding DNA to create nanoscale shapes and patterns. *Nature* **2006**, *440*, 297−302.
(2) Douglas, S. M.; Dietz, H.; Liedl, T.; Högberg, B.; Graf, F.; Shih, W. M. Self-assembly of DNA into nanoscale three-dimensional shapes. *Nature* **2009**, *459*, 414−418.
(3) Seeman, N. C. Nanomaterials based on DNA. *Annu. Rev. Biochem.* **2010**, *79*, 65−87.
(4) Han, D.; Pal, S.; Nangreave, J.; Deng, Z.; Liu, Y.; Yan, H. DNA origami with complex curvatures in three-dimensional space. *Science* **2011**, *332*, 342−346.
(5) Wei, B.; Dai, M.; Yin, P. Complex shapes self-assembled from single-stranded DNA tiles. *Nature* **2012**, *485*, 623−626.
(6) Benson, E.; Mohammed, A.; Gardell, J.; Masich, S.; Czeizler, E.; Orponen, P.; Högberg, B. DNA rendering of polyhedral meshes at the nanoscale. *Nature* **2015**, *523*, 441−444.
(7) Kauert, D. J.; Kurth, T.; Liedl, T.; Seidel, R. Direct mechanical measurements reveal the material properties of three-dimensional DNA origami. *Nano Lett.* **2011**, *11*, 5558−5563.
(8) Mikkilä, J.; Eskelinen, A.-P.; Niemelä, E. H.; Linko, V.; Frilander, M. J.; Törmä, P.; Kostiainen, M. A. Virus-encapsulated DNA origami nanostructures for cellular delivery. *Nano Lett.* **2014**, *14*, 2196−2200.
(9) Voigt, N. V.; Tørring, T.; Rotaru, A.; Jacobsen, M. F.; Ravnsbaek, J. B.; Subramani, R.; Mamdouh, W.; Kjems, J.; Mokhir, A.; Besenbacher, F.; Gothelf, K. V. Single-molecule chemical reactions on DNA origami. *Nat. Nanotechnol.* **2010**, *5*, 200−203.
(10) Hemmig, E. A.; Creatore, C.; Wünsch, B.; Hecker, L.; Mair, P.; Parker, M. A.; Emmott, S.; Tinnefeld, P.; Keyser, U. F.; Chin, A. W. Programming Light-Harvesting Efficiency Using DNA Origami. *Nano Lett.* **2016**, *16*, 2369−2374.
(11) Steinhauer, C.; Jungmann, R.; Sobey, T. L.; Simmel, F. C.; Tinnefeld, P. DNA origami as a nanoscopic ruler for super-resolution microscopy. *Angew. Chem., Int. Ed.* **2009**, *48*, 8870−8873.
(12) Gür, F. N.; Schwarz, F. W.; Ye, J.; Diez, S.; Schmidt, T. L. Toward Self-Assembled Plasmonic Devices: High-Yield Arrangement of Gold Nanoparticles on DNA Origami Templates. *ACS Nano* **2016**, *10*, 5374−5382.
(13) Thacker, V. V.; Herrmann, L. O.; Sigle, D. O.; Zhang, T.; Liedl, T.; Baumberg, J. J.; Keyser, U. F. DNA origami based assembly of gold nanoparticle dimers for surface-enhanced Raman scattering. *Nat. Commun.* **2014**, *5*, 3448.
(14) Kuzyk, A.; Schreiber, R.; Fan, Z.; Pardatscher, G.; Roller, E.-M.; Högele, A.; Simmel, F. C.; Govorov, A. O.; Liedl, T. DNA-based self-assembly of chiral plasmonic nanostructures with tailored optical response. *Nature* **2012**, *483*, 311−314.
(15) Yang, Y.; Wang, J.; Shigematsu, H.; Xu, W.; Shih, W. M.; Rothman, J. E.; Lin, C. Self-assembly of size-controlled liposomes on DNA nanotemplates. *Nat. Chem.* **2016**, *8*, 476−483.
(16) Czogalla, A.; Kauert, D. J.; Franquelim, H. G.; Uzunova, V.; Zhang, Y.; Seidel, R.; Schwille, P. Amphipathic DNA origami nanoparticles to scaffold and deform lipid membrane vesicles. *Angew. Chem., Int. Ed.* **2015**, *54*, 6501−6505.
(17) Livshits, G. I.; Stern, A.; Rotem, D.; Borovok, N.; Eidelshtein, G.; Migliore, A.; Penzo, E.; Wind, S. J.; Di Felice, R.; Skourtis, S. S.; Cuevas, J. C.; Gurevich, L.; Kotlyar, A. B.; Porath, D. Long-range charge transport in single G-quadruplex DNA molecules. *Nat. Nanotechnol.* **2014**, *9*, 1040−1046.
(18) Seidel, R.; Ciacchi, L. C.; Weigel, M.; Pompe, W.; Mertig, M. Synthesis of platinum cluster chains on DNA templates: Conditions for a template-controlled cluster growth. *J. Phys. Chem. B* **2004**, *108*, 10801−10811.
(19) Braun, E.; Eichen, Y.; Sivan, U.; Ben-Yoseph, G. DNA-templated assembly and electrode attachment of a conducting silver wire. *Nature* **1998**, *391*, 775−778.
(20) Mertig, M.; Ciacchi, L. C.; Seidel, R.; Pompe, W.; De Vita, A. DNA as a selective metallization template. *Nano Lett.* **2002**, *2*, 841−844.
(21) Wirges, C. T.; Timper, J.; Fischler, M.; Sologubenko, A. S.; Mayer, J.; Simon, U.; Carell, T. Controlled nucleation of DNA metallization. *Angew. Chem., Int. Ed.* **2009**, *48*, 219−223.
(22) Teschome, B.; Facsko, S.; Schönherr, T.; Kerbusch, J.; Keller, A.; Erbe, A. Temperature-Dependent Charge Transport through Individually Contacted DNA Origami-Based Au Nanowires. *Langmuir* **2016**, *32*, 10159−10165.
(23) Schreiber, R.; Kempter, S.; Holler, S.; Schüller, V.; Schiffels, D.; Simmel, S. S.; Nickels, P. C.; Liedl, T. DNA origami-templated growth of arbitrarily shaped metal nanoparticles. *Small* **2011**, *7*, 1795−1799.
(24) Liu, J.; Geng, Y.; Pound, E.; Gyawali, S.; Ashton, J. R.; Hickey, J.; Woolley, A. T.; Harb, J. N. Metallization of branched DNA origami for nanoelectronic circuit fabrication. *ACS Nano* **2011**, *5*, 2240−2247.
(25) Schreiber, R.; Do, J.; Roller, E.-M.; Zhang, T.; Schüller, V. J.; Nickels, P. C.; Feldmann, J.; Liedl, T. Hierarchical assembly of metal nanoparticles, quantum dots and organic dyes using DNA origami scaffolds. *Nat. Nanotechnol.* **2014**, *9*, 74−78.
(26) Uprety, B.; Gates, E. P.; Geng, Y.; Woolley, A. T.; Harb, J. N. Site-specific metallization of multiple metals on a single DNA origami template. *Langmuir* **2014**, *30*, 1134−1141.




DOI: 10.1021/acs.nanolett.8b00344
*Nano Lett.* 2018, 18, 2116−2123

(27) Richter, J.; Seidel, R.; Kirsch, R.; Mertig, M.; Pompe, W.; Plaschke, J.; Schackert, H. K. Nanoscale palladium metallization of DNA. *Adv. Mater.* **2000**, *12*, 507−510.
(28) Tian, C.; Cordeiro, M. A. L.; Lhermitte, J.; Xin, H. L.; Shani, L.; Liu, M.; Ma, C.; Yeshurun, Y.; DiMarzio, D.; Gang, O. Supra-Nanoparticle Functional Assemblies through Programmable Stacking. *ACS Nano* **2017**, *11*, 7036.
(29) Richter, J.; Mertig, M.; Pompe, W.; Mönch, I.; Schackert, H. K. Construction of highly conductive nanowires on a DNA template. *Appl. Phys. Lett.* **2001**, *78*, 536−538.
(30) Lund, J.; Dong, J.; Deng, Z.; Mao, C.; Parviz, B. A. Electrical conduction in 7 nm wires constructed on λ-DNA. *Nanotechnology* **2006**, *17*, 2752.
(31) Geng, Y.; Pearson, A. C.; Gates, E. P.; Uprety, B.; Davis, R. C.; Harb, J. N.; Woolley, A. T. Electrically conductive gold- and copper-metallized DNA origami nanostructures. *Langmuir* **2013**, *29*, 3482−3490.
(32) Pearson, A. C.; Liu, J.; Pound, E.; Uprety, B.; Woolley, A. T.; Davis, R. C.; Harb, J. N. DNA origami metallized site specifically to form electrically conductive nanowires. *J. Phys. Chem. B* **2012**, *116*, 10551−10560.
(33) Park, S. H.; Prior, M. W.; LaBean, T. H.; Finkelstein, G. Optimized fabrication and electrical analysis of silver nanowires templated on DNA molecules. *Appl. Phys. Lett.* **2006**, *89*, 033901.
(34) Harnack, O.; Ford, W. E.; Yasuda, A.; Wessels, J. M. Tris(hydroxymethyl)phosphine-capped gold particles templated by DNA as nanowire precursors. *Nano Lett.* **2002**, *2*, 919−923.
(35) Uprety, B.; Westover, T.; Stoddard, M.; Brinkerhoff, K.; Jensen, J.; Davis, R. C.; Woolley, A. T.; Harb, J. N. Anisotropic Electroless Deposition on DNA Origami Templates To Form Small Diameter Conductive Nanowires. *Langmuir* **2017**, *33*, 726−735.
(36) Wong, K. K.; Mann, S. Biomimetic synthesis of cadmium sulfide-ferritin nanocomposites. *Adv. Mater.* **1996**, *8*, 928−932.
(37) Balci, S.; Hahn, K.; Kopold, P.; Kadri, A.; Wege, C.; Kern, K.; Bittner, A. M. Electroless synthesis of 3 nm wide alloy nanowires inside Tobacco mosaic virus. *Nanotechnology* **2012**, *23*, 045603.
(38) Sun, W.; Boulais, E.; Hakobyan, Y.; Wang, W. L.; Guan, A.; Bathe, M.; Yin, P. Casting inorganic structures with DNA molds. *Science* **2014**, *346*, 1258361.
(39) Helmi, S.; Ziegler, C.; Kauert, D. J.; Seidel, R. Shape-controlled synthesis of gold nanostructures using DNA origami molds. *Nano Lett.* **2014**, *14*, 6693−6698.
(40) Ding, B.; Deng, Z.; Yan, H.; Cabrini, S.; Zuckermann, R. N.; Bokor, J. Gold nanoparticle self-similar chain structure organized by DNA origami. *J. Am. Chem. Soc.* **2010**, *132*, 3248−3249.
(41) Zhao, Z.; Jacovetty, E. L.; Liu, Y.; Yan, H. Encapsulation of gold nanoparticles in a DNA origami cage. *Angew. Chem., Int. Ed.* **2011**, *50*, 2041−2044.
(42) Stahl, E.; Martin, T. G.; Praetorius, F.; Dietz, H. Facile and scalable preparation of pure and dense DNA origami solutions. *Angew. Chem., Int. Ed.* **2014**, *53*, 12735−12740.
(43) Seol, S. K.; Kim, D.; Jung, S.; Chang, W. S.; Kim, J. T. One-step synthesis of PEG-coated gold nanoparticles by rapid microwave heating. *J. Nanomater.* **2013**, *2013*.110.1155/2013/531760
(44) Morris, J.; Coutts, T. Electrical conduction in discontinuous metal films: A discussion. *Thin Solid Films* **1977**, *47*, 3−65.
(45) Barwinski, B. Temperature dependence of electrical conduction in discontinuous gold films on sapphire substrates. *Thin Solid Films* **1985**, *128*, 1−9.
(46) Brust, M.; Bethell, D.; Kiely, C. J.; Schiffrin, D. J. Self-Assembled Gold Nanoparticle Thin Films with Nonmetallic Optical and Electronic Properties. *Langmuir* **1998**, *14*, 5425−5429.
(47) Douglas, S. M.; Marblestone, A. H.; Teerapittayanon, S.; Vazquez, A.; Church, G. M.; Shih, W. M. Rapid prototyping of 3D DNA-origami shapes with caDNAno. *Nucleic Acids Res.* **2009**, *37*, 5001−5006.
(48) Ke, Y.; Douglas, S. M.; Liu, M.; Sharma, J.; Cheng, A.; Leung, A.; Liu, Y.; Shih, W. M.; Yan, H. Multilayer DNA origami packed on a square lattice. *J. Am. Chem. Soc.* **2009**, *131*, 15903−15908.
(49) Hill, H. D.; Mirkin, C. A. The bio-barcode assay for the detection of protein and nucleic acid targets using DTT-induced ligand exchange. *Nat. Protoc.* **2006**, *1*, 324−336.



DOI: 10.1021/acs.nanolett.8b00344
*Nano Lett.* 2018, 18, 2116−2123

# 5. DNA-mediated Fabrication of Defined Semiconductor Nanorod Assemblies

## 5.1 Introduction

For emerging applications in nanoelectronics, nanooptics, and photocatalysis, an important material is semiconducting nanostructures with interesting anisotropic electronic and optical properties. So far, the DNA-based arrangement of semiconducting nanostructures was limited by the lack of a DNA-compatible functionalization.

In this chapter, an easily applicable method for the synthesis and DNA functionalization of semiconducting nanorods was established. The achieved high functionalization densities allowed assembling the nanorods at defined docking positions on the modular platform with a yield of up to 90%. Utilizing the mold-based modular platform, the formation of nanorod dimers with defined relative orientations as well as the dimerization of the mold element via a single semiconducting nanorod were demonstrated. Furthermore, metal-semiconductor heterostructures were formed by positioning both the semiconducting nanorods and the gold nanoparticles at defined locations on the platform. By using an electroless gold deposition, a direct metal-semiconductor interface was achieved which is a key component in nanoelectronic applications.

The achieved DNA functionalization of semiconducting rods can be further applied to other similar materials. This highly efficient approach of DNA-based integration of semiconducting nanorods into DNA origami structures provides a crucial basis to employ semiconductors in self-assembly structures for optical and electronic devices fabrication.

## 5.2 Associated Publication P3

**DNA-Mediated Self-Assembly and Metallization of Semiconductor Nanorods for the Fabrication of Nanoelectronic Interfaces**

by

Richard Weichelt,* Jingjing Ye,* Uri Banin, Alexander Eychmüller, Ralf Seidel

*equal contribution

published in

CHEMISTRY-A European Journal 2019, 25, 9012-9016

ChemPubSoc Europe

DOI: 10.1002/chem.201902148

CHEMISTRY A European Journal Communication

Nanomaterials

# DNA-Mediated Self-Assembly and Metallization of Semiconductor Nanorods for the Fabrication of Nanoelectronic Interfaces

Richard Weichelt[+],[a] Jingjing Ye[+],[b] Uri Banin,[c] Alexander Eychmüller,*[a] and Ralf Seidel*[b]

**Abstract:** DNA nanostructures provide a powerful platform for the programmable assembly of nanomaterials. Here, this approach is extended to semiconductor nanorods that possess interesting electrical properties and could be utilized for the bottom-up fabrication of nanoelectronic building blocks. The assembly scheme is based on an efficient DNA functionalization of the nanorods. A complete coverage of the rod surface with DNA ensures a high colloidal stability while maintaining the rod size and shape. It furthermore supports the assembly of the nanorods at defined docking positions of a DNA origami platform with binding efficiencies of up to 90% as well as the formation of nanorod dimers with defined relative orientations. By incorporating orthogonal binding sites for gold nanoparticles, defined metal-semiconductor heterostructures can be fabricated. Subsequent application of a seeded growth procedure onto the gold nanoparticles (AuNPs) allows for to establish a direct metal-semiconductor interface as a crucial basis for the integration of semiconductors in self-assembled nanoelectronic devices.

The bottom-up fabrication of programmable frameworks and building blocks by using complementary DNA base-pairing enabled the construction of nanomaterial systems with tightly controlled dimensions, stoichiometries, orientations, shapes and compositions.[1–3] The versatility of this concept has raised interest in areas that are typically covered by top-down methods, such as lithography processes for the fabrication of nanoelectronic elements. In the near future, combined top-down and bottom-up methods could be a promising way to realize the implementation into real-world applications.[4] In particular, recent developments in DNA nanotechnology, such as the DNA origami technique,[5] provided a straightforward route to fabricate 2D[6] and 3D[7] scaffolds that allowed for a precise arrangement of different materials through DNA-strand hybridization. Prominent examples include the demonstration of an DNA-templated carbon nanotube field-effect transistor[8] and the assembly of conductive gold nanowires.[9–11] To this end, one-dimensional semiconductor nanorods (SC NRs) are another promising material type, due to their synthetically designable anisotropic optical[12–14] and electrical[15,16] properties. DNA origami can serve as molecular breadboards for the precise arrangement of these SC NRs with defined spatial orientation and interparticle distances and allow for the construction of more complex nanoscale structures, including metal-SC heterostructures. Various approaches for the DNA-functionalization of zero-dimensional SC nanoparticles, so-called quantum dots (QDs) and their assembly onto DNA origami have been already developed.[17–22] However, these studies focused on their optical rather than electrical applications. Additionally, the elongated shape of SC NRs is more suitable to align these structures and establish electrical contacts through metal tips at the NR ends.[23] So far, only one study tried to assemble SC NRs onto DNA origami to investigate their optical properties but suffered from low oligonucleotide conjugation numbers, poor colloidal stability and reduced origami attachment yields.[24] In our study, we propose a new approach towards the DNA-mediated assembly of SC NRs. Particularly, we present a straightforward protocol for the synthesis and oligonucleotide functionalization of SC NRs to enable their self-assembly onto DNA origami structures at defined docking positions (Figure 1). Based on the precise arrangement of the NRs with high binding efficiencies, we also demonstrate the assembly of linear Au NP–SC NR heterostructures. These structures then undergo an electroless gold deposition process to form direct nanoscale metal-SC interfaces that could facilitate their integration into nanoelectronics applications.

To fabricate DNA-functionalized SC NRs, we employed a multistep procedure (Figure 1). Initially, CdS NRs were synthesized by using a two-step seeded growth protocol, adapted from the literature.[25] An elongated CdS shell was formed around a spherical CdS core particle. Thereby, phosphonic acids acted as ligands to stabilize the NRs and to induce a preferential shell growth along the *c* axis of the crystal lattice. Due to the high reaction temperature of 350 °C, the NRs gained a defined crystal structure and a uniform shape with narrow size distribution. As depicted in the corresponding TEM image (Figure 2a), a

[a] *R. Weichelt,[+] Prof. Dr. A. Eychmüller*
*Physical Chemistry, Center for Advancing Electronics Dresden (cfaed)*
*TU Dresden, 01069 Dresden (Germany)*
*E-mail: alexander.eychmüller@tu-dresden.de*

[b] *J. Ye,[+] Prof. Dr. R. Seidel*
*Peter Debye Institute for Soft Matter Physics*
*Center for Advancing Electronics Dresden (cfaed), Universität Leipzig*
*04103 Leipzig (Germany)*
*E-mail: ralf.seidel@physik.uni-leipzig.de*

[c] *Prof. Dr. U. Banin*
*Institute of Chemistry and Center for Nanoscience and Nanotechnology*
*The Hebrew University, Jerusalem, 91904 (Israel)*

[+] *These authors contributed equally to this work.*

*Supporting information and the ORCID identification number(s) for the author(s) of this article can be found under: https://doi.org/10.1002/chem.201902148.*

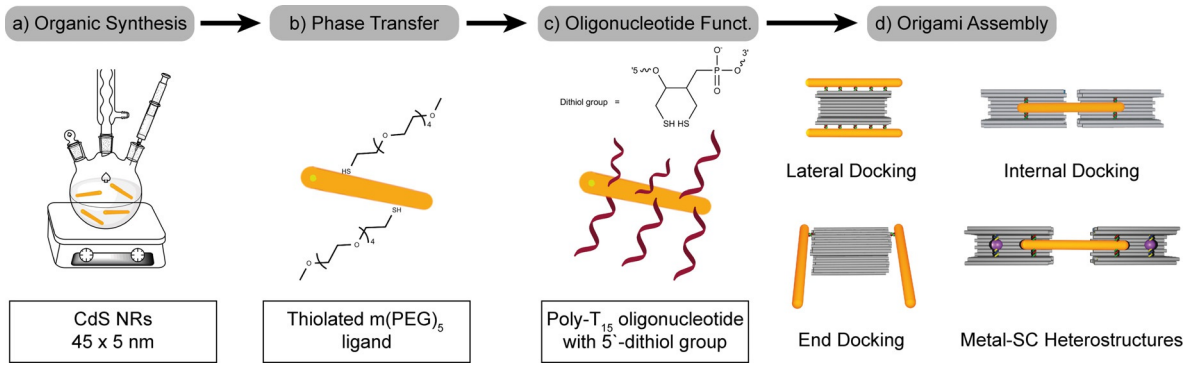


**Figure 1.** Fabrication scheme of the defined assemblies of SC NRs. (a) Synthesis of CdS NRs. (b) Phase transfer into water by using dithiolated $m(PEG)_5$ oligomers. (c) Oligonucleotide functionalization with dithiolated poly-$T_{15}$ to fully cover the NRs. (d) Arrangement of Poly-$T_{15}$@CdS at defined positions on a DNA origami mold platform, including the lateral docking, end docking and internal docking. Molds preloaded with AuNPs provide the formation of metal-SC heterostructures.

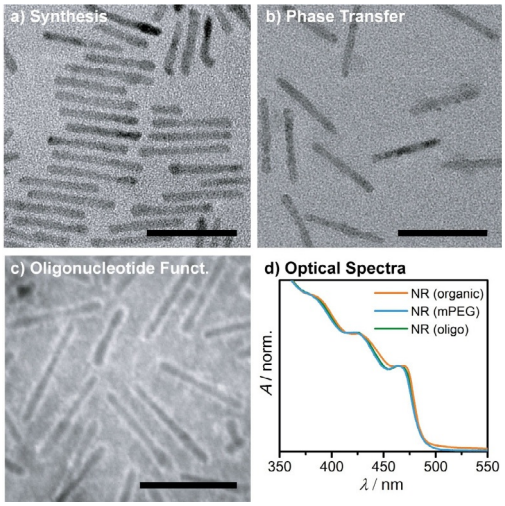


**Figure 2.** TEM images of CdS NRs after (a) organic synthesis with dimensions of 45×5 nm, (b) functionalization with m(PEG) and phase transfer into aqueous medium at preserved size and shape and (c) functionalization with a dense poly-$T_{15}$ oligonucleotide brush being visible due to a negative stain of the sample. Scale bars in all TEM images are 50 nm. (d) Absorbance spectra of the samples shown in (a)–(c).

typical synthesis yielded NRs with an aspect ratio of nine and dimensions of 45×5 nm. To facilitate the oligonucleotide functionalization and to allow for their attachment to origami platforms, the NRs had to be transferred from the organic to the aqueous phase. This required an exchange of the organic ligands of the NRs with water soluble molecules that would support a high stability in aqueous buffer solutions at a pH ranging from 7 to 8 in the presence of considerable concentrations of magnesium and sodium ions (up to 12 and 350 mM, respectively). Carboxylic acids, like MPA (mercaptopropionic acid or MUA (mercaptoundecanoic acid), and glutathione are typically excellent candidates for the transfer of organic SC NRs to the aqueous phase.[26]

Unfortunately, nanomaterials prepared with these ligands tend to aggregate under the required ionic conditions due to the coordination of magnesium ions with the carboxylic acid groups on the particle surface.[27] Alternatively, functionalized polymers that form a very dense ligand shell can prevent aggregation and provide higher stability. Known examples include polyethylene-glycol (PEG) and polyethylenimine (PEI) for the stabilization of AuNPs[28] and SC NRs.[26] The thicker ligand shell and the stronger attachment of the polymers to the NR surface may, however, significantly reduce the efficiency of a subsequent oligonucleotide functionalization. We thus combined the advantages of short thiolated molecules with the chemical inertness and colloidal stability of polymer coated NRs and used a short-length methoxy PEG5 Thiol $(mPEG)_5$ ligand for a fast and reproducible phase transfer. Following the successful ligand exchange, CdS NRs were transferred to 0.5× Tris-HCl buffer and diluted to a final concentration of approximately150 nM to test their stability in the aqueous phase. After 24-h storage at room temperature, absorbance spectra were recorded (Figure 2d, blue line) and compared to the spectra of NRs dissolved in toluene (orange line). No significant changes of the optical properties were detected. A minor blueshift of 6 nm was possibly due to the increased removal of larger NRs during multiple filtration steps. The stability of the NRs in the aqueous medium was confirmed by TEM images that displayed NRs with maintained size and shape (Figure 2b). In fact, CdS NRs that were passivated with mPEG-SH maintained their colloidal stability for more than two years without changes of their optical properties. After the phase transfer the NRs were functionalized, by using dithiol-modified DNA oligonucleotides containing fifteen thymine bases (poly-$T_{15}$). Two thiol groups per DNA strand can increase the overall binding efficiency at the particle surface as well as the stability of the formed bond compared to a monothiol group.[29] Considering that the CdS NRs already carried thiolated mPEG molecules on their surface, the dithiol functionalization of the DNA oligonucleotide was important to ensure an efficient ligand replacement. Following the oligonucleotide functionalization, including a so-called salt aging step with sodium chloride and overnight incubation, oligonucleotide functionalized NRs were purified through multiple filtration steps (see the experimental section of the Supporting Information). The recorded absorbance spectra (see Figure 2d, green line) indicated no changes in size, morphology as well as optical properties of the DNA functionalized NRs.

Due to the high extinction coefficient of the NRs at wavelengths $<400$ nm, and the absorbance of the oligonucleotides is at 260 nm, hence the final DNA concentration could not be obtained directly. To estimate the number of oligonucleotides attached to the NR surface, we collected the excess of unbound oligonucleotides after the functionalization and measured their concentration from the absorbance spectra. An approximately 50% reduced concentration of the excess oligonucleotides compared to the initially added oligonucleotides, indicated that about 250 oligonucleotides were bound to each NR. Given a surface area of around 760 $nm^2$ for a single NR, each oligonucleotide thus occupied an average area of approximately 3 $nm^2$. These results agreed with TEM images of the stained functionalized NR sample (Figure 2c), that displayed a dense oligonucleotide brush on the NR surface.

We next tested whether the freshly functionalized NRs can be bound on a DNA origami platform at defined positions (see scheme in Figure 1d). The origami structure was a so-called DNA mold, being a tube with quadratic cross section composed of 64 helices with outer dimensions of $25\times25\times40$ nm and a cavity of $15\times15\times40$ nm (for details see Supporting Information Figure S8–S10).[9] Complementary poly-$A_{15}$ capture strands were incorporated at specific positions on the out- or inside of the mold to allow binding of the functionalized NRs. In total, two different external and one internal binding configurations were introduced. The first tested external configuration carried out was a so-called lateral docking (Figure 3a,b), in which five capture strands were placed alongside a mold sidewall. For a one-sided lateral docking the capture strands were located only on one side wall, whereas for a two-sided lateral docking, yielding a parallel alignment of two NRs, two opposite side walls were modified. The NRs were incubated with the corresponding mold platform in an approximately 2:1 excess over NR binding sites. TEM imaging revealed that a lateral attachment of the NRs along the side wall and approximately parallel to the long axis of the origami structure could be achieved. Average binding efficiencies were determined from the overview TEM images (Figures S3–S6, Supporting Information). They were calculated as the percentage of filled docking positions on the origami platforms including occasional docking events where a single NR connected two origami. The obtained binding efficiencies for lateral docking reached $90\pm2\%$ ($N=566$) for both configurations. The second tested external binding configuration was end docking (Figure 3c,d) of NRs to a mold structure that was equipped with two capture strands on one or both ends, respectively. For end docking the average binding efficiencies reached also $90\pm3\%$ ($N=376$). Occasionally, the formation of short mold-NR chains was observed that could be prevented by increasing the proportion of the NRs and diluting the assembly solution (see Figures S5 and S6, Supporting Information). An internal docking was realized by placing four capture strands in the center of the mold cavity, such that one NR can either bind to one mold and form a NR-mold monomer or bind to two molds to form a dimer structure (Figure 3e,f). On average $80\pm7\%$ ($N=404$) of the molds had at least one NR internally attached. Out of these molds 20% were mold dimer structures (Figure 3f). As a control, we tested the binding of the functionalized NRs to

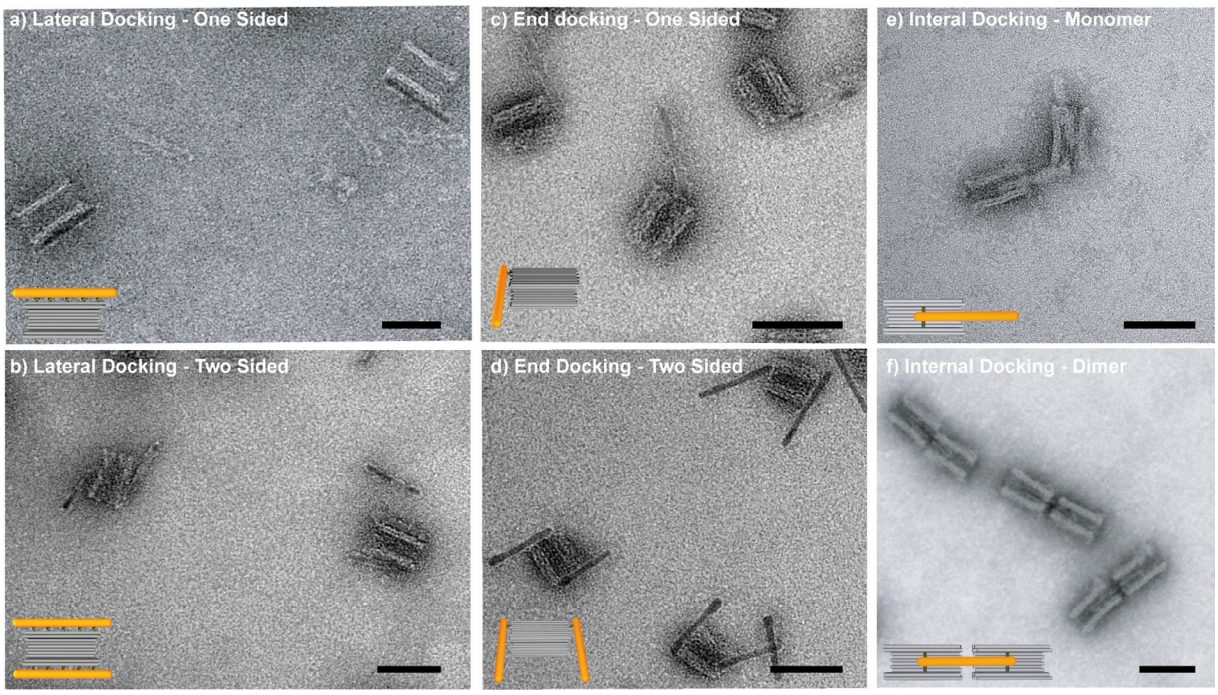


**Figure 3.** Representative TEM images displaying Poly-$T_{15}$@CdS NRs assembled onto DNA origami molds platforms. Different positions of capture strands allow different NR arrangements incl. (a) lateral docking to one mold wall (b) lateral docking to two opposite mold walls, (c) docking to a single mold end (d) docking to two mold ends, (e) internal NR binding with a single end (f) internal binding of both nanorod ends to two molds. Note that the tips of internally bound Poly-$T_{15}$@CdS NRs are precisely positioned in the middle of the mold cavity. Scale bars in all TEM images are 50 nm.

mold structures without poly-$A_{15}$ capture strand (Figure S2, Supporting Information). No binding was observed in this sample, that is, NR-mold binding stringently depends on the specific interactions to the introduced capture strands. Despite an excess of NRs that each carried a dense oligonucleotide brush, the binding efficiency for internal docking was significantly lower than for external docking. This suggests a limited accessibility of the internal compared to the external docking sites. Clearly, the surrounding mold walls will lower the probability of a random encounter between the internal capture strands and the NRs.[30]

Recently, we demonstrated, however, that the decoration of molds chains with AuNPs at efficiencies of 96±2% by using identical internal positions of capture strands.[9] We therefore attribute the limited accessibility to the internal docking sites to the anisotropic NR geometry. Compared to the spherical shape of a 5 nm AuNP, an elongated NR can only enter the mold cavity if it is oriented approximately parallel to the long axis of the mold. We think that this required orientational alignment strongly limits the assembly kinetics such that internal docking of SC NRs remains less efficient compared to external docking at the applied time scales. After demonstrating the SC NR docking at different positions of the origami platform, we tested whether our assembly scheme would also allow for attachment of additional objects at the orthogonal binding sites of the mold platform. Particularly, we probed the binding of AuNPs to form metal-SC heterostructures. To this end, an internal binding site for an AuNP by using a modified capture strand sequence different from CdS NR was placed in close proximity to an internal CdS NR binding site (Figure 4a).

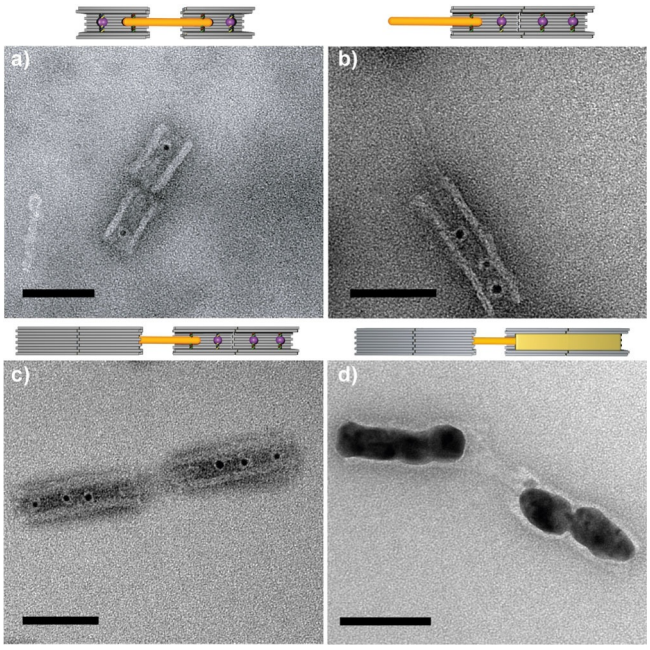


**Figure 4.** TEM images of self-assembled metal-SC heterostructures. (a) SC NR bound at either end to an AuNP preloaded mold monomer. (b,c) SC NRs bound at one or both ends to preformed mold dimers that were loaded with three AuNPs. (d) Structure shown in (c) after seeded gold growth. Scale bars in all TEM images are 50 nm.

After incubation of the molds with DNA functionalized AuNPs, TEM imaging (Figure S7, Supporting Information) confirmed that AuNPs attached only to one side of the mold cavity. Subsequently, the DNA functionalized NRs were added to the AuNP decorated structures, such that molds decorated with both particle types were obtained (Figure 4a). The decoration yield of the NR docking sites in the heterostructures was 70± 7% ($N$=510), that is, only slightly reduced compared to the simple internal NR docking. The additional blocking of one side of the mold cavity by the AuNP may explain the binding efficiency decrease, as well as the reduced percentage of mold dimer heterostructures to 10% (Figure 4a). The distance between the AuNPs and CdS NRs inside the mold was between 5–10 nm, which coincides with the designed capture strand positions. The bound AuNPs in the mold cavity allowed the SC NRs to enter from only one mold end which was proximal to the NR docking side. This provided a defined mold end on the AuNP side. By using end-to-end docking,[31] it should then allow for the structures to bind additional origami structures at the AuNP side. This would provide an increased complexity as well as allowing for an interfacing of the metal-SC heterostructures. To test this, mold ends on the AuNP side were extended by one additional origami mold that contained two AuNPs (Figure S7, Supporting Information). The specific interface design limited the extension to only a single mold. After assembly, SC NRs were found carrying either two AuNP-decorated molds on a single (Figure 4b) or at both ends (Figure 4c). All together the final structures contained one NR and either two molds with three AuNPs or four molds with six AuNPs. By using conventional synthesis approaches, Au island can be grown on the tips of SC NRs, yet they cannot exceed diameters larger than 3–5 nm without starting to cover the NR sides or without dissolution of one Au island due to Ostwald ripening.[32] The addition of 5 nm AuNPs in short distance to the NR tips allows for the growth of much larger Au contacts with a direct metal SC connection. To this end, we adapted a seeded growth procedure for AuNPs inside DNA molds[9,33] and applied it to the heterostructures. TEM imaging (Figure 4d) revealed an equal growth of the AuNPs to final diameters of 15–22 nm and formation of contacts between the metallic parts and the SC NR. We anticipate that the arrangement of the growing AuNPs is constrained by the mold sidewalls, which allows the outer AuNPs to push the inner ones closer to the NR tip. The reduced distance supports the merging of the NR tips with the growing AuNP. At the same time, the growth of small Au islands on the NR is prevented because most of the gold precursor is consumed by the large AuNPs.

In summary, we presented a new approach for the oligonucleotide functionalization of CdS NRs. The implementation of a robust phase transfer to the aqueous phase by using short thiolated mPEG molecules ensured a high colloidal stability of the CdS NRs. This enabled the usage of the NRs in DNA-origami-mediated self-assembly approaches. Dithiolated oligonucleotides formed a dense brush around the NRs, which allowed for a successful assembly onto five different DNA origami structures with binding efficiencies of 90 and 80% for external and internal docking, respectively. The obtained structures

could further be loaded with AuNPs such that defined metal-SC heterostructures were obtained. By using seeded growth, gold contacts were grown at the NR tips that were large enough to be interfaced with conventional top-down procedures. In general, the flexibility of our modular mold approach would enable the incorporation of additional molds or other materials, which potentially allows for a self-assembly of nanoelectronic device structures. Our functionalization protocol has also the potential to be adapted for other materials.

## *Acknowledgements*

This work was supported by the Deutsche Forschungsgemeinschaft within the Cluster of Excellence Center for Advancing Electronics Dresden (cfaed/TU Dresden) as well as grant SE 1646/8-1 to R.S. We gratefully acknowledge Markus Löffler and the Dresden Center for Nanoanalysis for access, training and support for the TEM imaging.

## Conflict of interest

The authors declare no conflict of interest.

**Keywords:** DNA origami · metallization · nanoelectronics · nanorods · self-assembly

[1] N. Liu, T. Liedl, *Chem. Rev.* **2018**, *118*, 3032 – 3053.
[2] F. Hong, F. Zhang, Y. Liu, H. Yan, *Chem. Rev.* **2017**, *117*, 12584 – 12640.
[3] K. F. Wagenbauer, C. Sigl, H. Dietz, *Nature* **2017**, *552*, 78 – 83.
[4] E. P. Gates, A. M. Dearden, A. T. Woolley, *Crit. Rev. Anal. Chem.* **2014**, *44*, 354 – 370.
[5] P. W. K. Rothemund, *Nature* **2006**, *440*, 297 – 302.
[6] Z. Zhao, Y. Liu, H. Yan, *Nano Lett.* **2011**, *11*, 2997 – 3002.
[7] E. S. Andersen, M. Dong, M. M. Nielsen, K. Jahn, R. Subramani, W. Mamdouh, M. M. Golas, B. Sander, H. Stark, C. L. P. Oliveira, J. S. Pedersen, V. Birkedal, F. Besenbacher, K. V. Gothelf, J. Kjems, *Nature* **2009**, *459*, 73.
[8] K. Keren, R. S. Berman, E. Buchstab, U. Sivan, E. Braun, *Science* **2003**, *302*, 1380 – 1382.
[9] T. Bayrak, S. Helmi, J. Ye, D. Kauert, J. Kelling, T. Schönherr, R. Weichelt, A. Erbe, R. Seidel, *Nano Lett.* **2018**, *18*, 2116 – 2123.
[10] B. Uprety, J. Jensen, B. R. Aryal, R. C. Davis, A. T. Woolley, J. N. Harb, *Langmuir* **2017**, *33*, 10143 – 10152.
[11] A. Stern, G. Eidelshtein, R. Zhuravel, G. I. Livshits, D. Rotem, A. Kotlyar, D. Porath, *Adv. Mater.* **2018**, *30*, 1800433.
[12] H. Pühringer, J. Roither, M. V. Kovalenko, M. Eibelhuber, T. Schwarzl, D. V. Talapin, W. Heiss, *Appl. Phys. Lett.* **2010**, *97*, 111115.
[13] Y. E. Panfil, M. Oded, U. Banin, *Angew. Chem. Int. Ed.* **2018**, *57*, 4274 – 4295; *Angew. Chem.* **2018**, *130*, 4354 – 4376.
[14] A. Sitt, I. Hadar, U. Banin, *Nano Today* **2013**, *8*, 494 – 513.
[15] R. Krahne, G. Morello, A. Figuerola, C. George, S. Deka, L. Manna, *Phys. Rep.* **2011**, *501*, 75 – 221.
[16] P.-E. Trudeau, M. Sheldon, V. Altoe, A. P. Alivisatos, *Nano Lett.* **2008**, *8*, 1936 – 1939.
[17] A. Banerjee, T. Pons, N. Lequeux, B. Dubertret, *Interface Focus* **2016**, *6*, 20160064.
[18] J. B. Blanco-Canosa, M. Wu, K. Susumu, E. Petryayeva, T. L. Jennings, P. E. Dawson, W. R. Algar, I. L. Medintz, *Coord. Chem. Rev.* **2014**, *263*, 101 – 137.
[19] A. Banerjee, C. Grazon, B. Nadal, T. Pons, Y. Krishnan, B. Dubertret, *Bioconjugate Chem.* **2015**, *26*, 1582 – 1589.
[20] R. Weichelt, S. Leubner, A. Henning-Knechtel, M. Mertig, N. Gaponik, T.-L. Schmidt, A. Eychmüller, *Small* **2016**, *12*, 4763 – 4771.
[21] A. Samanta, Z. Deng, Y. Liu, *Nanoscale* **2014**, *6*, 4486 – 4490.
[22] M. Rahman, D. Neff, M. L. Norton, *Chem. Commun.* **2014**, *50*, 3413 – 3416.
[23] M. T. Sheldon, P.-E. Trudeau, T. Mokari, L.-W. Wang, A. P. Alivisatos, *Nano Lett.* **2009**, *9*, 3676 – 3682.
[24] T. L. Doane, R. Alam, M. M. Maye, *Nanoscale* **2015**, *7*, 2883 – 2888.
[25] Y. Ben-Shahar, F. Scotognella, I. Kriegel, L. Moretti, G. Cerullo, E. Rabani, U. Banin, *Nat. Commun.* **2016**, *7*, 10413.
[26] Y. Ben-Shahar, F. Scotognella, N. Waiskopf, I. Kriegel, S. Dal Conte, G. Cerullo, U. Banin, *Small* **2015**, *11*, 462 – 471.
[27] A. Kondoh, T. Oi, *Z. Naturforsch.* **1997**, *52a*, 351 – 357.
[28] R. Wang, I. Bowling, W. Liu, *RSC Adv.* **2017**, *7*, 3676 – 3679.
[29] B. C. Mei, E. Oh, K. Susumu, D. Farrell, T. J. Mountziaris, H. Mattoussi, *Langmuir* **2009**, *25*, 10604 – 10611.
[30] M. T. Strauss, F. Schueder, D. Haas, P. C. Nickels, R. Jungmann, *Nat. Commun.* **2018**, *9*, 1600.
[31] J. Ye, S. Helmi, J. Teske, R. Seidel, *Nano Lett.* **2019**, *19*, 2707 – 2714.
[32] T. Mokari, C. G. Sztrum, A. Salant, E. Rabani, U. Banin, *Nat. Mater.* **2005**, *4*, 855 – 863.
[33] S. Helmi, C. Ziegler, D. J. Kauert, R. Seidel, *Nano Lett.* **2014**, *14*, 6693 – 6698.

Manuscript received: May 9, 2019
Accepted manuscript online: May 13, 2019
Version of record online: June 6, 2019

# 6. Conclusion and Outlook

Subject of this thesis was the development of a modular platform for the fabrication of complex inorganic nanoparticles based on a DNA origami mold system to solve the challenges towards the nanoelectroic applications: deficiency in size control of the synthesised particles which leads to inhomogeneities; avoiding background nucleation while maintaining the fully homogeneous and continuous targeted metal growth; controllable multi-dimensional geometries and high addressability of each metal nanoparticle; and the integration of multi-materials with distinct electronic properties. The versatility of the mold system fabrication was first studied using linear mold elements with different interfaces for mold-mold docking. By establishing a set of specific interfaces, linear mold superstructures with controllable length in which the monomers remained addressable could be fabricated. The concept was extended by integrating additional mold-based elements with different shapes that nonetheless followed the interface design rules. Different structures were integrated to allow formation of various shapes including complex metal structures and even branched structures. Furthermore, the metallic behaviour of the fabricated metal nanostructures was examined by temperature-dependent conductivity measurements. Moreover, the diversity and ubiquity of this modular platform was tested by integrating semiconducting rods together with gold nanoparticles inside the DNA molds. Metal-semiconductor complex heterostructures were successfully built providing this way a fundamental component for future nanoelectronic device fabrication. To further improve the electronic performance of the fabricated nanostructures, a thorough and systematic study for optimization of the metal deposition inside DNA molds was carried out. An improved electroless metal deposition protocol was established, allowing the formation of rod-shaped like, high aspect ratio gold nanoparticle from a single seed.

Specifically, in **Chapter 3**, the mold-based platform was constructed and metal structures with programmable length and pattern were synthesized. Four orthogonal high-affinity interfaces between mold monomers were established, enabling the fabrication of higher-order mold superstructures. Based on different selections of attractive and repulsive helices for the docking reaction with either 3’ or 5’ feature multiple terminal interfaces were developed. The fine-tuned interface affinities at each addressable monomer in the superstructures could reach yields of 74%, 46% and 41.3% for pentameric, octameric and nonameric mold assemblies, respectively. Different metallization patterns within pentamer structures were achieved as designed, demonstrating that this modular platform can be further expanded for the generation of larger and more complex higher-order DNA templates for inorganic nanostructures. In addition, the developed strategy represents the basis for fabrication of more arbitrary interfaces using different patterns of attractive and repulsive helices.

In **Chapter 4**, the developed platform was used to fabricate highly homogeneous and conductive gold nanowires and their electronic properties were characterized. High seed decoration efficiency (96±2%) was achieved for each mold monomer of the wire structures. By placing the complementary interfaces between mold-mold in an alternating manner, micron range periodic linear mold nanowires with homogeneous width (20-30 nm) were achieved comprising dozens of mold monomers and. To identify the charge transport mechanism in the fabricated gold nanowires, temperature-dependent conductance measurements were enabled by high-precision contacting of the gold nanowires using electron beam lithography. Some of the wires exhibited high metal-like conductivity with resistances of 90 Ω up to 30 kΩ. Such micrometer-long nanowires with high conductive property are ideal for interconnecting nano and micro range electronic devices.

In **Chapter 5**, CdS semiconducting rods were used to further utilize this platform for the integration of multi-functional material. A new approach for the oligonucleotide functionalization of CdS nanorods was demonstrated. Short thiolated mPEG molecules were used for a robust phase transfer to the aqueous phase, ensuring high colloidal stability of the CdS nanorods. Dithiolated oligonucleotides formed a dense brush around the NRs that allowed a successful assembly onto DNA origami structures with five different attachment schemes. The binding efficiencies reached yields of 90 % and 80 % for external and internal docking, respectively. Gold nanoparticles and CdS nanorods could be loaded into the platform at different positions to achieve defined metal-SC heterostructures.

Additionally, within the Ph.D. time frame, extra work were conducted for the development of the modular platform and they were summarized in unpublished manuscripts (**P4** and **P5**, refer to **List of Publications**). In manuscript **P4**, the versatility of the mold-based assembly platform was expanded by integrating differently shaped mold-based elements. Three additional DNA mold elements were introduced: mold lid elements with a DNA filled cavity, 3-wall elements with providing linear molds with a smaller cavity diameter and junction elements which allow to establish branches. Specific interfaces for the different elements were designed to allow the specific integration into the modular platform. Mold superstructures with various geometries were obtained. Using lid and mold elements, a DNA cage was created. Followed by a subsequent gold deposition, DNA-caged particles were achieved. Using standard molds and 3-wall elements which have smaller cavity diameters, allowed to fabricate rolling pin- and dumbbell-shaped particles. In addition, T-shaped and loop-shaped particles with high continuity were realized using junction elements. All the obtained metal nanostructures displayed high homogeneity and continuity. An effort has also been made to connect the loop structure into a larger network.

In manuscript **P5**, further improvement of the electroless gold deposition inside the mold was established to achieve more robust and straightforward rod-shaped like nanoparticles synthesis to improve the performance for future electronic applications. Based on the modular platform from **Chapter 3**, different alternating chain patterns were utilized to create certain interparticle distances (80 nm, 120 nm and 160 nm) between the 5 nm gold nanoparticle seeds inside the mold wires. A systematic study of possible parameters during the gold deposition process was conducted: different ratios of reducing agent and gold precursor were investigated (1:1 ratio resulting in the best gold growth); salt concentrations (NaCl) were varied to obtain the best particle merging condition (no NaCl turned out to give elongated growth); overall gold ion concentration was adjusted to fill up the gap between two AuNPs. Continuous and high aspect ratios of gold nanoparticles (up to 1:7) were achieved from one single AuNP seed with optimized conditions. It should on theory improved the conductivity performance of the gold nanowires and thus provided a robust gold rod assembly with the help of DNA origami mold.

The realization of functional nanoelectronic devices based on the established mold-based platform will represent a challenge for future studies. Expanded from **Chapter 3**, while this study utilized so far only four different interfaces for the mold element interaction, it will certainly be possible to introduce extra interfaces design to reach the limits of cross-sectional DNA origami design. Furthermore, different interface design strategies besides the already established attractive and repulsive helices scheme can be developed. In addition, a thorough study of affinities and dynamics during the higher-order assembly would be interesting to reveal the relation between different forces for self-organization. Expanded from **Chapter 4**, further characterization of the fabricated nanowire would be straightforward to test the structure performance. A combination of top-down strategy and bottom-up fabrication would be an alternative to guide the controlled deposition of metal nanostructures on the substrate and building interconnections between different electronic units. Expanded from **Chapter 5**, characterization of the metal-semiconducting heterostructures would be interesting as well as back gate constructing on top of the structures to achieve a real transistor. Expanded from manuscript **P4**, a new design of the junction elements (rigid top and bottom connection or new asymmetric interfaces) would be helpful for loop structures and a large network construction. Furthermore, different metal materials or magnetic materials could be incorporated to achieve a particular functionality. Different material seeds in specific molds should support the electroless growth of different metals at the desired location.

Overall, the modular platform for inorganic particles synthesis was developed. More homogeneous and continues metal deposition was achieved with improved electronic performance comparable to the bulk material. Furthermore, multiple materials were integrated compatibly into the

platform with highly controlled orientation. With the developed metal deposition protocol, this modular platform is ready to be used to fabricate nanoelectronic circuit for actual applications. All the prerequisites for the realization of nanoelectronic devices based on the DNA origami modular platform are reached. How to utilize these principles and protocols to design the target nanoelectronic devices is the key interest. Defined geometry can be designed for certain device constructions. Targeted metal composition can be fabricated at designed positions which will intrigue exciting phenomena. All together with further optimized controllable material deposition on silicon wafer, a real nanoelectronic device will be fabricated based on this modular platform for commercial usage.

# 7. Bibliography


[1] H. F. Sleiman and N. C. Seeman, "DNA nanotechnology," *Nat. Rev. Mater.*, vol. 3, p. 17068, Nov. 2017.

[2] F. Hong, F. Zhang, Y. Liu, and H. Yan, "DNA Origami: Scaffolds for Creating Higher Order Structures," *Chem. Rev.*, Jun. 2017.

[3] L. L. Ong *et al.*, "Programmable self-assembly of three-dimensional nanostructures from 10,000 unique components," *Nature*, vol. 552, no. 7683, p. 72, Dec. 2017.

[4] G. Tikhomirov, P. Petersen, and L. Qian, "Fractal assembly of micrometre-scale DNA origami arrays with arbitrary patterns," *Nature*, vol. 552, no. 7683, p. 67, Dec. 2017.

[5] K. F. Wagenbauer, C. Sigl, and H. Dietz, "Gigadalton-scale shape-programmable DNA assemblies," *Nature*, vol. 552, no. 7683, p. 78, Dec. 2017.

[6] T. L. Schmidt *et al.*, "Scalable amplification of strand subsets from chip-synthesized oligonucleotide libraries," *Nat. Commun.*, vol. 6, p. 8634, Nov. 2015.

[7] F. Praetorius, B. Kick, K. L. Behler, M. N. Honemann, D. Weuster-Botz, and H. Dietz, "Biotechnological mass production of DNA origami," *Nature*, vol. 552, no. 7683, p. 84, Dec. 2017.

[8] R. M. Zadegan and M. L. Norton, "Structural DNA Nanotechnology: From Design to Applications," *Int. J. Mol. Sci.*, vol. 13, no. 6, pp. 7149–7162, Jun. 2012.

[9] A. V. Pinheiro, D. Han, W. M. Shih, and H. Yan, "Challenges and opportunities for structural DNA nanotechnology," *Nat. Nanotechnol.*, vol. 6, no. 12, p. 763, Dec. 2011.

[10] R. Dahm, "Discovering DNA: Friedrich Miescher and the early years of nucleic acid research," *Hum. Genet.*, vol. 122, no. 6, pp. 565–581, Jan. 2008.

[11] O. T. Avery, C. M. MacLeod, and M. McCarty, "STUDIES ON THE CHEMICAL NATURE OF THE SUBSTANCE INDUCING TRANSFORMATION OF PNEUMOCOCCAL TYPES," *J. Exp. Med.*, vol. 79, no. 2, pp. 137–158, Feb. 1944.

[12] A. D. Hershey and M. Chase, "Independent functions of viral protein and nucleic acid in growth of bacteriophage," *J. Gen. Physiol.*, vol. 36, no. 1, pp. 39–56, May 1952.

[13] F. H. C. Crick and J. D. Watson, "Molecular Structure of Nucleic Acids: A Structure for Deoxyribose Nucleic Acid," *Nature*, vol. 171, no. 4356, p. 737, Apr. 1953.

[14] R. E. Franklin and R. G. Gosling, "Molecular Configuration in Sodium Thymonucleate," *Nature*, vol. 171, no. 4356, pp. 740–741, Apr. 1953.

[15] E. Chargaff, "Chemical specificity of nucleic acids and mechanism of their enzymatic degradation," *Experientia*, vol. 6, no. 6, pp. 201–209, Jun. 1950.

[16] M. Mandelkern, J. G. Elias, D. Eden, and D. M. Crothers, "The dimensions of DNA in solution," *J. Mol. Biol.*, vol. 152, no. 1, pp. 153–161, Oct. 1981.

[17] L. Pray, "Discovery of DNA structure and function: Watson and Crick," *Nat. Educ.*, vol. 1, no. 1, p. 100, 2008.

[18] C. Broka *et al.*, "Crystal structure analysis of a complete turn of B-DNA," *Nature*, vol. 287, no. 5784, p. 755, Oct. 1980.

[19] A. Ghosh and M. Bansal, "A glossary of DNA structures from A to Z," *Acta Crystallogr. D Biol. Crystallogr.*, vol. 59, no. 4, pp. 620–626, Apr. 2003.

[20] H. S. Basu, B. G. Feuerstein, D. A. Zarling, R. H. Shaffer, and L. J. Marton, "Recognition of Z-RNA and Z-DNA Determinants by Polyamines in Solution: Experimental and Theoretical Studies," *J. Biomol. Struct. Dyn.*, vol. 6, no. 2, pp. 299–309, Oct. 1988.

[21] F. H. C. Crick and J. D. Watson, "The complementary structure of deoxyribonucleic acid," *Proc R Soc Lond A*, vol. 223, no. 1152, pp. 80–96, Apr. 1954.

[22] A. Klug, "The Discovery of the DNA Double Helix," *J. Mol. Biol.*, vol. 335, no. 1, pp. 3–26, Jan. 2004.

[23] J. Šponer, J. Leszczynski, and P. Hobza, "Hydrogen Bonding and Stacking of DNA Bases: A Review of Quantum-chemical ab initio Studies," *J. Biomol. Struct. Dyn.*, vol. 14, no. 1, pp. 117–135, Aug. 1996.

[24] George A. Jeffrey and W. Saenger, *Hydrogen Bonding in Biological Structures*. Springer Berlin Heidelberg, 1991.
[25] E. T. Kool, "Hydrogen Bonding, Base Stacking, and Steric Effects in DNA Replication," *Annu. Rev. Biophys. Biomol. Struct.*, vol. 30, no. 1, pp. 1–22, 2001.
[26] Jr. John SantaLucia and D. Hicks, "The Thermodynamics of DNA Structural Motifs," *Annu. Rev. Biophys. Biomol. Struct.*, vol. 33, no. 1, pp. 415–440, 2004.
[27] P. Yakovchuk, E. Protozanova, and M. D. Frank-Kamenetskii, "Base-stacking and base-pairing contributions into thermal stability of the DNA double helix," *Nucleic Acids Res.*, vol. 34, no. 2, pp. 564–574, 2006.
[28] "Base pair," *Wikipedia*. 03-Jun-2019.
[29] N. C. Seeman, "Nucleic acid junctions and lattices," *J. Theor. Biol.*, vol. 99, no. 2, pp. 237–247, Nov. 1982.
[30] F. Zhang, J. Nangreave, Y. Liu, and H. Yan, "Structural DNA Nanotechnology: State of the Art and Future Perspective," *J. Am. Chem. Soc.*, vol. 136, no. 32, pp. 11198–11211, Aug. 2014.
[31] C. Bustamante, J. F. Marko, E. D. Siggia, and S. Smith, "Entropic elasticity of lambda-phage DNA.," *Science*, vol. 265, no. 5178, pp. 1599–1600, Sep. 1994.
[32] M. H. Caruthers, "Gene synthesis machines: DNA chemistry and its uses," *Science*, vol. 230, no. 4723, pp. 281–285, Oct. 1985.
[33] S. N. Cohen, A. C. Y. Chang, H. W. Boyer, and R. B. Helling, "Construction of Biologically Functional Bacterial Plasmids In Vitro," *Proc. Natl. Acad. Sci. U. S. A.*, vol. 70, no. 11, pp. 3240–3244, Nov. 1973.
[34] R. Holliday, "A mechanism for gene conversion in fungi," *Genet. Res.*, vol. 5, no. 2, pp. 282–304, Jul. 1964.
[35] I. G. Panyutin and P. Hsieh, "The kinetics of spontaneous DNA branch migration," *Proc. Natl. Acad. Sci.*, vol. 91, no. 6, pp. 2021–2025, Mar. 1994.
[36] C. Mao, W. Sun, and N. C. Seeman, "Designed Two-Dimensional DNA Holliday Junction Arrays Visualized by Atomic Force Microscopy," *J. Am. Chem. Soc.*, vol. 121, no. 23, pp. 5437–5443, Jun. 1999.
[37] N. C. Seeman, "Nucleic acid junctions and lattices," *J. Theor. Biol.*, vol. 99, no. 2, pp. 237–247, Nov. 1982.
[38] J. Chen and N. C. Seeman, "Synthesis from DNA of a molecule with the connectivity of a cube," *Nature*, vol. 350, no. 6319, p. 631, Apr. 1991.
[39] T. J. Fu and N. C. Seeman, "DNA double-crossover molecules," *Biochemistry*, vol. 32, no. 13, pp. 3211–3220, Apr. 1993.
[40] C. Mao, J. H. Reif, N. C. Seeman, and T. H. LaBean, "Logical computation using algorithmic self-assembly of DNA triple-crossover molecules," *Nature*, vol. 407, no. 6803, p. 493, Sep. 2000.
[41] T. H. LaBean *et al.*, "Construction, Analysis, Ligation, and Self-Assembly of DNA Triple Crossover Complexes," *J. Am. Chem. Soc.*, vol. 122, no. 9, pp. 1848–1860, Mar. 2000.
[42] E. Winfree, F. Liu, L. A. Wenzler, and N. C. Seeman, "Design and self-assembly of two-dimensional DNA crystals," *Nature*, vol. 394, no. 6693, p. 539, Aug. 1998.
[43] C. Lin, Y. Liu, S. Rinker, and H. Yan, "DNA Tile Based Self-Assembly: Building Complex Nanoarchitectures," *ChemPhysChem*, vol. 7, no. 8, pp. 1641–1647, Aug. 2006.
[44] B. Wei, M. Dai, and P. Yin, "Complex shapes self-assembled from single-stranded DNA tiles," *Nature*, vol. 485, no. 7400, p. 623, May 2012.
[45] W. M. Shih, J. D. Quispe, and G. F. Joyce, "A 1.7-kilobase single-stranded DNA that folds into a nanoscale octahedron," *Nature*, vol. 427, no. 6975, pp. 618–621, Feb. 2004.
[46] P. W. K. Rothemund, "Folding DNA to create nanoscale shapes and patterns," *Nature*, vol. 440, no. 7082, pp. 297–302, Mar. 2006.

[47] S. M. Douglas, H. Dietz, T. Liedl, B. Högberg, F. Graf, and W. M. Shih, "Self-assembly of DNA into nanoscale three-dimensional shapes," *Nature*, vol. 459, no. 7245, pp. 414–418, May 2009.
[48] Y. Ke *et al.*, "Multilayer DNA Origami Packed on a Square Lattice," *J. Am. Chem. Soc.*, vol. 131, no. 43, pp. 15903–15908, Nov. 2009.
[49] S. M. Douglas, A. H. Marblestone, S. Teerapittayanon, A. Vazquez, G. M. Church, and W. M. Shih, "Rapid prototyping of 3D DNA-origami shapes with caDNAno," *Nucleic Acids Res.*, p. gkp436, Jun. 2009.
[50] P. W. K. Rothemund, "Folding DNA to create nanoscale shapes and patterns," *Nature*, vol. 440, no. 7082, pp. 297–302, Mar. 2006.
[51] S. M. Douglas, H. Dietz, T. Liedl, B. Hogberg, F. Graf, and W. M. Shih, "Self-assembly of DNA into nanoscale three-dimensional shapes," *Nature*, vol. 459, no. 7245, pp. 414–418, May 2009.
[52] E. S. Andersen *et al.*, "Self-assembly of a nanoscale DNA box with a controllable lid," *Nature*, vol. 459, no. 7243, p. 73, May 2009.
[53] H. Dietz, S. M. Douglas, and W. M. Shih, "Folding DNA into Twisted and Curved Nanoscale Shapes," *Science*, vol. 325, no. 5941, pp. 725–730, Aug. 2009.
[54] T. Gerling, K. F. Wagenbauer, A. M. Neuner, and H. Dietz, "Dynamic DNA devices and assemblies formed by shape-complementary, non–base pairing 3D components," *Science*, vol. 347, no. 6229, pp. 1446–1452, Mar. 2015.
[55] E. Benson *et al.*, "DNA rendering of polyhedral meshes at the nanoscale," *Nature*, vol. 523, no. 7561, pp. 441–444, Jul. 2015.
[56] M. Matthies, N. P. Agarwal, and T. L. Schmidt, "Design and Synthesis of Triangulated DNA Origami Trusses," *Nano Lett.*, vol. 16, no. 3, pp. 2108–2113, Mar. 2016.
[57] F. Zhang *et al.*, "Complex wireframe DNA origami nanostructures with multi-arm junction vertices," *Nat. Nanotechnol.*, vol. 10, no. 9, p. 779, Sep. 2015.
[58] J. Mikkilä *et al.*, "Virus-Encapsulated DNA Origami Nanostructures for Cellular Delivery," *Nano Lett.*, vol. 14, no. 4, pp. 2196–2200, Apr. 2014.
[59] G. P. Acuna, F. M. Möller, P. Holzmeister, S. Beater, B. Lalkens, and P. Tinnefeld, "Fluorescence Enhancement at Docking Sites of DNA-Directed Self-Assembled Nanoantennas," *Science*, vol. 338, no. 6106, pp. 506–510, Oct. 2012.
[60] C. Heck, Y. Kanehira, J. Kneipp, and I. Bald, "Placement of Single Proteins within the SERS Hot Spots of Self-Assembled Silver Nanolenses," *Angew. Chem. Int. Ed.*, vol. 57, no. 25, pp. 7444–7447, Jun. 2018.
[61] V. V. Thacker *et al.*, "DNA origami based assembly of gold nanoparticle dimers for surface-enhanced Raman scattering," *Nat. Commun.*, vol. 5, p. 3448, Mar. 2014.
[62] J. Zessin *et al.*, "Tunable Fluorescence of a Semiconducting Polythiophene Positioned on DNA Origami," *Nano Lett.*, vol. 17, no. 8, pp. 5163–5170, Aug. 2017.
[63] F. N. Gür, F. W. Schwarz, J. Ye, S. Diez, and T. L. Schmidt, "Toward Self-Assembled Plasmonic Devices: High-Yield Arrangement of Gold Nanoparticles on DNA Origami Templates," *ACS Nano*, vol. 10, no. 5, pp. 5374–5382, May 2016.
[64] A. Kuzyk *et al.*, "DNA-based self-assembly of chiral plasmonic nanostructures with tailored optical response," *Nature*, vol. 483, no. 7389, pp. 311–314, Mar. 2012.
[65] F. Hong, F. Zhang, Y. Liu, and H. Yan, "DNA Origami: Scaffolds for Creating Higher Order Structures," *Chem. Rev.*, vol. 117, no. 20, pp. 12584–12640, Oct. 2017.
[66] W. Pfeifer and B. Saccà, "From Nano to Macro through Hierarchical Self-Assembly: The DNA Paradigm," *ChemBioChem*, vol. 17, no. 12, pp. 1063–1080, Jun. 2016.
[67] R. Iinuma, Y. Ke, R. Jungmann, T. Schlichthaerle, J. B. Woehrstein, and P. Yin, "Polyhedra Self-Assembled from DNA Tripods and Characterized with 3D DNA-PAINT," *Science*, vol. 344, no. 6179, pp. 65–69, Apr. 2014.
[68] W. Liu, H. Zhong, R. Wang, and N. C. Seeman, "Crystalline Two-Dimensional DNA-Origami Arrays," *Angew. Chem. Int. Ed.*, vol. 50, no. 1, pp. 264–267, Jan. 2011.

[69] P. Wang, S. Gaitanaros, S. Lee, M. Bathe, W. M. Shih, and Y. Ke, "Programming Self-Assembly of DNA Origami Honeycomb Two-Dimensional Lattices and Plasmonic Metamaterials," *J. Am. Chem. Soc.*, vol. 138, no. 24, pp. 7733–7740, 22 2016.

[70] H. Yan, T. H. LaBean, L. Feng, and J. H. Reif, "Directed nucleation assembly of DNA tile complexes for barcode-patterned lattices," *Proc. Natl. Acad. Sci.*, vol. 100, no. 14, pp. 8103–8108, Jul. 2003.

[71] S. Woo and P. W. K. Rothemund, "Programmable molecular recognition based on the geometry of DNA nanostructures," *Nat. Chem.*, vol. 3, no. 8, pp. 620–627, Aug. 2011.

[72] T. Gerling, K. F. Wagenbauer, A. M. Neuner, and H. Dietz, "Dynamic DNA devices and assemblies formed by shape-complementary, non–base pairing 3D components," *Science*, vol. 347, no. 6229, pp. 1446–1452, Mar. 2015.

[73] M. Endo, T. Sugita, Y. Katsuda, K. Hidaka, and H. Sugiyama, "Programmed-Assembly System Using DNA Jigsaw Pieces," *Chem. – Eur. J.*, vol. 16, no. 18, pp. 5362–5368, 2010.

[74] A. Rajendran, M. Endo, Y. Katsuda, K. Hidaka, and H. Sugiyama, "Programmed Two-Dimensional Self-Assembly of Multiple DNA Origami Jigsaw Pieces," *ACS Nano*, vol. 5, no. 1, pp. 665–671, Jan. 2011.

[75] G. Tikhomirov, P. Petersen, and L. Qian, "Programmable disorder in random DNA tilings," *Nat. Nanotechnol.*, vol. 12, no. 3, pp. 251–259, Mar. 2017.

[76] T. Zhang *et al.*, "3D DNA Origami Crystals," *Adv. Mater.*, vol. 30, no. 28, p. 1800273, Jul. 2018.

[77] K. F. Wagenbauer, C. Sigl, and H. Dietz, "Gigadalton-scale shape-programmable DNA assemblies," *Nature*, vol. 552, no. 7683, pp. 78–83, Dec. 2017.

[78] G. Tikhomirov, P. Petersen, and L. Qian, "Fractal assembly of micrometre-scale DNA origami arrays with arbitrary patterns," *Nature*, vol. 552, no. 7683, pp. 67–71, Dec. 2017.

[79] H. Zhang, J. Chao, D. Pan, H. Liu, Q. Huang, and C. Fan, "Folding super-sized DNA origami with scaffold strands from long-range PCR," *Chem. Commun.*, vol. 48, no. 51, pp. 6405–6407, May 2012.

[80] A. N. Marchi, I. Saaem, B. N. Vogen, S. Brown, and T. H. LaBean, "Toward Larger DNA Origami," *Nano Lett.*, vol. 14, no. 10, pp. 5740–5747, Oct. 2014.

[81] B. Högberg, T. Liedl, and W. M. Shih, "Folding DNA Origami from a Double-Stranded Source of Scaffold," *J. Am. Chem. Soc.*, vol. 131, no. 26, pp. 9154–9155, Jul. 2009.

[82] Z. Zhao, H. Yan, and Y. Liu, "A Route to Scale Up DNA Origami Using DNA Tiles as Folding Staples," *Angew. Chem. Int. Ed.*, vol. 49, no. 8, pp. 1414–1417, Feb. 2010.

[83] Z. Zhao, Y. Liu, and H. Yan, "Organizing DNA Origami Tiles into Larger Structures Using Preformed Scaffold Frames," *Nano Lett.*, vol. 11, no. 7, pp. 2997–3002, Jul. 2011.

[84] S. Woo and P. W. K. Rothemund, "Self-assembly of two-dimensional DNA origami lattices using cation-controlled surface diffusion," *Nat. Commun.*, vol. 5, p. 4889, Sep. 2014.

[85] S. Kocabey *et al.*, "Membrane-Assisted Growth of DNA Origami Nanostructure Arrays," *ACS Nano*, vol. 9, no. 4, pp. 3530–3539, Apr. 2015.

[86] A. P. Lyubartsev and A. Laaksonen, "Effective potentials for ion–DNA interactions," *J. Chem. Phys.*, vol. 111, no. 24, pp. 11207–11215, Dec. 1999.

[87] J. G. Duguid, V. A. Bloomfield, J. M. Benevides, and G. J. Thomas, "Raman spectroscopy of DNA-metal complexes. II. The thermal denaturation of DNA in the presence of Sr2+, Ba2+, Mg2+, Ca2+, Mn2+, Co2+, Ni2+, and Cd2+," *Biophys. J.*, vol. 69, no. 6, pp. 2623–2641, Dec. 1995.

[88] G. O. Mallory, J. B. Hajdu, A. Electroplaters, and S. F. Society, *Electroless plating : fundamentals and applications*, Reprint ed. Orlando, Fla. : American Electroplaters and Surface Finishers Society, 1990.

[89] "Modern Electroplating, 5th Edition | Electrochemistry | Chemistry | Subjects | Wiley." [Online]. Available: https://www.wiley.com/en-us/Modern+Electroplating%2C+5th+Edition-p-9780470167786. [Accessed: 21-Aug-2019].

[90] W. J. Cheong, B. L. Luan, and D. W. Shoesmith, "The effects of stabilizers on the bath stability of electroless Ni deposition and the deposit," *Appl. Surf. Sci.*, vol. 229, no. 1, pp. 282–300, May 2004.
[91] J. L. Coffer *et al.*, "Dictation of the shape of mesoscale semiconductor nanoparticle assemblies by plasmid DNA," *Appl. Phys. Lett.*, vol. 69, no. 25, pp. 3851–3853, Dec. 1996.
[92] E. Braun, Y. Eichen, U. Sivan, and G. Ben-Yoseph, "DNA-templated assembly and electrode attachment of a conducting silver wire," *Nature*, vol. 391, no. 6669, pp. 775–778, Feb. 1998.
[93] J. Richter, M. Mertig, W. Pompe, I. Mönch, and H. K. Schackert, "Construction of highly conductive nanowires on a DNA template," *Appl. Phys. Lett.*, vol. 78, no. 4, pp. 536–538, Jan. 2001.
[94] M. Mertig, L. Colombi Ciacchi, R. Seidel, W. Pompe, and A. De Vita, "DNA as a Selective Metallization Template," *Nano Lett.*, vol. 2, no. 8, pp. 841–844, Aug. 2002.
[95] R. Seidel, L. C. Ciacchi, M. Weigel, W. Pompe, and M. Mertig*, "Synthesis of Platinum Cluster Chains on DNA Templates: Conditions for a Template-Controlled Cluster Growth," 2004.
[96] Hector A. Becerril, Paul Ludtke, and Barry M. Willardson, and A. T. Woolley*, "DNA-Templated Nickel Nanostructures and Protein Assemblies," 2006.
[97] P. Atanasova *et al.*, "DNA-templated synthesis of ZnO thin layers and nanowires," *Nanotechnology*, vol. 20, no. 36, p. 365302, Sep. 2009.
[98] A. S. Swami, N. Brun, and D. Langevin, "Phase Transfer of Gold Metallized DNA," *J. Clust. Sci.*, vol. 20, no. 2, pp. 281–290, Jun. 2009.
[99] M. Fischler *et al.*, "Formation of Bimetallic Ag–Au Nanowires by Metallization of Artificial DNA Duplexes," *Small*, vol. 3, no. 6, pp. 1049–1055, Jun. 2007.
[100] C. F. M. and and A. T. Woolley*, "DNA-Templated Construction of Copper Nanowires," 2003.
[101] K. Keren, M. Krueger, R. Gilad, G. Ben-Yoseph, U. Sivan, and E. Braun, "Sequence-Specific Molecular Lithography on Single DNA Molecules," *Science*, vol. 297, no. 5578, pp. 72–75, Jul. 2002.
[102] H. Yan, S. H. Park, G. Finkelstein, J. H. Reif, and T. H. LaBean, "DNA-Templated Self-Assembly of Protein Arrays and Highly Conductive Nanowires," *Science*, vol. 301, no. 5641, pp. 1882–1884, Sep. 2003.
[103] D. Liu, S. H. Park, J. H. Reif, and T. H. LaBean, "DNA nanotubes self-assembled from triple-crossover tiles as templates for conductive nanowires.," *Proc. Natl. Acad. Sci. U. S. A.*, vol. 101, no. 3, pp. 717–22, Jan. 2004.
[104] H. Liu, Y. Chen, Y. He, A. E. Ribbe, and C. Mao, "Approaching The Limit: Can One DNA Oligonucleotide Assemble into Large Nanostructures?," *Angew. Chem. Int. Ed.*, vol. 45, no. 12, pp. 1942–1945, Mar. 2006.
[105] J. Liu *et al.*, "Metallization of Branched DNA Origami for Nanoelectronic Circuit Fabrication," *ACS Nano*, vol. 5, no. 3, pp. 2240–2247, Mar. 2011.
[106] Y. Geng, J. Liu, A. T. Woolley, E. Pound, and J. N. Harbb, "Rapid metallization of lambda DNA and DNA origami using a Pd seeding method," *J. Mater. Chem.*, vol. 21, no. 32, p. 12126, 2011.
[107] Y. Geng *et al.*, "Electrically Conductive Gold- and Copper-Metallized DNA Origami Nanostructures," *Langmuir*, vol. 29, no. 10, pp. 3482–3490, Mar. 2013.
[108] R. Schreiber *et al.*, "DNA Origami-Templated Growth of Arbitrarily Shaped Metal Nanoparticles," *Small*, vol. 7, no. 13, pp. 1795–1799, Jul. 2011.
[109] J. Zhou, J. Ralston, R. Sedev, and D. A. Beattie, "Functionalized gold nanoparticles: Synthesis, structure and colloid stability," *J. Colloid Interface Sci.*, vol. 331, no. 2, pp. 251–262, 2009.

[110] R. A. Sperling and W. J. Parak, "Surface modification, functionalization and bioconjugation of colloidal inorganic nanoparticles," *Philos. Trans. R. Soc. Lond. Math. Phys. Eng. Sci.*, vol. 368, no. 1915, 2010.
[111] J. Turkevich, P. C. Stevenson, and J. Hillier, "The Formation of Colloidal Gold," *J. Phys. Chem.*, vol. 57, no. 7, pp. 670–673, Jul. 1953.
[112] C. A. Mirkin, R. L. Letsinger, R. C. Mucic, and J. J. Storhoff, "A DNA-based method for rationally assembling nanoparticles into macroscopic materials," *Nature*, vol. 382, no. 6592, pp. 607–609, Aug. 1996.
[113] J. Pérez-Juste, I. Pastoriza-Santos, L. M. Liz-Marzán, and P. Mulvaney, "Gold nanorods: Synthesis, characterization and applications," *Coord. Chem. Rev.*, vol. 249, no. 17, pp. 1870–1901, 2005.
[114] S. C. and and D. L. Carroll, "Synthesis and Characterization of Truncated Triangular Silver Nanoplates," 2002.
[115] A. Umar, M. S. Akhtar, G. N. Dar, and S. Baskoutas, "Low-temperature synthesis of α-Fe2O3 hexagonal nanoparticles for environmental remediation and smart sensor applications," *Talanta*, vol. 116, pp. 1060–1066, 2013.
[116] M. Brust *et al.*, "Synthesis of thiol-derivatised gold nanoparticles in a two-phase Liquid–Liquid system," *J Chem Soc Chem Commun*, vol. 0, no. 7, pp. 801–802, 1994.
[117] C. A. Mirkin, R. L. Letsinger, R. C. Mucic, and J. J. Storhoff, "A DNA-based method for rationally assembling nanoparticles into macroscopic materials.," *Nature*, vol. 382, no. 6592, pp. 607–609, 1996.
[118] A. P. Alivisatos *et al.*, "Organization of 'nanocrystal molecules' using DNA.," *Nature*, vol. 382, no. 6592, pp. 609–11, Aug. 1996.
[119] D. S. Sebba, J. J. Mock, D. R. Smith, T. H. LaBean, and A. A. Lazarides, "Reconfigurable Core−Satellite Nanoassemblies as Molecularly-Driven Plasmonic Switches," *Nano Lett.*, vol. 8, no. 7, pp. 1803–1808, Jul. 2008.
[120] J. Sharma, R. Chhabra, C. S. Andersen, K. V. Gothelf, H. Yan, and Y. Liu, "Toward Reliable Gold Nanoparticle Patterning On Self-Assembled DNA Nanoscaffold," *J. Am. Chem. Soc.*, vol. 130, no. 25, pp. 7820–7821, Jun. 2008.
[121] B. Ding, Z. Deng, H. Yan, S. Cabrini, R. N. Zuckermann, and J. Bokor, "Gold Nanoparticle Self-Similar Chain Structure Organized by DNA Origami," *J. Am. Chem. Soc.*, vol. 132, no. 10, pp. 3248–3249, Mar. 2010.
[122] X. Shen *et al.*, "Rolling Up Gold Nanoparticle-Dressed DNA Origami into Three-Dimensional Plasmonic Chiral Nanostructures," *J. Am. Chem. Soc.*, vol. 134, no. 1, pp. 146–149, Jan. 2012.
[123] Z. Zhao, E. L. Jacovetty, Y. Liu, and H. Yan, "Encapsulation of Gold Nanoparticles in a DNA Origami Cage," *Angew. Chem. Int. Ed.*, vol. 50, no. 9, pp. 2041–2044, Feb. 2011.
[124] A. Kuzyk *et al.*, "DNA-based self-assembly of chiral plasmonic nanostructures with tailored optical response," *Nature*, vol. 483, no. 7389, pp. 311–314, Mar. 2012.
[125] M. Pilo-Pais, S. Goldberg, E. Samano, T. H. Labean, and G. Finkelstein, "Connecting the nanodots: Programmable nanofabrication of fused metal shapes on DNA templates," *Nano Lett.*, vol. 11, no. 8, pp. 3489–3492, Aug. 2011.
[126] A. C. Pearson *et al.*, "DNA Origami Metallized Site Specifically to Form Electrically Conductive Nanowires," *J. Phys. Chem. B*, vol. 116, no. 35, pp. 10551–10560, Sep. 2012.
[127] B. Teschome, S. Facsko, T. Schönherr, J. Kerbusch, A. Keller, and A. Erbe, "Temperature-Dependent Charge Transport through Individually Contacted DNA Origami-Based Au Nanowires," *Langmuir*, vol. 32, no. 40, pp. 10159–10165, Oct. 2016.
[128] B. Uprety, E. P. Gates, Y. Geng, A. T. Woolley, and J. N. Harb, "Site-Specific Metallization of Multiple Metals on a Single DNA Origami Template," *Langmuir*, vol. 30, no. 4, pp. 1134–1141, Feb. 2014.

[129] B. Uprety *et al.*, "Anisotropic Electroless Deposition on DNA Origami Templates To Form Small Diameter Conductive Nanowires," *Langmuir*, vol. 33, no. 3, pp. 726–735, Jan. 2017.
[130] B. Uprety, J. Jensen, B. R. Aryal, R. C. Davis, A. T. Woolley, and J. N. Harb, "Directional Growth of DNA-Functionalized Nanorods to Enable Continuous, Site-Specific Metallization of DNA Origami Templates," *Langmuir*, vol. 33, no. 39, pp. 10143–10152, Oct. 2017.
[131] B. R. Aryal *et al.*, "Four-Point Probe Electrical Measurements on Templated Gold Nanowires Formed on Single DNA Origami Tiles," *Langmuir*, vol. 34, no. 49, pp. 15069–15077, Dec. 2018.
[132] W. Sun *et al.*, "Casting inorganic structures with DNA molds," *Science*, p. 1258361, Oct. 2014.
[133] S. Helmi, C. Ziegler, D. J. Kauert, and R. Seidel, "Shape-Controlled Synthesis of Gold Nanostructures Using DNA Origami Molds," *Nano Lett.*, vol. 14, no. 11, pp. 6693–6698, Nov. 2014.
[134] T. Bayrak, N. S. Jagtap, and A. Erbe, "Review of the Electrical Characterization of Metallic Nanowires on DNA Templates," *Int. J. Mol. Sci.*, vol. 19, no. 10, Oct. 2018.
[135] F. Léonard and A. A. Talin, "Size-Dependent Effects on Electrical Contacts to Nanotubes and Nanowires," *Phys. Rev. Lett.*, vol. 97, no. 2, p. 026804, Jul. 2006.
[136] M. P. J. van Staveren, H. B. Brom, and L. J. de Jongh, "Metal-cluster compounds and universal features of the hopping conductivity of solids," *Phys. Rep.*, vol. 208, pp. 1–96, Oct. 1991.
[137] B. Abeles, P. Sheng, M. D. Coutts, and Y. Arie, "Structural and electrical properties of granular metal films," *Adv. Phys.*, vol. 24, no. 3, pp. 407–461, May 1975.
[138] A. Zabet-Khosousi and A.-A. Dhirani, "Charge Transport in Nanoparticle Assemblies," *Chem. Rev.*, vol. 108, no. 10, pp. 4072–4124, Oct. 2008.
[139] J. G. Simmons, "Electric Tunnel Effect between Dissimilar Electrodes Separated by a Thin Insulating Film," *J. Appl. Phys.*, vol. 34, no. 9, pp. 2581–2590, Sep. 1963.
[140] "Physics of Semiconductor Devices | Wiley Online Books." [Online]. Available: https://onlinelibrary.wiley.com/doi/book/10.1002/0470068329. [Accessed: 27-Aug-2019].
[141] T. Lee, W. Wang, and M. A. Reed, "Mechanism of electron conduction in self-assembled alkanethiol monolayer devices," *Ann. N. Y. Acad. Sci.*, vol. 1006, pp. 21–35, Dec. 2003.
[142] D. L. Klein, R. Roth, A. K. L. Lim, A. P. Alivisatos, and P. L. McEuen, "A single-electron transistor made from a cadmium selenide nanocrystal," *Nature*, vol. 389, no. 6652, pp. 699–701, Oct. 1997.
[143] null Andres *et al.*, "'Coulomb Staircase' at Room Temperature in a Self-Assembled Molecular Nanostructure," *Science*, vol. 272, no. 5266, pp. 1323–1325, May 1996.
[144] T. Henning, "Charging effects in niobium nanostructures," *ArXivcond-Mat9901308*, Jan. 1999.
[145] K. Miyaji and T. Hiramoto, "5.08 - Silicon Single Electron Transistors Operating at Room Temperature and Their Applications," in *Comprehensive Semiconductor Science and Technology*, P. Bhattacharya, R. Fornari, and H. Kamimura, Eds. Amsterdam: Elsevier, 2011, pp. 340–382.
[146] T. Bayrak *et al.*, "DNA-Mold Templated Assembly of Conductive Gold Nanowires," *Nano Lett.*, vol. 18, no. 3, pp. 2116–2123, Mar. 2018.
[147] A. C. Pearson *et al.*, "DNA origami metallized site specifically to form electrically conductive nanowires.," *J Phys Chem B*, vol. 116, no. 35, pp. 10551–10560, Sep. 2012.
[148] J. Liu *et al.*, "Metallization of Branched DNA Origami for Nanoelectronic Circuit Fabrication," *ACS Nano*, vol. 5, no. 3, pp. 2240–2247, Mar. 2011.
[149] P. Rai-Choudhury, *Handbook of Microlithography, Micromachining, and Microfabrication. Volume 1: Microlithography*. SPIE PRESS, 1997.

[150] A. A. Tseng, Kuan Chen, C. D. Chen, and K. J. Ma, "Electron beam lithography in nanoscale fabrication: recent development," *IEEE Trans. Electron. Packag. Manuf.*, vol. 26, no. 2, pp. 141–149, Apr. 2003.
[151] "Overview - EBL Patterning - Electron Beam Lithography - The University of Sheffield." [Online]. Available: https://www.sheffield.ac.uk/ebl/patterning. [Accessed: 11-Sep-2019].
[152] A. Ponce, S. Mejía-Rosales, and M. José-Yacamán, "Scanning transmission electron microscopy methods for the analysis of nanoparticles," *Methods Mol. Biol. Clifton NJ*, vol. 906, pp. 453–471, 2012.
[153] F. Krumeick, "Properties of electrons, their interactions with matter and applications in electron microscopy," *Lab. Inorg. Chem. Disponível Em Httpwww Microsc. Ethz ChdownloadsInteractions Pdf Consult. Em*, pp. 3–08, 2011.
[154] J. Ye, S. Helmi, J. Teske, and R. Seidel, "Fabrication of Metal Nanostructures with Programmable Length and Patterns Using a Modular DNA Platform," *Nano Lett.*, vol. 19, no. 4, pp. 2707–2714, Apr. 2019.
[155] R. Weichelt, J. Ye, U. Banin, A. Eychmüller, and R. Seidel, "DNA-Mediated Self-Assembly and Metallization of Semiconductor Nanorods for the Fabrication of Nanoelectronic Interfaces," *Chem. – Eur. J.*, vol. 25, no. 38, pp. 9012–9016, 2019.

# 8. Appendix

Supporting Information for Associated Publication P1

Supporting Information for Associated Publication P2

Supporting Information for Associated Publication P3

# Supporting Information for Associated Publication P1

## Supporting Information

## Fabrication of Metal Nanostructures with Programmable Length and Patterns Using a Modular DNA Platform

by

Jingjing Ye, Seham Helmi, Josephine Teske, Ralf Seidel

published in

Nano Letter 2019, 19, 4, 2707-2714

# Supporting Information

## Fabrication of metal nanostructures with programmable length and patterns using a modular DNA platform

Jingjing Ye[†,§],Seham Helmi[§,¶],Josephine Teske[§] and Ralf Seidel [†,§]

[†] Cluster of Excellence Center for Advancing Electronics Dresden (cfaed), TU Dresden, 01062 Dresden, Germany

[§] Molecular Biophysics group, Peter Debye Institute for Soft Matter Physics, Universität Leipzig, 04103 Leipzig, Germany

[¶] Present address: Department of Physics, University of Oxford, Oxford OX13PU, UK

Coresponding author contacts: ralf.seidel@physik.uni-leipzig.de Tel.+49 341 97 32501

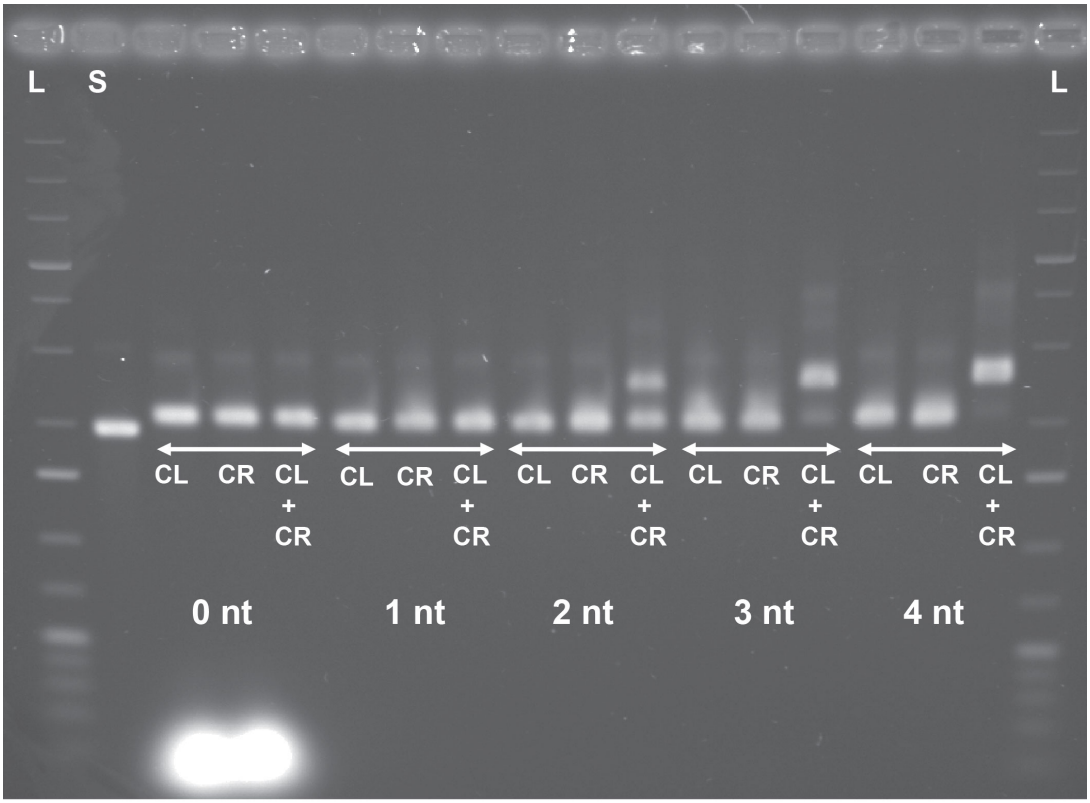


| overhang length | 0 nt | 1 nt | 2 nt | 3 nt | 4 nt |
|---|---|---|---|---|---|
| Monomer | 1 | 1 | 0.56 | 0.19 | 0.06 |
| Dimer | 0 | 0 | 0.44 | 0.81 | 0.94 |

**Figure S1.** Mold dimerization as function of the overhang length at attractive helix ends analyzed by gel electrophoresis. Dimer formation was tested between two molds carrying either an L-end or an R-end of the C-interface. Lanes labeled with L and S correspond to a 1 kb DNA size marker and the p8064 scaffold, respectively. Overhang length varied between 0 nt and 4 nt as indicated. For each overhang length the monomer with the left side of the interface (CL), the monomer with the right side of the interface (CR) and the mixture of both monomers (CL+CR) was analyzed. Dimer band started to appear for overhang length of 2 nt or larger. The table underneath the gel image provides the fractions of monomer and dimer bands in the CL+CR lane. The monomers with 0 nt overhangs were analyzed on the gel before purification, such that a bright band from the stable oligonucleotides is seen.

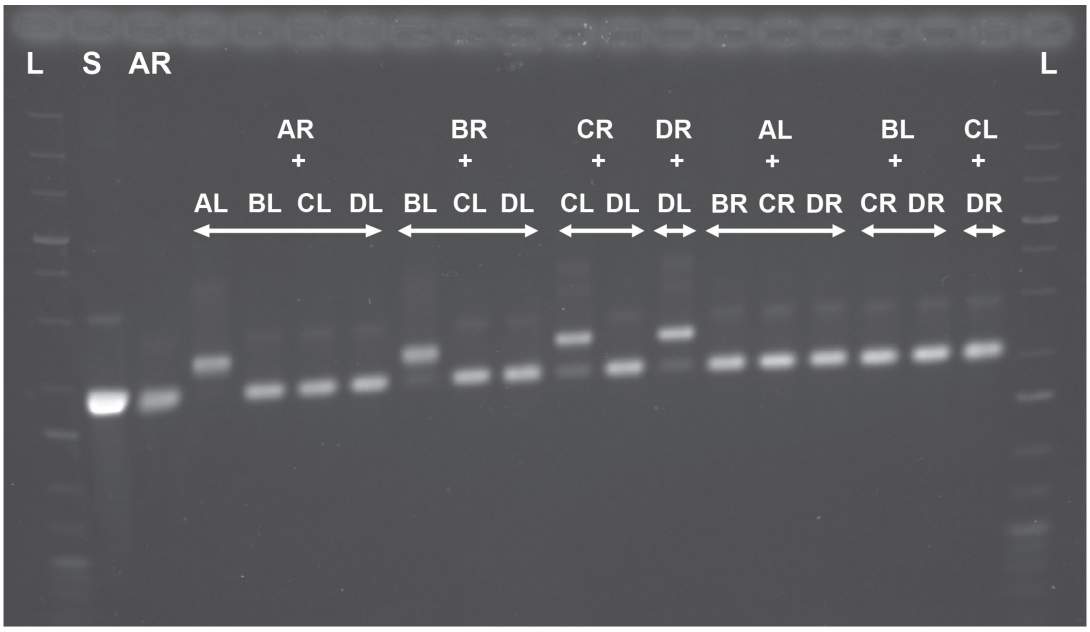


| | AL | BL | CL | DL |
|---|---|---|---|---|
| AR | 1 | 0 | 0 | 0 |
| BR | 0 | 0.9 | 0 | 0 |
| CR | 0 | 0 | 0.79 | 0 |
| DR | 0 | 0 | 0 | 0.86 |

**Figure S2.** Testing the dimerization for all possible combinations of interface L-ends with interface R-ends to verify the specificity of the designed interfaces. Molds with an attractive L-end were mixed at equal stoichiometry with molds with an attractive R-end and analyzed by agarose gel electrophoresis. Lanes labeled with L and S correspond to a 1 kb DNA size marker and the p8064 scaffold, respectively. Different mold mixtures are indicated by XR+YL, where X and Y indicate the particular interface. Dimerization occurs only when L-end and R-end monomers are from the same interface type. The table underneath the gel image provides the fractions of formed mold dimers.

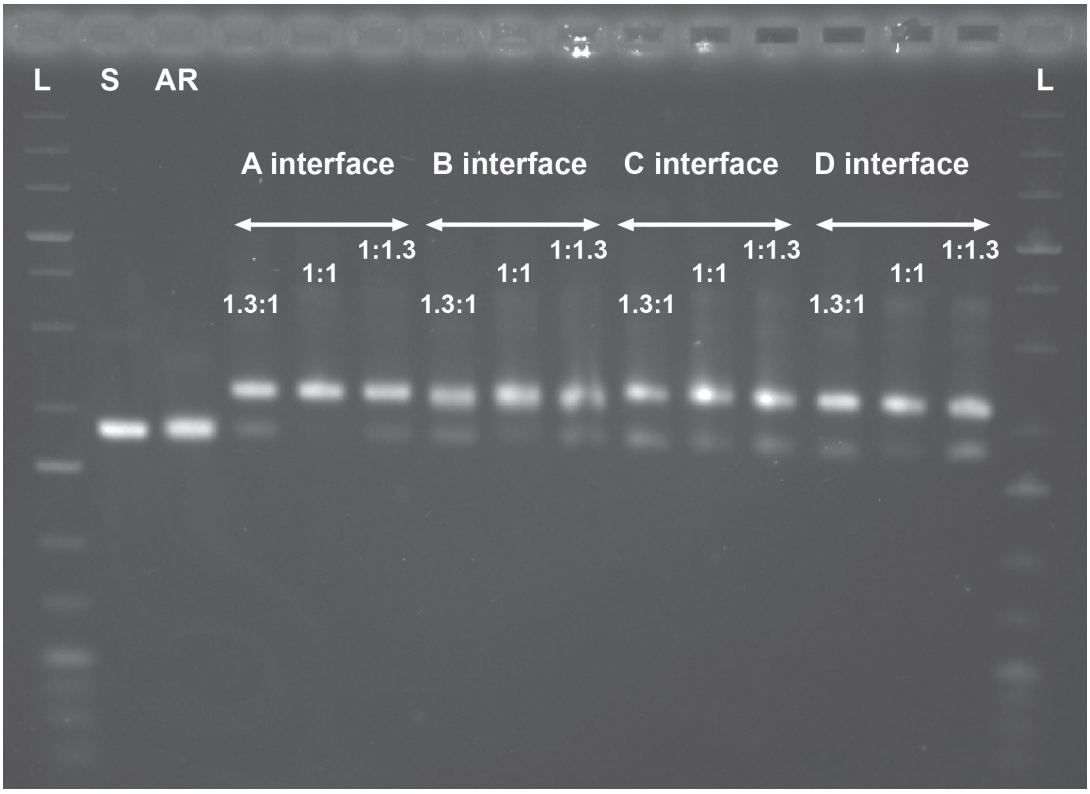


**Figure S3.** Mold mixing at the stoichiometric optimum was confirmed by gel electrophoresis. Lanes labeled with L and S correspond to a 1 kb DNA size marker and the p8064 scaffold, respectively. L-end molds were mixed with R-end molds of the same interface type at stoichiometries of 1.3:1, 1:1 and 1:1.3 as indicated in the image. Optimal dimerization, i.e. minimum monomer formation occurred for a 1:1 mixture of monomers.

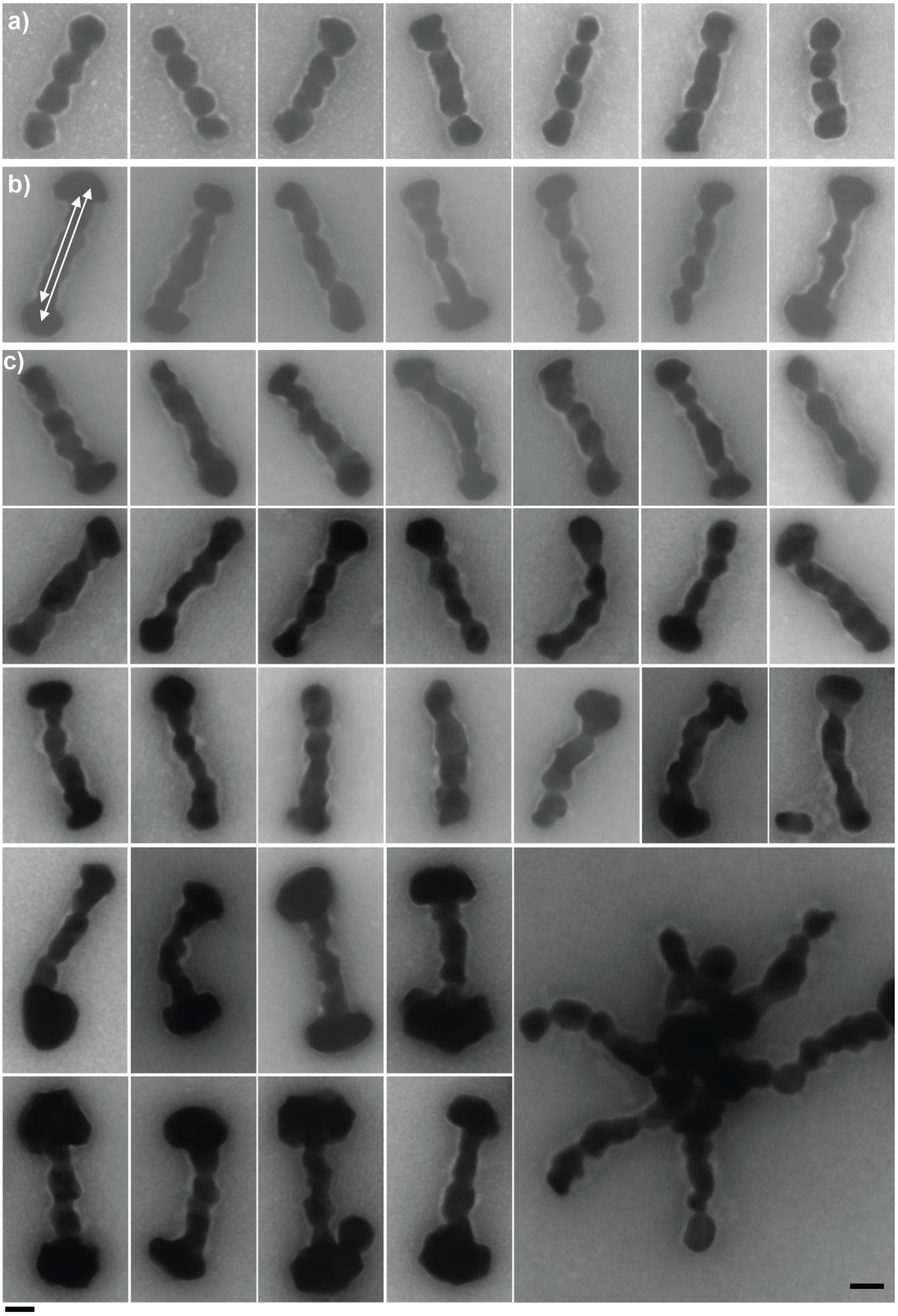


**Figure S4.** Selection of mold dimers after metal deposition. For a seed concentration of 2 nM the metallization used either: a) 450$\mu$M, b) 562.5$\mu$M or c) 675$\mu$M of H[$AuCl_4$]. Average lengths of the formed metal structures were obtained from the average of the stem length and the full length of the structures (see arrows in b). The image at the bottom right shows the aggregated dimers due to the gold outgrowth at the mold ends. The scale bars correspond to 20 nm.

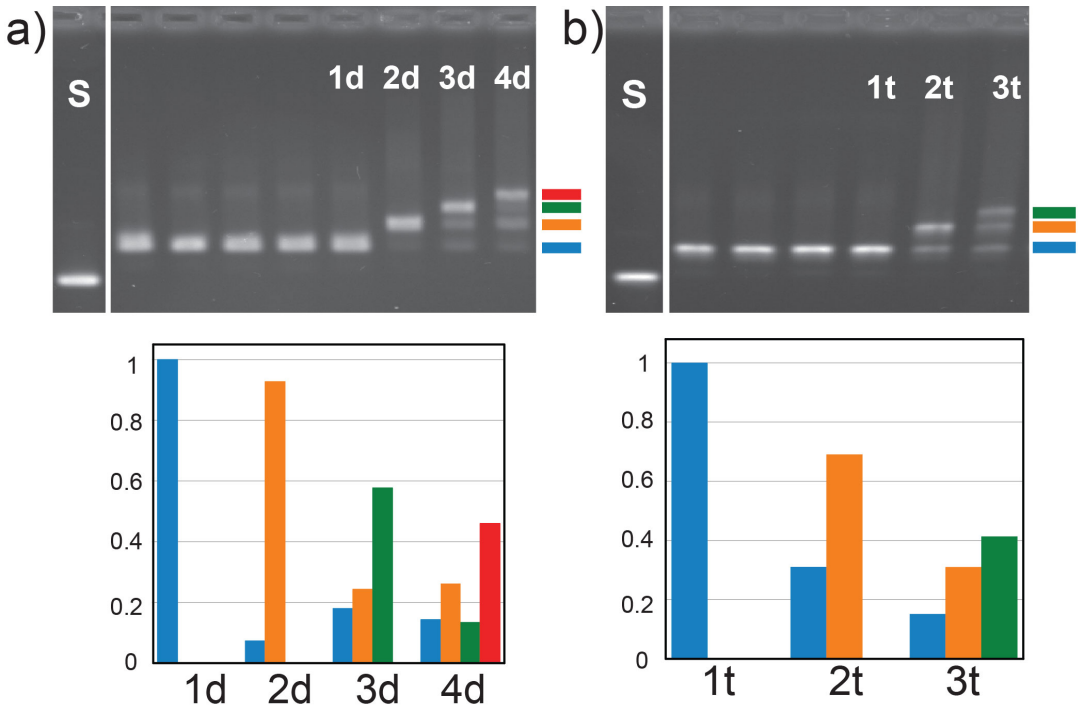


**Figure S5.** a) Controlled multimerization of dimers and trimers analyzed by agarose gel electrophoresis (see image 3 in the main text). a) Dimer multimerization. Gel lanes include the p8064 scaffold (S), the four different dimers and the reactions of forming a monomer, dimer, trimer and tetramer of dimers (labelled 1d, 2d, 3d, 4d, respectively). Color bars indicate the positions of the different multimers in the gel (blue, orange, green and res for monomer, dimer , trimer and multimer , respectively). The bar graph at the bottom shows the fraction of the different multimers as analyzed from the band intensities in the gel images. Notably, the efficiency to form the octamer reaches almost 50 %. b) Trimer multimerization. Gel lanes include the p8064 scaffold (S), the three different dimers and the reactions of forming a monomer, dimer and trimer of trimers (labelled 1d, 2d, 3d, 4d, respectively). The bar graph at the bottom shows the fraction of the different multimers. The yield of nonamer formation exceeded 40 %.

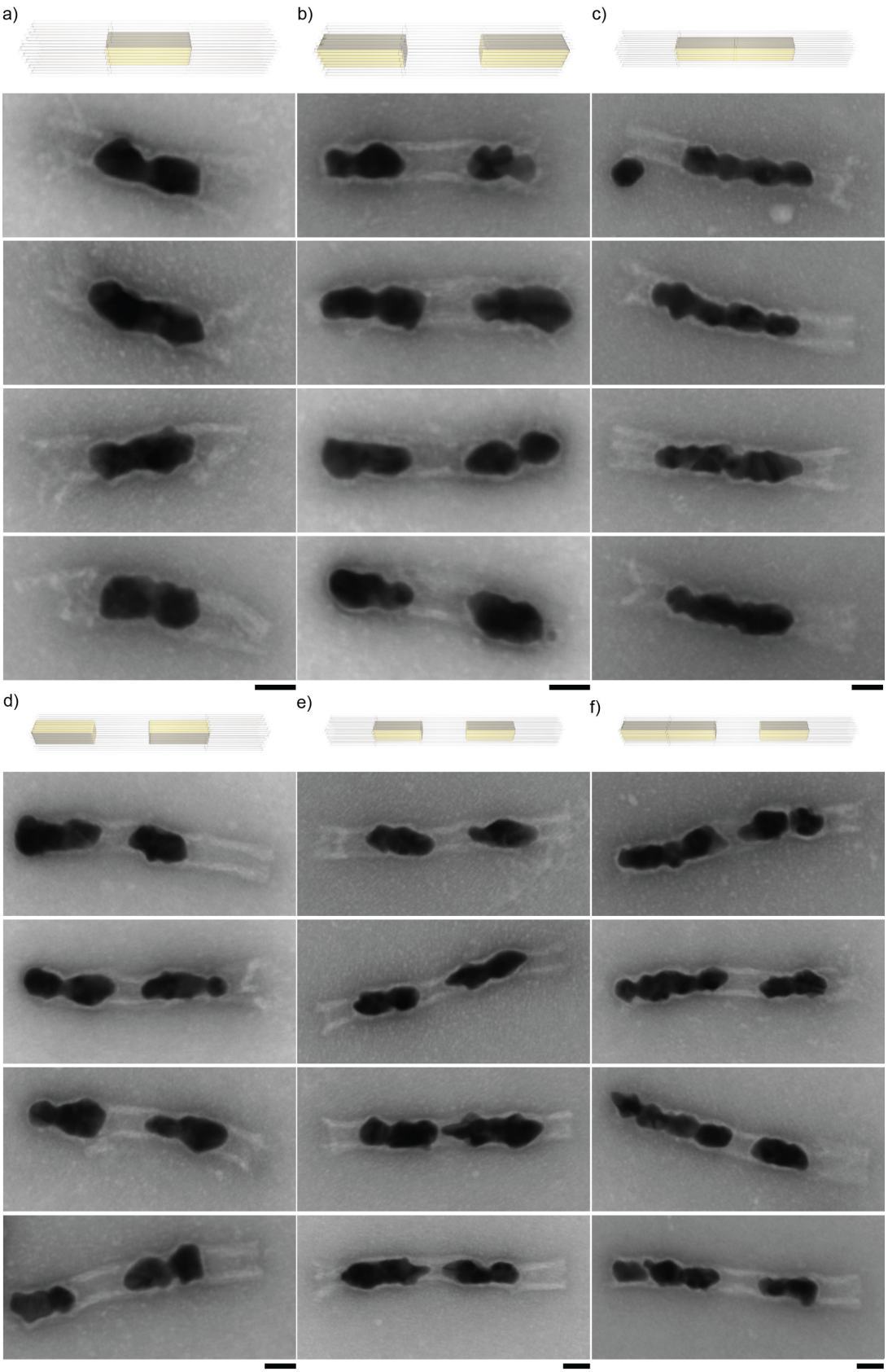


**Figure S6.** tSEM images of trimeric, tetrameric and pentameric mold superstructures after site-specific metal deposition. The intended metal deposition pattern as indicated in the cartoon above the images. The scale bars correspond to 50 nm.

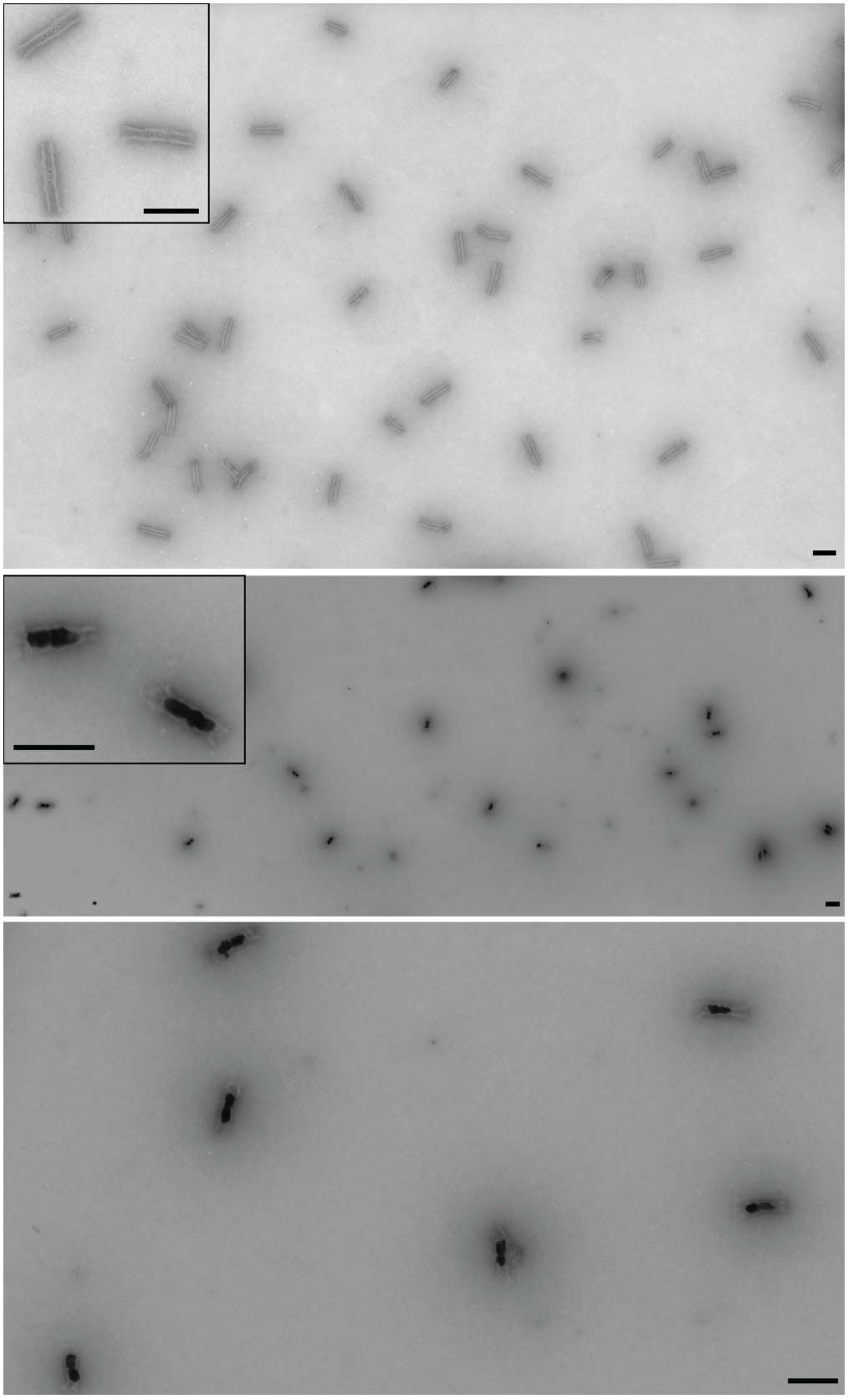

**Figure S7.** Overview tSEM images of a mold trimer with a single central gold block before and after metallization (see Figure S6a). The scale bars correspond to 100 nm.

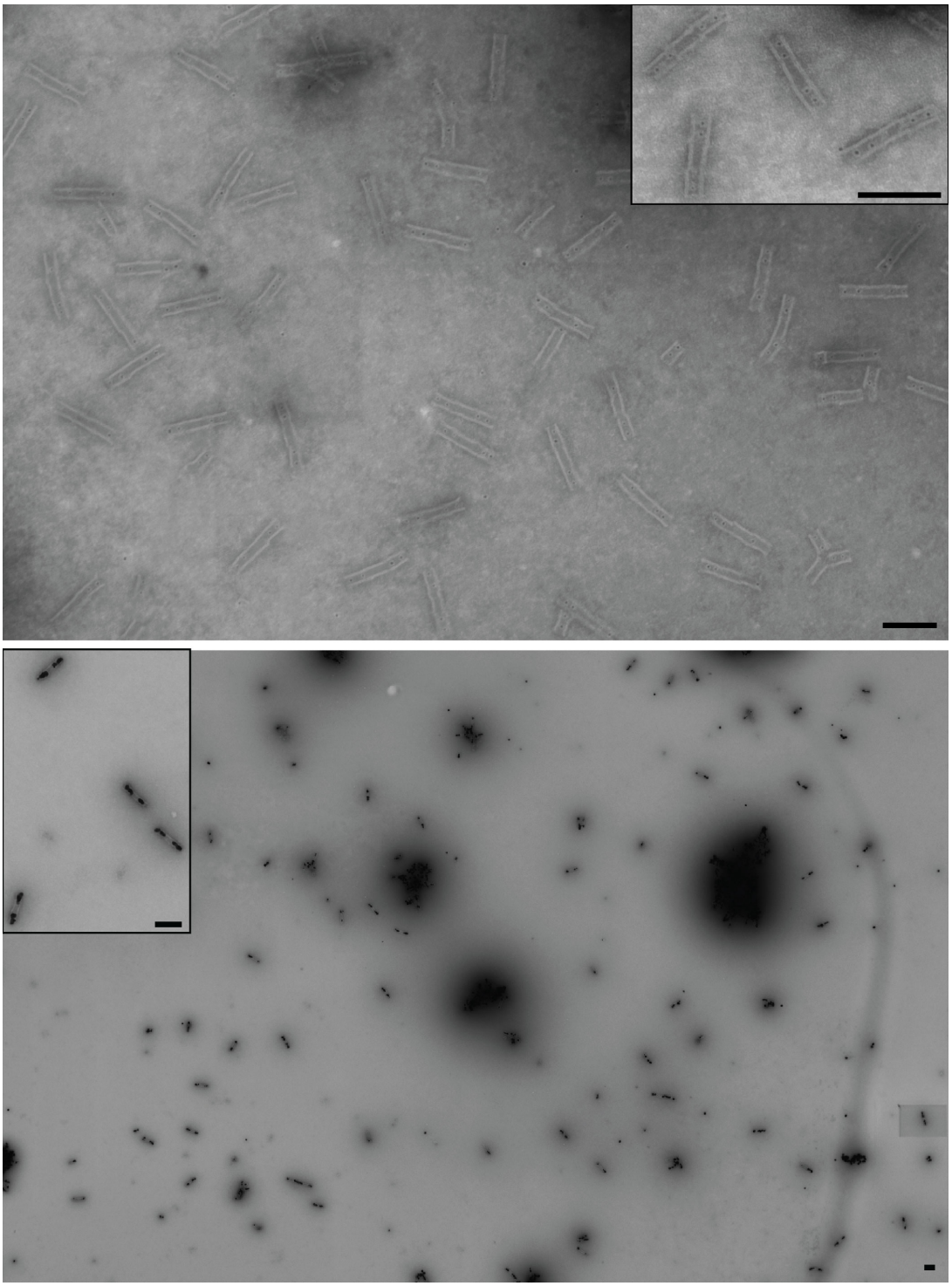

**Figure S8.** Overview tSEM images of a mold trimer with two terminal gold blocks separated by a gap before and after metallization (see Figure S6b). The scale bars correspond to 100 nm.

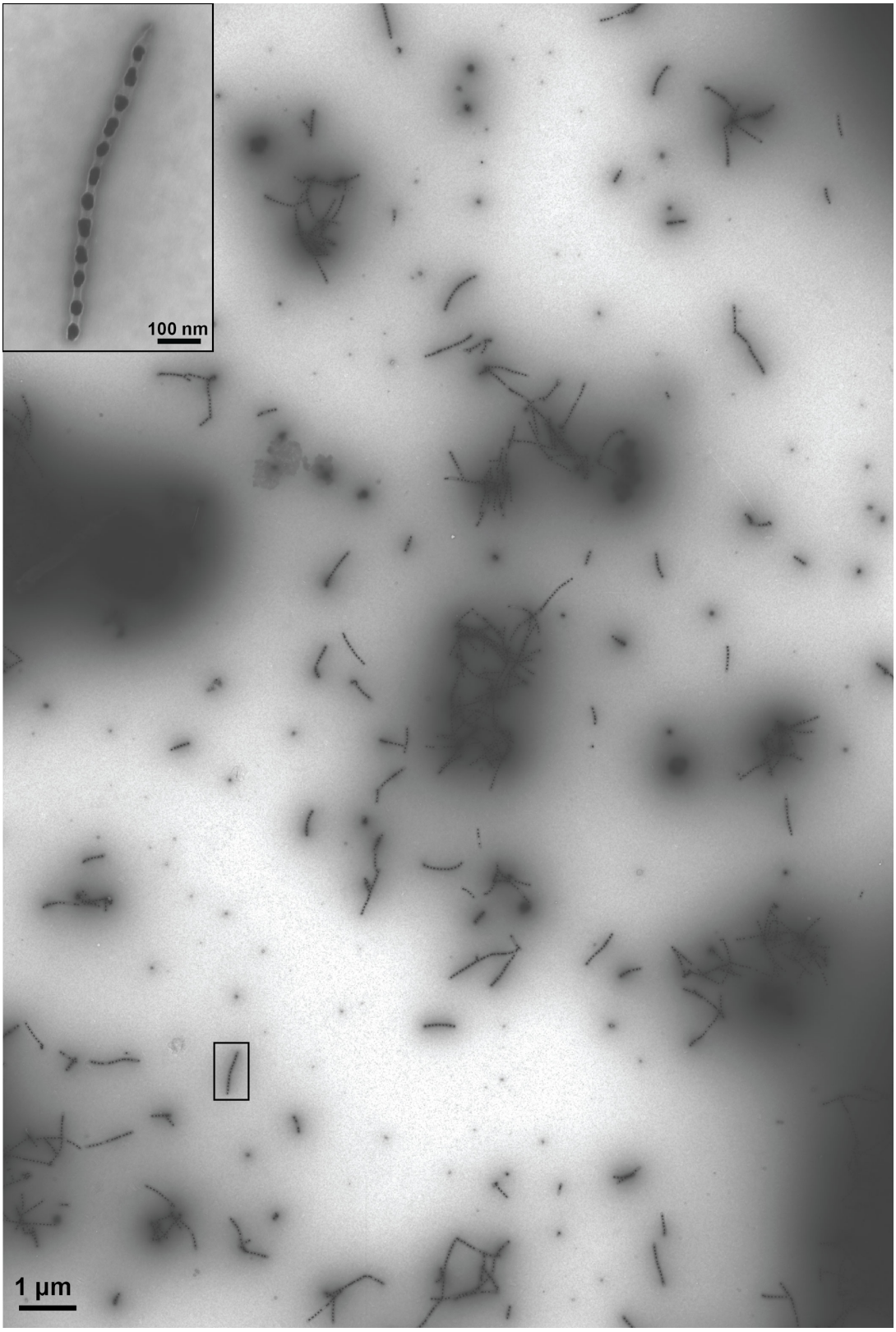


**Figure S9.** Overview tSEM image of the alternating chain pattern of one empty and one gold-filled mold using two interfaces (see Figure 5a, main text). The formation of $\mu$m-long linear structures is observed.

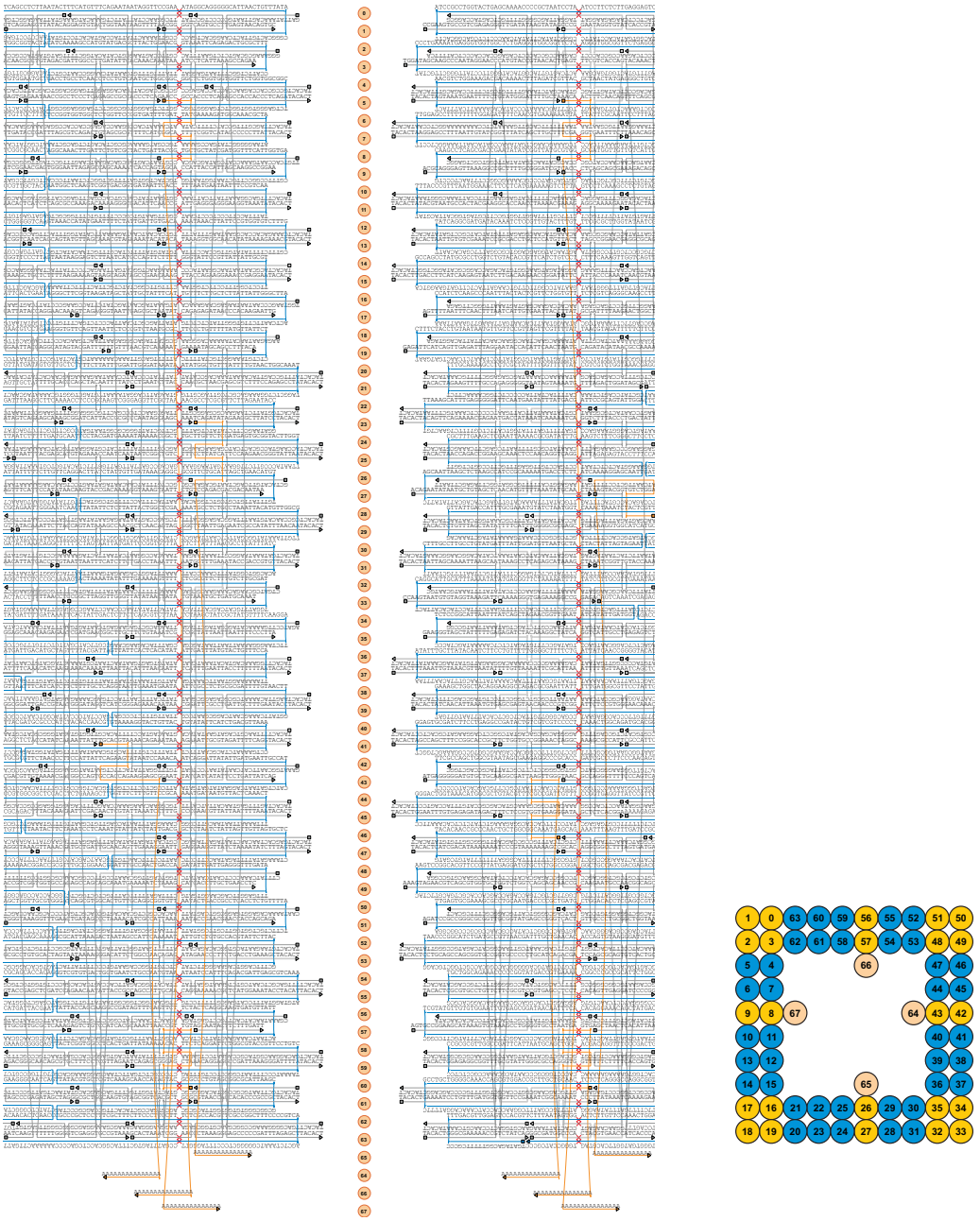

**Figure S10. Design template for a mold with Interface A at either end.** Shown is the detailed sequence and folding of the 8064 nt scaffold (blue) and the various staples (other colors) used to create the structure. For better visualization of the AL-AR interface docking the design was cut into two parts to place the interface sides opposite to each other. Repulsive ends carry a 5'-TACACT ssDNA extension at the 5' and 3'-ends (repulsive helices are marked in blue in the scheme on the right). Attractive helices of the A interface have a 3 nt **5' end extension** and a 3 nt **3' end recession** (attractive helices are marked in yellow in the scheme on the right). Staples in yellow represent the capture strands that carry 15 nt 3'-polyadenine overhangs for attaching two DNA-coated AuNP seeds. Squares and triangles at the staple ends symbolize the 5'- and the 3'-end, respectively. The core design template was created using CaDNAno[1]. Red crosses are imaginary gaps that were introduced for better graphical representation. This was done in order to fit the 8 bp lattice size (corresponding to about 270° turns) into the 63 bp unit cell (six helical turns of dsDNA) that underly the square-lattice arrangement of DNA helices.

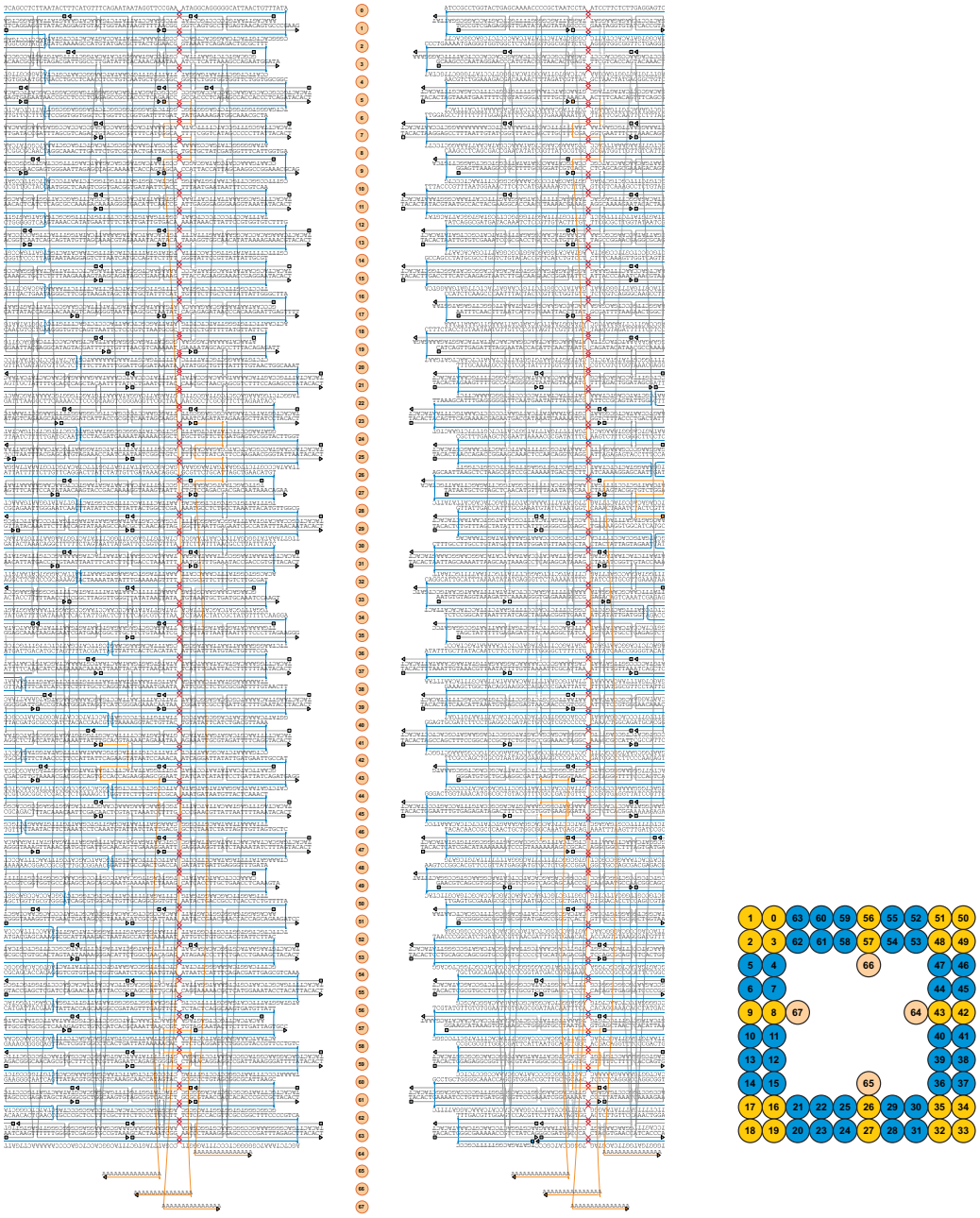

**Figure S11. Design template for a mold with Interface B at either end.** Repulsive ends marked in blue carry a 5'-TACACT ssDNA extension at the 5' and 3'-ends. Attractive helix ends (marked in yellow) of the B interface have a 3 nt **5' end recession** and a 3 nt **3' end extension**. Colors and symbols are as in Supplementary Figure S10.

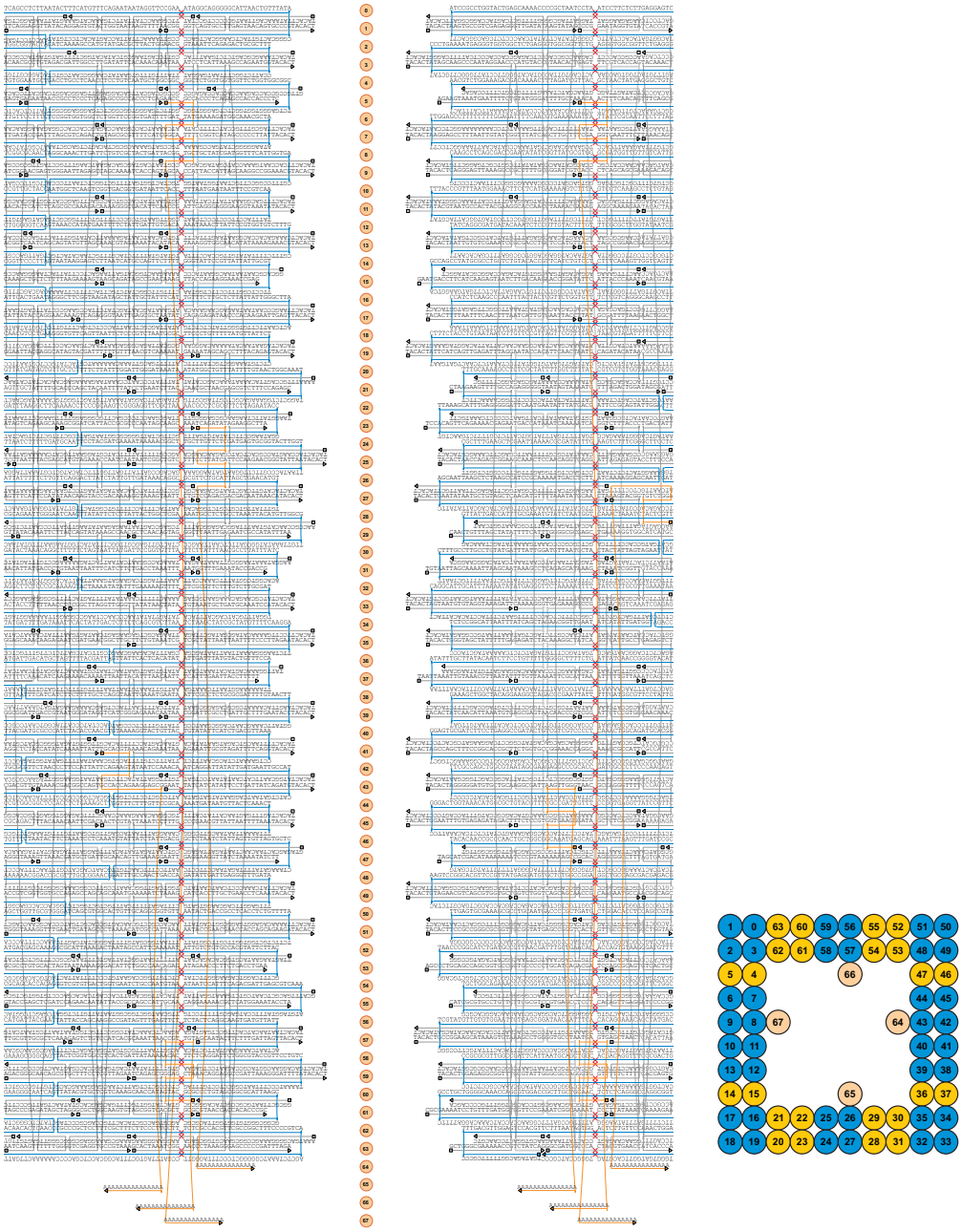

**Figure S12. Design template for a mold with Interface C at either end.** Repulsive ends (marked in blue) carry a 5'-TACACT ssDNA extension at the 5' and 3'-ends. Attractive helix ends (marked in yellow) of the C interface have a 3 nt **5' end extension** and a 3 nt **3' end recession**. Colors and symbols are as in Supplementary Figure S10.

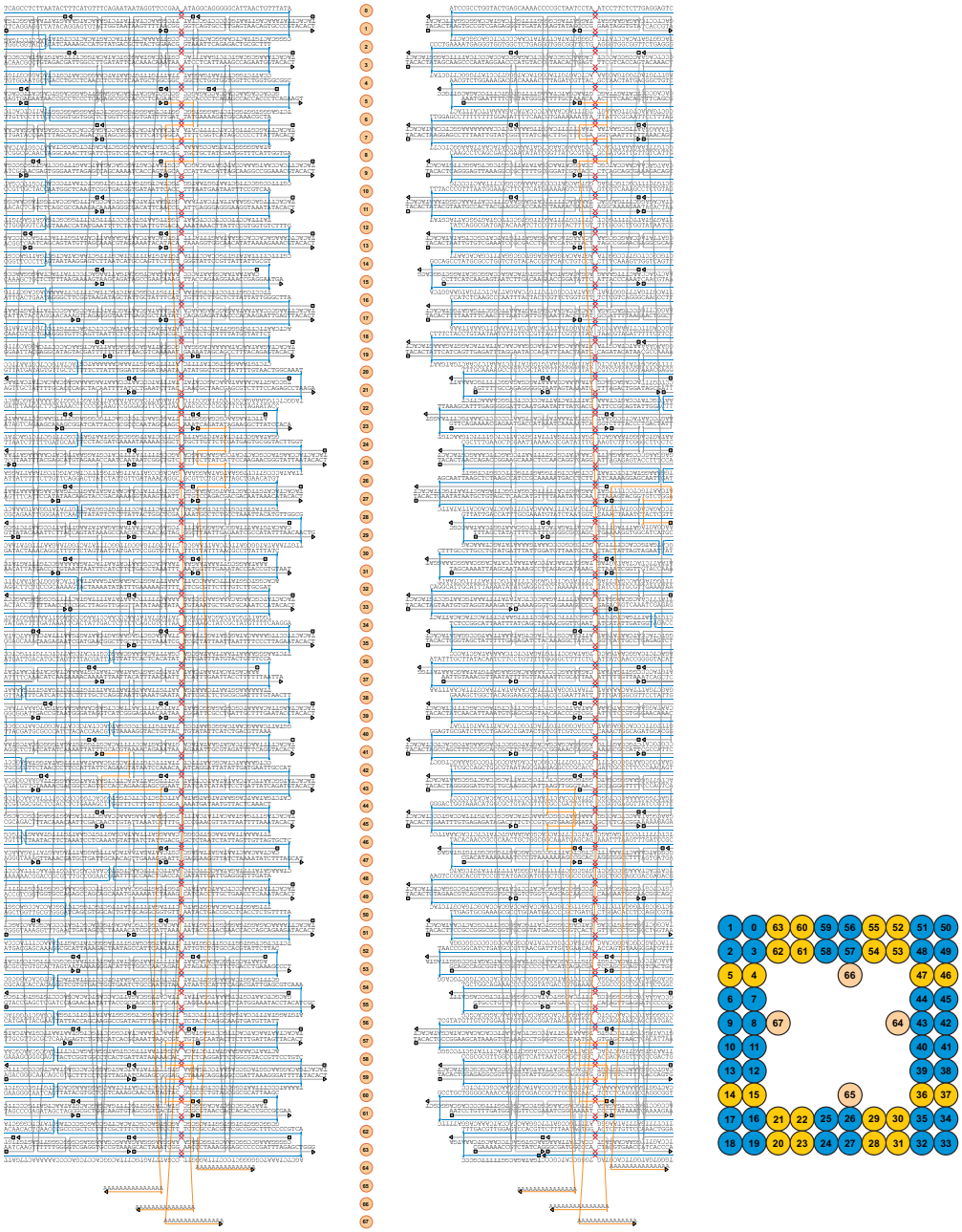

**Figure S13. Design template fora mold with Interface D at either end.** Repulsive ends (marked in blue) carry a 5'-TACACT ssDNA extension at the 5' and 3'-ends. Attractive helices (marked in yellow) of the B interface have a 3 nt **5'-end recession** and a 3 nt **3' end extension**. Colors and symbols are as in Supplementary Figure S10.

## References


1. Douglas, S. M.; Marblestone, A. H.; Teerapittayanon, S.; Vazquez, A.; Church, G. M.; Shih, W. M. *Nucleic Acids Research* **2009**, *37*, 5001–5006.

# Supporting Information for Associated Publication P2

## Supporting Information

## DNA-Mold Templated Assembly of Conductive Gold Nanowires

by

Türkan Bayrak,* Seham Helmi,* Jingjing Ye,* Dominik Kauert, Jeffrey Kelling, Tommy Schönherr, Artur Erbe, Ralf Seidel

*equal contribution

published in

Nano Letter 2018, 18, 3, 2116-2123

# Supporting Information

## DNA mold templated assembly of conductive gold nanowires

Türkan Bayrak[†,‡,♯], Seham Helmi[§,¶,♯], Jingjing Ye[‡,§,♯], Dominik J. Kauert[§], Jeffrey Kelling[$], Tommy Schoenherr[†], Richard Weichelt[&,‡], Artur Erbe[†,‡,*] and Ralf Seidel[‡,§,*]

[†] Institute of Ion Beam Physics and Materials Research, Helmholtz-Zentrum Dresden-Rossendorf, 01328 Dresden, Germany

[‡] Cluster of Excellence Center for Advancing Electronics Dresden (cfaed), TU Dresden, 01062 Dresden, Germany

[§] Molecular Biophysics group, Peter Debye Institute for Soft Matter Physics, Universität Leipzig, 04103 Leipzig, Germany

[$] Department of Information Services and Computing, Helmholtz-Zentrum Dresden-Rossendorf, 01328 Dresden, Germany

[&] Institute of Physical Chemistry, TU Dresden, 01062 Dresden, Germany

[¶] Present address: Department of Physics, University of Oxford, Oxford OX13PU, UK

[♯] These authors contributed equally to the presented work

[*] Correspondence should be addressed to Artur Erbe (a.erbe@hzdr.de, Tel. +49 351 260 2366) or Ralf Seidel (ralf.seidel@physik.uni-leipzig.de, Tel. +49 341 97 32501)

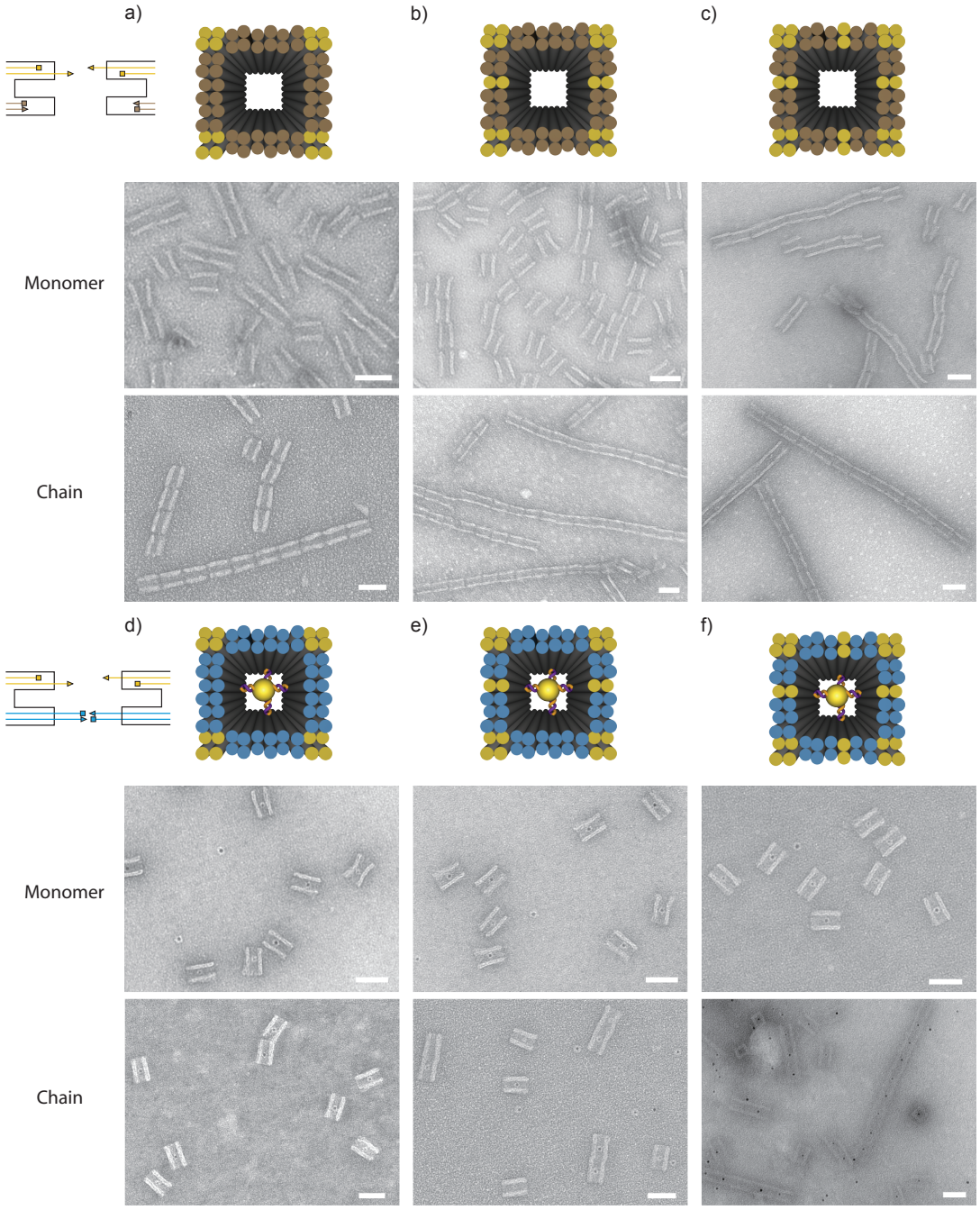


**Figure S1.** (a-c) Molds with attractive and non-attractive helix ends. Cartoons in the top row of each subfigure indicate the positions of attractive (in yellow) and non-attractive ends (in brown) that were obtained by omitting end staples at these positions (see cartoon on the left side of figure). TEM images below the cartoons were recorded for a single monomer type and by mixing both monomers types as indicated. We tested (a) 16, (b) 20 and (c) 24 attractive ends. While non-specific chain formation was strongest for 24 attractive ends, dimeric and trimeric chains in staggered conformations were still found for 20 and 16 attractive ends. All versions supported the formation of longer linear, non-staggered assemblies when mixing both monomer types.
(d-f) Molds with attractive and repulsive helix ends shown in the cartoons in yellow and blue, respectively. The figures show the same set of experiments as for molds with with non-attractive ends. Molds of a single type remained monomeric for all tested numbers of attractive helices. When mixing both monomer types, linear chain formation was only observed for 24 attractive helices. The scale bar in all TEM images is 50 nm.

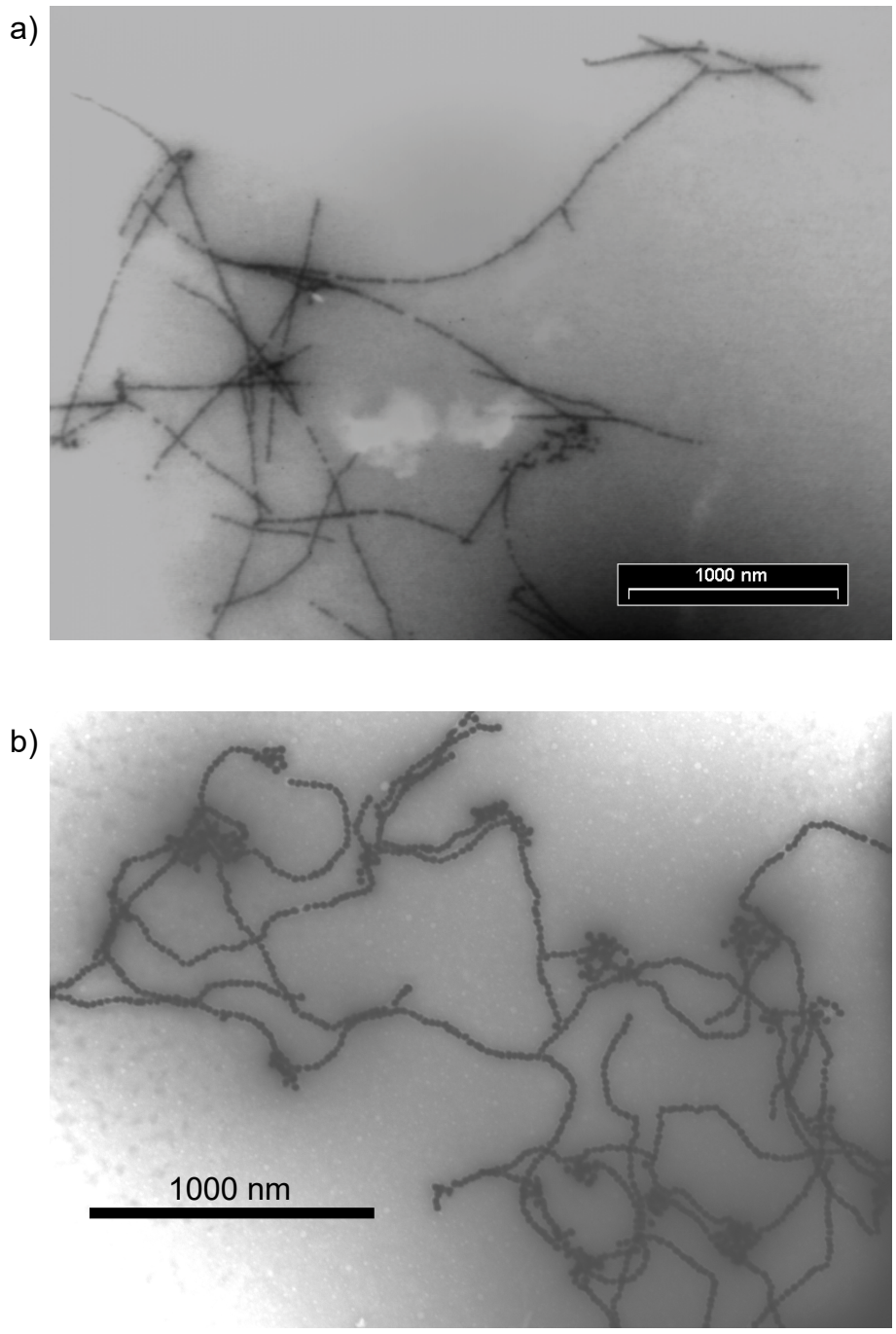


**Figure S2. Overview TEM images of linear gold structures after metallization.** The shown images correspond to a a) 1-fold and b) 4-fold relative gold concentration (see Figure 3, main text). The formation of $\mu$m long linear structures is observed.

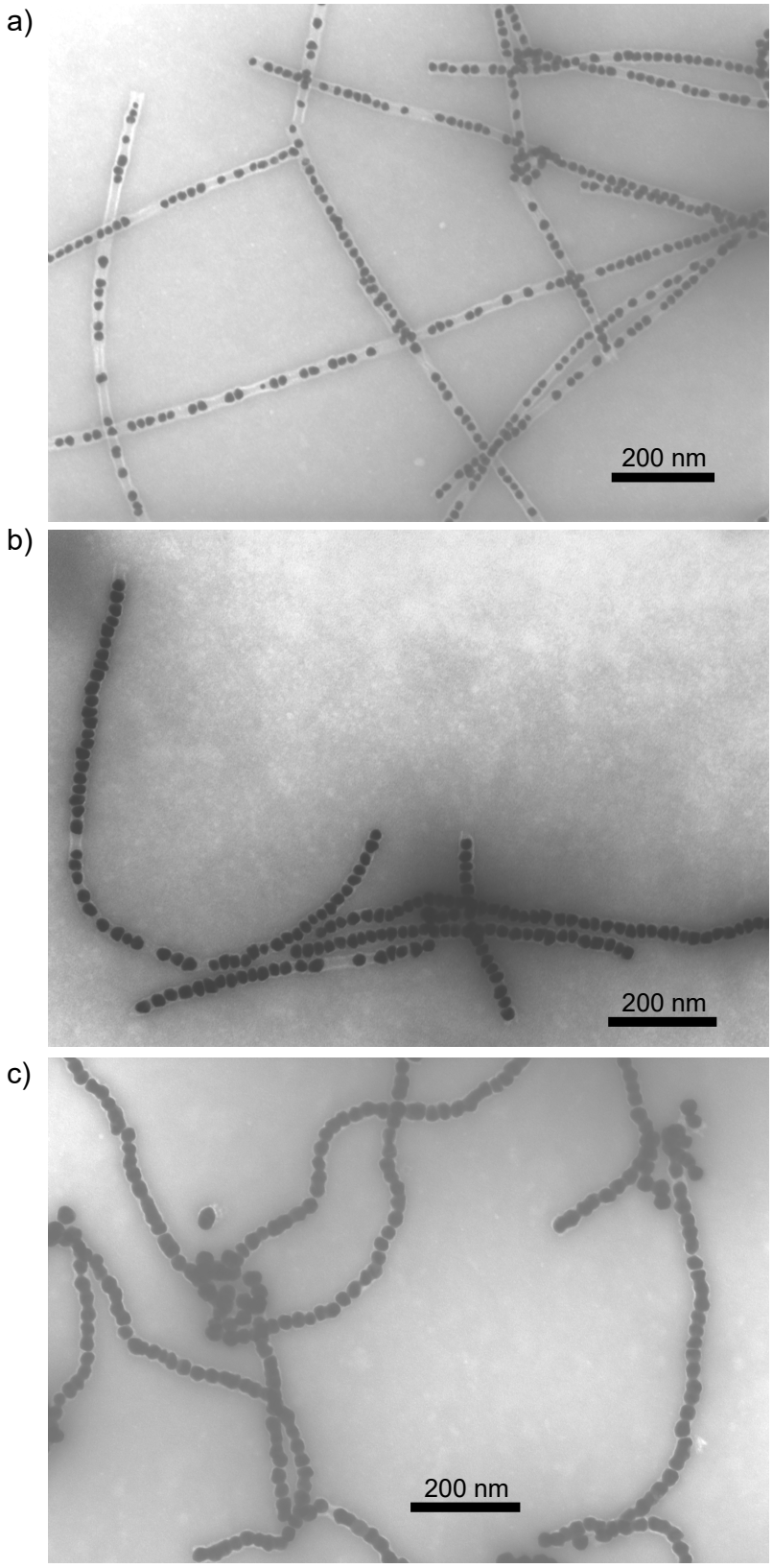


**Figure S3. TEM images of linear gold structures after metallization on a $\mu$m-scale.** The shown images correspond to a a) 1-fold, b) 2-fold and c) 4-fold relative gold concentration (see Figure 3, main text). With increasing gold deposition, the structures become more continuous but also slightly curved.

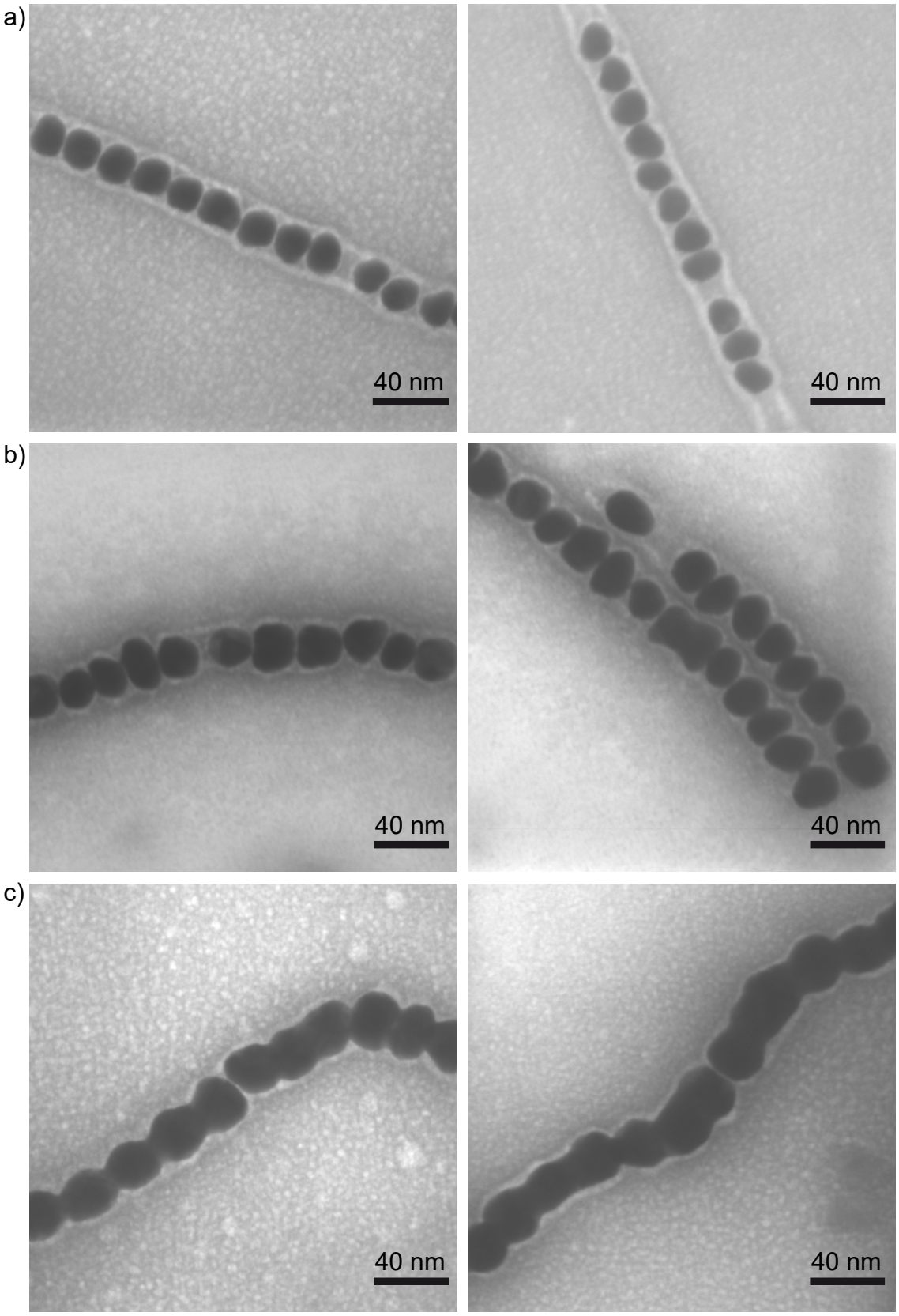


**Figure S4. High magnification TEM images of linear gold structures after metallization.** The shown images correspond to a a) 1-fold, b) 2-fold and c) 4-fold relative gold concentration (see Figure 3, main text). At the highest applied gold concentration many of the individual gold clusters become connected to each other, though nm-sized gaps between individual clusters remain occasionally.

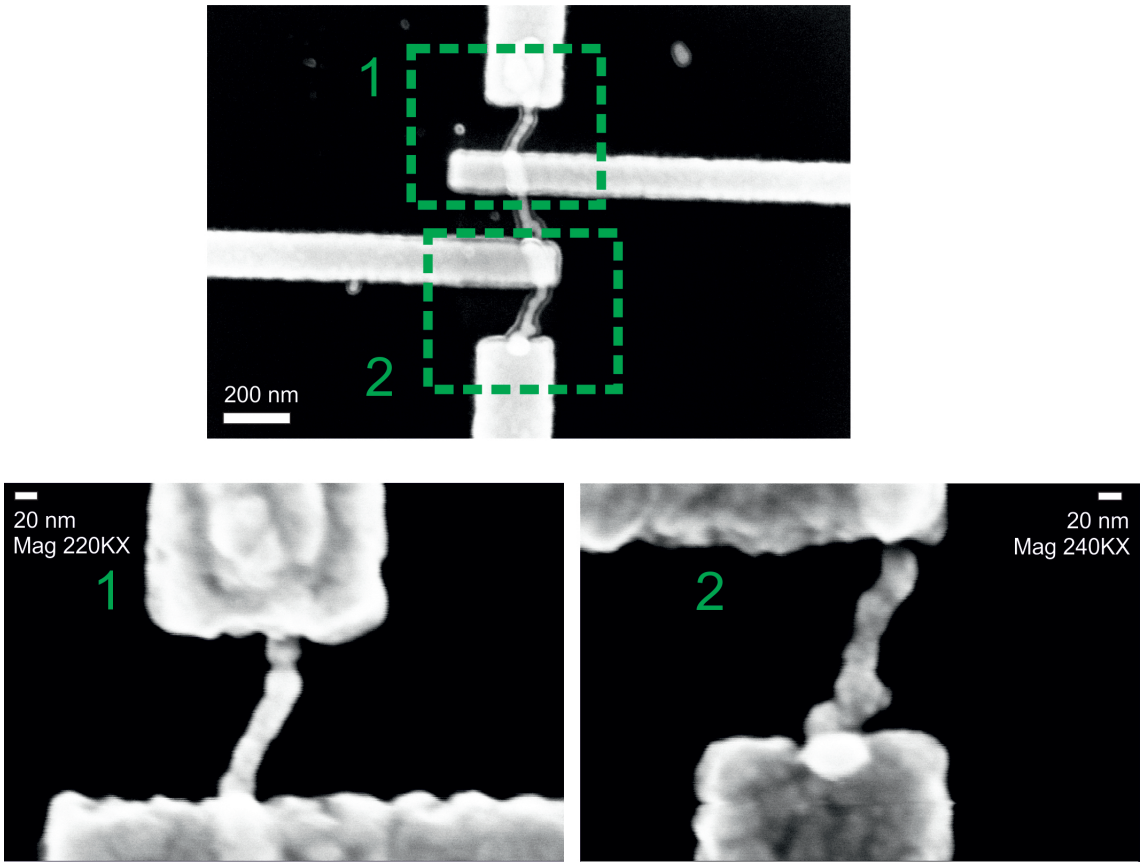


**Figure S5. SEM images of a wire with four contacts, which was found to be non-conductive** ($R > 260\,G\Omega$). The limited resolution of SEM imaging on the $SiO_2$ substrate did not allow to resolve residual gaps within the wire that blocked the conductivity.

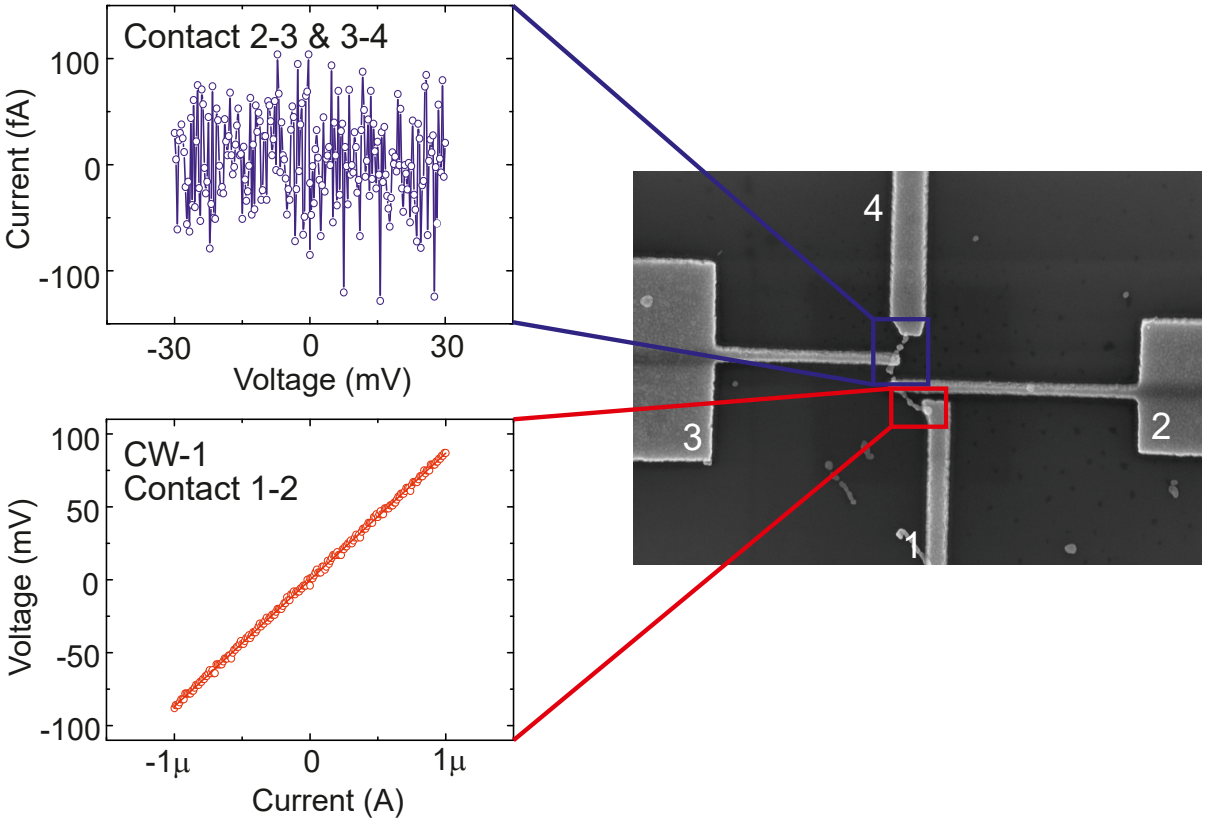


**Figure S6. Conductance measurements between different contacts of the structure containing CW-1.** Shown are an SEM image of the wire with the four contacts, the V-I curve of CW-1 measured between contacts 1-2 (measured by applying a defined current) and the I-V curve of the wire measured between contacts 3-4 (measured by applying a defined voltage bias). The latter indicates an insulating behavior of the wire between contacts 3-4. A similar behavior was found between contacts 2-3.

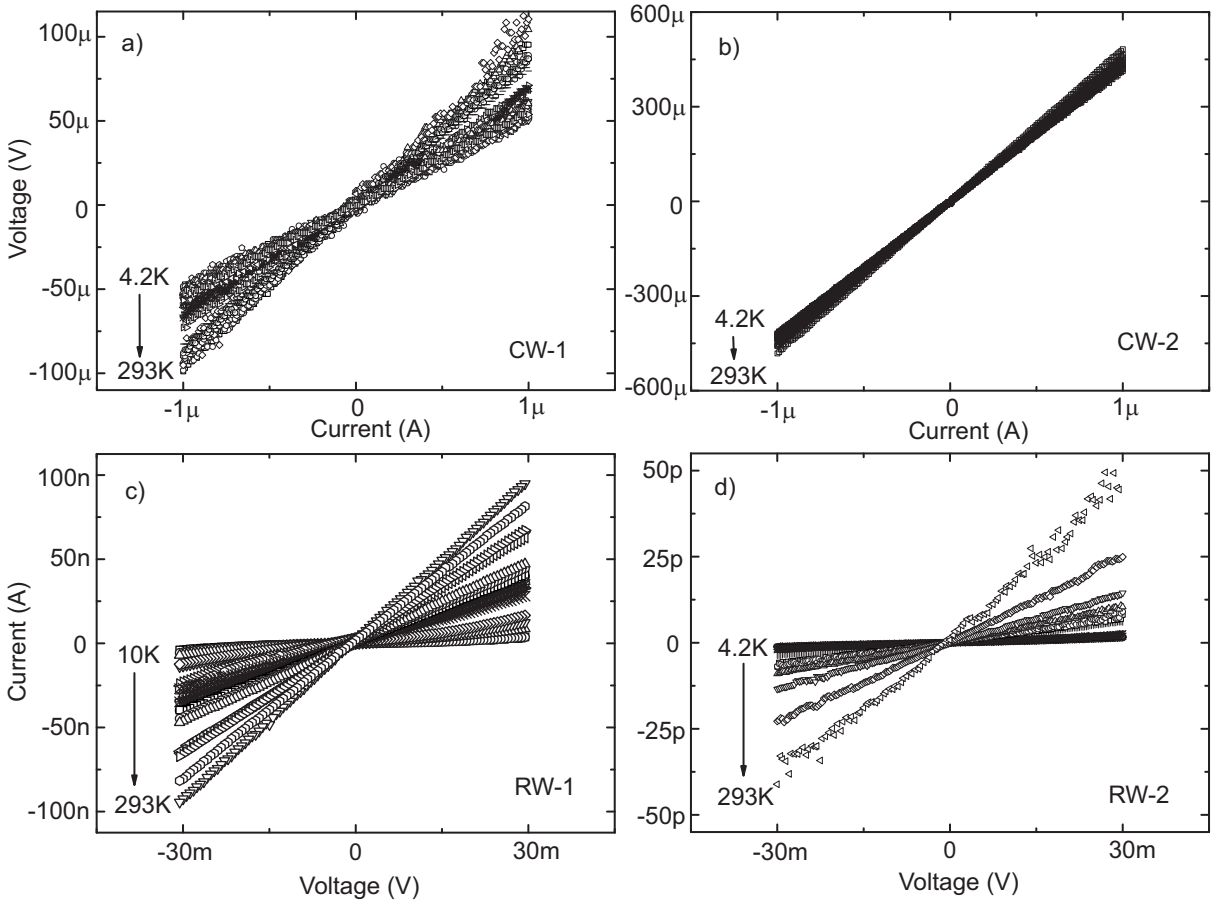


**Figure S7. Temperature dependent I-V behavior of CW-1, CW-2, RW-1 and RW-2 over the temperature range from 4.2 to 293 K.** (a,b) Curves for conductive wires CW-1 and CW-2 that were measured by applying a defined current. (c,d) Curves for the more resistive wires RW-1 and RW-2 that were measured by applying a defined voltage bias.

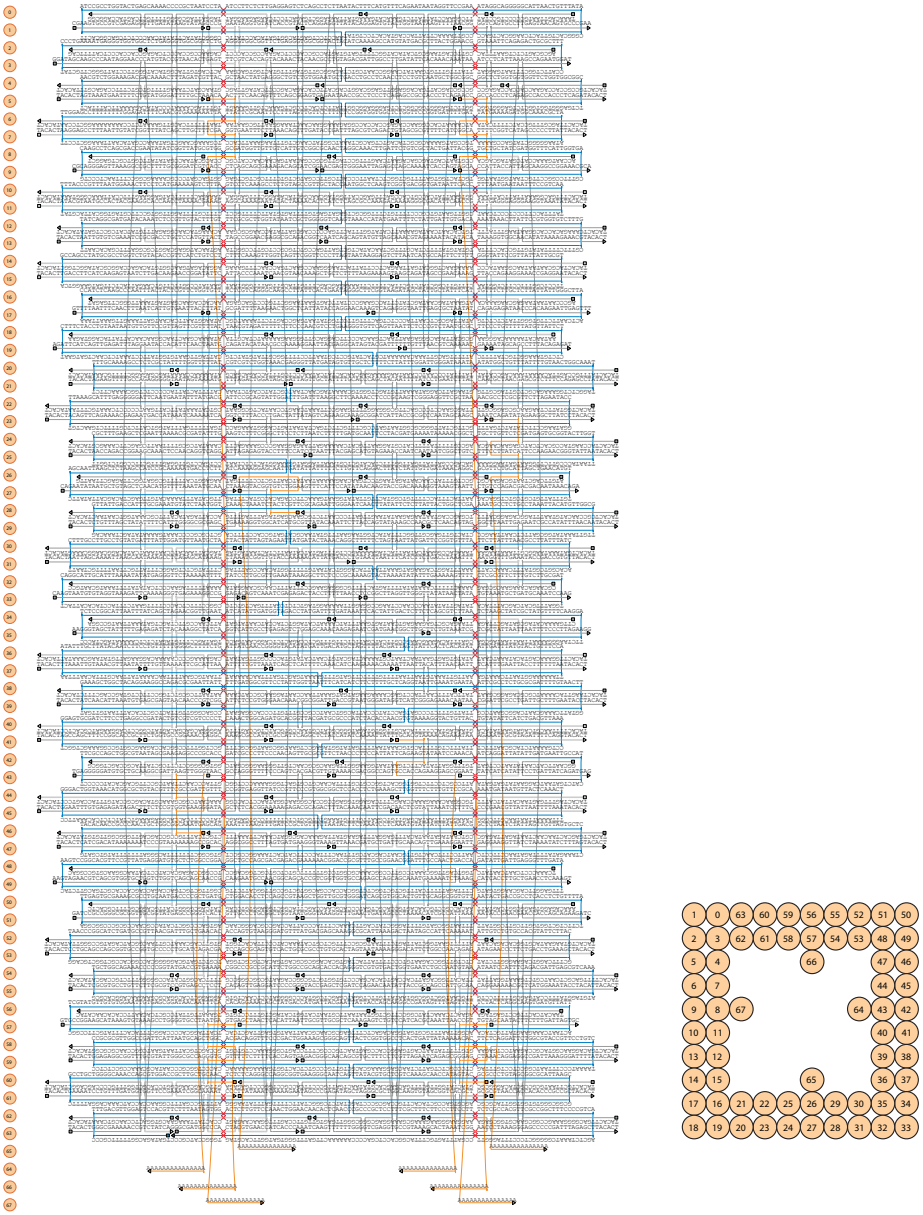

**Figure S8. Design template for the AB' DNA origami mold with 24 attractive and 40 repulsive helix ends.** Shown is the detailed sequence and folding of the 8064 nt scaffold (blue) and the various staples (other colors) used to create the structure. Repulsive ends carry a 5'-TACACT ssDNA extension both at 5' and 3'-ends. Attractive helices carry on the A interface (left side) either a 2 nt 5'-staple end extension or a 2 nt 3'-staple end recession. Correspondingly, attractive helices carry on the B' interface (right side) either a 2 nt 3'-staple end extension or a 2 nt 5'-staple end recession. Staples in yellow represent the capture strands that carry 15 nt 3'-polyadenine overhangs for attaching two DNA-coated AuNP seeds. Squares and triangles at the staple ends symbolize the 5'- and the 3'-end, respectively. The core design template was created using CaDNAno[1]. Red crosses are imaginary gaps that were introduced for better graphical representation. This was done in order to fit the 8 bp lattice size (corresponding to about 270° turns) into the 63 bp unit cell (six helical turns of dsDNA) that underly the square-lattice arrangement of DNA helices.

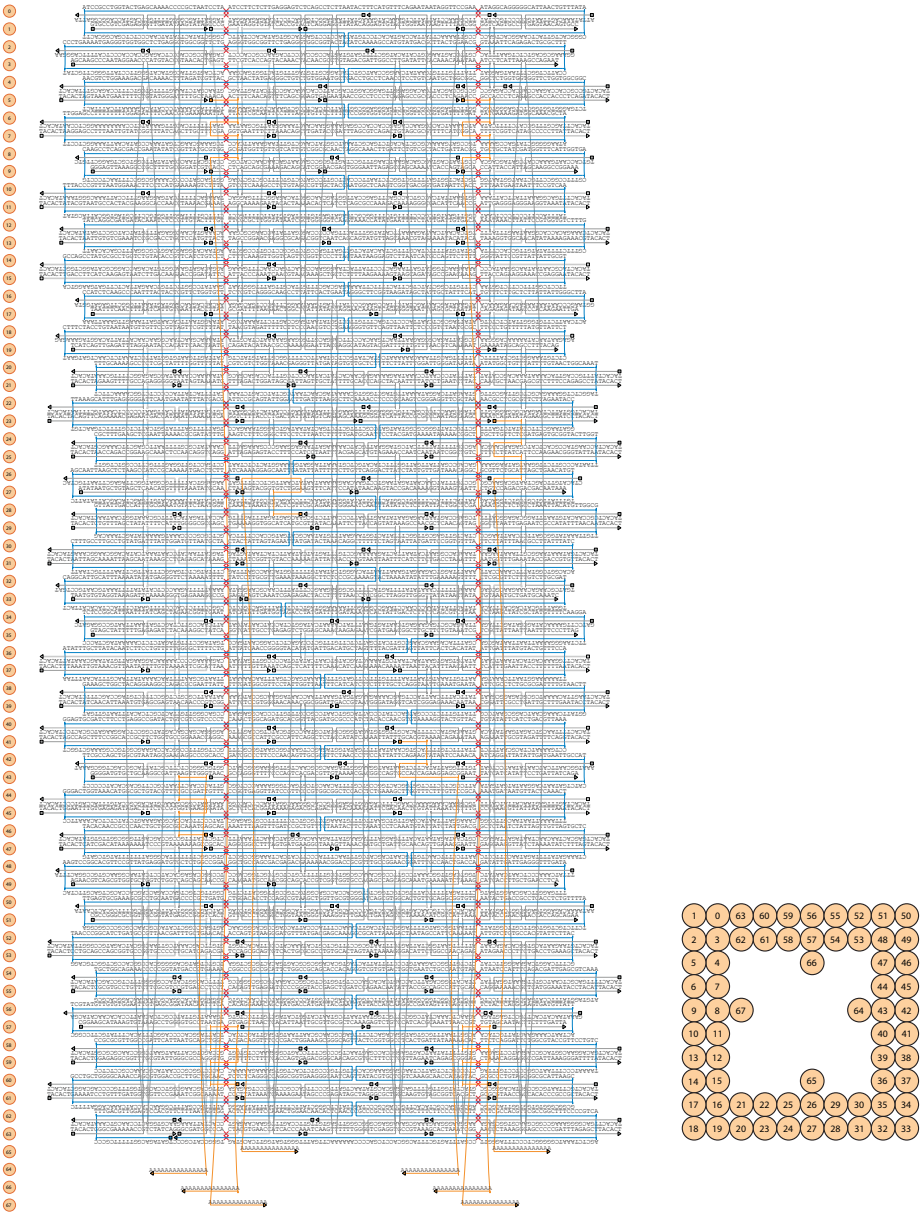

**Figure S9. Design template for the BA' DNA origami mold with 24 attractive and 40 repulsive helix ends.** The ends are complementary to the ends of the mold with AB' ends. Attractive helices carry on the B interface (left side) either a 2 nt 3'-staple end extension or a 2 nt 5'-staple end recession. Correspondingly, attractive helices carry on the A' interface either a 2 nt 5'-staple end extension or a 2 nt 3'-staple end recession. Colors and symbols are as in Supplementary Figure S5.

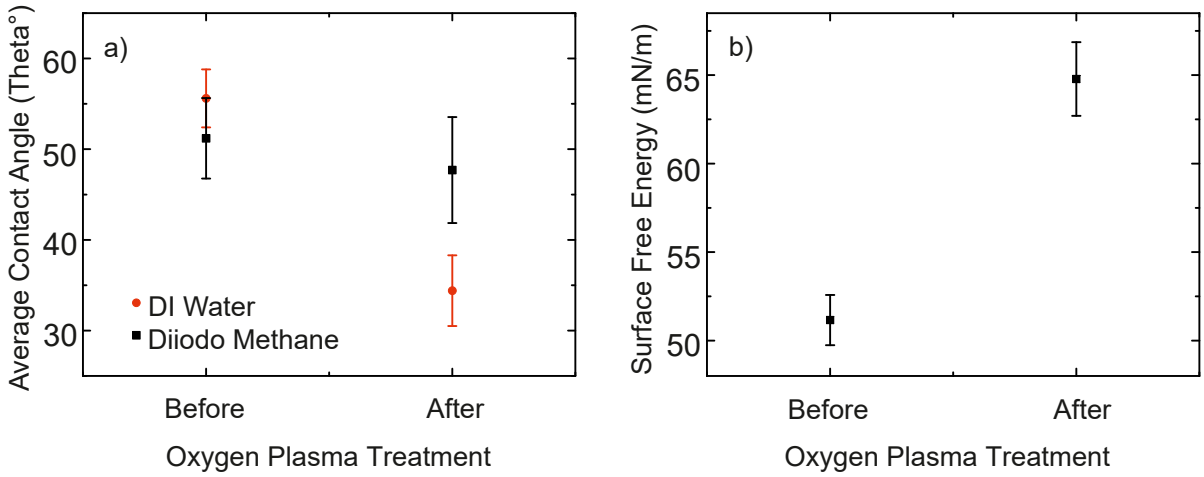


**Figure S10. Contact angles and surface energies of a $SiO_2$ substrate before and after the oxygen plasma treatment.** (a) To understand the influence of plasma treatment on the adsorption of the nanowires at $O_2$ surfaces, contact angles on 300 nm$SiO_2$ surfaces (precleaned 10 s with water and 10 s with ETOH) were measured before and after plasma treatment. To this end small droplets of either deionized water $2.54 \pm 0.18 \mu l$ or diiodo-methane $2.83 \pm 0.49 \mu l$ were deposited on $SiO_2$ surface and imaged using a Drop Shape Analysis System (Krüss , DSA 10Mk2). Contact angles were determined from images recorded at a optimally adjusted viewing angle. Oxygen plasma treatment reduced the contact angle strongly for water and moderately for diiodo-methane. The strong decrease for water can be explained by an increased electrostatic charge on the surface thus increasing its hydrophylicity. (b) The surface free energy of the $SiO_2$-liquids interface including of disperse and polar contributions were calculated by the Owens-Wendt method by using the Drop Shape Analysis Software version 1.80.0.2. The plasma treatment caused a significant increase of the surface energy.

## References

1. Douglas, S. M.; Marblestone, A. H.; Teerapittayanon, S.; Vazquez, A.; Church, G. M.; Shih, W. M. *Nucleic Acids Res.* **2009**, *37*, 5001–5006.

# Supporting Information for Associated Publication P3

## Supporting Information

## DNA-Mediated Self-Assembly and Metallization of Semiconductor Nanorods for the Fabrication of Nanoelectronic Interfaces

by

Richard Weichelt,* Jingjing Ye,* Uri Banin, Alexander Eychmüller, Ralf Seidel

*equal contribution

published in

CHEMISTRY-A European Journal 2019, 25, 9012-9016

CHEMISTRY
A European Journal

Supporting Information

# DNA-Mediated Self-Assembly and Metallization of Semiconductor Nanorods for the Fabrication of Nanoelectronic Interfaces

Richard Weichelt[+],[a] Jingjing Ye[+],[b] Uri Banin,[c] Alexander Eychmüller,*[a] and Ralf Seidel*[b]

chem_201902148_sm_miscellaneous_information.pdf

# SUPPORTING INFORMATION

**Table of Contents**

## 1. Experimental Procedures

Materials and Characterization techniques

Unless otherwise noted, all used chemicals and filters were purchased from Merck (Darmstadt, Germany). Oligonucleotides for DNA origami assembly were purchased from Eurofins while oligonucleotides for the SC NR and Au NP functionalization were obtained from Biomers.net GmbH (Ulm, Germany) (sequences given in Table 1)

**Table 1.** Overview of the different oligonucleotides used in this study.

| Nanomaterial | Sequence | 5´ - Modification |
|---|---|---|
| CdS NR | TTTTT TTTTT TTTTT | Dithiol group |
| Au NP | TTTTT TTTTT TTTTT | Monothiol group |
| Au NP (for metal-SC dimer) | TTTAC CAGTG CTCCT | Monothiol group |

TEM imaging was performed using a JEOL JEM 1400 plus TEM or a Zeiss Gemini 500 SEM at 120 kV or 20 kV, respectively. HRTEM imaging of CdS NRs was performed using a FEI Tecnai F30 at 300 kV. Absorption spectra were recorded with a Cary 60 UV-Vis Spectrophotometer from Agilent Technologies.

### 1.1 CdS seed synthesis

Cadmium oxide (0.8 mmol), oleic acid (8 mmol) and 1-octadecene (20 g) were mixed in a 100 ml flask. The mixture was heated to 120°C and placed under vacuum for 1 h followed by three times argon purging. Afterwards, the solution was heated to 260°C to obtain a clear colorless solution. At 260 °C 0.04 mmol sulfur in 7 ml 1-octadecene was rapidly injected into the hot solution. After 90 s the reaction was quenched by cooling with a fan and the mixture was purified by precipitation with acetone followed by centrifugation. After precipitation, the seeds were purged with argon and stored in the glovebox under nitrogen atmosphere for further rod synthesis.

### 1.2 CdS NR synthesis

Cadmium oxide (0.93 mmol), trioctylphosphine oxide (6 g), octadecylphosphonic acid (2 mmol, PlasmaChem) and hexylphosphonic acid (0.24 mmol, PlasmaChem) were mixed in a 100 ml flask. The mixture was heated to 120°C and placed under vacuum for 1 h followed by three times argon purging. The solution was heated to 350°C to dissolve the CdO (clear colorless solution). At this temperature 1.8 ml trioctylphosphine was injected and the solution was cooled down to 120 °C again and placed under vacuum for another hour. Meanwhile, the CdS seeds were dissolved in 2.4 ml trioctylphosphine with sulfur (0,075 g/ml). After heating up the CdO solution to 365°C this mixture was rapidly injected. The reaction was quenched by cooling down after 9 min at 350 °C.

### 1.3 Phase transfer & oligonucleotide functionalization of CdS NRs

NRs were dissolved in toluene, precipitated with methanol (4:1) and centrifuged to remove excess organic compounds. The procedure was repeated up to three times in order to get a concentrated NR solution. Afterwards, 200 µl of a freshly prepared methoxy-polyethylenglycol-thiol solution (0.37 mmol, JenKem Technology) and KOH (0.53 mmol) in 1 ml methanol was added to 1 ml of NRs. The mixture was vortexed for 3 sec, followed by addition of 2 ml based Milli-Q water (pH 11) and subsequently centrifuged for another 5 min. Afterwards, phases were separated. The NR containing aqueous phase is washed three times with 10 ml 0.5x Tris-HCl (pH 8) using a Vivaspin 20 spin column (100,000 MWCO).

The dithiolated oligonucleotides (for sequences refer to table 1) were incubated with tris(2-carboxyethyl)phosphine hydrochloride (TCEP) at a 1:1 molar ratio (20 mM final concentration) for 12 h and cleaned with a G25 column filter to remove excess TCEP. The NRs in aqueous solution were immediately mixed with the functionalized oligonucleotides (molar ratio 1:600). In a salt aging process sodium chloride was added to the solution stepwise up to a final concentration of 300 mM NaCl. Afterwards the sample was incubated for 24 h. To remove excess oligos, the sample was filtered eight times with 0.5x Tris-HCl (pH 8) using 100 kDa Amicon filters.

### 1.4 Oligonucleotide functionalization of Au NPs

For the oligonucleotide functionalization of AuNPs a previously described method was utilized.[1,2] 5 nm AuNPs (Sigma-Aldrich) were densely coated with 15 nt poly-thymidine oligonucleotides carrying a 5'-thiol modification by salt aging. The final Au NP concentration was calculated from the absorbance signal at 520 nm.

### 1.5 Origami folding

The DNA origami molds[3] (Supporting information, Figures S8) were designed using CaDNAno[4] comprising parallel helices arranged in a square lattice.[5] 10 nM single-stranded p8064 scaffold DNA (tilibit nanosystems, Garching, Germany) was mixed in folding buffer containing 5 mM Tris-HCl, 1 mM EDTA and 11 mM $MgCl_2$ ( pH 8.0) with staple strands and capture strands (Eurofins) in a molar ratio of 1:10:1 (per individual sequence). The reaction was heated to 80°C for 5 min, and cooled to 25°C over 15 h using a non-linear temperature ramp with the slowest temperature decrease occurring between 55°C to 45°C. Subsequently, the molds were purified using precipitation with polyethylene glycol to remove excess staples[6]. For TEM imaging, 2-3 µl of a diluted origami solution (1-2 nM) was applied to glow-discharged carbon-coated grids. The sample was subsequently stained using a filtered 2% solution of uranyl formate in 5 mM NaOH for 2 min.

### 1.6 Attachment of SC NRs and Au NPs to DNA-origami structures

Freshly filtered CdS NRs were mixed with origami molds in 0.5x Tris-HCl buffer (pH 8) supplemented with 300 mM NaCl and 11 mM $MgCl_2$. The chosen NR amount was typically twice the number of attachment sites, i.e. for a mold structure with one attachment site the molar NR-origami ratio was 2:1. The mixture was then slowly heated to 40°C and afterwards cooled down to 23°C over the course of a 5 h time period. Finally, the sample was incubated at 20°C for 24-72 h. The attachment of AuNPs followed the same procedure, with a molar ratio of 3:1 or 6:1 for molds with one or two seed binding sites, respectively. Molds were purified from excess AuNPs using PEG precipitation[6]. For the assembly of heterostructures, mold monomers were first loaded with Au NPs and following PEG precipitation the mold concentration was measured. Subsequently, a 0.5 molar ratio of CdS NRs was added to form the final heterostructure.

### 1.7 Formation of mold dimers

To form heterostructures based on preformed mold dimers, two mold monomers each carrying a corresponding complementary interface to support dimerization (Interface A, design details see Figure S9 and S10) were assembled and preloaded with Au NPs. The two monomers were then mixed at a 1:1 ratio in folding buffer supplemented with 350 mM NaCl and left overnight for the dimerization.

**1.8 Seeded-growth of gold within the molds of SC NR heterostructures**

The concentration of the mold superstructures was adjusted with folding buffer, such that 1 nM mold monomers were present in solution. Then hydroxyl amine ($NH_2OH$) was added at a 6-fold molar access over the subsequently added gold precursor. The gold growth was initiated by injecting 3.6 µl of 25 mM $H[AuCl_4]$ into 100 µl final volume of the $NH_2OH$ containing mold solution.[3] During growth the solution was vigorously stirred and after 1 min the grown structures were deposited on TEM grids.

## 2. Results and Discussion

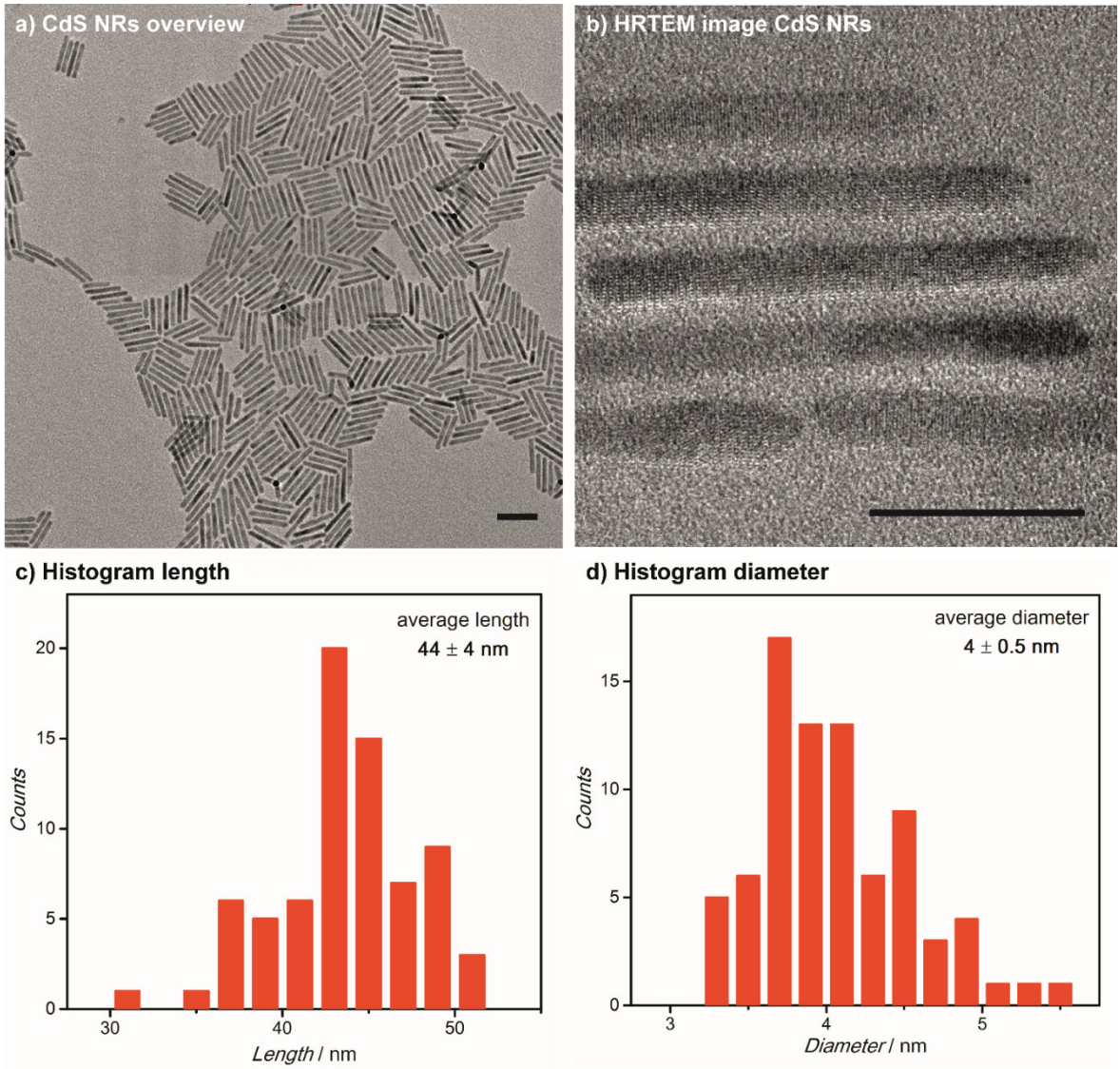


**Figure S1.** Analysis of CdS NRs following the organic synthesis. (a) Overview TEM (scale bar: 50 nm) and (b) HRTEM images (scale bar: 20nm), as well as histograms for (c) the average length and (d) the diameter of the rods

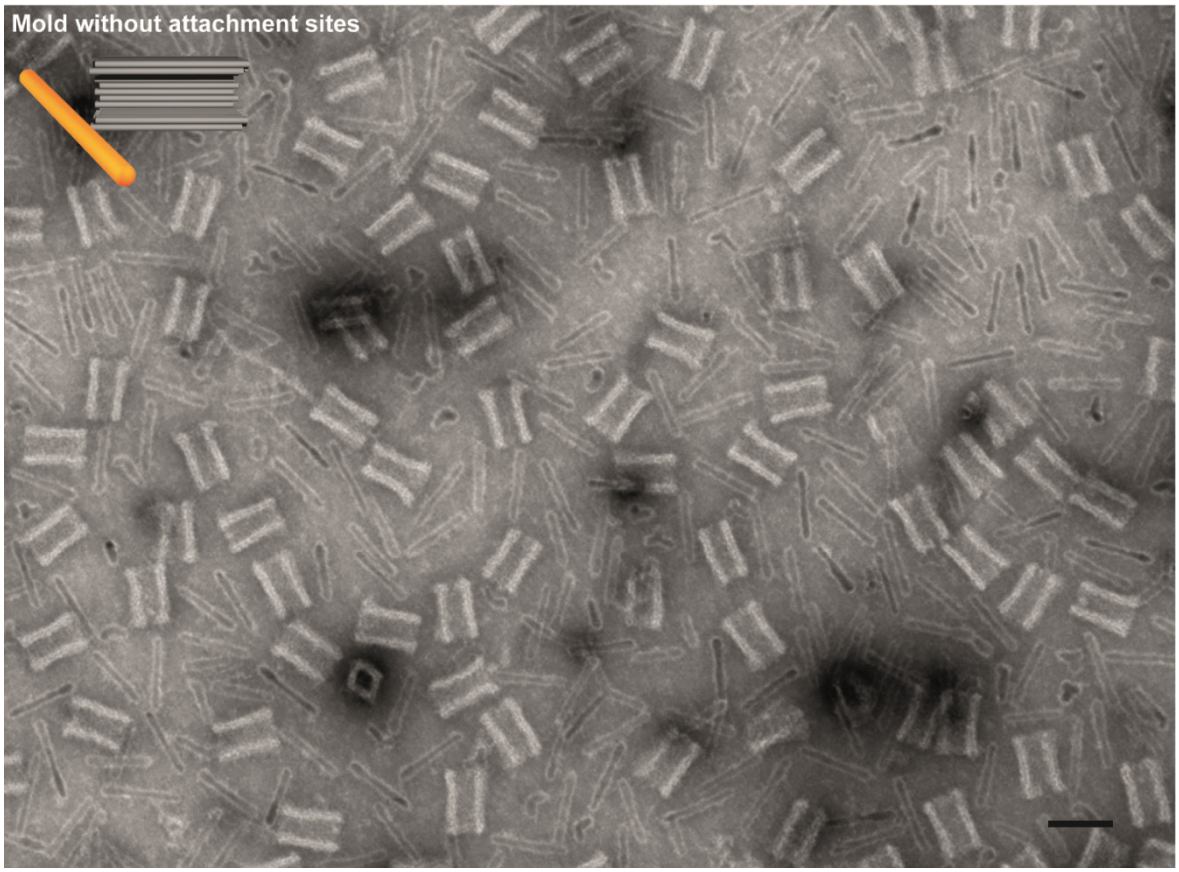


**Figure S2.** TEM image of oligonucleotide functionalized SC NRs incubated with molds containing no poly-A15 attachment sites. Despite the high densities no nonspecific interactions between the objects were observed. (scale bar: 50 nm)

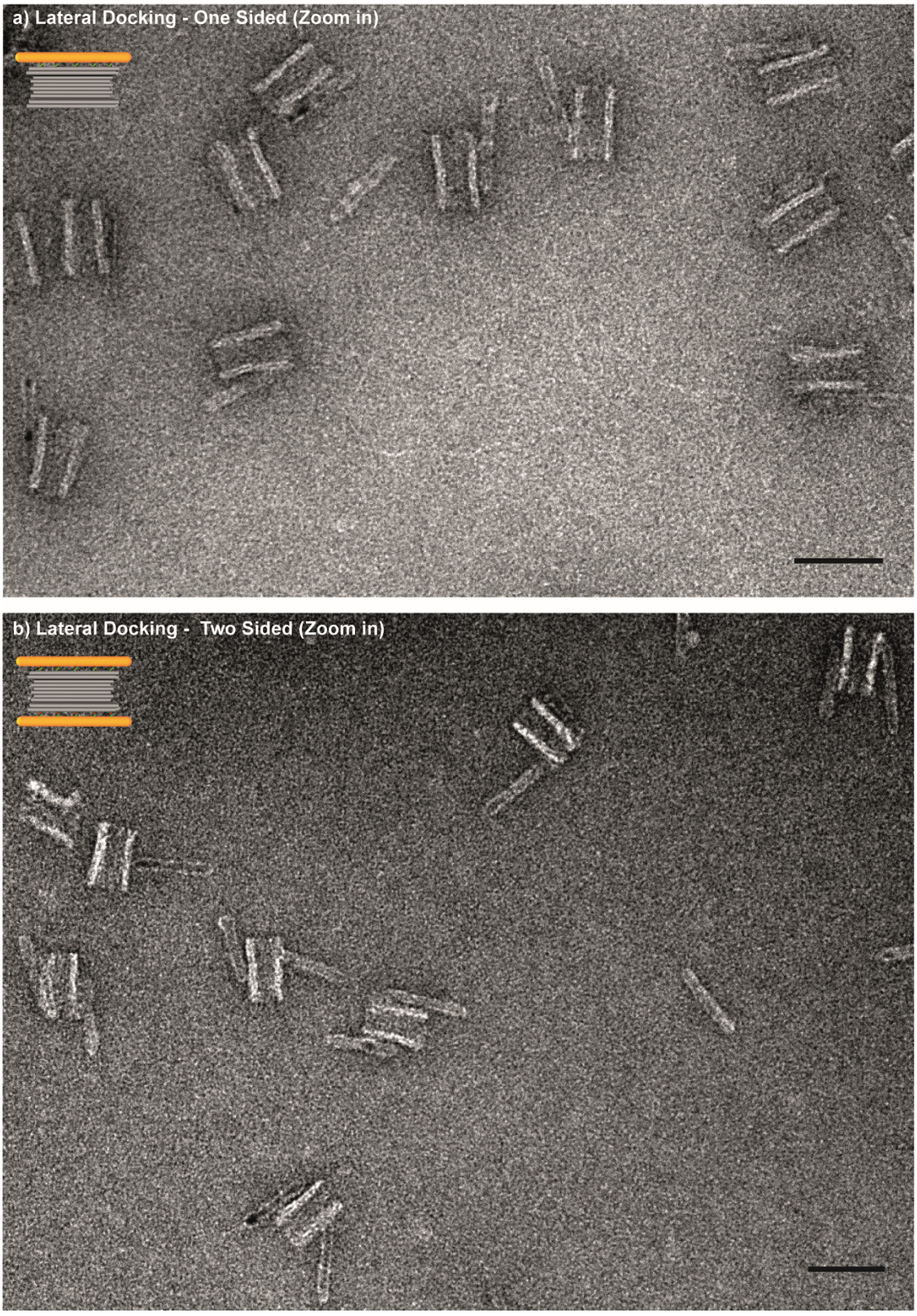


**Figure S3.** Zoom in TEM image for the (a) one and (b) two sided lateral docking display NR-mold monomer and dimer structures. (scale bar: 50 nm)

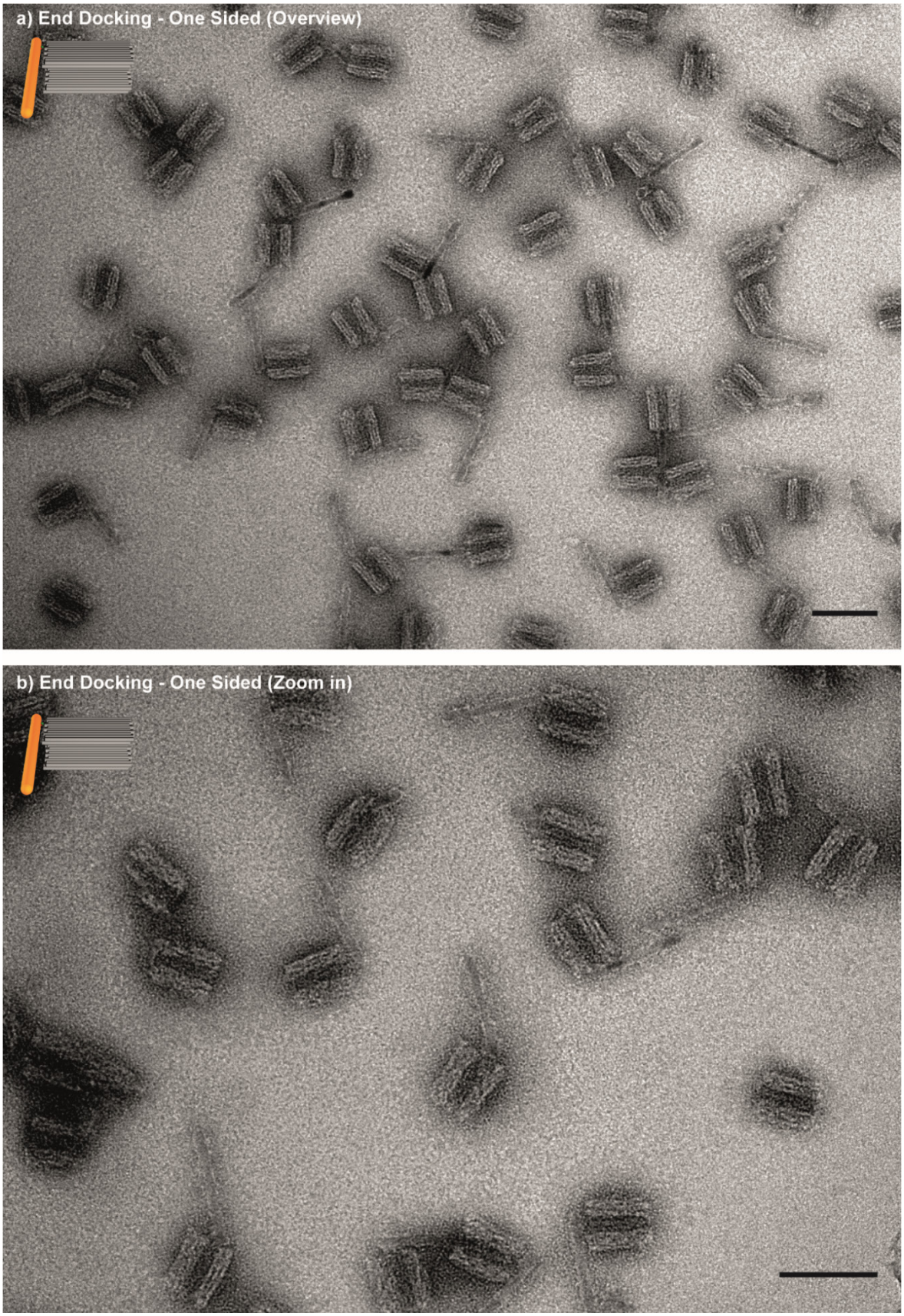


**Figure S4.** (a) Overview and (b) Zoom-in TEM images for one-sided external docking displays molds with single bound NRs. (scale bar: 50 nm)

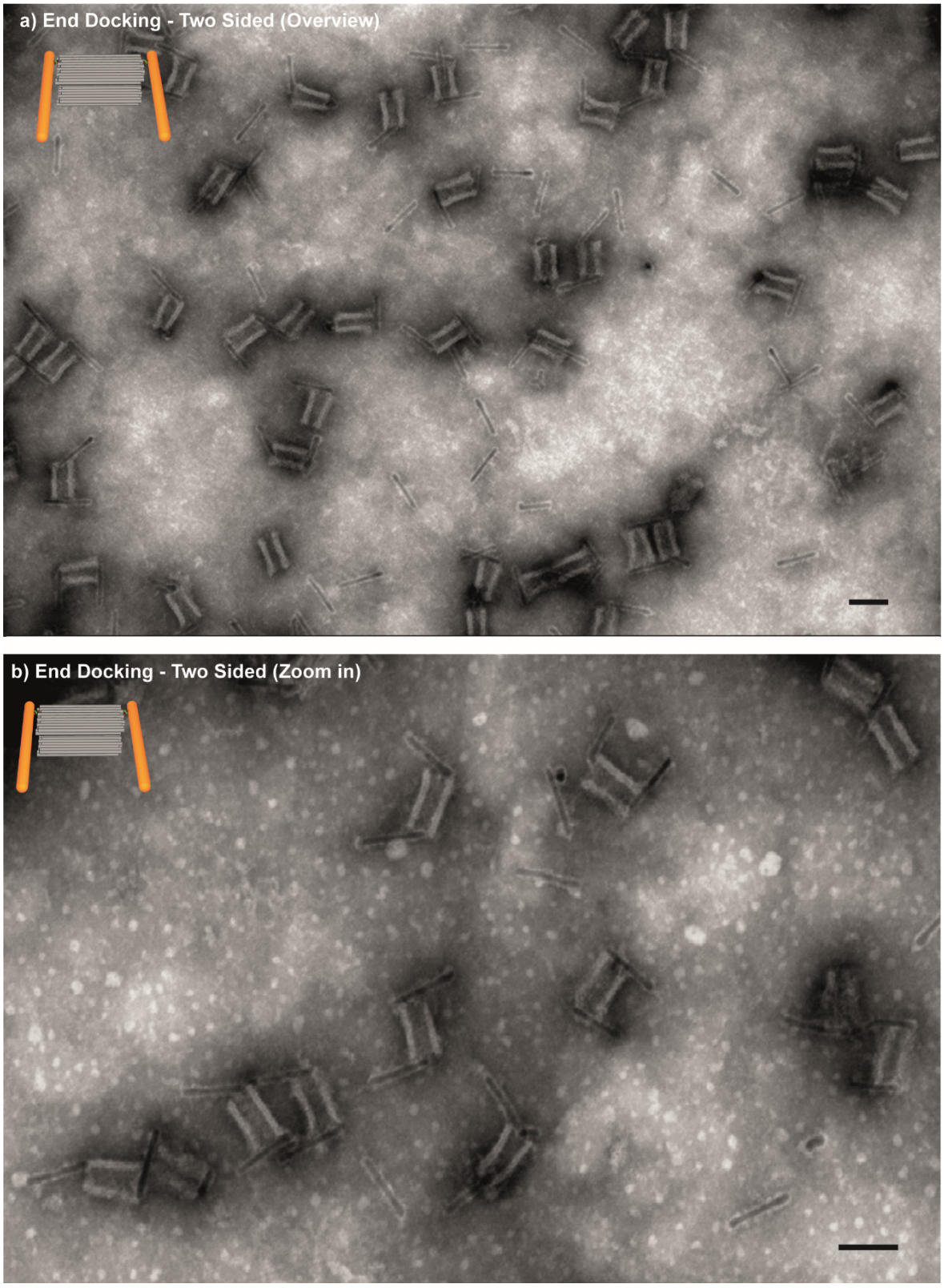


**Figure S5.** (a) Overview and (b) Zoom in TEM image for two-sided external docking display molds with two bound NRs. Thereby, some NRs connected with two molds and assembled chain-like structures. (scale bar: 50 nm)

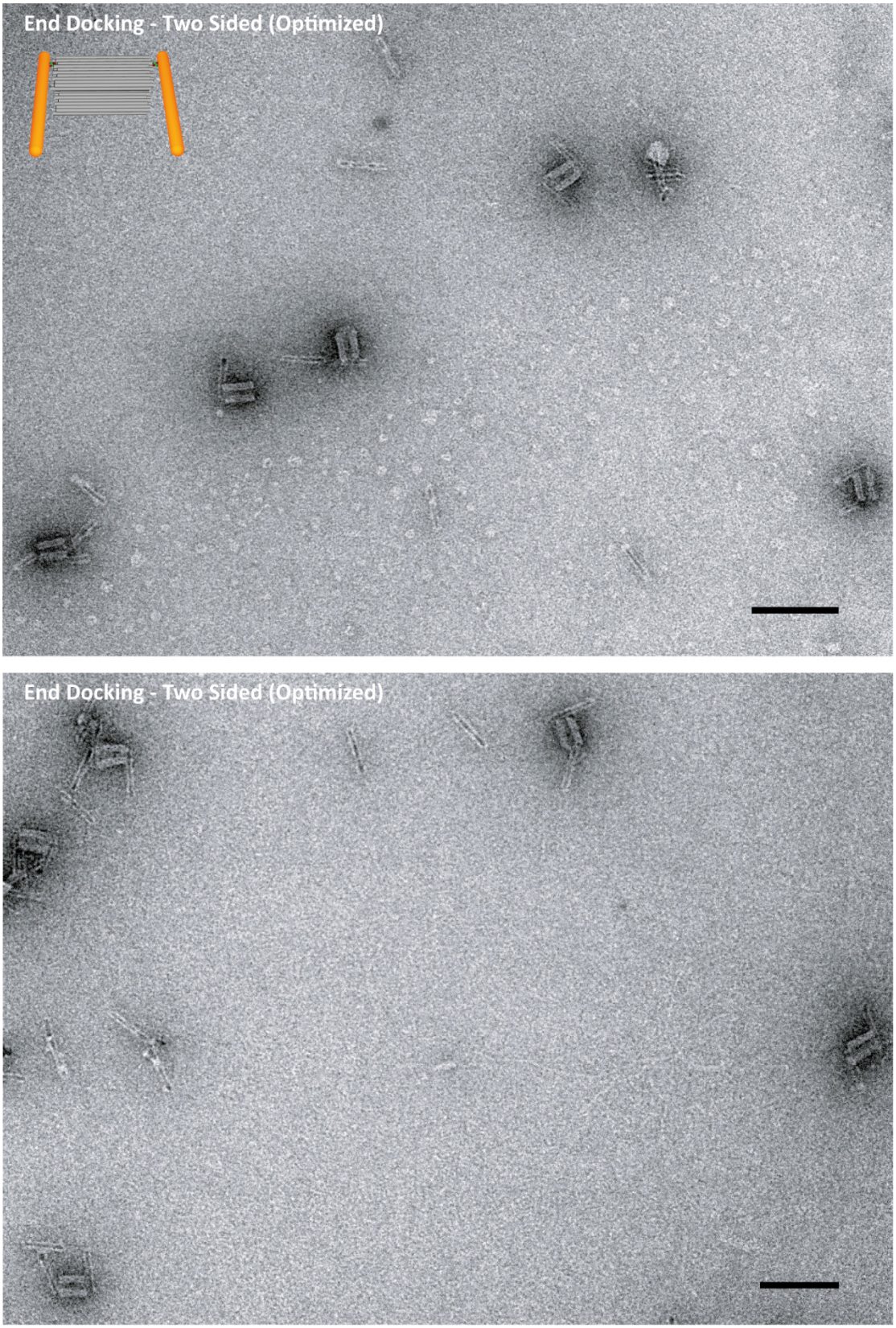


**Figure S6.** Overview TEM images for the optimized two-sided external docking displays molds with two bound NRs but without the formation of short chain structures. This was achieved by an enhancement of the SC NR proportion over the DNA origami molds and the four times dilution the overall concentration of all components in the assembly solution. (scale bar: 100 nm)

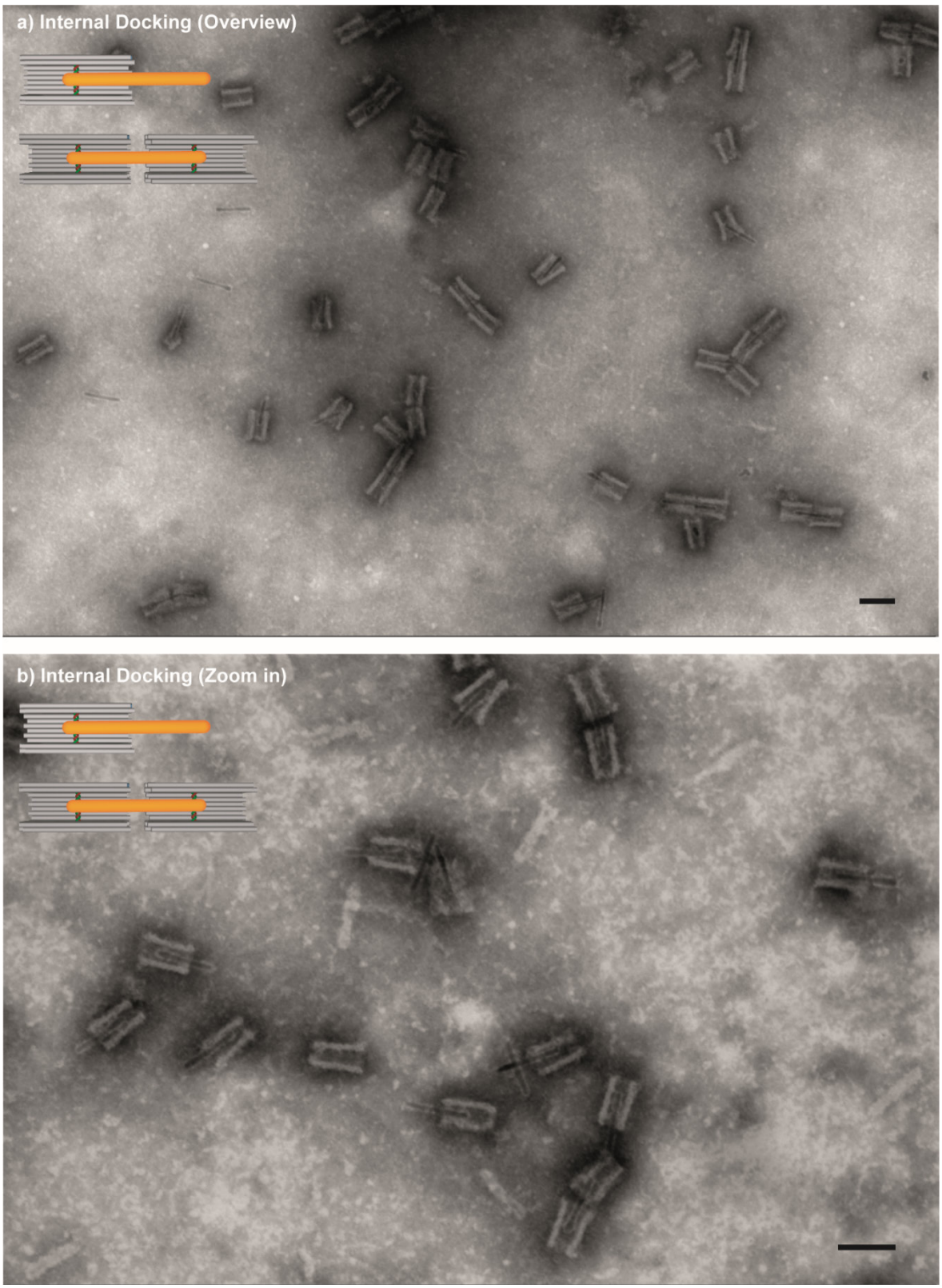


**Figure S7.** (a) Overview and (b) Zoom-in TEM images for the internal docking displaying NR-mold monomer and dimer structures. (scale bar: 50 nm)

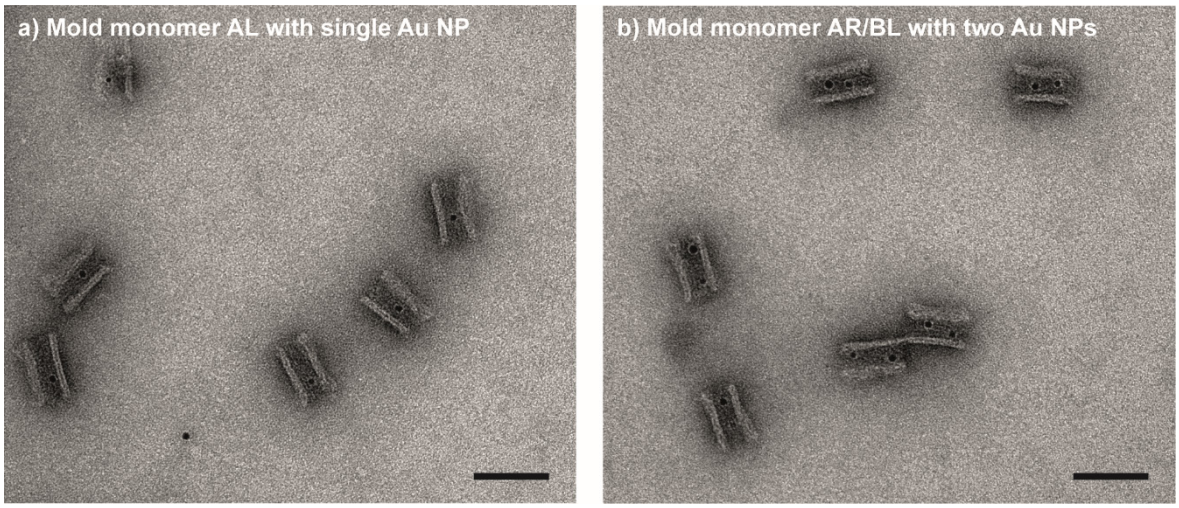


**Figure S8.** TEM images of (a) mold monomer structures that were preloaded with a single Au NP and (b) mold monomer structures that were preloaded with two Au NPs. (scale bar: 50 nm)

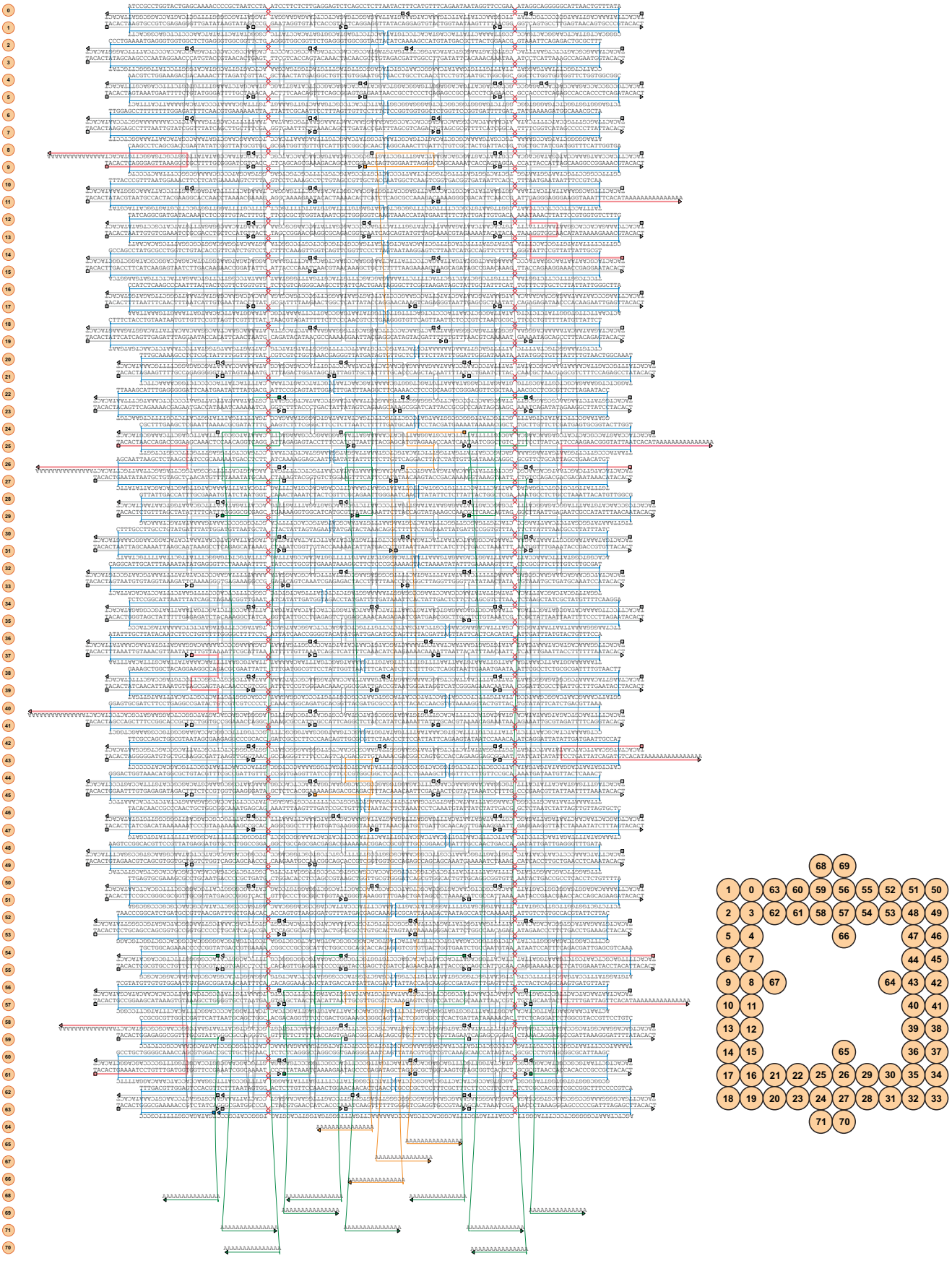

**Figure S9.** Design template for a mold structure with different binding sites for the attachment of nanorods. Shown is the detailed sequence and folding of the 8064 nt scaffold (blue) and the various staples (other colors) used to create the structure.The core design template was created using CaDNAno[4]. Red crosses are imaginary gaps that were introduced for better graphical representation. This was done in order to fit the 8 bp lattice size (corresponding to about 270 turns) into the 63 bp unit cell (six helical turns of dsDNA) that underly the square-lattice arrangement of DNA helices. Repulsive ends carry a 5'-TACACT ssDNA extension at the 5' and 3'-ends. Staples in green represent the capture strands for lateral docking. Staples in red represent the capture strands for end docking. Staples in yellow represent the capture strands for internal docking. All the capture strands carry 15 nt 3'-polyadenine overhangs for attaching DNA-coated NR. Squares and triangles at the staple ends symbolize the 5'- and the 3'-end, respectively.

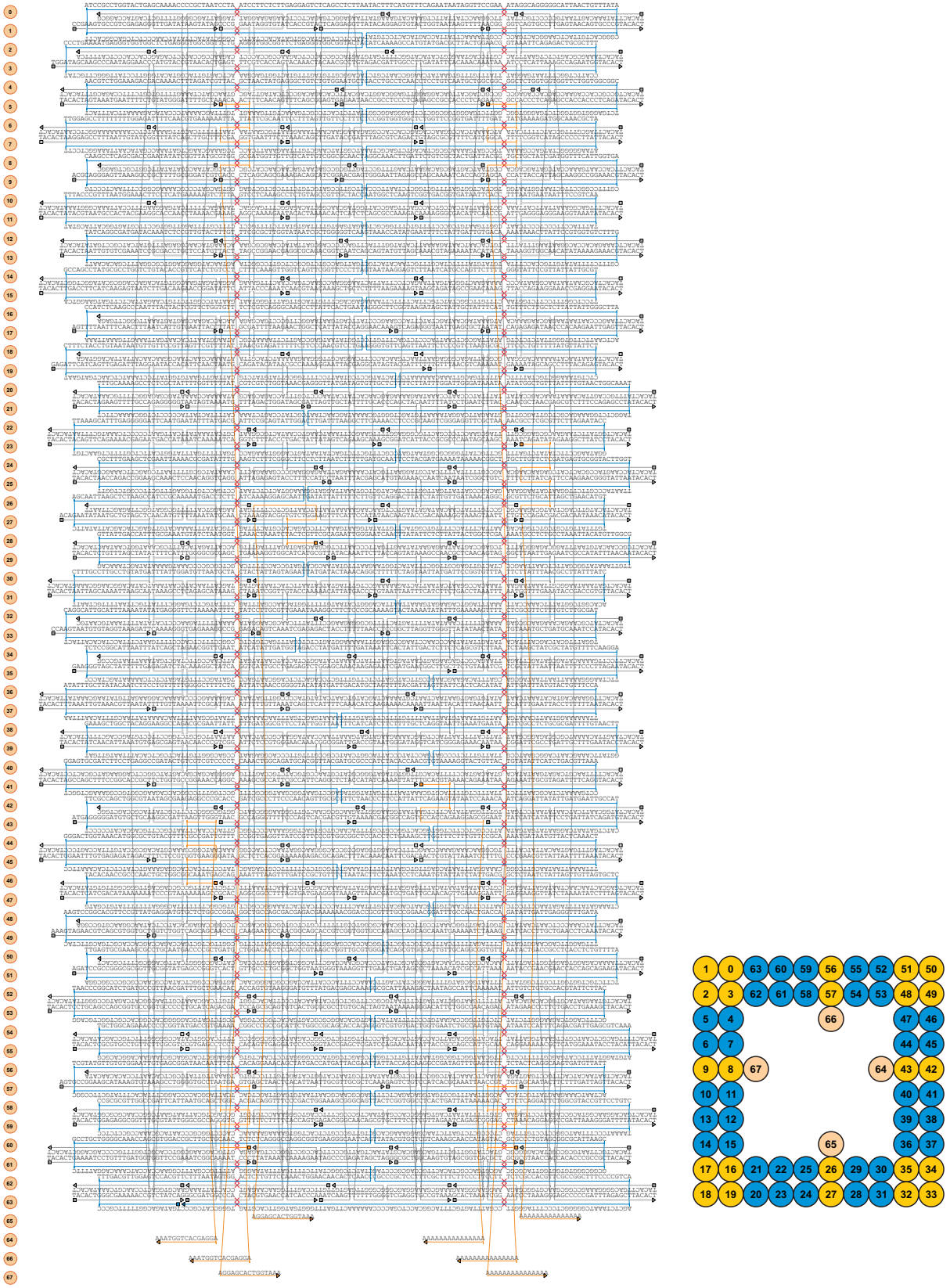


**Figure S10.** Design template for a mold with Interface A at the left end. Repulsive ends of the interface carry a 5'-TACACT ssDNA extension at the 5' and 3'-ends (repulsive helices are marked in blue in the scheme on the right). Attractive helices of the A interface have a 3 nt 5' end extension and a 3 nt 3' end recession (attractive helices are marked in yellow in the scheme on the right). Staples in yellow represent the capture strands for attaching a DNA-coated AuNP in the left part and NR in the right part. Colors and symbols are as in Supplementary Figure S8.

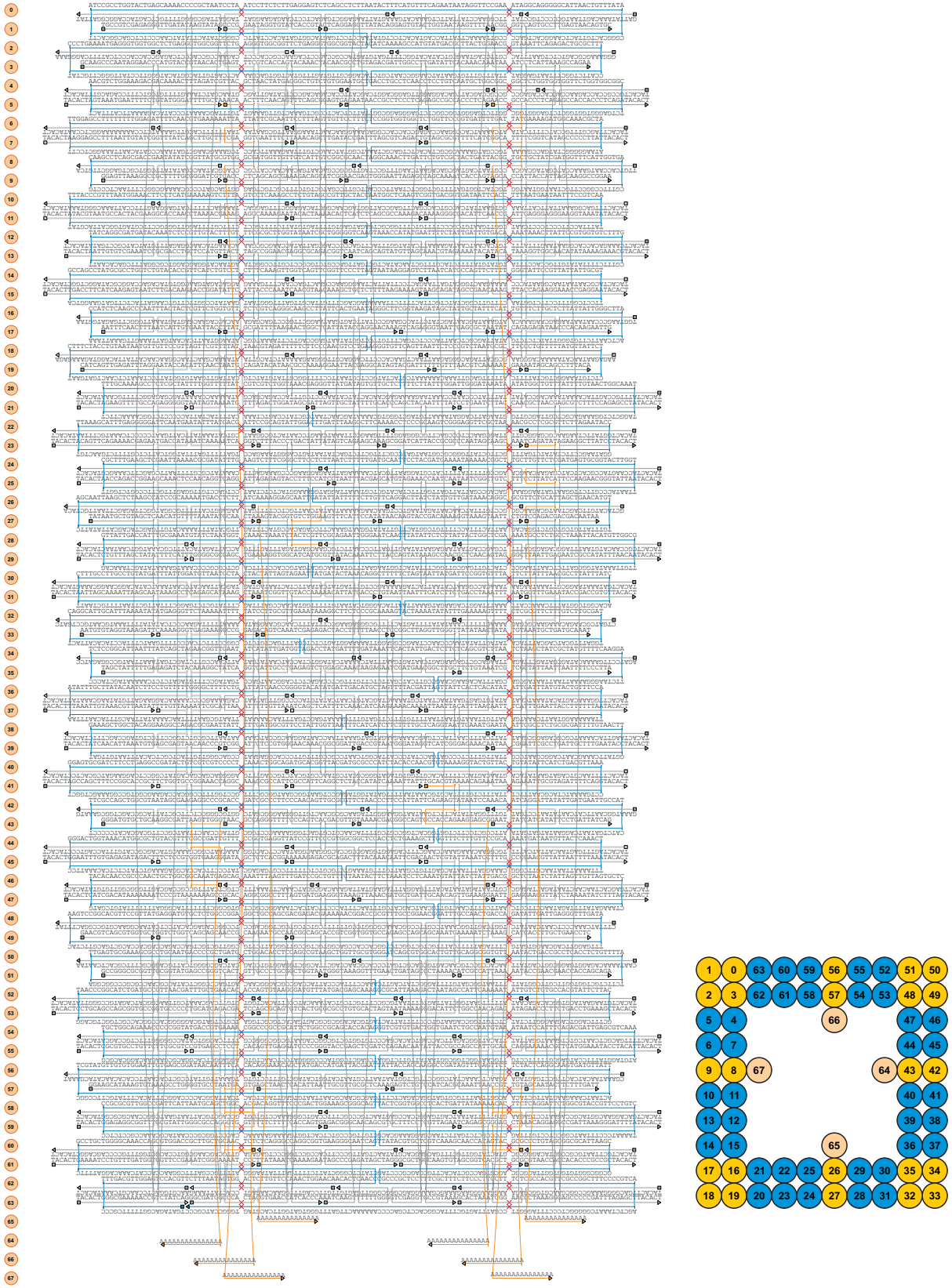


**Figure S11.** Design template for a mold with Interface B at left end and interface A at the right. Repulsive ends marked in blue carry a 5'-TACACT ssDNA extension at the 5' and 3'-ends. Attractive helix ends (marked in yellow) of the B interface at the left end have a 3 nt 5' end recession and a 3 nt 3' end extension. Attractive helix ends (marked in yellow) of the A interface at the right end have a 3 nt 3' end recession and a 3 nt 5' end extension. Colors and symbols are as in Supplementary Figure S8.

## 3. References

[1] F. N. Gür, F. W. Schwarz, J. Ye, S. Diez, T. L. Schmidt, *ACS Nano* **2016**, *10*, 5374–5382.

[2] S. Helmi, C. Ziegler, D. J. Kauert, R. Seidel, *Nano Lett.* **2014**, *14*, 6693–6698.

[3] T. Bayrak, S. Helmi, J. Ye, D. Kauert, J. Kelling, T. Schönherr, R. Weichelt, A. Erbe, R. Seidel, *Nano Lett.* **2018**, *18*, 2116–2123.

[4] S. M. Douglas, A. H. Marblestone, S. Teerapittayanon, A. Vazquez, G. M. Church, W. M. Shih, *Nucleic Acids Res.* **2009**, *37*, 5001–5006.

[5] Y. Ke, S. M. Douglas, M. Liu, J. Sharma, A. Cheng, A. Leung, Y. Liu, W. M. Shih, H. Yan, *J. Am. Chem. Soc.* **2009**, *131*, 15903–15908.

[6] E. Stahl, T. G. Martin, F. Praetorius, H. Dietz, *Angew. Chemie Int. Ed.* **2014**, *53*, 12735–12740.

## 4. Author Contributions

U.B., A.E. and R.S. designed the study. R.W. and J.Y. carried out the experiments and analyzed the data. R.W. (lead) and R.S. (supporting) wrote the manuscript. R.W. and J.Y. contributed equally to the experimental part of the study.

# List of Figures

# List of Tables

# Selbstständigkeitserklärung

Hiermit versichere ich, dass ich die vorliegende Arbeit selbstständig und ohne unzulässige Hilfe oder Benutzung anderer als der angegebenen Hilfsmittel angefertigt habe. Ich habe keine anderen als die im Literaturverzeichnis aufgeführten Quellen benutzt und alle Textstellen, die wörtlich oder sinngemäß aus veröffentlichten oder unveröffentlichten Schriften entnommen wurden, als solche kenntlich gemacht. Alles aus anderen Quellen oder von anderen Personen übernommene Material, das in der Arbeit verwendet wurde oder auf das direkt Bezug genommen wird, wurde als solches gekennzeichnet. Insbesondere wurden alle Personen genannt, die an der direkten Entstehung der vorliegenden Arbeit beteiligt waren. Ich versichere, dass Dritte von mir weder unmittelbar noch mittelbar geldwerte Leistungen für Arbeiten erhalten haben, die im Zusammenhang mit dem Inhalt der vorliegenden Dissertation stehen und dass die vorgelegte Arbeit weder im Inland noch im Ausland in gleicher oder ähnlicher Form einer anderen Prüfungsbehörde zum Zwecke einer Dissertation oder eines anderen Prüfungsverfahrens vorgelegt wurde.

_____ _____

Ort, Datum Jingjing Ye

# Author Contributions

**P1:** *Fabrication of Metal Nanostructures with Programmable Length and Patterns Using a Modular DNA Platform*

Jingjing Ye, Seham Helmi, Josephine Teske, Ralf Seidel

Nano Letter 2019, 19, 4, 2707-2714

Project concept was designed by R. Seidel and me. S. Helmi drafted an original design which was further improved and developed by me. I performed all the experiments and analysed the data. Under my supervision, J. Teske additionally analysed the length distribution of the nanostructures. The manuscript was drafted by me. All the authors critically revised and approved the manuscript.

**P2:** *DNA-Mold Templated Assembly of Conductive Gold Nanowires*

Türkan Bayrak,* Seham Helmi,* Jingjing Ye,* Dominik Kauert, Jeffrey Kelling, Tommy Schönherr, Artur Erbe, Ralf Seidel

Nano Letter 2018, 18, 3, 2116-2123

*These authors contributed equally to this work

A. Erbe and R. Seidel designed the study. S. Helmi worked out the design of the DNA template and the metallization; I prepared the gold nanowires for the characterisation; T. Bayrak performed the conductivity measurement. T. Bayrak, S. Helmi and I contributed equally to the experimental part of the study. T. Bayrak, A. Erbe, R. Seidel and I wrote the manuscript. All the authors critically revised and approved the manuscript.

**P3:** *DNA-Mediated Self-Assembly and Metallization of Semiconductor Nanorods for the Fabrication of Nanoelectronic Interfaces*

Richard Weichelt,* Jingjing Ye,* Uri Banin, Alexander Eychmüller, Ralf Seidel

CHEMISTRY-A European Journal 2019, 25, 9012-9016

*These authors contributed equally to this work

U. Banin, A. Eychmüller and R. Seidel designed the study. R. Weichelt carried out the synthesis of the semiconductor nanorods; I designed and prepared all the DNA origami structures. The gold growth protocol was developed in the joint manner by R. Weichelt and me. R. Weichelt and I contributed equally to the experimental part of the study. All the authors contributed to the manuscript writing.

## Thesis Advising Committee (University of Leipzig):

**Prof. Dr. Frank Cichos (Chairman)**
Peter Debye Institute for Soft Matter Physics
University of Leipzig
Linnéstraße 5
04103 Leipzig
Germany

**Prof. Dr. Ralf Seidel (Supervisor)**
Peter Debye Institute for Soft Matter Physics
University of Leipzig
Linnéstraße 5
04103 Leipzig
Germany

**Prof. Dr. Tilo Pompe**
Institute for Biochemistry
University of Leipzig
Johannisallee 21-23
04103 Leipzig
Germany

Also obligated to

**Cfaed (Center for Advancing Electronics Dresden) postgraduate program**

**International Helmholtz Research School for Nanoelectronics Networks (IHRS NANONET) doctoral program**

## Thesis Advising Committee:

**Primary supervisor: Prof. Dr. Ralf Seidel**

Peter Debye Institute for Soft Matter Physics

University of Leipzig

Linnéstraße 5

04103 Leipzig

Germany

**Scientific Co-supervisor: Prof. Dr. Thorsten Lars Schmidt**

Physics Department

Kent State University

800 E Summit St, Kent, OH 44240

USA

**External Co-supervisor: PD Dr. Artur Erbe**

Institute of Ion Beam Physics and Materials Research

Helmholtz-Zentrum Dresden-Rossendorf

01328 Dresden

Germany

# Acknowledgement

I would like to foremost express my deep gratitude to Prof. Ralf Seidel, my supervisor, for his patient guidance, enthusiastic encouragement and useful critiques for this research work. His valuable and constructive suggestions during my PhD helped me to develop this research work and my scientific skills. His willingness to give his time generously for discussing the projects and his support for my German courses has been very much appreciated. The last three and a half years have been truly a great experience.

I would like to express my very great appreciation to my thesis advisory committee within the cfaed frame: PD Dr. Artur Erbe, Dr. Thorsten Schmidt and Prof. Ralf Seidel for their guidance, support, and advice throughout my PhD period. I would like to thank Dr. Artur Erbe for introducing me to the Nanonet PhD program and providing me a different view of my project. I would like to thank Dr. Thorsten Schmidt for all the useful discussions. All have been an invaluable asset.

I would like to thank cfaed and Nanonet, the two PhD program that I am involved in. For financing the PhD project and providing me support for the language course. They offered me unlimited opportunities and workshops to develop and explore myself. Special thanks go to Dr. Peter Zahn, coordinator of Nanonet, for always encouraging and supporting me throughout my PhD.

My special thanks are extended to two amazing collaborators, Richard Weichelt from Prof. Alexander Eychmüller group in TU-Dresden and Türkan Bayrak from Dr. Artur Erbe in HZDR. Not only being excellent collaborators but also sharing precious insights and friendships. I was definitely lucky to work with them. I thank Dr. Markus Löffler and Alexander Tahn for the training and supporting of using electron microscope in DCN (Dresden center for nanoanalysis).

I am very grateful to Dr. Martin Göse and Dr. Nicole Weizenmann for proofreading this thesis. I would also like to thank Dr. Richard Weichelt for the German translation of the abstract.

I would like to thank all the former and current AG Seidel group members, for creating an amazing working atmosphere, for all the short weekend trips, fun dinner party, and cakes! Many thanks particularly to Dominik and Seham for always having time for short discussion. Special thanks to our three secretary/lab managers, Nicole, Cordula and Kerstin for their generous help and support whenever I needed. I would also like to thank my office mates, Pierre and Ulrich for sharing the lovely office and time. I want to thank our excellent student whom I supervised, Josephine! It has been a pleasure to work together with you for almost two and a half years. I learned a lot from you. I would like to also thank the Nanonet gang in Dresden, Türkan, Filip, Bilal, Alex,

and Hagen, for all the fun road trips, workshops and conferences. I would like to thank all my former colleagues from my master study in Dresden for their continuous support especially at the beginning of my PhD.

Many thanks to all my friends for always supporting me. To share all the bad and good times with joys and sadness. Thanks for being there and make me feel at home in Germany. I would also like to thank my German study group, Anna my German teacher, Andrea, Amy, Atefeh and Alberto for all the lovely evening time.

Finally, I would like to thank my friends back home for always empowering and supporting me. My biggest thanks go to my family who always loves me and believes in me, always there to support me unconditionally. In the end, I would like to thank Uzay for always being there for me.

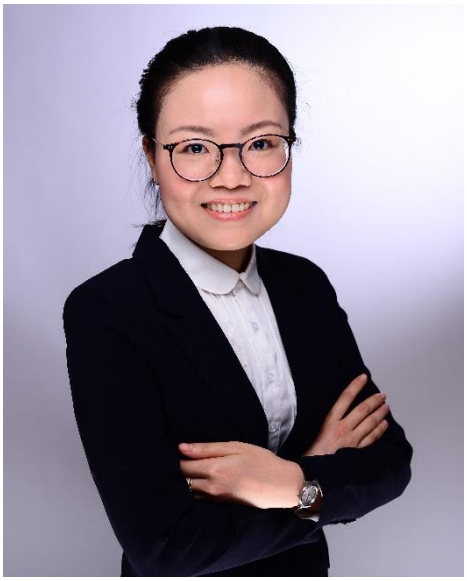

# Jingjing Ye

**Birthday**
23.09.1991
**Place of birth**
Zhejiang, China
**Address**
Albert-Schweitzer-Str. 12, 04317, Leipzig, Germany
**E-Mail**
jingjing.ye@physik.uni-leipzig.de

## EDUCATION

| | |
|---|---|
| **03/2016-Current** | **Doctor rerum naturalium - Physics**<br>University Leipzig, Germany |
| **09/2013-10/2015** | **Master of Science - Nanoscience and Nanotechnology**<br>Specialization Nano-electronics<br>Technische Universität Dresden, Germany and<br>Katholieke Universiteit Leuven, Belgium |
| **09/2009-06/2013** | **Bachelor of Science - Physics**<br>Harbin Institute of Technology, China |
| **02/2012-07/2012** | **Exchange Student - Physics**<br>Fudan University, China |

## PERSONAL EXPERIENCE

**03/2016-present PhD Thesis: Nano-electronic components built from DNA templates**

Supervisor: Prof. Dr. Ralf Seidel, University Leipzig, Germany

- Fabrication of complex inorganic nanostructures for nano-electronics in a lego-brick like fashion using mold-based particle synthesis.

**03/2015-10/2015 Master Thesis: Multi-step assembly on solid support**

Supervisor: Dr. Thorsten-Lars Schmidt, Center for advancing electronics Dresden (Cfaed), Germany

- Purification of DNA origami structure by using magnetic beads to capture and release; assembly plasmonic waveguides directly on solid support.

**07/2014-09/2014 Internship: Optical characterization of optoprobes**

Supervisor: Dr. Dries Braeken, IMEC, Belgium

- On-chip waveguides characterization to investigate optical losses in the substrate and the efficiency of coupling light into and from the substrate. Parameters of

efficient stimulation were studied by using optical imaging and electrical recording techniques.

**09/2012-06/2013 Undergraduate Thesis: Excited state energy relaxation of organic material from ultrafast optical spectroscopy**

Supervisor: Prof. Yanqiang Yang, Physics Department, Harbin Institute of Technology, China

- Constructed time resolved transient absorption spectroscopy; collected data of F8BT dynamic process; combined with other optical spectroscopies, analyzed intramolecular charge transfer of F8BT.

## SKILLS

| | |
|---|---|
| **Languages** | Chinese (Mother tongue); English (Fluent); German (B2) |
| **Computer skills** | MS office applications; Origin; Maya; Adobe Illustrator; Coreldraw; Matlab |
| **Hobbies** | Chinese painting and calligraphy; Piano; Travelling |